Mechanistic Investigations of Palladium-Catalyzed Cross-Coupling Reactions Using Advanced Mass Spectrometric Methodologies

by

Ian Chikumbutso Chagunda

B.Sc. Chemistry, Simon Fraser University, 2020

A dissertation submitted in partial fulfilment of the requirements for the degree of

Doctor of Philosophy

in the

Department of Chemistry

University of Victoria

We acknowledge and respect the Lək̓ʷəŋən (Songhees and Xʷsepsəm/Esquimalt) Peoples on whose territory the university stands, and the Lək̓ʷəŋən and W̱SÁNEĆ Peoples whose historical relationships with the land continue to this day.

Mechanistic Investigations of Palladium-Catalyzed Cross-Coupling Reactions Using Advanced Mass Spectrometric Methodologies

by

Ian Chikumbutso Chagunda

B.Sc. Chemistry, Simon Fraser University, 2020

Supervisory Committee

Prof. Dr. J. Scott McIndoe, Supervisor

Department of Chemistry, University of Victoria

Prof. Dr. Ian Manners (deceased), Departmental Member

Department of Chemistry, University of Victoria

Prof. Dr. David C. Leitch, Departmental Member

Department of Chemistry, University of Victoria

Prof. Dr. Alisdair Boraston, External Member

Department of Biochemistry and Microbiology, University of Victoria

Abstract

This dissertation explores the application of mass spectrometry (MS) as a tool for investigating the mechanisms of palladium-catalyzed cross-coupling (PdCC) reactions. By integrating advanced MS techniques with reaction monitoring methodologies, this work provides insights into catalytic activation processes, the role of intermediates, and the limitations of MS in analyzing complex chemical systems. The research is presented across five chapters, each examining specific aspects of MS in the context of organometallic catalysis.

The first chapter establishes the foundational context, detailing the principles of MS and its role in studying PdCC reactions. A particular focus is placed on electrospray ionization mass spectrometry (ESI-MS) and pressurized sample infusion (PSI), highlighting their advantages and challenges in capturing transient catalytic species. Chapter 2 discusses the inherent limitations of MS in characterizing high molecular weight polymers, a common product of PdCC reactions. Factors such as diminishing signal-to-noise (S/N) ratios, isotope pattern broadening, and ionization inefficiencies are examined, and strategies for improving polymer analysis via MS are proposed.

Chapter 3 evaluates the performance of ESI-MS across different instruments, particularly in detecting fragile organometallic complexes. A multi-instrument comparative study reveals significant variability in instrument performance, emphasizing the necessity for optimizing instrument parameters to preserve weakly bound catalytic species. Chapter 4 critically re-examines the mercury drop test, a widely used method for distinguishing between homogeneous and heterogeneous catalysis. This analysis demonstrates that mercury interacts with Pd intermediates through redox-transmetallation and amalgamation processes, leading to potential misinterpretations of catalytic activity.

Finally, Chapter 5 investigates a new-generation palladium precatalyst, $(^{DMP}DAB)Pd(CH_2SiMe_3)_2$, providing mechanistic insights into ligand substitution, catalyst activation, and oxidative addition processes. The combination of PSI-ESI-MS and real-time monitoring enabled the identification of key catalytic intermediates, contributing to the development of more efficient and selective Pd-based catalysts. Collectively, this

dissertation advances the understanding of MS as a tool for elucidating catalytic processes, offering methodological improvements and new perspectives on PdCC reaction mechanisms. The findings have broad implications for catalyst design, sustainability, and the continued evolution of mass spectrometric techniques in organometallic chemistry.

Table of Contents

Abbreviations and Definitions

API : Atmospheric pressure ionization

CA : Catalyst activation

CE : Collision energy

CEM : Chain ejection model

CID : Collision-induced dissociation

CRM : Charged residue model

Cy : Cyclohexyl group

Da : Dalton

dba : Dibenzylideneacetone

DC : Direct current

DFT : Density functional theory

^{DMP}DAB : *N*,*N*′-bis(2,6-dimethylphenyl)diazabutadiene

E_{el} : Electric potential energy

E_{Kin} : Kinetic energy

ESI : Electrospray ionization

Et : Ethyl group

FT : Fourier transform

FWHM : Full width at half maximum

GC : Gas chromatography

HPLC : High performance liquid chromatography

ICR : Ion cyclotron resonance

IEM : Ion evaporation model

***i*-Pr** : Isopropyl group

IR : Infrared spectroscopy

kV : Kilovolts

L : Ligand

LC : Liquid chromatography

M : Metal

m/z : Mass-to-charge ratio

MAH : Maleic anhydride

MALDI : Matrix-assisted laser desorption/ionization

MeOH : Methanol, CH_3OH

MMD : Molar mass distribution

MRM : Multiple reaction monitoring

MS : Mass spectrometry

MS/MS : Tandem mass spectrometry

NMR : Nuclear magnetic resonance

Nu : Nucleophile

OA : Oxidative addition

OAc : Acetoxy group

OAC : Oxidative addition complex

OTf : Triflate group

OTs : Tosylate group

PEEK : Polyether ether ketone

PPN : Bis(triphenylphosphine)iminium

PSI : Pressurized sample infusion

PVC : Poly(vinyl chloride)

Q-TOF : Quadrupole Time-of-flight

RE : Reductive elimination

RF : Radiofrequency

S/N : Signal-to-noise ratio

SEC : Size exclusion chromatography

SIR : Selected ion recording

SM : Suzuki-Miyaura

SPC : Suzuki polycondensation

***t*-Bu** : Tertbutyl group

THF : Tetrahydofuran

TIC : Total ion current

TM : Transmetallation

TOF : Time-of-flight

TQD : Tandem Quadrupole Detector™

List of Publications

This dissertation contains the following original publications.

Thomas, G. T.; Donnecke, S.; **Chagunda, I. C.**; McIndoe, J. S. Pressurized Sample Infusion. *Chemistry–Methods* **2022**, *2* (1), e202100068. doi.org/10.1002/cmtd.202100068.

Chagunda, I. C.; Russell, G. T.; McIndoe, J. S. The Signal-to-Noise Issue in Mass Spectrometric Analysis of Polymers. *Polymer Chemistry* **2021**, *12* (31), 4451–4461. doi.org/10.1039/D1PY00461A.

Chagunda, I. C.; Williams, P. J. H.; Fisher, T.; Stock, N. L.; Beach, D. G.; Thomas, G. T.; Zhu, J.; McIndoe, J. S. Comparative Assessment of ESI-MS Softness for Inorganic Complexes: How Soft Is Your ESI-MS? *European Journal of Inorganic Chemistry* **2024**, No. 27, e202400077. doi.org/10.1002/ejic.202400077.

Chagunda, I. C.; Fisher, T.; Schierling, M.; McIndoe, J. S. Poisonous Truth about the Mercury Drop Test: The Effect of Elemental Mercury on Pd(0) and Pd(II)ArX Intermediates. *Organometallics* **2023**, *42* (19), 2938–2945. doi.org/10.1021/acs.organomet.3c003400.

Chagunda, I. C.; Kropp, A.; Leitch, D. C.; McIndoe, J. S. Ligand Substitution, Catalyst Activation, and Oxidative Addition Studies of a Stable Dialkyl Palladium Precatalyst. *Organometallics* **2025**, *44* (5), 628–636. doi.org/10.1021/acs.organomet.4c00463.

Additional Publications

The following is a list of publications contributed to during my PhD studies, but not included in this dissertation.

Ting, M. Y. C.; Yunker, L. P. E.; **Chagunda, I. C.**; Hatlelid, K.; Vieweg, M.; McIndoe, J. S. A Mechanistic Investigation of the Suzuki Polycondensation Reaction Using MS/MS Methods. *Catalysis Science & Technology* **2021**, *11* (13), 4406–4416. doi.org/10.1039/D1CY00743B.

Williams, P. J. H.; Killeen, C.; **Chagunda, I. C.**; Henderson, B.; Donnecke, S.; Munro, W.; Sidhu, J.; Kraft, D.; Harrington, D. A.; McIndoe, J. S. Continuous Addition Kinetic Elucidation: Catalyst and Reactant Order, Rate Constant, and Poisoning from a Single Experiment. *Chemical Science* **2023**, *14* (36), 9970–9977. doi.org/10.1039/D3SC02698A.

Williams, P. J. H.; **Chagunda, I. C.**; McIndoe, J. S. OptiMS: An Accessible Program for Automating Mass Spectrometry Parameter Optimization and Configuration. *Journal of the American Society for Mass Spectrometry.* **2024**, *35* (3), 449–455. doi.org/10.1021/jasms.3c00354.

Levy, J.; **Chagunda, I. C.**; Iosub, V.; Leitch, D. C.; McIndoe, J. S. MoleculAR: An Augmented Reality Application for Understanding 3D Geometry. *Journal of Chemical Education* **2024**, *101* (6), 2533–2539. doi.org/10.1021/acs.jchemed.3c01045.

Killeen, C.; Kropp, A.; **Chagunda, I. C.**; Jackson, E. C.; McIndoe, J. S. The Amenability of Different Solvents to Electrospray Ionization Mass Spectrometry. *International Journal of Mass Spectrometry* **2024**, *506*, 117349. doi.org/10.1016/j.ijms.2024.117349.

Thind, S. S.; Ryane, B. A.; Hayden, J. B.; **Chagunda, I. C.**; Paul, M.; McIndoe, J. S. Bias Enhanced Electro-Photocatalysis on TiO_2 Nanoporous Materials for Decomposition of Forever Chemicals in Saltwater. *Environmental Science: Advances* **2025**, Advance Article. doi.org/10.1039/D4VA00423J.

List of Figures

List of Tables

List of Schemes

Acknowledgements

This dissertation would not have been possible without the help, encouragement, guidance, patience, critique, advise, and support of so many people. I will try to mention you all…

First, a heartfelt thank you to Scott for taking me on in 2020, in the midst of a global pandemic. Beginning a PhD is daunting under normal circumstances, but doing so in a time of such uncertainty was even more challenging. Your support through those first few months made all the difference. Thank you for your guidance, for the encouragement to explore different ideas in the lab, and to step out and engage with opportunities beyond our group. Your willingness to share travel, research, and scholarship opportunities has been instrumental in my growth as a researcher and person.

I also must also acknowledge Gilian (now Dr. Thomas) for being a guiding light in the early days in the lab. Your patience in teaching the practicalities of the lab and setting an example for staying organized and focused through the grind, was invaluable. Thank you to the rest of the McIndoe group, past and present, who made the day to day more fun and enjoyable. Peter, Charlie, Sofia, Nick, Tanner, Jack, Nadini, Bobby, Bragi; we shared a lot of experiences and discussions that have shaped me as a researcher in ways I can't fully quantify. To past group members who lay the foundations for my work; Krista, Eric, Lars, Michelle, your papers were a great source of inspiration and direction. Special extra mention to Lars for PythoMS!

I also need to acknowledge the broader chemistry community and friends at UVic. I won't name you all, but if we have chatted over seminar coffee, or shared a beer at Grad House, know that I appreciate you. A special thank you also to Erin and Hiromi, without whom I would have been completely lost in the administrative maze of graduate school. Thanks to Ori and Tyler for instrument assistance, knowledge-sharing, and the occasional few grams of standards to calibrate our instruments. You saved me countless troubleshooting headaches, and probably also saved Scott a lot of money!

This work would have been a whole lot more challenging without the financial support from numerous private donors through the Faculty of Graduate Studies. I am especially grateful to NSERC for the CGS-D. I was incredibly privileged to be in this situation, which is not lost

on me. But it should not require a national scholarship to be able to support oneself through graduate school comfortably. I sincerely hope that the many initiatives and advocacy efforts around graduate stipends continues so that all students can be lifted up to work productively without financial strain.

One of the other great privileges of my PhD was mentoring undergraduates in our lab. Nimrod, Jaspreet, Maryam, Lena, Sam, Makenna, Tiago, Gwyneth, Antonia, Harrison; thank you for your hard work, dedication and curiosity. It was my joy to help you through your studies and research journeys, and hopefully inspire you to push on with Chemistry. Your questions and inquisitive natures often challenged my own knowledge and pushed me to grow both as a scientist and a communicator. More importantly, you all helped me get through some difficult moments, and for that I am deeply grateful.

A special thank you to my friends, near and far. Toby, I wouldn't be here if we hadn't been out on the slopes, and you gave me the push I needed to just get on with it and get back to school. Your friendship through the years, shared music, SauceBoss playlists, and videochats have meant the world to me. Noel, for always being a phone call away, and always seeing the best in me, even when I don't. Millie, you have been there at every key moment over the past decade. Thank you for your friendship, encouragement, and reminders that I am capable of this have kept me going. And to others who have been there at different points; Erlend, Chris, Victoria, Henry, Jake, Ryan, Mahanna, Jen, Peter, Gabe, Kavindra, Evangelia, Matt, Daniel, Jayme, Braden. I am eternally grateful for your presence, hospitality, guidance, for coffees dates, dinners, hikes, walks, and endless WhatApp chats. You've each played a role in keeping me grounded.

I also want to acknowledge the third spaces that provided some much-needed community and escape. To my Kickin' Chickens soccer crew, and FriendsWhoPunchThings at Forge and Victoria Martial Arts, sometimes all it takes is kicking a ball and punching a bag to reset your body and spirit. I'm grateful for every moment. And to the cafes with delicious coffees and free Wi-Fi that got me through writing this thing; Little June, Hide and Seek, Discovery, Habit, St. Ceclia, thank you.

To my family, mom, dad, and Astrid, your support has meant a lot to me. Thank you for championing me, even from across the world. To Azamaseya, whose sacrifices I will never fully understand, and whose grace and determination paved the way for me to be here.

Finally, endless love and gratitude to Jenn. None of this would have been possible without you. Your patience, love, generosity, and belief in me have carried me through the most difficult moments of this journey. Thank you for being my constant, my greatest supporter, my champion, my home, my heart. And Nora, you have brought so much love and light into our lives. I can't wait to tell you all about this!

The "get off the stage" music would probably have started playing about 3 paragraphs ago, so I'll stop here and say: to everyone who has been a part of this journey, thank you.

Now to sleep.

Ian C. Chagunda

Victoria BC, February 2025

Dedication

for Jenn and Nora,

forever and always.

Chapter 1 – Introduction

This chapter provides a general introduction to the essential concepts on mass spectrometry and palladium-catalyzed cross-coupling reactions relevant for this dissertation. Portions of this chapter (Section 1.1.5.3) have been reproduced from "Gilian T. Thomas, Sofia Donnecke, Ian C. Chagunda, and J. Scott McIndoe, *Chemistry—Methods*, **2022**, 2, e202100068" and adapted with permission from Wiley-VCH GmbH. This work was conceptualized by GTT and JSM. ICC contributed investigations into filtration techniques relevant to PSI-ESI-MS and writing discussions pertaining to that section. As Chapter 1 is not a comprehensive review of the fields, each subsequent chapter begins with an introduction specific to the research discussed therein.

1.1 Mass Spectrometry

Mass spectrometry (MS) is an indispensable analytical tool in chemistry and the natural sciences, widely used for applications such as environmental analysis, molecule discovery, structure elucidation, sequencing of biomolecules, and reaction monitoring.[1] At its core, MS measures the molecular masses of ions and analysing them with a mass analyzer.[2] It operates on the principle of separating ions based on their mass-to-charge (*m/z*) ratio and detecting them in either positive or negative ion modes to provide structural and quantitative information.[1]

This section of this chapter introduces the fundamental principles of MS. It begins with a brief history of the development of MS, followed by an overview of the key ionization sources and mass analyzers used in this work. The section also explores the use of off-line and on-line MS techniques for studying catalytic reactions, with a specific emphasis on its role in mechanistic studies of organometallic catalytic reactions. Special focus will be placed on the Pressurized Sample Infusion (PSI) technique for real-time reaction monitoring, which serves as a foundational method for the experiments described in subsequent

chapters. Through these discussions, the chapter aims to establish the central role of MS as both an analytical and mechanistic tool in modern catalysis research.

1.1.1 A Brief History

The origins of MS can be traced back to Sir J. J. Thomson, who developed the parabola mass spectrograph through his work on negatively and positively charged cathode rays in the late 19th century.[3,4] This early instrument, credited as the first to separate ions by their *m/z*, is considered the precursor to modern mass spectrometry. In the following decades, pioneering mass spectrometrists working with "home-built" instruments drove the field forward, with physicists such as Dempster,[5] Aston,[6] Bainbridge and Jordan,[7] and Nier,[8] making significant contributions to its development during the early 20th century.

In the 1940s, MS gained broader recognition, particularly in petroleum refining, with the first commercial mass spectrometer introduced in 1943.[9] The 1950s and 1960s saw further advancements, including time-of-flight (TOF),[10] ion cyclotron resonance (ICR),[11] quadrupole, and ion trap mass analyzers,[12] and the introduction of the gas chromatography (GC) MS systems,[13,14] all of which contributed to the analysis of complex mixtures. By the 1960s, MS had became a standard tool in organic chemistry, though its use in the biosciences was limited by challenges associated with ionizing complex non-volatile biological compounds.[1,2]

The 1980s marked a significant expansion in the applications of MS with the development of softer ionization techniques, including fast atom bombardment (FAB),[15] electrospray ionization (ESI),[16,17] and matrix-assisted laser desorption/ionization (MALDI),[18,19] and the coupling of High Performance Liquid Chromatography (HPLC) systems.[20] These breakthroughs extended the mass range beyond 100 kDa, revolutionizing research in biology and life sciences. The impact of these advancements was further recognized in 2002 when John Fenn and Koichi Tanaka won the Nobel Prize in Chemistry for their contributions to ESI and MALDI.[2]

With these many developments, the core components of a mass spectrometer have remained largely unchanged. A typical mass spectrometer consists of three key elements; an ionization source, a mass analyzer, and a detector, all operating under high vacuum conditions, in addition to a control and data management system found on modern instruments (Figure 1.1).[1] The sample is first introduced to the ionization source through an inlet for ionization into the gas-phase, with the resulting ions then accelerated through electric or magnetic fields to the mass analyzer, where they are separated based on their *m/z* ratios. The ions are then detected, and their abundance converted into readable signals.

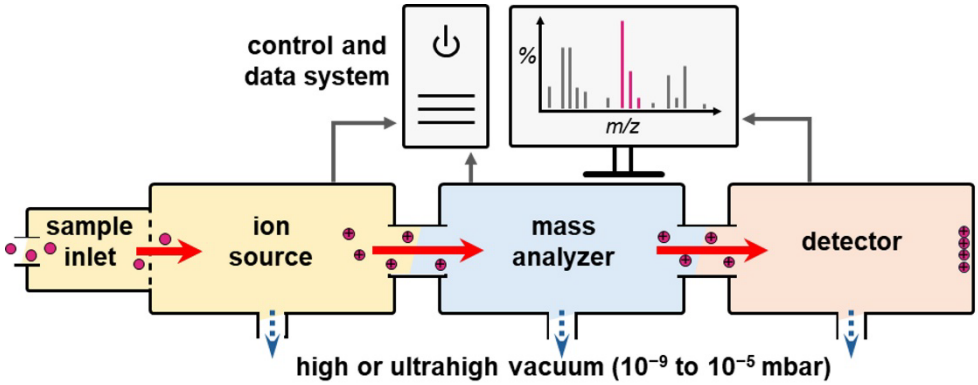

Figure 1.1: General layout of mass spectrometers, with key components of an ionization source, a mass analyzer, and a detector.

Various ionization methods and mass analyzers are used depending on the sample type and specific research objectives. These methods can include thermal ionization, ionization by electric fields, or ionization through interactions with energetic electrons, ions, or photons.[1] Similarly, mass analyzers come in various types: quadrupole, ion trap, orbitrap, Fourier transform (FT) ICR, and TOF analyzers. Each method has distinct design and performance characteristics, offering different advantages and limitations.[21] While a comprehensive discussion of all ionization techniques and mass analyzers and their underlying mechanisms is beyond the scope of this chapter, a more detailed overview of the electrospray ionization, and quadrupole and TOF mass analyzers, which are primarily used in these studies, will be provided below.

1.1.2 Electrospray Ionization

Electrospray ionization (ESI) is a prominent ionization technique for transferring ions from the liquid phase into the gas phase. ESI belongs to the group of atmospheric ionization (API) methods, where ionization starts at atmospheric pressure and incrementally proceeds into the high vacuum of the mass analyzer.[22] The technique is considered "soft" as it generates ions without causing significant fragmentation, making it particularly useful for analyzing non-volatile intact biomolecules, and weakly-coordinating organometallic species.[1,23,24] The conceptual development of ESI was introduced by the Dole group,[25] with the first successful ESI-MS systems then developed by Yamashita and Fenn in the mid-1980s.[16,17] By incorporating a quadrupole mass analyzer to an improved ESI source, Yamashita and Fenn's design allowed the detection of analytes with molecular weights of 100–2000 Da.

ESI involves transferring a dilute solution containing the analyte, typically at low concentrations (10^{-9} to 10^{-4} M depending on analyte type), through the source inlet into a spray capillary. A high voltage (3–5 kV relative to a surrounding cylindrical electrode) is applied to the capillary, which, when the instrument is operating in positive ion mode, serves as the anode in a specialized type of electrolytic cell. Electrochemical oxidation reactions generate an excess of cations at the capillary surface, influenced by the experimental conditions.[1] For instance, metallic capillaries introduce metal ions into solution through anodic erosion (Eq. 1), while solvent oxidation for example in methanol (Eq. 2), or discharge of anions (Eq. 3), can further enrich the surface charge.[26,27] Each case is illustrated with a net charge of 2+ for convenience, with analogous reduction reactions generating excess anions in negative ion mode.

$$M \rightarrow M^{2+} + 2e^- \qquad \text{Eq. 1}$$

$$CH_3OH \rightarrow HCHO + 2H^+ + 2e^- \qquad \text{Eq. 2}$$

$$2A^+ + 2B^- \rightarrow 2A^+ + B_2 + 2e^- \qquad \text{Eq. 3}$$

Charge enrichment destabilizes the solvent meniscus, forming a Taylor cone at the capillary tip and leading to the emission of a jet of charged droplets.[28,29] The droplets are

then carried through a heated gas stream, where solvent evaporation and Coulombic repulsion drive successive disintegration into smaller droplets, until highly charged, tiny droplets capable of producing gas-phase ions remain as illustrated in Figure 1.2. This transition of ions from the solution phase to the gas phase involves mechanisms such as the ion evaporation model (IEM), where ions are ejected directly from the droplet surface due to electrostatic forces, and the charged residue model (CRM), where complete solvent evaporation leaves behind desolvated ions.[26,30] For macromolecules such as proteins, the chain ejection model (CEM), in which largely unfolded chains are transferred into the gas phase due to electrostatic forces that destabilize the protein's native folded structure, can be dominant.[31]

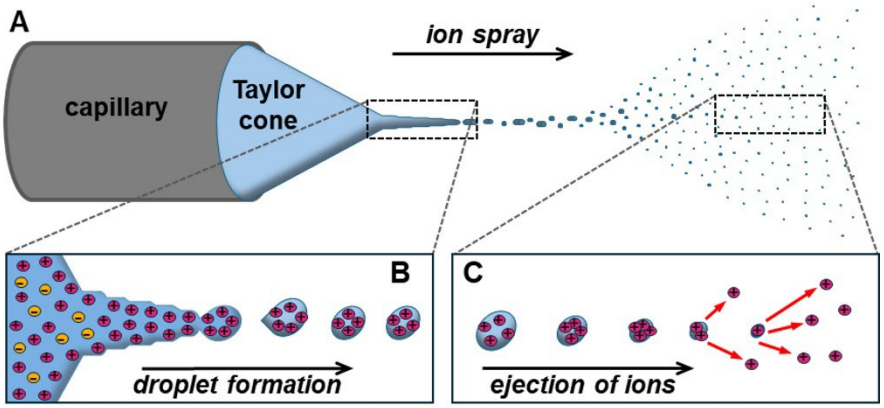

Figure 1.2: A) Taylor cone and droplet disintegration in ESI leading to formation of gas-phase ions for MS analysis. B) Detail of ion excess in the Taylor cone and transition of spray jet to droplets. C) Droplet shrinking and ejection of ions by ion evaporation mechanism (IEM). Figure shows positive mode mechanism for simplicity.

Following desolvation, gas-phase ions are then directed into the mass analyzer through differentially pumped interfaces. Modern ESI sources, such as the Z-spray interface developed by Waters Corporation, refine this process by introducing the spray at a 90° deflection angle, selectively diverting smaller, highly charged droplets towards the mass analyzer, reducing contamination and clogging issues.[38] The choice of solvent also plays a critical role in ensuring optimal ESI operation, as the solvent must be sufficiently polar to facilitate the electrochemical reactions that generate excess charge.[35,36] While non-polar solvents are generally incompatible due to low conductivity, their performance can be

improved with the addition of a ionic liquid, through care must be taken not to introduce unwanted reactivity with the analytes.[36]

1.1.3 Triple Quadrupole Mass Analyzer

Triple quadrupole mass spectrometers are among the most widely used instruments for ESI-MS, valued for their high sensitivity and robust capabilities in structure elucidation and mixture analysis. The instruments consists of three quadrupoles arranged sequentially: Q1, q2, and Q3.[37] Each quadrupole features four cylindrical or hyperbolic rods extending along the z-axis, as illustrated in Figure 1.3. Opposite rod pairs are electrically connected and subjected to a combination of radiofrequency (RF) and direct current (DC) potentials, which generate electric fields to control ion trajectories based on their *m/z*.[1,38] The resulting electric field stabilizes ions of specific *m/z* range, guiding them along the z-axis while inducing oscillating motion in the xy-plane.[39] By carefully tuning the RF and DC voltages, ions with stable trajectories are passed through the quadrupole to the detector, while ions outside the selected *m/z* range become destabilized, resulting in collisions with the rods and neutralization.

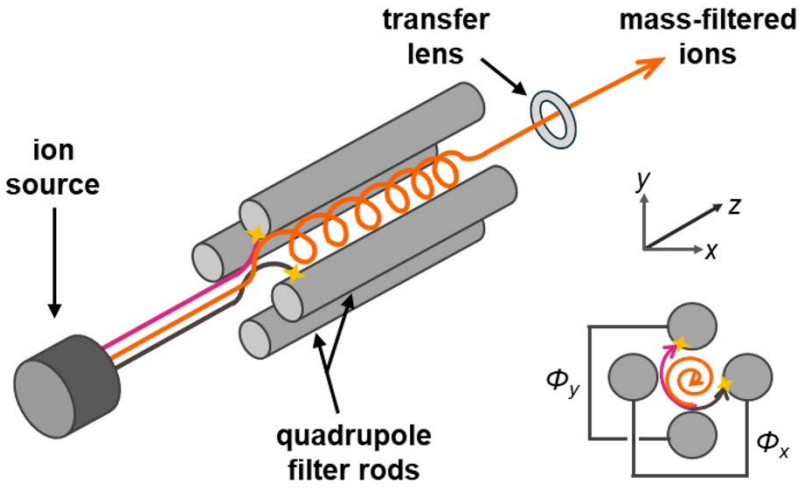

Figure 1.3: Schematic of a simple quadrupole mass analyzer, showing stable (orange line) and unstable (pink, grey lines) ion trajectories along z-axis. Inset shows potential on the electrode surfaces and ion trajectories.

Assuming a perfect quadrupole electric field, the stability of an ion's motion, determined by its *m/z*, is described mathematically by the Mathieu stability equations (Eq. 4 and Eq. 5).[39] These equations describe the ion's behavior under the combined influence of a static DC voltage (U) and oscillating RF voltage (V), with the total potential (Φ) and angular frequency (ω) in a set flight time (t) influencing the electric field dynamics.

$$\Phi_x = U + V_0\cos(\omega t) \qquad \text{Eq. 4}$$

$$\Phi_y = -\big(U + V_0\cos(\omega t)\big) \qquad \text{Eq. 5}$$

In the triple quadrupole arrangement, the second quadrupole (q2) functions as a collision cell that only experiences RF potentials. Here, ions can simply pass through with q2 operating as an ion guide. Alternatively, q2 can also be operated as a collision cell, where ions can undergo collision-induced dissociation (CID) through collisions with neutral collision gas molecules, typically argon. This dissociation process is integral to tandem mass spectrometry (MS/MS) experiments where detailed structural information may be discerned from the fragmentation patterns of product ions. The RF-only quadrupole field is used to refocus fragment ions, maintaining a reasonable instrument sensitivity. Though termed “triple quadrupole”, some modern instruments feature a hexapole or octapole, with six or eight rods instead of four, providing improved mass filtration efficacy.[21]

The Waters Tandem Quadrupole Detector (TQD), one of the primary instruments used in this dissertation, showcases the advanced functionality of modern triple quadrupole systems. It supports multiple MS and MS/MS operating modes, as illustrated in Figure 1.4. In MS full scan mode, the first quadrupole (Q1(acts as a mass filter, scanning across an *m/z* range while q2 and Q3 pass all ions through. This mode offers high sensitivity akin to single-quadrupole operation. Selected ion recording (SIR) fixes Q1 at a specific *m/z* ratio, enabling quantitation when fragment ions are unavailable or unsuitable for more targeted analysis.

In the product ion mode, a precursor ion is selected in Q1 at a fixed *m/z* ratio, fragmented in q2, and the resulting product ions are scanned in Q3. Conversely, precursor

ion mode fixes Q3 at a specific product ion *m/z* and scans Q1 for all precursors yielding the selected fragment. Neutral loss mode identifies precursors that lose a specific neutral fragment from unspecified precursors by scanning Q1 and Q3 simultaneously. This mode is particularly ideal for screening compounds that share common functional groups and exhibit characteristic fragmentation pathways. Finally, multiple reaction monitoring (MRM) is a highly selective mode that monitors multiple precursor-product ion pairs by fixing Q1 and Q3 at specified ion *m/z* values, while fragmenting ions in q2. MRM minimizes chemical noise and enhances sensitivity, making it a preferred methods for precise compound isolation. The TQD's operational flexibility, with its diverse scanning modes, makes it an essential tool for both qualitative and quantitative mass analysis.

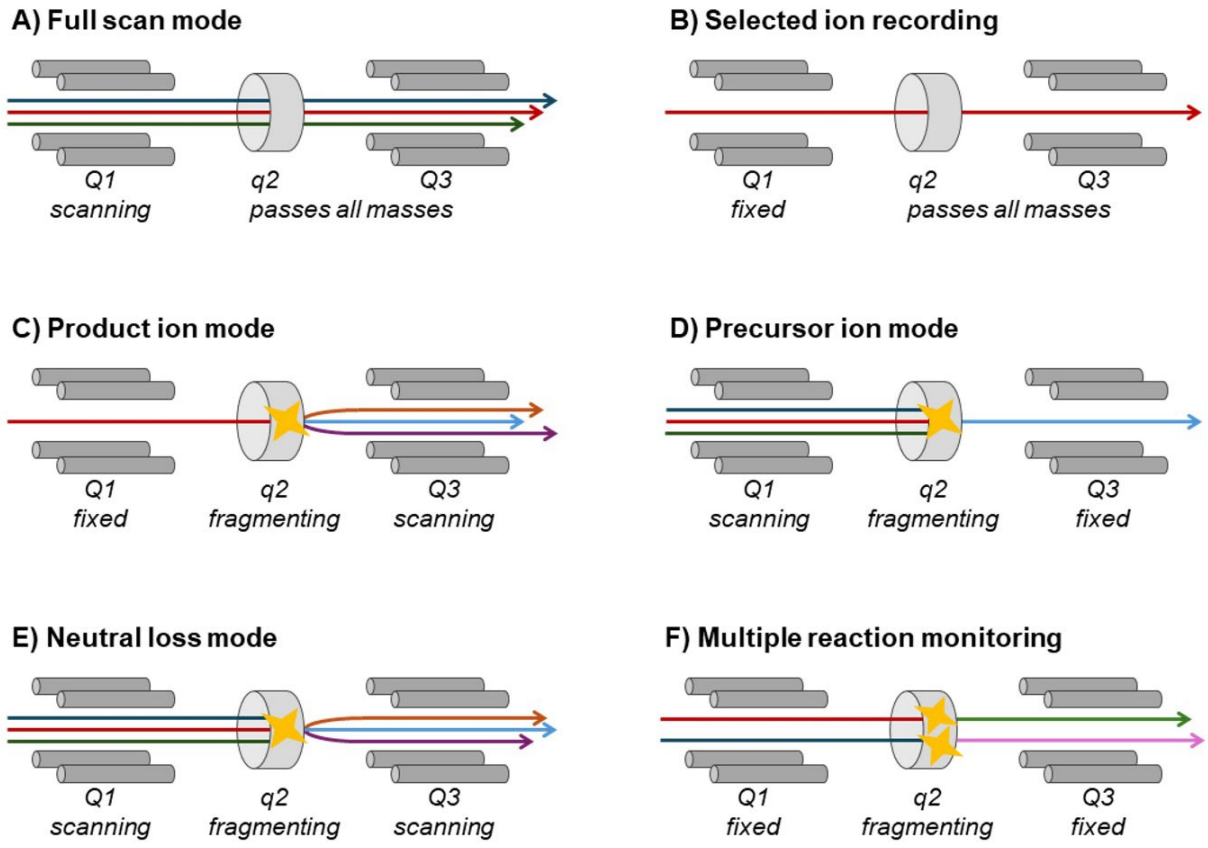

Figure 1.4: Scan modes on the TQD mass spectrometer: (A) full scan mode, (B) selected ion recording C) product ion scan, (D) precursor ion recording, (E) neutral loss mode, and (F) multiple reaction monitoring.

1.1.4 Quadrupole Time-of-Flight Mass Analyzer

Time-of-flight (TOF) mass analyzers are widely used in ESI-MS due to their simplicity, sensitivity, and rapid acquisition rates. Initially conceptualized by Wolff and Stephens in 1946, the TOF analyzer operates on the principle of separating ions based on their *m/z* ratios by measuring their flight times through a drift tube.[10,40,41] A key assumption is that ions with different mass-to-charge ratios, starting their journey simultaneously, will exhibit different velocities when accelerated by the same electric potential, leading to temporal separation at the detector, as shown in Figure 1.5.[1]

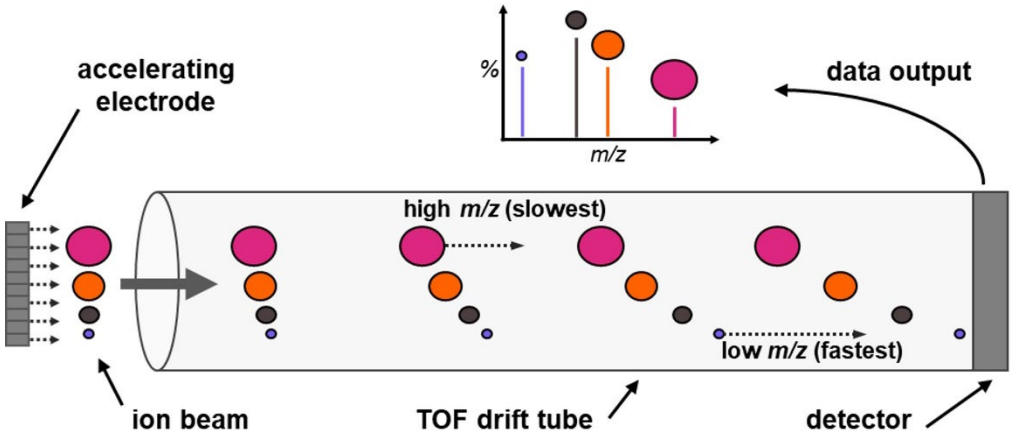

Figure 1.5: An illustration of the TOF mass analyzer.

The working principle of a TOF analyzer relies on the conversion of potential energy from an electric field into kinetic energy during ion acceleration. When an ion of mass m_i and charge q (where q is equal to an integer number z of elementary charges e) is accelerated through an electric field of voltage U, the potential energy E_{el} imparted to the ion is converted into kinetic energy E_{kin} with ion velocity v by Eq. 6.[1] Solving for v, the ion's velocity found is inversely proportional to the square root of its mass by Eq. 7.

$$E_{el} = qU = ezU = \frac{1}{2}m_i v^2 = E_{kin} \qquad \text{Eq. 6}$$

$$v = \sqrt{\frac{2ezU}{m_i}} \qquad \text{Eq. 7}$$

$$t = \frac{s}{\sqrt{2eU}}\sqrt{\frac{m_i}{z}} \qquad \text{Eq. 8}$$

Given the mathematical relationship between velocity, distance, and time, $v=s/t$, the time t taken for the ion to traverse a drift tube of length s in a field-free region is determined upon substitution of v by Eq. 7 and rearranging, giving an experimental value of t that is proportional to the square root of m_i/z by Eq. 8. Thus, small differences in flight time of ions of different mass m_i operating under otherwise identical field acceleration will be registered at the detector, with the known instrument parameters s and U used to calculate the ion's m/z. To ensure high accuracy in TOF measurements, the drift tube is maintained under high vacuum to eliminate collisions with background gas molecules, which could disrupt ion velocities.[40] Orthogonal acceleration, in which ions are introduced into the drift tube at right angles to the ion beam, also enhances resolution by minimizing initial spatial and energy dispersion.

The TOF analyzer is often sequentially combined with a quadrupole mass analyzer to form a hybrid Q-TOF instrument, as in the Waters Synapt G2-S*i* used in this dissertaion.[34] This hybrid setup combines the adaptability of a quadrupole with the high resolution, sensitivity, and mass accuracy of TOF analysis. A typical Q-TOF system consists of a series of quadrupoles, Q1 and q2, with the replacement of Q3 in a triple quadrupole by a TOF mass analyzer. This setup gives the benefits of high sensitivity, mass resolution and mass accuracy in both MS and MS/MS modes.[42]

In single MS mode, Q1 operates in RF-only mode, serving as a transmission element. The TOF analyzer records spectra by detecting all ions in parallel, avoiding the need for scanning. For MS/MS experiments, Q1 functions as a mass filter, isolating a specific precursor ion. The selected ion is then accelerated into the collision cell q2 where it undergoes CID. The resulting fragment ions, along with any remaining parent ions are then passed through ion guides for ion trapping, accumulation, release, and transfer to the TOF analyzer.[34] In the Synapt G2-S*i*, the ion guide can additionally function as an ion mobility

separator, where ions of nominal m/z can be separated based on their collisional cross section.[43]

Resolution and mass accuracy are critical parameters in evaluating the performance of mass analyzers like the triple quadrupole and Q-TOF systems used in this work. Mass accuracy measures the difference of the calculated, m_{calc}, and experimental, m_{exp}, m/z as expressed by Eq. 9. Resolution, typically defined as the ability to distinguish two peaks of different m/z, is in this work expressed using the full width at half maximum (FWHM) of a peak, defined by Eq. 10, where m is the m/z value of a single peak, and $\Delta m_{50\%}$ is the width of the peak at 50% of the peak's height.[1]

$$Mass\ accuracy\ (ppm) = \frac{m_{calc} - m_{exp}}{m_{exp}} \times 10^6 \qquad \text{Eq. 9}$$

$$Resolution\ (FWHM) = \frac{m}{\Delta m_{50\%}} \qquad \text{Eq. 10}$$

For example, the quadrupole instrument typically achieves a resolution of 2000 FWHM,[44] while TOF analyzers can achieve significantly higher resolution, up to 20,000–100,000 FWHM depending on the system.[34] Mass accuracy, which refers to the difference between the measured m/z and the true m/z of an ion, is particularly critical in Q-TOF systems. These instruments provide exceptional mass accuracy, within 1–5 ppm, compared to 100 ppm in the triple quadrupole system, allowing for highly precise molecular formula assignments. Together, these parameters ensure the reliable identification and characterization of analytes in complex reaction mixtures, as described in subsequent chapters.

1.1.5 Mass Spectrometric Reaction Monitoring of Catalytic Reactions

"I feel sure that there are many problems in Chemistry which could be solved with far greater ease by this than by any other method. The method is surprisingly sensitive—more so even than that of spectrum analysis—requires an infinitesimal amount of material and does not require this to be specially purified."[45]

– Sir J.J. Thomson, 1913.

Mass spectrometry has a storied history in chemistry, with its potential first articulated over a century ago by Sir J.J. Thomson. Thomson's foresight was remarkable, yet the applications of MS today far exceed what could have been envisioned in his era. While initially focused on determining the *m/z* ratio of organic compounds, modern MS has become an indispensable tool across numerous domains. It is now used to determine molecular structures, determine thermochemical and physical properties such as ionization energy, reaction enthalpies, proton and ion affinities, and gas-phase acidities, monitor and investigate reaction dynamics and kinetics, to name a few use-cases.[2]

This dissertation specifically focuses on the use of MS in monitoring catalytic reactions. Reaction monitoring can be broadly categorized based on the timing, location, and method of data acquisition. The two primary categorization discussed here are on-line monitoring, which involves continuous sampling directly from the reaction system to a connected external device for immediate analysis, and off-line monitoring, which requires discrete sample collection and external analysis, often introducing delays.[47] Each approach has trade-offs in terms of speed, accuracy, and practicality, depending on the reaction's complexity and requirements. For the work described in this dissertation, continuous on-line reaction monitoring is employed using ESI-MS and the Pressurized Sample Infusion methodology to be discussed in Section 1.1.5.3. Throughout this dissertation, the term real-time monitoring will refer specifically to continuous on-line methods that provide timely data, enabling immediate user feedback and reaction control.

1.1.5.1 Off-line Reaction Monitoring

Mass spectrometry has demonstrated success in monitoring reactions both off-line and on-line. In off-line reaction monitoring the solution composition and progression of a reaction is typically determined by drawing aliquots of the reaction mixture at specific time intervals. These aliquots are then quenched and/or diluted to stop the reaction at a particular point along the progression of the reaction, before being injected into the mass spectrometer for analysis.[46] HPLC is one of the most frequently used complementary technique in conjunction with MS, as it separates reaction components through a column, enables small-volume injections, and provides simpler or better-quantified spectra, enhancing characterization.[47]

Early examples of off-line reaction monitoring include work by Canary, who investigated Suzuki-Miyaura (SM) cross-coupling intermediates.[48] The groundbreaking study introduced the concept of using substrates specifically amenable to the ESI-MS process. In this case, a brominated pyridine substrate was chosen, which had a peripheral basic site that was uninvolved in the reaction's reactivity but was easily protonated to produce $[M+H]^+$ ions. This approach illuminated not only the substrate but also the intermediates, resting states, and decomposition products associated with it, capturing snapshots of the reaction's speciation as it progressed. Follow-up examinations by Frech and coworkers further examined the reaction kinetics using ESI-MS.[49] Similarly, Moreno-Mañas and coworkers performed off-line ESI-MS mechanistic investigations of the palladium-catalyzed oxidative self-coupling of arylboronic acids,[50] with Hinderling and Chen using off-line monitoring to develop a mass spectrometric assay of palladium-based polymerization catalysts for combinational screening.[51]

These examples demonstrated ESI-MS as a promising tool for catalytic reaction analysis. Its utility was particularly pronounced in cases where the reaction intermediates are stable enough to be observed after quenching and dilution, providing a detailed view of the reaction's progression. However, although real-time off-line monitoring is possible for slow reactions,[46] off-line reaction monitoring can encounter limitations in situations where there are short-lived intermediates or when the reaction kinetics are very fast.[52]

1.1.5.2 On-line Reaction Monitoring

On-line ESI-MS presents an alternative to off-line monitoring by directly coupling the reaction vessel to the ESI inlet. This approach enables observation of kinetic behaviours and molecular speciation, and enables the experimenter to react and make decisions on how to proceed in real-time.[46] This method can provide characterization of reactive intermediates with lifetimes down to the millisecond time regime, with the added benefit of capturing fleeting intermediates and track dynamic changes in substrates, intermediates, products, and even impurities without extensive sample pretreatment.[53]

Several methodologies have been developed to facilitate on-line monitoring of catalytic reactions.[47,53] Syringe pumps are often used due to their compatibility with many solvents and their ability to deliver samples at a controlled flow rate. However, these systems have limitations, including minimal control over reaction conditions such as temperature and mixing, and sequential addition of reaction components is challenging.[54] Microreactors connected to mass spectrometers provide another option, with rapid mixing of reactants prior to analysis enabling the collection of multiple data points.[55,56] For instance, Metzger and coworkers designed an on-line microreactor with separate lines for reactant solutions, that proved effective for monitoring reactions with short incubation times.[57,58] Eberlin and coworkers used a similar system to investigate the mechanisms of the Heck reaction with aryldiazonium salts, uncovering previously unknown intermediates in the oxidative addition steps.[59] Zhu and coworkers employed on-line MS to study the one-pot palladium-catalyzed cleavage of thiocarbonyl bonds, revealing a mechanism involving hydrolytic desulfurization and a trinuclear palladium cluster intermediate.[60]

The need for air- and moisture-free sample introduction is crucial for organometallic catalytic reactions, where sensitivity to atmospheric conditions can affect reaction outcomes. To address this need, techniques such as coupling nitrogen atmospheres to the mass spectrometer source via glove bags, sealed glass probes, or modified gloveboxes with feedthrough ports have been developed.[61–66] While effective, these approaches are often costly, complex, or incompatible with solution-phase samples. To address these challenges, the Pressurized Sample Infusion (PSI) method was developed

as a simple, robust, and cost-effective solution.[67] PSI has since become a cornerstone for real-time reaction monitoring in catalytic systems used in the McIndoe group.

1.1.5.3 Pressurized Sample Infusion (PSI)

First reported in 2010, PSI is a sample introduction method designed for on-line reaction monitoring of reaction solutions.[67] This technique involves a positive pressure cannula transfer of a reacting solution directly into an ESI mass spectrometer, eliminating the need for mechanical pumping, and allows for raw reaction mixtures to be infused without further treatment.[68] Avoiding a pumping system addresses two main challenges: the internal volume of even the smallest pumps can result in significant delays in transfer of the reaction solution to the mass spectrometer for this application, and the diverse materials within pumps can lack resistance to the wide variety of solvents, catalysts, and substrates used in reactions.

A Schlenk flask is placed close to the ESI inlet and is equipped with a rubber septum over the ground glass joint, and a rubber hose on the arm. A stir bar may be placed in the flask with reactants to ensure homogenous mixing. The rubber hose connects to a regulated cylinder of chosen gas, set at slightly above ambient pressure (2-5 psi; 0.14-0.34 bar). If reagents are not added to the flask inside a glovebox, they can be prepared on a Schlenk line and then safely transferred via syringe to the PSI flask for sample introduction.[69] The rubber septum is punctured with polyether ether ketone (PEEK) tubing that extends into the sealed reaction solution, with the other end of the tubing attached to the ESI inlet via a PEEK fitting. For heated reactions, a two-neck flask with a condenser or a specialized PSI flask with a built-in condenser may be used, as shown in Figure 1.6.[70] The PSI approach works at temperatures up to the boiling point of the solvent, as higher temperatures can over-pressurize the flask. While PSI can operate below ambient temperatures, practical limitations arise from the tubing and ESI source being at room and elevated temperatures, respectively. As such, temperatures below 0°C are not recommended unless the reaction is relatively slow.

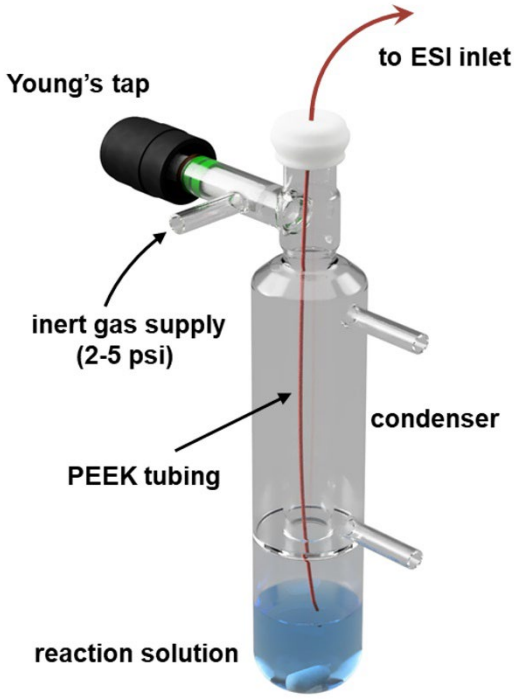

Figure 1.6: Custom Schlenk flask for PSI setup.

As in a cannula transfer, solutions may be filtered by securing filter material to the end of the tubing in the reaction flask. Blockage can occur relatively easily due to the narrow internal diameter of tubing; however, a narrow diameter is necessary to minimize the time between reaction sampling and measurement. To prevent blockages, the end of the capillary can be protected with (a suitably cut) filter paper, cotton wool, glass wool, or any other filter material, and secured by use of polytetrafluoroethylene (PTFE) sealant tape. An example is illustrated in Figure 1.7, where standard filter papers (Watman, 55Ø) are used with standard density PTFE tape to secure the filter paper to PEEK tubing. To avoid compromising flow rate or retention time, it is important to use the minimal amount of filter material necessary.

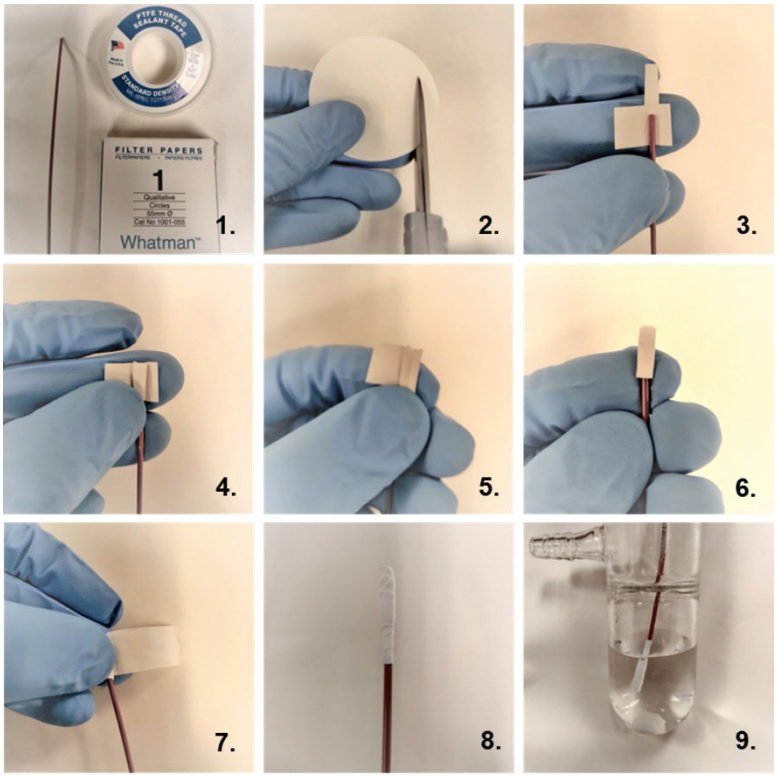

Figure 1.7: Steps 1-9 for preparing PSI PEEK tubing filter using Watman 55Ø filter papers and PTFE tape.

The effects of filtration on the PSI flow rate were tested in the McIndoe group, with the results illustrated in Figure 1.8. A PSI flask was set up as described in Figure 1.6, however the end of the tubing that would be attached to the ESI source inlet was instead suspended above a flask that was placed on an analytical balance. The mass of solution flowing from the PEEK tubing was measured as a function of time, providing the PSI flow rate. A control trial with a homogeneous solution of tetrahydofuran (THF) and no filtration (green) resulted in a consistent flow rate. In contrast, for a fine suspension (purple) (K_3PO_4 in THF), the flow rate was seen to drastically drop after a minute of monitoring, indicating presence of a blockage. By attaching the filter described in Figure 1.7, clogging was effectively prevented.

Reagents can be prepared off-line, and the flask degassed as needed for air-sensitive reactions. A reaction is typically initiated by adding the catalyst via an air-tight syringe. When a small overpressure is applied to the flask, continuous injection of the reaction solution into the source enables acquisition of time-resolved data.[71] This simple setup has

good reproducibility, and intensity fluctuations can be normalized against an internal standard, the total ion current (TIC), or the summed integration of the relevant species intensities.[68,72]

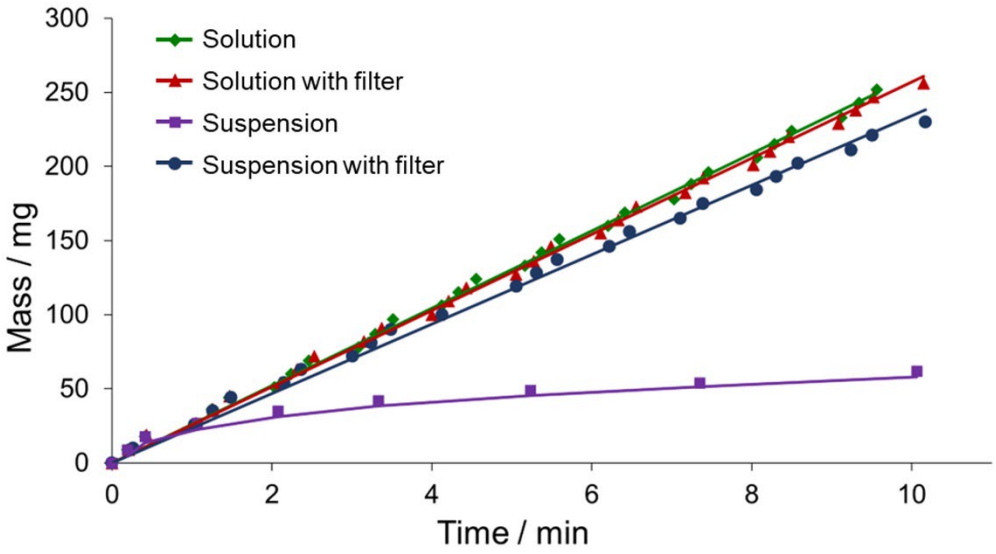

Figure 1.8: Mass of solution vs. time, illustrating the effect of attaching a filter to PEEK tubing in a heterogeneous reaction solution.

PSI-ESI-MS provides temporal intensity profiles for charged components of the reaction.[67,73] By monitoring the behavior of these species over time, the roles of individual species in the reaction mechanism can be assigned. The persistence or disappearance of specific species often reveals their function, whether as reactants, products, precatalyst, intermediates, resting states, decomposition products, or inactive impurities, as outlined in Figure 1.9. This temporal information, coupled with the ion isotope pattern assignment, lays the foundation for deciphering the mechanistic pathways of catalytic reactions.

The ability to acquire data on catalyst resting state and overall reaction progress simultaneously is a significant advantage of the technique and can be improved further via combination with orthogonal methods. As MS is so sensitive, it is especially effective for analyzing reaction components at low concentration, such as species related to the catalyst, while orthogonal methods monitor overall reaction progress by tracking the disappearance of reactant(s) and/or appearance of product(s). Flow infrared (IR) spectroscopy is an ideal

candidate for this type of analysis.[73] Additionally, this method becomes even more powerful when combined with computation, which can provide further structural information and bond dissociation energies.[74,75]

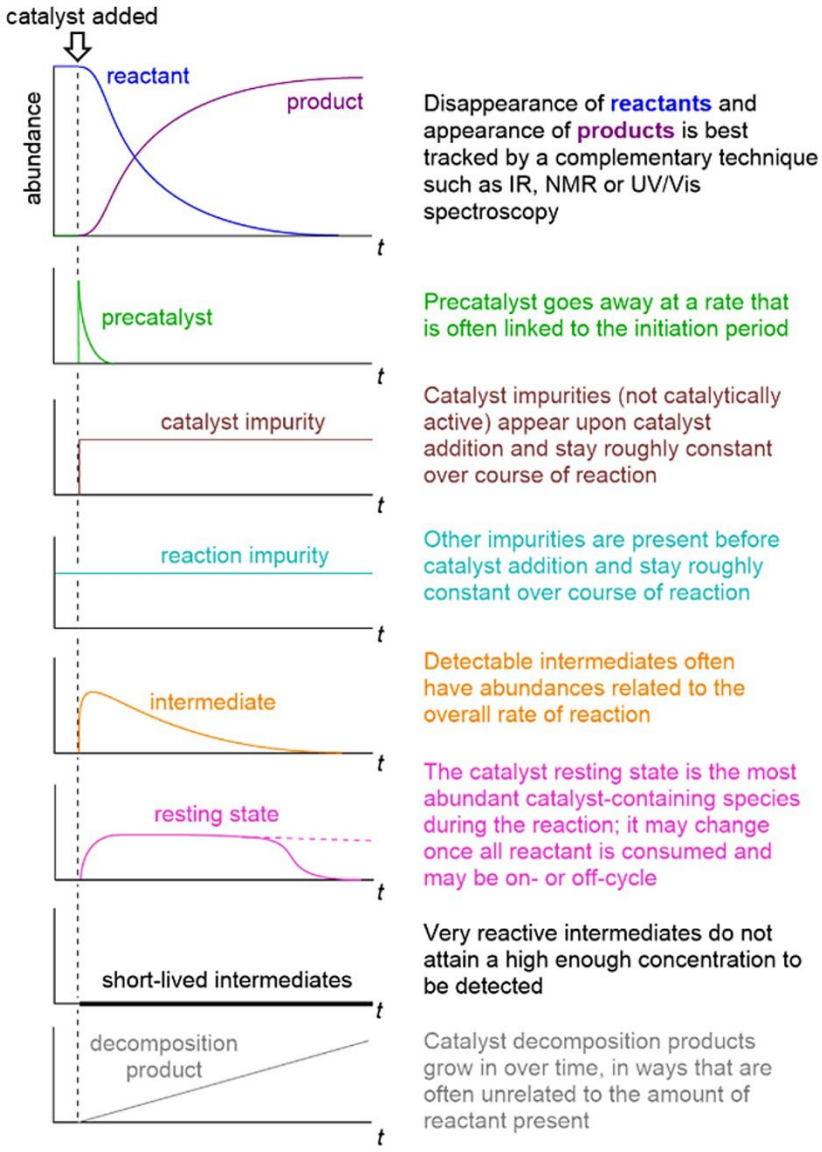

Figure 1.9: Idealized temporal profiles for different reaction components over the course of a reaction. These dynamics provide important clues as to which reaction role a given species is most likely playing. Reprinted with permission from Theron *et al.* at ref. 73. Copyright 2016 American Chemical Society.

In the McIndoe group, we routinely use PSI-ESI-MS to study various air-sensitive catalytic reactions and other transformations.[72,76–80] The PSI-ESI-MS methodology can be combined with any type of mass analyzer. When using a quadrupole time-of-flight (Q-TOF) spectrometer precision to four decimal places is obtained, yielding accurate mass identification of analytes.[81–84] Triple quadrupole instruments provide a lower level of resolution; however analyte identification can be confirmed via CID. The resulting fragments can be used to create multiple reaction monitoring (MRM) transitions effectively eliminating isobaric species, and analytes of interest can be observed in real-time when coupled with PSI.[77]

We demonstrated this method by monitoring the Suzuki Polycondensation (SPC) reaction where a charge-tagged phosphine ligand was used to track the catalytically relevant species (Figure 1.10).[85] Each component was added to the reaction flask sequentially to fully visualize each step in the catalytic cycle. The strategy of charge-tagging a ligand—adding a charged moiety such as a phosphonium group away from the ligand's reactive site—is one we have used extensively, with the reactivity of the charge-tagged ligands closely mirroring that of their neutral analogues.[86] This approach enables the observation of ordinarily neutral catalytic species that are otherwise unobservable by MS. While characterization of molar mass distribution (MMD) and composition is often the first step in the analysis of polymeric materials using both MALDI and ESI-MS,[87,88] this work demonstrated how ESI-MS enables detailed monitoring of the polymerization process.

Real-time MS reaction monitoring generates large data sets as mass spectra can be collected rapidly. Therefore one key component of data management that has been developed in the McIndoe group is an open-source set Python-based software.[89,90] These tools allow for simple data organisation, identifying and assigning of isotope patterns, and data visualisation, and was used extensively in this project. Additionally, the development of open-source software for semi-automated optimisation of instrument parameters has resulted in faster optimisation, improved data quality, more reliable and reproducible analysis.[91]

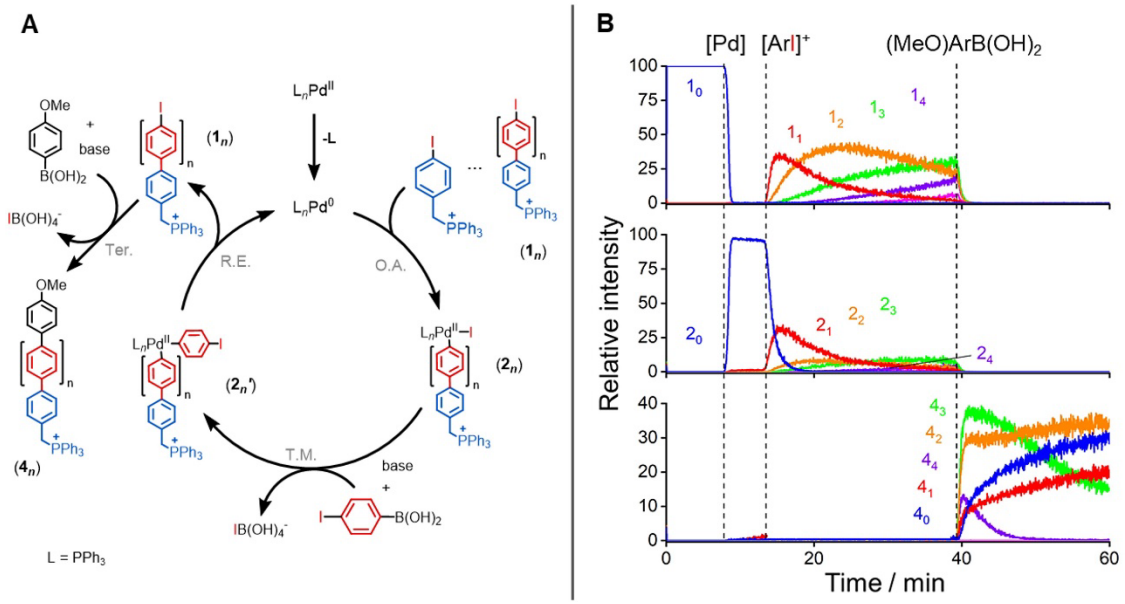

Figure 1.10: A) Proposed SPC catalytic cycle where a charge-tagged aryl iodide, and monomer *p*-iodophenylboronic acid were used for polymer propagation, with *p*-methoxyphenyl boronic used in the terminating step. B) The normalized PSI-ESI-MS MRM chronogram of the SPC showing the relative intensity of aryl iodide species label as 1_n, intermediates as 2_n, and capped oligomer products as 4_n (n = 0–4). Reproduced from Ting *et al.* at ref. 85 with permission from Royal Society of Chemistry.

Another tool developed within the McIndoe group is Continuous Addition Kinetic Elucidation (CAKE), which simplifies the kinetic analysis of catalytic reactions.[92] This technique involves continuously adding a catalyst into a reaction mixture while monitoring reaction progress over time. By analyzing the resulting concentration profiles, CAKE is used to determine kinetic parameters such as the order of reactants and catalysts, rate constants, and the extent of catalyst poisoning from a single experiment. This method was demonstrated in many catalytic systems, including analysis of a Suzuki–Miyaura reaction.

Increasingly, a growing number of other researchers have adopted PSI-ESI-MS. This includes work by Ananikov and coworkers, who applied PSI-ESI-MS to investigate R–NHC coupling for various Pd/NHC species with reactive aryl iodides.[93] They also explored asymmetric alkylation of indoles with α-diazoesters, revealing the interplay between highly reactive mononuclear Pd species, and polynuclear Pd species and nanoparticles which do not contribute to the enantioselective pathway.[94] Similarly, Koszinowski and coworkers leveraged PSI-ESI-MS to track the dynamic behavior of Pd/diene catalyzed cross-coupling

reactions, observing the evolution of mononuclear, dinuclear, and polynuclear palladium species alongside catalyst degradation over time.[95] Additionally, the study discovered that the transmetallation step in these reactions precedes the oxidative addition step in the catalytic cycle.

Beller and coworkers used PSI-ESI-MS to elucidate catalytic behavior of Mo_3S_4 hydride clusters during the reduction of functionalized nitroarenes,[96] while Mack and coworkers uncovered the degradation mechanism of their [$(dtbpy)_2Ru(CO_3)$] pre-catalyst (dtbpy = 4,4′-di-tert-butyl-2,2′-bipyridine), determining that ligand dissociation was the primary limiting turnover, rather than catalyst dimerization.[97] Work from the Newman group investigated the chemoselectivity of the Kumada-Corriu cross-coupling reaction, identifying optimal reagent addition rates to minimize side products and enhance yields.[98] These studies highlight the growing recognition of PSI-ESI-MS as a tool for elucidating mechanistic details, validating active species, and optimizing reaction conditions in diverse catalytic systems.

1.1.6 Challenges and Limitations of PSI-ESI-MS

While ESI-MS is undoubtably a powerful technique for reaction monitoring and mechanistic studies, several challenges must be considered when applying it to catalytic systems. One major limitation is the requirement for analytes to be readily ionizable. Neutral species, which are often critical components in catalytic reactions, exhibit poor ESI performance, limiting the technique's ability to provide a comprehensive picture of all species present in solution. To address this, charge-tagged analogues of analyte molecules are used to enhance the detectability of otherwise neutral species.[86] However, this approach often requires synthesizing analogues that may not be readily commercially available, and introduces challenges such as altered substrate solubility, and additional time and expense. Additionally, high salt concentrations and varying solvent compositions can significantly impact ionization efficiency, leading to signal suppression or complex spectral interferences.[99,100]

PSI-ESI-MS, as an on-line reaction monitoring tool, introduces additional challenges. One notable limitation is its incompatibility with high-concentration process-level reactions, as ESI-MS is inherently optimized for highly dilute systems.[26] This restricts its direct application in industrial-scale monitoring, necessitating additional instrumentation for sample dilution or alternative ionization strategies to bridge this gap. Additionally, inconsistent PSI flow rates, compounded with inherent challenges associated with flow-rate in ESI-MS, such as inefficient ionization, droplet formation issues, and signal instability,[26] further complicate accurate control and analysis.

Another limitation is the difficulty in monitoring catalytic reactions operating under biphasic or heterogeneous conditions. Since sampling from two immiscible phases simultaneously into a single inlet can be problematic, this technique is limited to homogeneous reaction systems. Addressing this challenge may require adapting methodologies from other biphasic analysis techniques, such as the dual-phase online HPLC and flow NMR spectroscopy approach by Hein and coworkers, which incorporates an additional inlet to enable concurrent analysis of both organic and aqueous phases.[101]

Lastly, mass spectrometric techniques, including PSI-ESI-MS, must be interpreted with an understanding of their inherent limitations in representing the true solution-state chemistry.[26] The ionization process can introduce artifacts, selectively enhance or suppress species that does not accurately reflect equilibrium concentrations.[99,100] Furthermore, analyte desolvation and ionization into the gas phase may not fully preserve the complex dynamic equilibria present in solution, particularly for systems involving weakly bound intermediates or transient species. Careful calibration and thorough experimental design are therefore essential to mitigate these limitations and ensure that the insights gained from PSI-ESI-MS accurately reflect the underlying reaction mechanisms.

Despite these challenges, PSI-ESI-MS remains a powerful tool for real-time analysis due to its speed, ability to handle complex mixtures, relative ease of set-up, and high sensitivity.[68] Developing a more robust sample delivery system capable of extending these advantages to higher concentration and complex solvent systems is an important next step in the evolution of this technique. As will be discussed in this dissertation, PSI-ESI-MS was instrumental in studying mechanisms insights of PdCC reactions.

1.2 Palladium-Catalyzed Cross-Coupling Reactions

Palladium-catalyzed cross-coupling (PdCC) is one of the most transformative tools in modern synthetic chemistry, a contribution so impactful that it was recognized with the 2010 Nobel Prize for Chemistry.[102] This class of reactions has revolutionized how chemists approach the construction of complex molecules, enabling late-stage, highly-selective functionalization of diverse substrates. PdCC methodologies have become indispensable for the synthesis of pharmaceuticals, agrochemicals, and advanced materials.

This section of the chapter provides a brief history of the development of PdCC reactions, tracking the pivotal discoveries and advancements that have shaped our understanding of these processes. As will be explored in later chapters of this dissertation, PdCC reactions serve as an ideal system for mechanistic studies using PSI-ESI-MS. Focus will be placed on catalyst behaviors and reaction pathways associated with the catalyst activation and oxidative addition steps, which are key to efficient operation of these reactions. These steps are also the primary focus of the literature examples discussed in this section, as they relate to the mechanistic work presented in later chapters. This section will also briefly survey select applications of PdCC in diverse fields, along with its current challenges and limitations that highlight opportunities for further advancement in PdCC chemistry.

1.2.1 A History of Incremental Progress

Following the post-World War II economic boom in Europe, the demand for inexpensive precursors for fine chemicals and plastic production spurred significant advances in metal-catalyzed synthesis.[102] A pivotal development was the discovery of the palladium-catalyzed Wacker Process, which enabled the synthesis of acetaldehyde from ethylene. Based on these early studies on palladium chemistry, Richard Heck in 1968 reported the stoichiometric reaction of organomercurial compounds with alkenes in the presence of lithium palladium chloride salts.[103] Due to the toxicity of organomercury compounds, Heck introduced alternate procedures, with the concurrent discoveries by Ei-ichi Mizokori demonstrating the first catalytic coupling of aryl halides and alkenes using palladium

salts.[104,105] These contributions as the now named Heck-Mizoroki reaction (Scheme 1.1), a foundational milestone in palladium-catalyzed cross-coupling chemistry, with Richard Heck jointly recognized with the 2010 Nobel Prize for Chemistry.

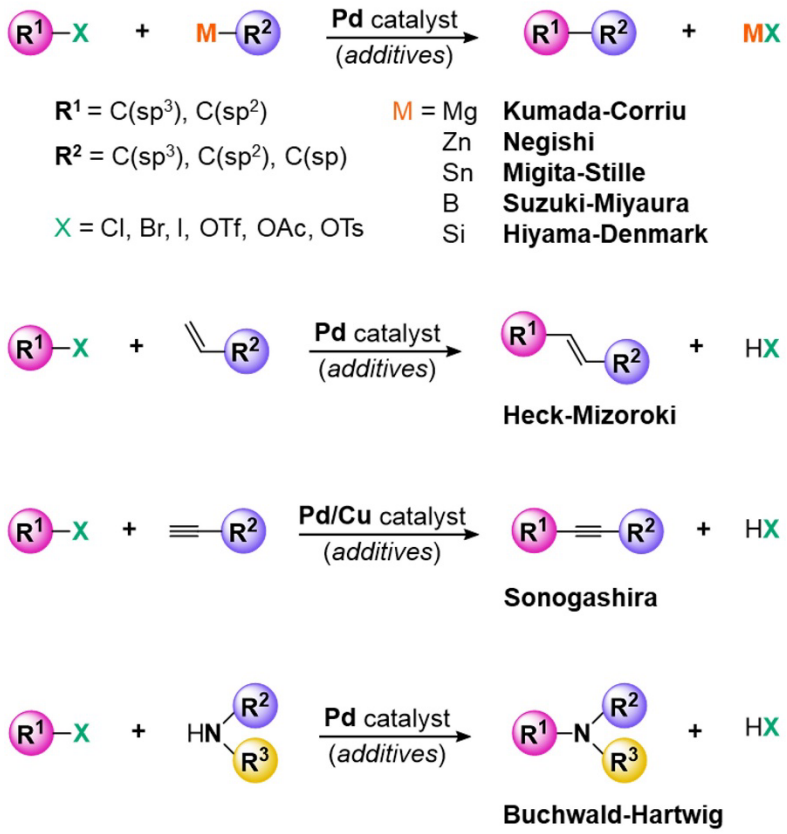

Scheme 1.1: General reaction schemes of palladium-catalyzed cross-coupling reactions.

Building on early investigations into Grignard reagents the Corriu[106] and Kumada[107] groups independently reported in 1972 the nickel-catalyzed cross-coupling of aryl and alkenyl halides with Grignard reagents (Scheme 1.1). This was further extended by Murahashi[108] in 1975, who demonstrated the cross-coupling with Grignard reagents under palladium catalysis. The scope of palladium-catalyzed coupling reactions was expanded by Kenkichi Sonogashira in 1975, coupling of terminal alkynes with aryl or vinyl halides (Scheme 1.1), using a copper co-catalyst.[109] This system allowed reactions to proceed under milder reaction conditions,[110] but the generated copper acetylides readily resulted in oxidative homocoupling products of the terminal alkynes when exposed to air. Despite

these challenges, the Sonogashira reaction opened a versatile route for C(sp)–C(sp^2) bond formation, with further improvements aimed at eliminating the need for copper salts.[111]

As chemists sought to find more convenient organometallic reagents, another step forward was reported by Ei-ichi Negishi in 1976 by introducing a method for assembling aryl halides with zinc-, boron-, or tin-based organometallic reagents.[112,113] This approach significantly broadened the cross-coupling approach and set the stage for using milder, less electropositive metal coupling species.[114] Following Negishi's work, John K. Stille in 1978 achieved a palladium-catalyzed cross-coupling of acyl chlorides with organotin nucleophiles,[115] and demonstrated the reaction's versatility and functional-group tolerance, though the toxicity of organotin compounds restricted large-scale pharmaceutical applications.[116] Migita's contributions further refined this reaction by enabling the coupling of organotin reagents with aryl bromides.[117]

In 1979, Akira Suzuki and Norio Miyaura introduced a reaction using boronic acids or boronic esters with organohalide coupling partners, using a Pd(0) catalyst and a base to synthesize biaryl compounds through C(sp^2)–C(sp^2) linkages (Scheme 1.1).[118] Extensive studies on the role of the base revealed its function in activating poorly nucleophilic borane reagents into more reactive boronate complexes, enabling the coupling of organometallic reagents unable to undergo transmetallation under standard conditions.[119,120] This discovery opened the door to coupling reactions involving nucleophiles with lower electronegativity differences between the metal and the organic moiety. The Suzuki-Miyaura (SM) reaction has since become a powerful and general method for C–C bond formation, with several advantageous features: (1) air- and moisture-stable organoboron starting materials; (2) mild and convenient reaction conditions, and (3) the relatively easy removal of less-toxic inorganic byproducts. These attributes make the SM coupling reaction especially valuable for industrial applications.

The push towards less-toxic organometallic nucleophiles is exemplified by work from Hiyama and coworkers in 1988, where palladium- and nickel-catalyzed coupling of organosilanes with aryl halides and triflates was achieved using a fluoride source as an activator.[121] This method provided a relatively safer and more environmentally friendly

alternative to traditional organometallic reagents of the time. Subsequent advancements by Denmark in 1999 and others explored silicon derivatives, such as siloxanes, further expanding the Hiyama coupling's applications.[122] The now-named Hiyama-Denmark reaction highlights the potential for broader adoption of silicon-based reagents in synthesis.

The 1990s witnessed expansion into non-carbon-based nucleophiles participating in PdCC reactions.[102] One such advancement was the amination of aryl, vinyl, and heteroaryl halides through carbon–nitrogen (C–N) coupling as reported by Stephen L. Buchwald and John F. Hartwig in 1998 and 1999.[123,124] This C–N bond formation is particularly significant due to the prevalence of aromatic amines in pharmaceuticals and natural products. The synthetic effectiveness of the Buchwald-Hartwig amination (Scheme 1.1) expanded the cross-coupling substrate scope, offering a flexible strategy for the synthesis of (hetero)arylamines.[125]

1.2.2 Mechanisms of PdCC Reactions

A major factor in the widespread use of PdCC reactions is their reliability and reproducibility.[126] Undoubtedly, detailed understanding of the mechanism of cross-coupling reactions, including knowledge about the nature of the organometallic intermediates and catalyst decomposition pathways, has contributed to the dependability of these reactions.[72,102,127–131]In general, the widely accepted mechanism of palladium-catalyzed cross-coupling involves a Pd(0)/Pd(II) catalytic cycle as shown in Scheme 1.2.

The elementary steps involved in catalysis are: (1) oxidative addition of the organo(pseudo)halide electrophile (R^1–X) to the coordinatively unsaturated Pd(0) catalyst, where the C–X bond is polarized to afford a Pd(II) complex; (2) transmetallation of the nucleophile, where an organic group (or hydride) from the main group organometallic compound (M–R^2) is transferred to the Pd(II) oxidative addition complex; and (3) the reductive elimination step where elimination of the two ligands gives rise to a coupled product (R^1–R^2), and regenerates the L_nPd(0) catalyst.[130] A catalyst activation step often precedes oxidative addition to generate the active catalytic species from a precatalyst, as

well as cis-trans isomerization of the transmetallation intermediate preceding reductive elimination.

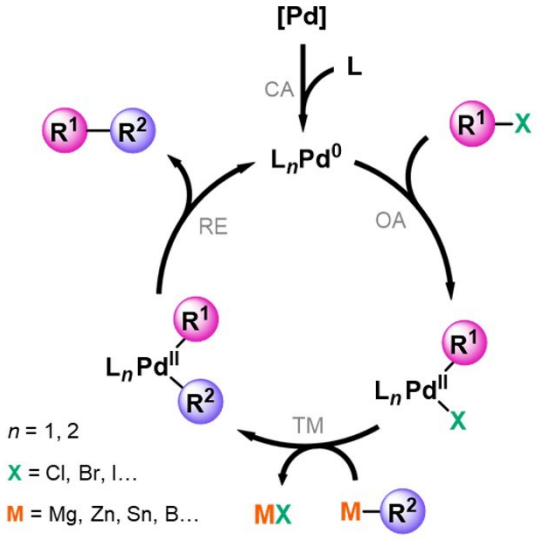

Scheme 1.2: Generalized mechanism for palladium-catalyzed cross-coupling reactions. Key: CA = catalyst activation, OA = oxidative addition, TM = transmetallation, RE = reductive elimination. (cis–trans isomerization step omitted for clarity)

Beyond the elementary catalytic steps shown in Scheme 1.2, additional catalytic pathways specific to certain types of cross-coupling reactions have been elucidated. In the Heck-Mizoroki reaction, coordination of an alkene to the Pd(II) oxidative addition complex (OAC), followed by syn migratory insertion at the Pd–C bond, and succeeded by syn β-hydride elimination form the coupled alkene product and a [L_nPd(H)(X)] complex. Base-assisted elimination of HX from [L_nPd(H)(X)] occurs to regenerate the L_nPd(0) catalyst.[132] In the Sonogashira reaction, after OAC formation, the palladium cycle intersects with the co-catalyzed copper (or palladium for Cu-free Sonogashira reaction)[111] cycle. A copper acetylide, formed through deprotonation of a π-alkyne-copper complex, undergoes transmetallation to generate a palladium acetylide complex, with cis-trans isomerization and reductive elimination following to produce the final product.[110] For the Buchwald-Hartwig amination, the mechanism involves amine coordination and deprotonation rather than direct transmetallation.[125]

Extensive experimental and computational evidence has been discovered to support these pathways, shedding light on factors influencing each elementary step.[133] These detailed mechanistic investigations have been instrumental in driving the development and improvement of cross-coupling reactions, enabling their broad application in modern synthetic chemistry.[102,127–130] The emergence of Pd(II)/Pd(IV) catalytic cycles is also of growing significance, as highlighted in recent reviews.[134,135] While these Pd(II)/Pd(IV) systems are beyond the scope of this dissertation, they represent a promising avenue for future research, with the potential to expand the utility and versatility of palladium-catalyzed processes in novel and challenging transformations.

1.2.2.1 Catalyst Activation

As shown in Scheme 1.2, to catalyze a reaction, the palladium precatalyst must be activated to produce a coordinatively unsaturated $L_nPd(0)$ species. The catalyst activation step directly affects the overall rate and performance of the cross-coupling reaction, yet remains poorly understood.[136] This is further complicated by the reactive nature of these complexes, making then challenging to isolate and study.[137–139] Traditionally, active species were obtained *in situ* by mixing an excess of a ligand with a Pd source, with early palladium-based catalysts using simple phosphines such as PPh_3 as ligands.[102]

The drive to achieve challenging substrate transformations with higher selectivity under milder reaction conditions has fueled advances in ligand design. Strongly electron-donating and sterically bulky ligands, such as biaryldialkyl phosphines, QPhos and YPhos ligands, or *N*-heterocyclic carbenes (NHCs) as those developed by the Herrmann, Glorius, Organ, and Nolan groups, have proven to be superior in challenging coupling reactions.[140–144] Many of these offer tunable electronic and steric properties through modifications to their backbones and axillary functional groups.

Activation of palladium catalysts *in situ* can be divided into two general groups: (1) from Pd(0) precatalysts, such as $Pd(PPh_3)_4$ or $Pd_2(dba)_3$•*solvent*, via ligand dissociation and exchange, or (2) from Pd(II) precatalysts, such as $Pd(OAc)_2$, $PdCl_2(PPh_3)_2$, or $[Pd(\eta^3\text{-allyl})Cl]_2$, via reductive elimination with the help of external bases or ligands (Scheme 1.3A).[145] These activation mechanisms depend on several factors, including the precatalyst

source, orders of addition, and reaction conditions.[146–149] Fairlamb and coworkers have recently put forth a case for studying catalyst activation, showing systems involving various types of catalytic centers (palladium complexes, clusters, and nanoparticles) all involved in complementary linked pathways.[150–153] Wei and coworkers also demonstrated that base-assisted reduction of Pd(II) can proceed via two distinct pathways, leading to either mono- or bisligated Pd(0) complexes.[154] Controlling the desired ligation state therefore remains a challenge, as many simple Pd sources can form both mono- and bisligated species in solution. As will be discussed in Chapter 5, *in situ* control of catalyst activation can be achieved through careful design of the precatalyst, ligand, and reaction conditions.

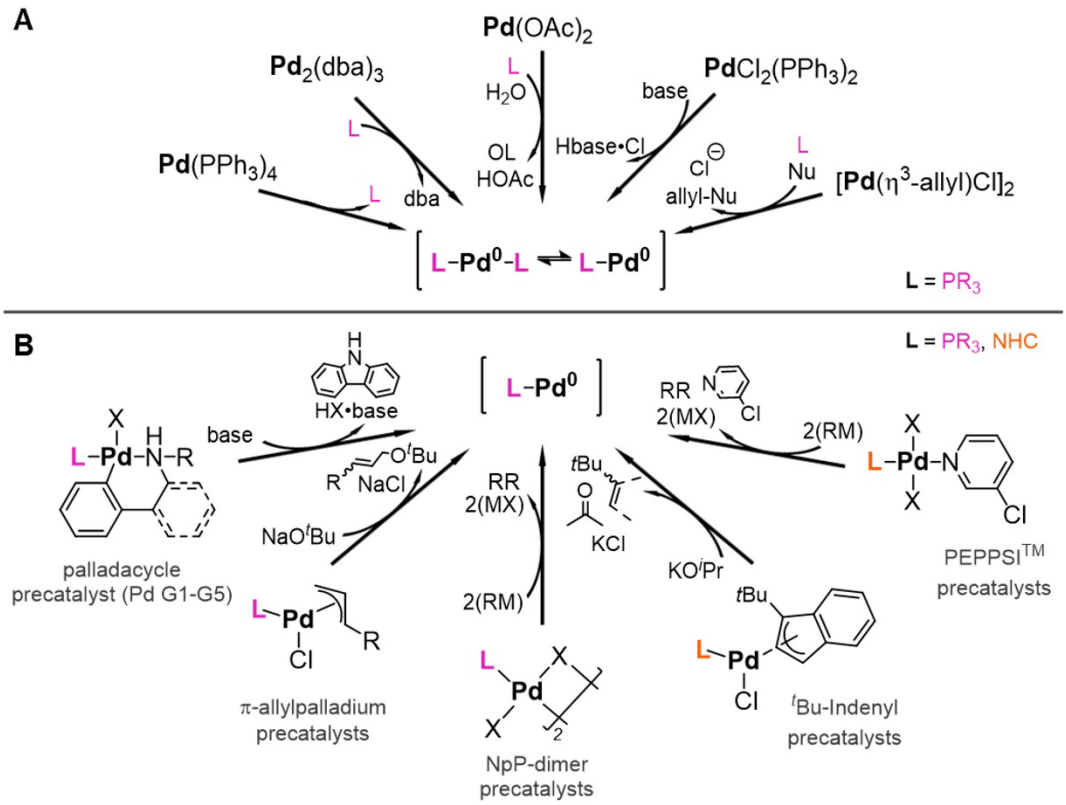

Scheme 1.3: A) *In situ* activation pathways for select simple Pd(0) and Pd(II) precatalysts, where controlling the ligation state can be challenging. B) Select pre-ligated Pd(II) precatalysts for controlled monoligated catalyst activation.

Studies have highlighted that monoligated catalysts, LPd(0), are often favoured as active species over bisligated L_2Pd(0).[154,155] Monoligated species typically exhibit superior catalytic activity compared to their bisligated counterpart, even with the same ligand

used.[155,156] The ligation state also influences mechanistic pathways for oxidative addition leading to differential site-selectivity preferences in specific reactions.[157–160] To optimize catalytic performance, developments have focused on precatalysts that ensure a 1:1 palladium-to-ligand ratio thus providing better control for catalytic activity. This includes single-component precatalysts with desired supporting ligands already pre-installed.[161]

Single-component precatalysts include biphenylamine-based palladacycles developed by Buchwald and coworkers, which are generally activated by deprotonation of the Pd-bound amine followed by C–N reductive elimination, yielding LPd(0) and indoline or carbazole byproducts (Scheme 1.3B).[162–164] Shaughnessy and coworkers demonstrated that $[LPdX_2]_2$ dimer complexes with preinstalling neopentyl phosphine (NpP) ligands disfavoured Pd(I) dimer formation, instead yielding Pd(II) complexes that undergo reductive elimination to yield LPd(0).[165,166] Similarly, the Pd(π-allyl)(L)Cl precatalysts, where L = di(tert-butyl)(neopentyl)phosphine (DTBNpP), published jointly by the Shaughnessy and Colacot groups, serve as Pd(0) sources through nucleophilic addition and reductive elimination (Scheme 1.3B).[167,168] These systems generate highly reactive LPd(0) species, outperforming $L_2Pd(0)$ complexes or *in situ* systems generated from $Pd_2(dba)_3$–DTBNpP (1:1).

Hazari and coworkers iterated on the Pd(π-allyl)(L)Cl design with NHC-based systems, showing that increasing steric bulk at the allyl ligand reduces comproportionation, preserving more of the active LPd(0) species (Scheme 1.3B).[169,170] NHC-based systems have also been advanced by Organ and coworkers, with Pyridine Enhanced Precatalyst Preparation Stabilization and Initiation (PEPPSI) systems, which generate monoligated LPd(0) upon activation by a strong nucleophilic coupling partner or a base, with 3-chloropyridine as a throwaway stabilizing ligand.[171]

These pre-ligated precatalysts enhance catalytic performance in specific transformation by eliminating the need for ligand substitution steps and enabling site- and substrate-selective activation pathways. However, challenges remain, including complex and costly multistep syntheses, slower initiation at room temperature in the presence of weak bases, and limited flexibility in accommodating different ancillary ligands. The examples discussed above illustrate how mechanistic investigations of catalyst activation

processes, coupled with iterative improvements in catalyst design, have significantly enhanced the utility and reactivity of Pd catalysts. The work in this dissertation aims to contribute to these advancements by providing deeper mechanistic insights and guiding future catalyst development.

1.2.2.2 Oxidative Addition

The oxidative addition (OA) of organic electrophiles to Pd(0) is a cornerstone of organopalladium chemistry and a critical step in palladium-catalyzed cross-coupling reactions. This elementary step involves the breaking of a substrate's bond (e.g., C–X, where X is a (pseudo)halogen) and the formation of Pd–C and Pd–X bonds.[172,173] The efficiency of OA is central to the overall success of cross-coupling reactions, making it an area of intense investigation in both theoretical and applied research.

Mechanistic studies have identified different pathways for OA, depending on the nature of the substrate and the reaction environment. Three primary mechanisms have been proposed as in Scheme 1.4: (1) an S_N2-type nucleophilic displacement mechanism via an attack of Pd on C, generating Pd–C^+ and X^- fragments, which further reacts yielding the OAC; (2) a three-centered concerted insertion, simultaneously forming the Pd–X and Pd–C bond as the C–X bond is broken; and (3) a radical process where an X radical is abstracted from C in the initial step.[172] For aliphatic halides, the nucleophilic displacement mechanism is often favored in polar solvents due to the formation of ion pairs, whereas for aromatic halides, the three-center mechanism is typically lower in energy.[174,175] This is attributed to the backdonation from the Pd(0) center to the π-system of the aromatic ring, facilitated by its lower HOMO-LUMO gap compared to aliphatic substrates.[176] The bond dissociation energy also plays a critical role, with reactivity following the trend I > Br > Cl > F.[177] In addition, the balance between steric repulsion and attractive weak interactions on the OA influences reactivity, with the OA energy barriers increasing along with the degree of substitution of the carbon atom.[178]

The role of the ligation state of palladium in OA cannot be understated. In solutions containing L/Pd, two potential reactive species, mono- and bisligated Pd complexes typically coexist in equilibrium. This balance is influenced by steric and electronic

properties of the ligands.[155,179–181] Bulky, electron-rich monophosphine ligands, such as P(*t*-Bu)$_3$, often favor the formation of highly reactive monoligated Pd(0) species. These bulky ligands have been critical in enabling cross-coupling reactions with less reactive substrates, such as aryl chlorides and alkyl tosylates, under milder conditions.[161] The ligation state also plays a pivotal role in dictating the efficiency of OA, with ligand properties modulating OA kinetics and selectivity.[182–184]

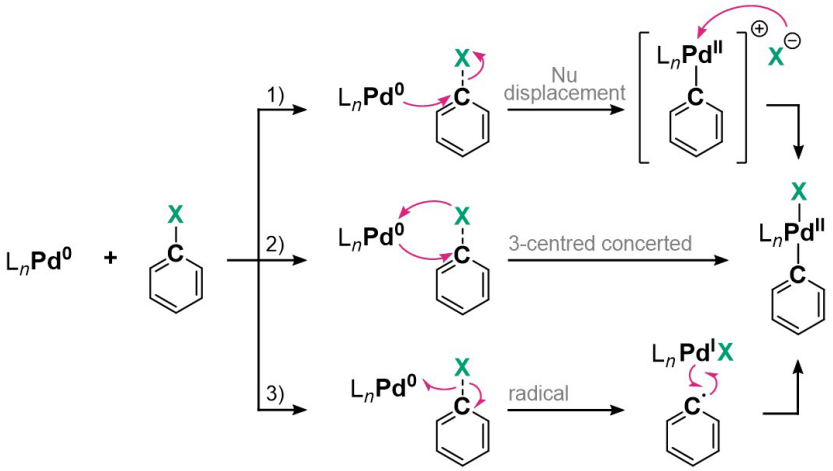

Scheme 1.4: General mechanisms for oxidative addition of a simple aryl halide to Pd in cross-coupling reactions.

This ability to tune OA by controlling ligand steric and electronic factors lays the groundwork for further exploration of OACs as mechanistic tools. Isolating these relatively stable on-cycle species allows for the stoichiometric analysis of intermediates along the catalytic cycle. Such studies have been instrumental in understanding catalyst deactivation pathways,[185] guiding the design of new ligand scaffolds,[186,187] and optimizing catalytic conditions for challenging substrates.[188] Although not successfully isolable in the studies presented in the following chapters, this application presents a desirable pathway for further exploration in future studies building on the findings of this dissertation.

OACs have also proven useful as precatalysts for specific transformations. For example, Shaughnessy and coworkers reported [(PNp$_3$)Pd(Ar)Br]$_2$ (PNp$_3$ = trineopentylphosphine) complexes as one of the first examples of OACs as a precatalyst, demonstrating exceptional activity in coupling sterically hindered aryl bromides and

aniline derivatives.[189,166] Similarly, Buchwald and coworkers demonstrated the utility of (AlPhos)Pd(Ar)X OACs in the fluorination of aryl bromides.[190] More recently, Colacot and coworkers developed a series of 89 air-stable OACs with a general formula (*t*-Bu$_3$P)Pd(Ar)X as precatalysts for challenging Suzuki–Miyaura reactions of polyfluorinated arylboron reagents.[191] These precatalysts demonstrated superior catalytic activities than that of the many reported "state-of-the art" catalyst systems, revealing the hidden potential in the often-used commercially availability P(*t*-Bu)$_3$ ligand. The ability of OACs to bypass the catalyst activation step required by traditional precatalysts makes them particularly attractive for late-stage functionalization and pharmaceutical applications.[192] However, challenges such as the synthesis and stability of these complexes, as well as their compatibility with diverse reaction conditions, remain areas for continued research.

1.2.3 Select Applications of PdCC Reactions

Palladium-catalyzed cross-coupling reactions have become vital tools in both academia and industry due to their versatility, efficiency, and reliability. They are widely applied in fields such as medicinal chemistry, agrochemistry, and polymer synthesis, where they address longstanding synthetic challenges with innovative solutions. In medicinal chemistry, PdCC reactions have revolutionized the synthesis of active pharmaceutical ingredients. A survey of commonly used reactions in this field shows that Suzuki-Miyaura, Buchwald-Hartwig, and Sonogashira couplings rank among the top 20 reactions.[126] An early and elegant industrial example is the Boots-Hoechst-Celanese process for manufacturing ibuprofen (Advil) in two catalytic steps—hydrogenation and carbonylation—from *p*-isobutylacetophenone (Scheme 1.5) with 100% atom economy.[193] This streamlined process replaced a classical multistep route.

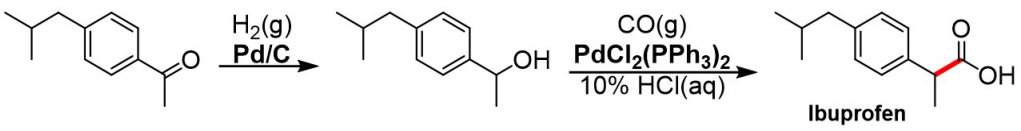

Scheme 1.5: Boots-Hoechst-Celanese ibuprofen synthesis by palladium-catalyzed hydrogenation and carbonylation.

Other examples of palladium catalysis in pharmaceutical synthesis (see Figure 1.11) include Losartan,[194] used to treat high blood pressure, and Imatinib,[195] a leukemia treatment, both listed on the World Health Organisation List of Essential Medicines.[196] These reactions offer excellent yields, chemoselectivity, and compatibility with functionalized substrates. Large-scale pharmaceutical manufacturing further underscore its industrial relevance, such as Pfizer's 40 kg-scale Heck reaction for a hepatitis C viral polymerase (HCVP) inhibitor,[197] and Novartis's 50 kg-scale Suzuki-Miyaura coupling for Crizotinib,[198] a potent anticancer agent. Similarly, the Suzuki-Miyaura coupling has been used in the synthesis of MK-0913, a potential treatment for rheumatoid arthritis, Crohn's disease, and psoriasis.[199]

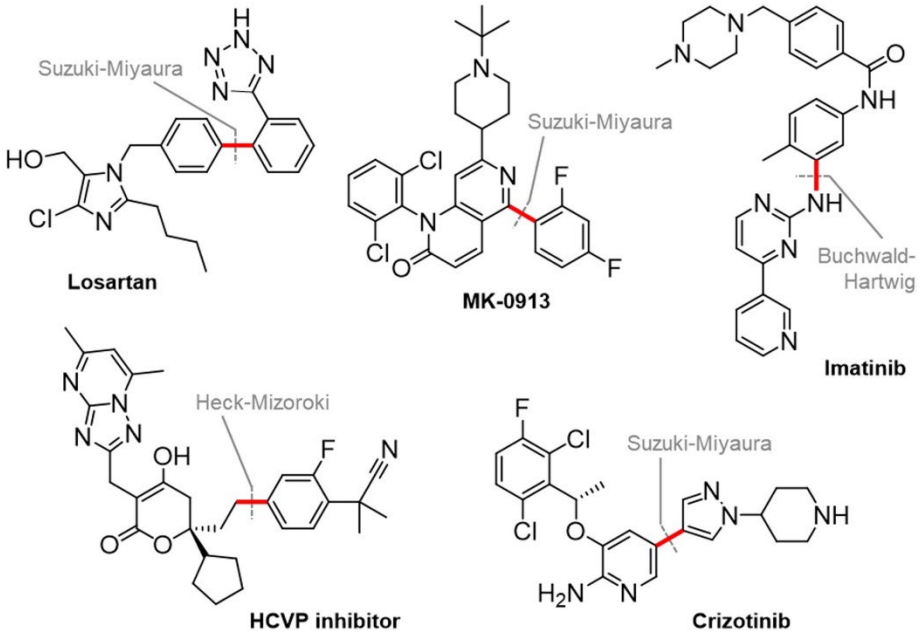

Figure 1.11: Select examples of active pharmaceutical ingredients, with PdCC bond formation highlighted.

Palladium-catalyzed cross-coupling reactions have also played a crucial role in the synthesis of polymers used in advanced materials. The Suzuki-Miyaura and Stille coupling reactions are commonly used to construct π-conjugated backbones for organic photovoltaics (OPVs), light-emitting diodes (OLEDs), and field-effect transistors (OFETs).[200,201] In one example, poly(3-hexylthiophene) (P3HT), a benchmark material for organic solar cells, is polymerized by cross-coupling as in Scheme 1.6, allowing for well-

defined molecular weights and controlled regioregularity.[202,203] Similarly, donor–acceptor conjugated polymers, used for efficient charge transport in electronic applications, are often synthesized using cross-coupling reactions to incorporate electron-rich and electron-deficient monomers with high functional group tolerance.[204]

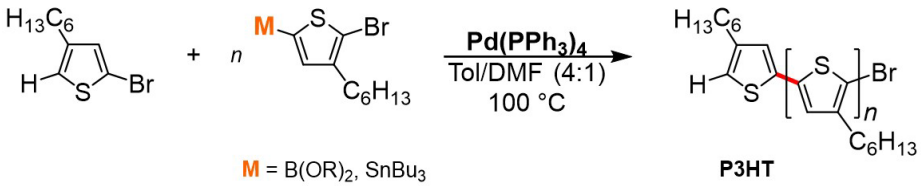

Scheme 1.6: Synthesis of poly(3-hexylthiophene) (P3HT) via Suzuki-Miyaura or Stille PdCC reaction.

In agrochemistry, PdCC reactions have been pivotal in developing modern agrochemicals with improved efficacy and environmental safety. Reactions such as the Heck, Suzuki-Miyaura, and Stille couplings have been used to synthesize intermediates for fungicides, herbicides, and insecticides, such as prosulfuron, boscalid, fenpropimorph, and bixafen.[205] The utility of palladium-catalyzed cross-coupling reactions lies not only in their ability to create bonds but also in their adaptability to diverse contexts. The availability of numerous coupling partners, including aromatic boronic acids, halides, and heteroatom-based electrophiles, enhances their versatility. Despite their success, ongoing research continues to address challenges in scalability, cost efficiency, and environmental impact, ensuring that PdCC reactions remain a cornerstone in modern synthetic chemistry.

1.2.4 Challenges of PdCC Reactions

Despite the transformative impact of palladium-catalyzed cross-coupling on synthetic chemistry, numerous limitations and challenges persist. Addressing these issues highlighted below is critical for advancing sustainable and efficient chemical processes in research and industry.

1.2.4.1 Toxicity, Cost, and Sustainability of Palladium

Palladium is an essential component of cross-coupling reactions, but its widespread use raises significant concerns. The environmental and human health risks associated with palladium stem from its toxicity and the challenges in removing residual metal from final products. Regulatory agencies, such as the European Medicines Agency, mandate stringent limits on metal impurities, typically below 10 ppm,[206] which can be costly and difficult to achieve.[207] Palladium mining and its widespread use as catalytic converters in cars also contributes to environmental contamination, with traces of the metal found in remote locations like Antarctica.[208]

From an economic perspective, palladium is a scarce and expensive precious metal, and its fluctuating price poses a challenge for industrial-scale applications. While strategies to reduce catalyst loading and enhance recycling efficiency have been developed,[209] these innovations are not yet universally applicable. Moreover, many state-of-the-art ligands that improve catalyst performance are costly, and industrial processes are often proprietary, introducing licensing costs and complicating the adoption of new methodologies.

1.2.4.2 Limitations of Organometallic and Organohalide Reagents

The reliance on organometallic nucleophiles which are often derived from organohalides, introduces additional challenges and undermines the sustainability of cross-coupling chemistry.[210,211] While pseudohalides generally offer lower toxicity compared to halides, they are not always straightforward replacements and often lead to divergent reactivity.[212] Furthermore, the instability of many organometallic reagents necessitate *in situ* generation under stringent reaction conditions, complicating scalability and increasing costs.[213,214]

As history has shown, efforts to move away from more toxic nucleophiles has driven progress towards less toxic alternatives like boronic acids and silanes. However, completely eliminating toxic coupling partners remains a distant goal. Recent advancements in cross-electrophile coupling reactions (Ullman-type) offer a promising alternative by coupling two electrophiles instead of an electrophile and organometallic nucleophile.[207,215] These reactions potentially simplify reaction setups and reduce waste, with nickel emerging as a leading catalyst due to its unique redox properties.[215,216]

Nevertheless, challenges remain, as both electrophiles can compete for oxidative addition, leading to mixtures of cross-coupled and homo-coupled products.[216] Further research is needed to address these issues and expand the applicability of this approach.

1.2.4.3 Environmental Impact and Solvent Use

The environmental impact of cross-coupling chemistry extends beyond the catalyst and substrates to include the solvents used, many of which pose significant health and environmental risks. Traditional solvents like chlorinated hydrocarbons and tetrahydrofuran (THF) are classified as problematic to highly hazardous in most solvent selection guides.[217] Recent efforts to adopt greener alternatives, such as cyclopentyl methyl ether (CPME),[218,219] *p*-cymene,[220] isopropyl acetate,[221] and organic carbonates,[222–224] are promising but highlight the need for further research into water-based and biomass-derived systems.[225]

Organic solvents dominate pharmaceutical manufacturing, with one survey revealing that solvents account for 56% of materials used in active pharmaceutical ingredients (APIs) production, while water contributes a further 32%.[226] The ideal case would be no solvent at all, but when required, water offers significant advantages: it is non-toxic, non-flammable, abundant, and inexpensive. Hence, catalytic reactions in aqueous media, including aqueous biphasic system, have been extensively studied,[225] with the latter enabling efficient catalyst recovery and recycling.[207,227] Innovations in solvent systems hold great potential to improve the sustainability of cross-coupling reactions.

1.2.4.4 Challenges in Scaling Up and Recovery

Scaling up cross-coupling reactions from laboratory to industrial scales introduces additional hurdles. Homogeneous catalysts, while highly effective, are difficult to recycle, resulting in increased waste and costs. The majority of industrial-scale catalyst systems developed remain heterogeneous in nature.[213] Heterogeneous catalysts offer practical advantages, including straightforward recovery via filtration or centrifugation and reuse after appropriate washing.[207] Polymer-supported palladium catalysts, functionalized with phosphine groups, serve as a hybrid class that combines the activity and selectivity of homogeneous catalysts with the recovery ease of heterogeneous systems. These catalysts

have been applied successfully in various coupling reactions and are more commonly used due to their simpler recycling compared to ligand-modified palladium catalysts.[228,229] Continuous-flow methods provide additional advantages for scaling up. They enable precise control over reaction parameters, such as heat transfer, mass transfer, and residence time, while simplifying workup.[230,231] These methods highlight the potential for scalable and efficient industrial applications of cross-coupling chemistry, especially in long-term and sequential catalyst systems.

1.2.4.5 Lack of Suitable Earth-Abundant Alternatives

While efforts to replace palladium with earth-abundant metals such as iron, nickel, and copper have shown promise, these alternatives often fall short in terms of activity, selectivity, and substrate scope.[208,232,233] For example, palladium catalysts generally exhibit superior performance in reactions involving less reactive (but often cheaper) substrates, such as aryl chlorides.[234] Transitioning these alternative systems from academic research to industrial applications remains a challenge due to their incompatibility with established reaction conditions. Uncovering the mechanistic intricacies of these reactions is a key step in addressing these challenges.

1.3 Objectives for Study and Dissertation Outline

1.3.1 Motivations and Objectives

Palladium-catalyzed cross-coupling reactions are a cornerstone of modern synthetic chemistry, celebrated for their efficiency and versatility. However, challenges remain as the demand for sustainable, economically viable, and scalable synthetic methods grows, further complicated by the increasing cost and environmental impact of palladium. This urgency is further heightened by current geopolitical instability in regions responsible for significant palladium mining.

While great strides have been made in developing non-precious metal alternatives, palladium remains the most reliable and widely used metal for cross-coupling reactions, with most practical applications of PdCC relying on *in situ* activation of a precatalyst with

auxiliary ligands. Gaining mechanistic insights into these processes is crucial for identifying bottlenecks, improving catalytic efficiency, and developing innovative ligand and catalyst systems to address current limitations.

Mass spectrometry has emerged as a powerful tool for probing catalytic mechanisms, offering insights into reaction dynamics. By integrating direct on-line sampling through PSI with the soft ionization capabilities of ESI and advanced ion characterization from tandem MS, this methodology enables the direct observation of reactive intermediates, resting states, and decomposition products. My objective is to leverage expertise in catalytic reaction monitoring developed in the McIndoe group to probe key mechanistic questions in PdCC reactions. The work will not only provide fundamental insights into palladium catalysis, but also explore the limitations of MS for analyzing complex chemical systems.

This dissertation is guided by two main research questions:

1) What are the limitations of ESI-MS in studying complex systems, and how can this methodology be optimized to better represent preserve weakly coordinating organometallic species?

2) What are the key intermediates and pathways involved in the *in situ* activation of palladium precatalysts, and how do these processes influence the formation and decomposition of palladium species?

1.3.2 Dissertation Outline

The dissertation addresses these research questions through studies presented in Chapters 2–5. It consists of self-contained chapters based on previously published work. As is common in collaborative research, contributions from coauthors and collaborators have been integral to the success of these projects. These contributions will be acknowledged and detailed at the beginning of each chapter.

Chapter 1 provides background on palladium-catalyzed cross-coupling reactions, mass spectrometry, and their relevance to this work. This foundational chapter sets the

stage for the investigations and methodologies explored in subsequent chapters. Chapter 2 examines the limitations of MS in characterizing high molecular weight polymers, some of which are synthesized via PdCC reactions. This chapter highlights the challenges and provides insights into improving its applicability for such materials. Chapter 3 evaluates ESI-MS performance across multiple instruments, focussing on preserving weak interactions in inorganic and organometallic complexes, and offering practical tests for instrument evaluation and optimization.

Chapters 4 and 5 explore the mechanisms of catalyst activation in palladium-catalyzed cross-coupling. In chapter 4, I investigate the activation of $Pd_2(dba)_3$, a classic Pd(0) source, and evaluate the mercury drop test, a widely used method for distinguishing the nature of active catalytic species. Chapter 5 examines the activation and oxidative addition processes of a new-generation palladium precatalyst, $(^{DMP}DAB)Pd(CH_2SiMe_3)_2$. This case study demonstrates the utility of PSI-ESI-MS for probing complex catalytic mechanisms and advancing the understanding of modern palladium precatalysts. Finally, Chapter 6 concludes with a summary of the key findings of this dissertation, and their implications for palladium catalysis and mass spectrometry. It also provides an outlook on potential directions for further research.

1.4 References

(1) Gross, J. H. *Mass Spectrometry: A Textbook*; Springer, 2017.
(2) Madeira, P. J. A.; Florêncio, M. H.; Madeira, P. J. A.; Florêncio, M. H. Applications of Tandem Mass Spectrometry: From Structural Analysis to Fundamental Studies. In *Tandem Mass Spectrometry - Applications and Principles*; IntechOpen, 2012. https://doi.org/10.5772/31736.
(3) Thomson, J. J. XL. Cathode Rays. *Lond. Edinb. Dublin Philos. Mag. J. Sci.* **1897**, *44* (269), 293–316. https://doi.org/10.1080/14786449708621070.
(4) Thomson, J. J. XLVII. On Rays of Positive Electricity. *Lond. Edinb. Dublin Philos. Mag. J. Sci.* **1907**, *13* (77), 561–575. https://doi.org/10.1080/14786440709463633.
(5) Dempster, A. J. A New Method of Positive Ray Analysis. *Phys. Rev.* **1918**, *11* (4), 316–325. https://doi.org/10.1103/PhysRev.11.316.
(6) Aston, F. W. LXXIV. A Positive Ray Spectrograph. *Lond. Edinb. Dublin Philos. Mag. J. Sci.* **1919**, *38* (228), 707–714. https://doi.org/10.1080/14786441208636004.
(7) Bainbridge, K. T.; Jordan, E. B. Mass Spectrum Analysis 1. The Mass Spectrograph. 2. The Existence of Isobars of Adjacent Elements.
(8) Nier, A. O. A Mass Spectrometer for Routine Isotope Abundance Measurements. *Rev. Sci. Instrum.* **1940**, *11* (7), 212–216. https://doi.org/10.1063/1.1751688.
(9) Hoover, J. H. Mass Spectrometer. US2341551A, February 15, 1944. https://patents.google.com/patent/US2341551A/en (accessed 2024-11-19).
(10) Wolff, M. M.; Stephens, W. E. A Pulsed Mass Spectrometer with Time Dispersion. *Rev. Sci. Instrum.* **1953**, *24* (8), 616–617. https://doi.org/10.1063/1.1770801.
(11) Sommer, H. The Measurement of e/M by Cyclotron Resonance. *Phys. Rev.* **1951**, *82* (5), 697–702. https://doi.org/10.1103/PhysRev.82.697.
(12) Paul, W. Electromagnetic Traps for Charged and Neutral Particles. *Rev. Mod. Phys.* **1990**, *62* (3), 531–540. https://doi.org/10.1103/RevModPhys.62.531.
(13) Ryhage, Ragnar. Use of a Mass Spectrometer as a Detector and Analyzer for Effluent Emerging from High Temperature Gas Liquid Chromatography Columns. *Anal. Chem.* **1964**, *36* (4), 759–764. https://doi.org/10.1021/ac60210a019.
(14) Watson, J. T.; Biemann, Klaus. Direct Recording of High Resolution Mass Spectra of Gas Chromatographic Effluents. *Anal. Chem.* **1965**, *37* (7), 844–851. https://doi.org/10.1021/ac60226a015.
(15) Barber, M.; Bordoli, R. S.; Sedgwick, R. D.; Tyler, A. N. Fast Atom Bombardment of Solids (F.A.B.): A New Ion Source for Mass Spectrometry. *J. Chem. Soc. Chem. Commun.* **1981**, No. 7, 325–327. https://doi.org/10.1039/C39810000325.
(16) Yamashita, M.; Fenn, J. B. Electrospray Ion Source. Another Variation on the Free-Jet Theme. *J. Phys. Chem.* **1984**, *88* (20), 4451–4459. https://doi.org/10.1021/j150664a002.
(17) Fenn, J. B.; Mann, M.; Meng, C. K.; Wong, S. F.; Whitehouse, C. M. Electrospray Ionization for Mass Spectrometry of Large Biomolecules. *Science* **1989**, *246* (4926), 64–71. https://doi.org/10.1126/science.2675315.
(18) Karas, Michael.; Hillenkamp, Franz. Laser Desorption Ionization of Proteins with Molecular Masses Exceeding 10,000 Daltons. *Anal. Chem.* **1988**, *60* (20), 2299–2301. https://doi.org/10.1021/ac00171a028.
(19) Tanaka, K.; Waki, H.; Ido, Y.; Akita, S.; Yoshida, Y.; Yoshida, T.; Matsuo, T. Protein and Polymer Analyses up to m/z 100 000 by Laser Ionization Time-of-Flight Mass Spectrometry. *Rapid Commun. Mass Spectrom.* **1988**, *2* (8), 151–153. https://doi.org/10.1002/rcm.1290020802.
(20) Abian, J. The Coupling of Gas and Liquid Chromatography with Mass Spectrometry. *J. Mass Spectrom.* **1999**, *34* (3), 157–168. https://doi.org/10.1002/(SICI)1096-9888(199903)34:3<157::AID-JMS804>3.0.CO;2-4.

(21) Enke, C. G. A Perspective on the Development of Tandem Mass Spectrometry. In *The Encyclopedia of Mass Spectrometry*; Gross, M. L., Caprioli, R. M., Eds.; Elsevier: Boston, 2016; pp 68–76. https://doi.org/10.1016/B978-0-08-043848-1.00026-2.
(22) Daub, C. D.; Cann, N. M. How Are Completely Desolvated Ions Produced in Electrospray Ionization: Insights from Molecular Dynamics Simulations. *Anal. Chem.* **2011**, *83* (22), 8372–8376. https://doi.org/10.1021/ac202103p.
(23) Cristoni, S.; Bernardi, L. R. Development of New Methodologies for the Mass Spectrometry Study of Bioorganic Macromolecules. *Mass Spectrom. Rev.* **2003**, *22* (6), 369–406. https://doi.org/10.1002/mas.10062.
(24) Wang, E. H.; Appulage, D. K.; McAllister, E. A.; Schug, K. A. Investigation of Ion Transmission Effects on Intact Protein Quantification in a Triple Quadrupole Mass Spectrometer. *J. Am. Soc. Mass Spectrom.* **2017**, *28* (9), 1977–1986. https://doi.org/10.1021/jasms.8b05636.
(25) Dole, M.; Mack, L. L.; Hines, R. L.; Mobley, R. C.; Ferguson, L. D.; Alice, M. B. Molecular Beams of Macroions. *J. Chem. Phys.* **1968**, *49* (5), 2240–2249. https://doi.org/10.1063/1.1670391.
(26) Kebarle, P.; Verkerk, U. H. Electrospray: From Ions in Solution to Ions in the Gas Phase, What We Know Now. *Mass Spectrom. Rev.* **2009**, *28* (6), 898–917. https://doi.org/10.1002/mas.20247.
(27) Mora, J. F. de la; Van Berkel, G. J.; Enke, C. G.; Cole, R. B.; Martinez-Sanchez, M.; Fenn, J. B. Electrochemical Processes in Electrospray Ionization Mass Spectrometry. *J. Mass Spectrom.* **2000**, *35* (8), 939–952. https://doi.org/10.1002/1096-9888(200008)35:8<939::AID-JMS36>3.0.CO;2-V.
(28) Rosell-Llompart, J.; Grifoll, J.; Loscertales, I. G. Electrosprays in the Cone-Jet Mode: From Taylor Cone Formation to Spray Development. *J. Aerosol Sci.* **2018**, *125*, 2–31. https://doi.org/10.1016/j.jaerosci.2018.04.008.
(29) Taylor, G. I. Disintegration of Water Drops in an Electric Field. *Proc. R. Soc. Lond. Ser. Math. Phys. Sci.* **1997**, *280* (1382), 383–397. https://doi.org/10.1098/rspa.1964.0151.
(30) Konermann, L.; Ahadi, E.; Rodriguez, A. D.; Vahidi, S. Unraveling the Mechanism of Electrospray Ionization. *Anal. Chem.* **2013**, *85* (1), 2–9. https://doi.org/10.1021/ac302789c.
(31) Konermann, L.; Metwally, H.; Duez, Q.; Peters, I. Charging and Supercharging of Proteins for Mass Spectrometry: Recent Insights into the Mechanisms of Electrospray Ionization. *Analyst* **2019**, *144* (21), 6157–6171. https://doi.org/10.1039/C9AN01201J.
(32) Trivedi, V.; Upadhyay, V.; Yadav, M.; Shrivastav, P. S.; Sanyal, M. Impact of Electrospray Ion Source Platforms on Matrix Effect Due to Plasma Phospholipids in The Determination of Rivastigmine by LC–MS/MS. *Bioanalysis* **2014**, *6* (17), 2301–2316. https://doi.org/10.4155/bio.14.85.
(33) Banerjee, S.; Mazumdar, S. Electrospray Ionization Mass Spectrometry: A Technique to Access the Information beyond the Molecular Weight of the Analyte. *Int. J. Anal. Chem.* **2012**, *2012*, e282574. https://doi.org/10.1155/2012/282574.
(34) Corporation, W. *SYNAPT G2-Si HDMS Mass Spectrometer Overview and Maintenance Guide*; Overview and Maintenance Guide 715004159/Revision C; Waters Corporation: Milford, USA, 2016; pp 1–358. https://www.waters.com/webassets/cms/support/docs/715004159rc.pdf (accessed 2024-03-13).
(35) Killeen, C.; Kropp, A.; Chagunda, I. C.; Jackson, E. C.; Scott McIndoe, J. The Amenability of Different Solvents to Electrospray Ionization Mass Spectrometry. *Int. J. Mass Spectrom.* **2024**, *506*, 117349. https://doi.org/10.1016/j.ijms.2024.117349.
(36) Henderson, M. A.; Mcindoe, J. S. Ionic Liquids Enable Electrospray Ionisation Mass Spectrometry in Hexane. *Chem Commun* **2006**, 2872–2874. https://doi.org/10.1039/b606938j.

(37) Gross, J. H. Tandem Mass Spectrometry. In *Mass Spectrometry: A Textbook*; Gross, J. H., Ed.; Springer International Publishing: Cham, 2017; pp 539–612. https://doi.org/10.1007/978-3-319-54398-7_9.
(38) Reuben, A. J.; Smith, G. B.; Moses, P.; Vagov, A. V.; Woods, M. D.; Gordon, D. B.; Munn, R. W. Ion Trajectories in Exactly Determined Quadrupole Fields. *Int. J. Mass Spectrom. Ion Process.* **1996**, *154* (1), 43–59. https://doi.org/10.1016/0168-1176(96)04374-1.
(39) Douglas, D. J.; Konenkov, N. V. Mass Resolution of Linear Quadrupole Ion Traps with Round Rods. *Rapid Commun. Mass Spectrom.* **2014**, *28* (21), 2252–2258. https://doi.org/10.1002/rcm.7018.
(40) Guilhaus, M.; Selby, D.; Mlynski, V. Orthogonal Acceleration Time-of-Flight Mass Spectrometry. *Mass Spectrom. Rev.* **2000**, *19* (2), 65–107. https://doi.org/10.1002/(SICI)1098-2787(2000)19:2<65::AID-MAS1>3.0.CO;2-E.
(41) Guilhaus, M.; Mlynski, V.; Selby, D. Perfect Timing: Time-of-Flight Mass Spectrometry†. *Rapid Commun. Mass Spectrom.* **1997**, *11* (9), 951–962. https://doi.org/10.1002/(SICI)1097-0231(19970615)11:9<951::AID-RCM785>3.0.CO;2-H.
(42) Chernushevich, I. V.; Loboda, A. V.; Thomson, B. A. An Introduction to Quadrupole–Time-of-Flight Mass Spectrometry. *J. Mass Spectrom.* **2001**, *36* (8), 849–865. https://doi.org/10.1002/jms.207.
(43) Borsdorf, H.; Eiceman, G. A. Ion Mobility Spectrometry: Principles and Applications. *Appl. Spectrosc. Rev.* **2006**, *41* (4), 323–375. https://doi.org/10.1080/05704920600663469.
(44) Gross, J. H. *Mass Spectrometry*, 3rd ed.; Springer International Publishing: Cham, 2017. https://doi.org/10.1007/978-3-319-54398-7.
(45) Thomson, J. J. (Joseph J. *Rays of Positive Electricity and Their Application to Chemical Analyses*; London ; New York : Longmans, Green, 1913.
(46) Santos, L. S.; Knaack, L.; Metzger, J. O. Investigation of Chemical Reactions in Solution Using API-MS. *Int. J. Mass Spectrom.* **2005**, *246* (1), 84–104. https://doi.org/10.1016/j.ijms.2005.08.016.
(47) Ray, A.; Bristow, T.; Whitmore, C.; Mosely, J. On-Line Reaction Monitoring by Mass Spectrometry, Modern Approaches for the Analysis of Chemical Reactions. *Mass Spectrom. Rev.* **2018**, *37* (4), 565–579. https://doi.org/10.1002/mas.21539.
(48) Aliprantis, A. O.; Canary, J. W. Observation of Catalytic Intermediates in the Suzuki Reaction by Electrospray Mass Spectrometry. *J. Am. Chem. Soc.* **1994**, *116* (15), 6985–6986. https://doi.org/10.1021/ja00094a083.
(49) Agrawal, D.; Schröder, D.; Frech, C. M. Observation of Binuclear Palladium Clusters upon ESI-MS Monitoring of the Suzuki–Miyaura Cross-Coupling Catalyzed by a Dichloro-Bis(Aminophosphine) Complex of Palladium. *Organometallics* **2011**, *30* (13), 3579–3587. https://doi.org/10.1021/om200274z.
(50) Moreno-Mañas, M.; Pérez, M.; Pleixats, R. Palladium-Catalyzed Suzuki-Type Self-Coupling of Arylboronic Acids. A Mechanistic Study. *J. Org. Chem.* **1996**, *61* (7), 2346–2351. https://doi.org/10.1021/jo9514329.
(51) Hinderling, null; Chen, null. Rapid Screening of Olefin Polymerization Catalyst Libraries by Electrospray Ionization Tandem Mass Spectrometry. *Angew. Chem. Int. Ed Engl.* **1999**, *38* (15), 2253–2256.
(52) Zhu, W.; Yuan, Y.; Zhou, P.; Zeng, L.; Wang, H.; Tang, L.; Guo, B.; Chen, B. The Expanding Role of Electrospray Ionization Mass Spectrometry for Probing Reactive Intermediates in Solution. *Molecules* **2012**, *17* (10), 11507–11537. https://doi.org/10.3390/molecules171011507.
(53) Sun, J.; Yin, Y.; Li, W.; Jin, O.; Na, N. Chemical Reaction Monitoring by Ambient Mass Spectrometry. *Mass Spectrom. Rev.* **2022**, *41* (1), 70–99. https://doi.org/10.1002/mas.21668.

(54) Bethem, R., A.; Basic, C.; Boyd, R., K. Tools of the Trade I. The Classical Tools. In *Trace Quantitative Analysis by Mass Spectrometry*; John Wiley & Sons, Ltd, 2008; pp 17–49. https://doi.org/10.1002/9780470727140.ch2.
(55) Santos, L. S. Online Mechanistic Investigations of Catalyzed Reactions by Electrospray Ionization Mass Spectrometry: A Tool to Intercept Transient Species in Solution. *Eur. J. Org. Chem.* **2008**, *2008* (2), 235–253. https://doi.org/10.1002/ejoc.200700723.
(56) Santos, L. S. On-Line Monitoring Reactions by Electrospray Ionization Mass Spectrometry. In *Reactive Intermediates*; John Wiley & Sons, Ltd, 2009; pp 133–198. https://doi.org/10.1002/9783527628728.ch5.
(57) Fürmeier, S.; Metzger, J. O. Detection of Transient Radical Cations in Electron Transfer-Initiated Diels–Alder Reactions by Electrospray Ionization Mass Spectrometry. *J. Am. Chem. Soc.* **2004**, *126* (44), 14485–14492. https://doi.org/10.1021/ja046157z.
(58) Santos, L. S.; Metzger, J. O. Study of Homogeneously Catalyzed Ziegler–Natta Polymerization of Ethene by ESI-MS. *Angew. Chem. Int. Ed.* **2006**, *45* (6), 977–981. https://doi.org/10.1002/anie.200503307.
(59) Sabino, A. A.; Machado, A. H. L.; Correia, C. R. D.; Eberlin, M. N. Probing the Mechanism of the Heck Reaction with Arene Diazonium Salts by Electrospray Mass and Tandem Mass Spectrometry. *Angew. Chem.* **2004**, *116* (19), 2568–2572. https://doi.org/10.1002/ange.200353076.
(60) Zhu, T.; Wu, X.; Yang, X.; Sharma, B.; Li, N.; Huang, J.; Wang, W.; Xing, W.; Zhao, Z.; Huang, H. One-Pot Catalytic Cleavage of C═S Double Bonds by Pd Catalysts at Room Temperature. *Inorg. Chem.* **2018**, *57* (15), 9266–9273. https://doi.org/10.1021/acs.inorgchem.8b01275.
(61) Bjarnason, A.; DesEnfants, R. E. I.; Barr, M. E.; Dahl, L. F. Fourier-Transform Mass Spectrometry of Several Organometallic Complexes: Laser-Desorption versus Electron-Impact Ionization. *Organometallics* **1990**, *9* (3), 657–661. https://doi.org/10.1021/om00117a020.
(62) Lubben, A. T.; McIndoe, J. S.; Weller, A. S. Coupling an Electrospray Ionization Mass Spectrometer with a Glovebox: A Straightforward, Powerful, and Convenient Combination for Analysis of Air-Sensitive Organometallics. *Organometallics* **2008**, *27* (13), 3303–3306. https://doi.org/10.1021/om800164e.
(63) Eelman, M. D.; Blacquiere, J. M.; Moriarty, M. M.; Fogg, D. E. Shining New Light on an Old Problem: Retooling MALDI Mass Spectrometry for Organotransition-Metal Catalysis. *Angew. Chem. Int. Ed.* **2008**, *47* (2), 303–306. https://doi.org/10.1002/anie.200704489.
(64) Penafiel, J.; Hesketh, A. V.; Granot, O.; McIndoe, J. S. Electron Ionization Mass Spectrometric Analysis of Air- and Moisture-Sensitive Organometallic Compounds. *Dalton Trans.* **2016**, *45* (39), 15552–15556. https://doi.org/10.1039/C6DT03020C.
(65) Naim, A.; Farenc, M.; Hubert-Roux, M.; Chavagnan, T.; Cirriez, V.; Welle, A.; Vantomme, A.; Kirillov, E.; Carpentier, J.-F.; Afonso, C.; Giusti, P. Paraffin-Inert Atmospheric Solid Analysis Probe: A Fast and Easy Approach To Characterize Extremely Air-Sensitive Organometallic Complexes by Mass Spectrometry. *Anal. Chem.* **2020**, *92* (4), 2922–2925. https://doi.org/10.1021/acs.analchem.9b04478.
(66) Strong, K. A.; Stokes, P.; Parker, D.; Buckley, A. K.; Mosely, J. A.; Brodie, C. N.; Dyer, P. W. Versatile, Cheap, Readily Modifiable Sample Delivery Method for Analysis of Air-/Moisture-Sensitive Samples Using Atmospheric Pressure Solids Analysis Probe Mass Spectrometry. *Anal. Chem.* **2022**, *94* (32), 11315–11320. https://doi.org/10.1021/acs.analchem.2c02039.
(67) Vikse, K. L.; Woods, M. P.; McIndoe, J. S. Pressurized Sample Infusion for the Continuous Analysis of Air- And Moisture-Sensitive Reactions Using Electrospray Ionization Mass Spectrometry. *Organometallics* **2010**, *29* (23), 6615–6618. https://doi.org/10.1021/om1008082.
(68) Thomas, G. T.; Donnecke, S.; Chagunda, I. C.; McIndoe, J. S. Pressurized Sample Infusion. *Chemistry–Methods* **2022**, *2* (1), e202100068. https://doi.org/10.1002/cmtd.202100068.

(69) Hesketh, A. V.; Nowicki, S.; Baxter, K.; Stoddard, R. L.; McIndoe, J. S. Simplified Real-Time Mass Spectrometric Analysis of Reactions. *Organometallics* **2015**, *34* (15), 3816–3819. https://doi.org/10.1021/acs.organomet.5b00460.
(70) Thomas, G. T.; MacGillivray, L.; Dean, N. L.; Stoddard, R. L.; Yunker, L. P. E.; McIndoe, J. S. Confounding Contaminants in Mass Spectrometric Reaction Monitoring. *Int J Mass Spectrom* **2019**, *441*, 14–18. https://doi.org/10.1016/J.IJMS.2019.04.001.
(71) Iacobucci, C.; Reale, S.; De Angelis, F. Elusive Reaction Intermediates in Solution Explored by ESI-MS: Reverse Periscope for Mechanistic Investigations. *Angew. Chem. Int. Ed.* **2016**, *55* (9), 2980–2993. https://doi.org/10.1002/anie.201507088.
(72) Yunker, L. P. E.; Ahmadi, Z.; Logan, J. R.; Wu, W.; Li, T.; Martindale, A.; Oliver, A. G.; McIndoe, J. S. Real-Time Mass Spectrometric Investigations into the Mechanism of the Suzuki–Miyaura Reaction. *Organometallics* **2018**, *37* (22), 4297–4308. https://doi.org/10.1021/acs.organomet.8b00705.
(73) Theron, R.; Wu, Y.; Yunker, L. P. E.; Hesketh, A. V; Pernik, I.; Weller, A. S.; Mcindoe, J. S. Simultaneous Orthogonal Methods for the Real-Time Analysis of Catalytic Reactions. *ACS Catal.* **2016**, *6*, 6911–6917. https://doi.org/10.1021/acscatal.6b01489.
(74) Cheng, G.-J.; Zhong, X.-M.; Wu, Y.-D.; Zhang, X. Mechanistic Understanding of Catalysis by Combining Mass Spectrometry and Computation. *Chem. Commun.* **2019**, *55* (85), 12749–12764. https://doi.org/10.1039/C9CC05458H.
(75) Kostyukovich, A. Yu.; Tsedilin, A. M.; Sushchenko, E. D.; Eremin, D. B.; Kashin, A. S.; Topchiy, M. A.; Asachenko, A. F.; Nechaev, M. S.; Ananikov, V. P. In Situ Transformations of Pd/NHC Complexes with N-Heterocyclic Carbene Ligands of Different Nature into Colloidal Pd Nanoparticles. *Inorg. Chem. Front.* **2019**, *6* (2), 482–492. https://doi.org/10.1039/c8qi01095a.
(76) Ahmadi, Z.; Yunker, L. P. E.; Oliver, A. G.; McIndoe, J. S. Mechanistic Features of the Copper-Free Sonogashira Reaction from ESI-MS. *Dalton Trans.* **2015**, *44* (47), 20367–20375. https://doi.org/10.1039/C5DT02889B.
(77) Thomas, G. T.; Janusson, E.; Zijlstra, H. S.; McIndoe, J. S. Step-by-Step Real Time Monitoring of a Catalytic Amination Reaction. *Chem Commun* **2019**, *55* (78), 11727–11730. https://doi.org/10.1039/C9CC05076K.
(78) Belli, R. G.; Wu, Y.; Ji, H.; Joshi, A.; Yunker, L. P. E.; McIndoe, J. S.; Rosenberg, L. Competitive Ligand Exchange and Dissociation in Ru Indenyl Complexes. *Inorg. Chem.* **2019**, *58* (1), 747–755. https://doi.org/10.1021/acs.inorgchem.8b02915.
(79) Joshi, A.; Zijlstra, H. S.; Collins, S.; McIndoe, J. S. Catalyst Deactivation Processes during 1-Hexene Polymerization. *ACS Catal.* **2020**, *10* (13), 7195–7206. https://doi.org/10.1021/acscatal.0c01607.
(80) Thomas, G. T.; Ronda, K.; McIndoe, J. S. A Mechanistic Investigation of the Pd-Catalyzed Cross-Coupling between N-Tosylhydrazones and Aryl Halides. *Dalton Trans.* **2021**, *50* (43), 15533–15537. https://doi.org/10.1039/D1DT03161A.
(81) McLuckey, S. A.; Wells, J. M. Mass Analysis at the Advent of the 21st Century. *Chem. Rev.* **2001**, *101* (2), 571–606. https://doi.org/10.1021/cr990087a.
(82) Guilhaus, M.; Selby, D.; Mlynski, V. Orthogonal Acceleration Time-of-Flight Mass Spectrometry. *Mass Spectrom. Rev.* **2000**, *19* (2), 65–107. https://doi.org/10.1002/(SICI)1098-2787(2000)19:2<65::AID-MAS1>3.0.CO;2-E.
(83) Chernushevich, I. V.; Loboda, A. V.; Thomson, B. A. An Introduction to Quadrupole-Time-of-Flight Mass Spectrometry. *J. Mass Spectrom.* **2001**, *36* (8), 849–865. https://doi.org/10.1002/jms.207.
(84) Burlingame, A. L.; Boyd, R. K.; Gaskell, S. J. Mass Spectrometry. *Anal. Chem.* **1994**, *66* (12), 634–683. https://doi.org/10.1021/ac00084a024.

(85) Ting, M. Y. C.; Yunker, L. P. E.; Chagunda, I. C.; Hatlelid, K.; Vieweg, M.; McIndoe, J. S. A Mechanistic Investigation of the Suzuki Polycondensation Reaction Using MS/MS Methods. *Catal. Sci. Technol.* **2021**, *11* (13), 4406–4416. https://doi.org/10.1039/D1CY00743B.
(86) Vikse, K. L.; Henderson, M. A.; Oliver, A. G.; McIndoe, J. S. Direct Observation of Key Intermediates by Negative-Ion Electrospray Ionisation Mass Spectrometry in Palladium-Catalysed Cross-Coupling. *Chem. Commun.* **2010**, *46* (39), 7412–7414. https://doi.org/10.1039/C0CC02773A.
(87) *Mass Spectrometry in Polymer Chemistry*; Barner-Kowollik, C., Gruendling, T., Falkenhagen, J., Weidner, S., Eds.; Wiley-VCH: Weinheim, 2012.
(88) Wesdemiotis, C.; Williams-Pavlantos, K. N.; Keating, A. R.; McGee, A. S.; Bochenek, C. Mass Spectrometry of Polymers: A Tutorial Review. *Mass Spectrom. Rev.* **2024**, *43* (3), 427–476. https://doi.org/10.1002/mas.21844.
(89) Yunker, L. P. E.; Donnecke, S.; Ting, M.; Yeung, D.; McIndoe, J. S. PythoMS: A Python Framework To Simplify and Assist in the Processing and Interpretation of Mass Spectrometric Data. *J. Chem. Inf. Model.* **2019**, *59* (4), 1295–1300. https://doi.org/10.1021/acs.jcim.9b00055.
(90) McFarlane, J.; Henderson, B.; Donnecke, S.; McIndoe, J. S. An Information-Rich Graphical Representation of Catalytic Cycles. *Organometallics* **2019**, *38* (21), 4051–4053. https://doi.org/10.1021/acs.organomet.9b00563.
(91) Williams, P. J. H.; Chagunda, I. C.; McIndoe, J. S. OptiMS: An Accessible Program for Automating Mass Spectrometry Parameter Optimization and Configuration. *J. Am. Soc. Mass Spectrom.* **2024**, *35* (3), 449–455. https://doi.org/10.1021/jasms.3c00354.
(92) Williams, P. J. H.; Killeen, C.; Chagunda, I. C.; Henderson, B.; Donnecke, S.; Munro, W.; Sidhu, J.; Kraft, D.; Harrington, D. A.; McIndoe, J. S. Continuous Addition Kinetic Elucidation: Catalyst and Reactant Order, Rate Constant, and Poisoning from a Single Experiment. *Chem. Sci.* **2023**, *14* (36), 9970–9977. https://doi.org/10.1039/D3SC02698A.
(93) Kostyukovich, A. Y.; Tsedilin, A. M.; Sushchenko, E. D.; Eremin, D. B.; Kashin, A. S.; Topchiy, M. A.; Asachenko, A. F.; Nechaev, M. S.; Ananikov, V. P. In Situ Transformations of Pd/NHC Complexes with N-Heterocyclic Carbene Ligands of Different Nature into Colloidal Pd Nanoparticles. *Inorg. Chem. Front.* **2019**, *6* (2), 482–492. https://doi.org/10.1039/C8QI01095A.
(94) Fukazawa, Y.; Vaganov, V. Yu.; Burykina, J. V.; Fakhrutdinov, A. N.; Safiullin, R. I.; Plasser, F.; Rubtsov, A. E.; Ananikov, V. P.; Malkov, A. V. Mechanistic Insight into Palladium-Catalyzed Asymmetric Alkylation of Indoles with Diazoesters Employing Bipyridine-N,N'-Dioxides as Chiral Controllers. *Adv. Synth. Catal.* **2024**, *366* (1), 121–133. https://doi.org/10.1002/adsc.202300845.
(95) Kolter, M.; Koszinowski, K. Formation of Transient Anionic Metal Clusters in Palladium/Diene-Catalyzed Cross-Coupling Reactions. *Chem. – Eur. J.* **2019**, *25* (58), 13376–13384. https://doi.org/10.1002/chem.201902610.
(96) Sorribes, I.; Wienhöfer, G.; Vicent, C.; Junge, K.; Llusar, R.; Beller, M. Chemoselective Transfer Hydrogenation to Nitroarenes Mediated by Cubane-Type Mo3S4 Cluster Catalysts. *Angew. Chem. Int. Ed.* **2012**, *51* (31), 7794–7798. https://doi.org/10.1002/anie.201202584.
(97) Mack, J. B. C.; Walker, K. L.; Robinson, S. G.; Zare, R. N.; Sigman, M. S.; Waymouth, R. M.; Du Bois, J. Mechanistic Study of Ruthenium-Catalyzed C–H Hydroxylation Reveals an Unexpected Pathway for Catalyst Arrest. *J. Am. Chem. Soc.* **2019**, *141* (2), 972–980. https://doi.org/10.1021/jacs.8b10950.
(98) Hua, X.; Masson-Makdissi, J.; Sullivan, R. J.; Newman, S. G. Inherent vs Apparent Chemoselectivity in the Kumada–Corriu Cross-Coupling Reaction. *Org. Lett.* **2016**, *18* (20), 5312–5315. https://doi.org/10.1021/acs.orglett.6b02631.

(99) Pape, J.; Vikse, K. L.; Janusson, E.; Taylor, N.; McIndoe, J. S. Solvent Effects on Surface Activity of Aggregate Ions in Electrospray Ionization. *Int. J. Mass Spectrom.* **2014**, *373*, 66–71. https://doi.org/10.1016/j.ijms.2014.09.009.
(100) Omari, I.; Randhawa, P.; Randhawa, J.; Yu, J.; McIndoe, J. S. Structure, Anion, and Solvent Effects on Cation Response in ESI-MS. *J. Am. Soc. Mass Spectrom.* **2019**, *30* (9), 1750–1757. https://doi.org/10.1007/s13361-019-02252-0.
(101) Sato, Y.; Liu, J.; Ndukwe, I. E.; Silva Elipe, M. V.; Griffin, D. J.; Murray, J. I.; Hein, J. E. Liquid/Liquid Heterogeneous Reaction Monitoring: Insights into Biphasic Suzuki-Miyaura Cross-Coupling. *Chem Catal.* **2023**, *3* (7), 100687. https://doi.org/10.1016/j.checat.2023.100687.
(102) Johansson Seechurn, C. C. C.; Kitching, M. O.; Colacot, T. J.; Snieckus, V. Palladium-Catalyzed Cross-Coupling: A Historical Contextual Perspective to the 2010 Nobel Prize. *Angew. Chem. Int. Ed.* **2012**, *51* (21), 5062–5085. https://doi.org/10.1002/anie.201107017.
(103) Heck, R. F. Aromatic Haloethylation with Palladium and Copper Halides. *J. Am. Chem. Soc.* **1968**, *90* (20), 5538–5542. https://doi.org/10.1021/ja01022a038.
(104) Mizoroki, T.; Mori, K.; Ozaki, A. Arylation of Olefin with Aryl Iodide Catalyzed by Palladium. *Bull. Chem. Soc. Jpn.* **1971**, *44* (2), 581–581. https://doi.org/10.1246/bcsj.44.581.
(105) Heck, R. F.; Nolley, J. P. Palladium-Catalyzed Vinylic Hydrogen Substitution Reactions with Aryl, Benzyl, and Styryl Halides. *J. Org. Chem.* **1972**, *37* (14), 2320–2322. https://doi.org/10.1021/jo00979a024.
(106) Corriu, R. J. P.; Masse, J. P. Activation of Grignard Reagents by Transition-Metal Complexes. A New and Simple Synthesis of Trans-Stilbenes and Polyphenyls. *J. Chem. Soc. Chem. Commun.* **1972**, No. 3, 144a–144a. https://doi.org/10.1039/C3972000144A.
(107) Tamao, K.; Sumitani, K.; Kumada, M. Selective Carbon-Carbon Bond Formation by Cross-Coupling of Grignard Reagents with Organic Halides. Catalysis by Nickel-Phosphine Complexes. *J. Am. Chem. Soc.* **1972**, *94* (12), 4374–4376. https://doi.org/10.1021/ja00767a075.
(108) Yamamura, M.; Moritani, I.; Murahashi, S.-I. The Reaction of σ-Vinylpalladium Complexes with Alkyllithiums. Stereospecific Syntheses of Olefins from Vinyl Halides and Alkyllithiums. *J. Organomet. Chem.* **1975**, *91* (2), C39–C42. https://doi.org/10.1016/S0022-328X(00)89636-9.
(109) Sonogashira, K.; Tohda, Y.; Hagihara, N. A Convenient Synthesis of Acetylenes: Catalytic Substitutions of Acetylenic Hydrogen with Bromoalkenes, Iodoarenes and Bromopyridines. *Tetrahedron Lett.* **1975**, *16* (50), 4467–4470. https://doi.org/10.1016/S0040-4039(00)91094-3.
(110) Chinchilla, R.; Nájera, C. The Sonogashira Reaction: A Booming Methodology in Synthetic Organic Chemistry. *Chem. Rev.* **2007**, *107* (3), 874–922. https://doi.org/10.1021/cr050992x.
(111) Gazvoda, M.; Virant, M.; Pinter, B.; Košmrlj, J. Mechanism of Copper-Free Sonogashira Reaction Operates through Palladium-Palladium Transmetallation. *Nat. Commun.* **2018**, *9* (1), 4814. https://doi.org/10.1038/s41467-018-07081-5.
(112) Negishi, E.; King, A. O.; Okukado, N. Selective Carbon-Carbon Bond Formation via Transition Metal Catalysis. 3. A Highly Selective Synthesis of Unsymmetrical Biaryls and Diarylmethanes by the Nickel- or Palladium-Catalyzed Reaction of Aryl- and Benzylzinc Derivatives with Aryl Halides. *J. Org. Chem.* **1977**, *42* (10), 1821–1823. https://doi.org/10.1021/jo00430a041.
(113) Negishi, E. Palladium- or Nickel-Catalyzed Cross Coupling. A New Selective Method for Carbon-Carbon Bond Formation. *Acc. Chem. Res.* **1982**, *15* (11), 340–348. https://doi.org/10.1021/ar00083a001.
(114) Haas, D.; Hammann, J. M.; Greiner, R.; Knochel, P. Recent Developments in Negishi Cross-Coupling Reactions. *ACS Catal.* **2016**, *6* (3), 1540–1552. https://doi.org/10.1021/acscatal.5b02718.
(115) Kosugi, M.; Fugami, K. A Historical Note of the Stille Reaction. *J. Organomet. Chem.* **2002**, *653* (1), 50–53. https://doi.org/10.1016/S0022-328X(02)01270-6.

(116) Cochran, J. C. The Stille Reaction (Farina, Vittorio; Krishnamurthy, Venkat; Scott, William J.). *J. Chem. Educ.* **1999**, *76* (10), 1344. https://doi.org/10.1021/ed076p1344.
(117) Kosugi, M.; Shimizu, Y.; Migita, T. Alkylation, Arylation, and Vinylation of Acyl Chlorides by Means of Organotin Compounds in the Presence of Catalytic Amounts of Tetrakis(Triphenylphosphine)Palladium(0). *Chem. Lett.* **1977**, *6* (12), 1423–1424. https://doi.org/10.1246/cl.1977.1423.
(118) Suzuki, A. Carbon–Carbon Bonding Made Easy. *Chem. Commun.* **2005**, No. 38, 4759–4763. https://doi.org/10.1039/B507375H.
(119) Matos, K.; Soderquist, J. A. Alkylboranes in the Suzuki−Miyaura Coupling: Stereochemical and Mechanistic Studies. *J. Org. Chem.* **1998**, *63* (3), 461–470. https://doi.org/10.1021/jo971681s.
(120) Braga, A. A. C.; Morgon, N. H.; Ujaque, G.; Maseras, F. Computational Characterization of the Role of the Base in the Suzuki−Miyaura Cross-Coupling Reaction. *J. Am. Chem. Soc.* **2005**, *127* (25), 9298–9307. https://doi.org/10.1021/ja050583i.
(121) Hatanaka, Y.; Hiyama, T. Cross-Coupling of Organosilanes with Organic Halides Mediated by a Palladium Catalyst and Tris(Diethylamino)Sulfonium Difluorotrimethylsilicate. *J. Org. Chem.* **1988**, *53* (4), 918–920. https://doi.org/10.1021/jo00239a056.
(122) Denmark, S. E.; Choi, J. Y. Highly Stereospecific, Cross-Coupling Reactions of Alkenylsilacyclobutanes. *J. Am. Chem. Soc.* **1999**, *121* (24), 5821–5822. https://doi.org/10.1021/ja9908117.
(123) Hartwig, J. F. Transition Metal Catalyzed Synthesis of Arylamines and Aryl Ethers from Aryl Halides and Triflates: Scope and Mechanism. *Angew. Chem. Int. Ed.* **1998**, *37* (15), 2046–2067. https://doi.org/10.1002/(SICI)1521-3773(19980817)37:15<2046::AID-ANIE2046>3.0.CO;2-L.
(124) Ruiz-Castillo, P.; Buchwald, S. L. Applications of Palladium-Catalyzed C–N Cross-Coupling Reactions. *Chem. Rev.* **2016**, *116* (19), 12564–12649. https://doi.org/10.1021/acs.chemrev.6b00512.
(125) Forero-Cortés, P. A.; Haydl, A. M. The 25th Anniversary of the Buchwald–Hartwig Amination: Development, Applications, and Outlook. *Org. Process Res. Dev.* **2019**, *23* (8), 1478–1483. https://doi.org/10.1021/acs.oprd.9b00161.
(126) Brown, D. G.; Boström, J. Analysis of Past and Present Synthetic Methodologies on Medicinal Chemistry: Where Have All the New Reactions Gone? *J. Med. Chem.* **2016**, *59* (10), 4443–4458. https://doi.org/10.1021/acs.jmedchem.5b01409.
(127) Gildner, P. G.; Colacot, T. J. Reactions of the 21st Century: Two Decades of Innovative Catalyst Design for Palladium-Catalyzed Cross-Couplings. *Organometallics* **2015**, *34* (23), 5497–5508. https://doi.org/10.1021/acs.organomet.5b00567.
(128) Nicolaou, K. C.; Bulger, P. G.; Sarlah, D. Palladium-Catalyzed Cross-Coupling Reactions in Total Synthesis. *Angew. Chem. Int. Ed.* **2005**, *44* (29), 4442–4489. https://doi.org/10.1002/anie.200500368.
(129) Burke, A. J.; Marques, C. S.; Turner, N. J.; Hermann, G. J. Catalytic Cross-Coupling Reactions – Nobel Prize Catalysis. In *Active Pharmaceutical Ingredients in Synthesis*; John Wiley & Sons, Ltd, 2018; pp 175–257. https://doi.org/10.1002/9783527807253.ch6.
(130) Campeau, L.-C.; Hazari, N. Cross-Coupling and Related Reactions: Connecting Past Success to the Development of New Reactions for the Future. *Organometallics* **2019**, *38* (1), 3–35. https://doi.org/10.1021/acs.organomet.8b00720.
(131) Amatore, C.; Le Duc, G.; Jutand, A. Mechanism of Palladium-Catalyzed Suzuki–Miyaura Reactions: Multiple and Antagonistic Roles of Anionic "Bases" and Their Countercations. *Chem. – Eur. J.* **2013**, *19* (31), 10082–10093. https://doi.org/10.1002/chem.201300177.
(132) P. Knowles, J.; Whiting, A. The Heck–Mizoroki Cross-Coupling Reaction: A Mechanistic Perspective. *Org. Biomol. Chem.* **2007**, *5* (1), 31–44. https://doi.org/10.1039/B611547K.

(133) D'Alterio, M. C.; Casals-Cruañas, È.; Tzouras, N. V.; Talarico, G.; Nolan, S. P.; Poater, A. Mechanistic Aspects of the Palladium-Catalyzed Suzuki-Miyaura Cross-Coupling Reaction. *Chem. – Eur. J.* **2021**, *27* (54), 13481–13493. https://doi.org/10.1002/chem.202101880.
(134) Sehnal, P.; Taylor, R. J. K.; Fairlamb, I. J. S. Emergence of Palladium(IV) Chemistry in Synthesis and Catalysis. *Chem. Rev.* **2010**, *110* (2), 824–889. https://doi.org/10.1021/cr9003242.
(135) Vicente-Hernández, I.; Chicote, M.-T.; Vicente, J.; Bautista, D. A New Type of Oxidative Addition of an Iodoarene to a Pd(II) Complex. *Chem. Commun.* **2015**, *52* (3), 594–596. https://doi.org/10.1039/C5CC07698F.
(136) Ahmadvand, Z.; Bayat, M.; Zolfigol, M. A. Toward Prediction of the Precatalyst Activation Mechanism through the Cross-Coupling Reactions: Reduction of Pd(II) to Pd(0) in Precatalyst of the Type Pd-PEPPSI. *J. Comput. Chem.* **2020**, *41* (26), 2296–2309. https://doi.org/10.1002/jcc.26393.
(137) Lau, S. H.; Chen, L.; Kevlishvili, I.; Davis, K.; Liu, P.; Carrow, B. Capturing the Most Active State of a Palladium(0) Cross-Coupling Catalyst. ChemRxiv October 13, 2021. https://doi.org/10.26434/chemrxiv-2021-477kn.
(138) Christmann, U.; Vilar, R. Monoligated Palladium Species as Catalysts in Cross-Coupling Reactions. *Angew. Chem. Int. Ed.* **2005**, *44* (3), 366–374. https://doi.org/10.1002/anie.200461189.
(139) Zheng, Q.; Liu, Y.; Chen, Q.; Hu, M.; Helmy, R.; Sherer, E. C.; Welch, C. J.; Chen, H. Capture of Reactive Monophosphine-Ligated Palladium(0) Intermediates by Mass Spectrometry. *J. Am. Chem. Soc.* **2015**, *137* (44), 14035–14038. https://doi.org/10.1021/jacs.5b08905.
(140) Sau, S. C.; Hota, P. K.; Mandal, S. K.; Soleilhavoup, M.; Bertrand, G. Stable Abnormal N-Heterocyclic Carbenes and Their Applications. *Chem. Soc. Rev.* **2020**, *49* (4), 1233–1252. https://doi.org/10.1039/C9CS00866G.
(141) Barder, T. E.; Walker, S. D.; Martinelli, J. R.; Buchwald, S. L. Catalysts for Suzuki–Miyaura Coupling Processes: Scope and Studies of the Effect of Ligand Structure. *J. Am. Chem. Soc.* **2005**, *127* (13), 4685–4696. https://doi.org/10.1021/ja042491j.
(142) Hamann, B. C.; Hartwig, J. F. Sterically Hindered Chelating Alkyl Phosphines Provide Large Rate Accelerations in Palladium-Catalyzed Amination of Aryl Iodides, Bromides, and Chlorides, and the First Amination of Aryl Tosylates. *J. Am. Chem. Soc.* **1998**, *120* (29), 7369–7370. https://doi.org/10.1021/ja981318i.
(143) Weber, P.; Scherpf, T.; Rodstein, I.; Lichte, D.; Scharf, L. T.; Gooßen, L. J.; Gessner, V. H. A Highly Active Ylide-Functionalized Phosphine for Palladium-Catalyzed Aminations of Aryl Chlorides. *Angew. Chem. Int. Ed.* **2019**, *58* (10), 3203–3207. https://doi.org/10.1002/anie.201810696.
(144) Lapointe, S.; Sarbajna, A.; Gessner, V. H. Ylide-Substituted Phosphines: A Platform of Strong Donor Ligands for Gold Catalysis and Palladium-Catalyzed Coupling Reactions. *Acc. Chem. Res.* **2022**, *55* (5), 770–782. https://doi.org/10.1021/acs.accounts.1c00797.
(145) Melvin, P. R.; Balcells, D.; Hazari, N.; Nova, A. Understanding Precatalyst Activation in Cross-Coupling Reactions: Alcohol Facilitated Reduction from Pd(II) to Pd(0) in Precatalysts of the Type (H3-Allyl)Pd(L)(Cl) and (H3-Indenyl)Pd(L)(Cl). *ACS Catal.* **2015**, *5* (9), 5596–5606. https://doi.org/10.1021/acscatal.5b01291.
(146) Strieter, E. R.; Blackmond, D. G.; Buchwald, S. L. Insights into the Origin of High Activity and Stability of Catalysts Derived from Bulky, Electron-Rich Monophosphinobiaryl Ligands in the Pd-Catalyzed C–N Bond Formation. *J. Am. Chem. Soc.* **2003**, *125* (46), 13978–13980. https://doi.org/10.1021/ja037932y.
(147) DeAngelis, A. J.; Gildner, P. G.; Chow, R.; Colacot, T. J. Generating Active "L-Pd(0)" via Neutral or Cationic π-Allylpalladium Complexes Featuring Biaryl/Bipyrazolylphosphines: Synthetic,

Mechanistic, and Structure–Activity Studies in Challenging Cross-Coupling Reactions. *J. Org. Chem.* **2015**, *80* (13), 6794–6813. https://doi.org/10.1021/acs.joc.5b01005.
(148) Weber, P.; Biafora, A.; Doppiu, A.; Bongard, H.-J.; Kelm, H.; Gooßen, L. J. A Comparative Study of Dibenzylideneacetone Palladium Complexes in Catalysis. *Org. Process Res. Dev.* **2019**, *23* (7), 1462–1470. https://doi.org/10.1021/acs.oprd.9b00214.
(149) Zalesskiy, S. S.; Ananikov, V. P. Pd2(Dba)3 as a Precursor of Soluble Metal Complexes and Nanoparticles: Determination of Palladium Active Species for Catalysis and Synthesis. *Organometallics* **2012**, *31* (6), 2302–2309. https://doi.org/10.1021/om201217r.
(150) Appleby, K. M.; Dzotsi, E.; Scott, N. W. J.; Dexin, G.; Jeddi, N.; Whitwood, A. C.; Pridmore, N. E.; Hart, S.; Duckett, S. B.; Fairlamb, I. J. S. Bridging the Gap from Mononuclear Pd^{II} Precatalysts to Pd Nanoparticles: Identification of Intermediate Linear $[Pd_3(XPh_3)_4]^{2+}$ Clusters as Catalytic Species for Suzuki–Miyaura Couplings (X = P, As). *Organometallics* **2021**, *40* (21), 3560–3570. https://doi.org/10.1021/acs.organomet.1c00452.
(151) Scott, N. W. J.; Ford, M. J.; Husbands, D. R.; Whitwood, A. C.; Fairlamb, I. J. S. Reactivity of a Dinuclear PdI Complex $[Pd_2(\mu\text{-}PPh_2)(\mu_2\text{-}OAc)(PPh_3)_2]$ with PPh_3: Implications for Cross-Coupling Catalysis Using the Ubiquitous $Pd(OAc)_2/nPPh_3$ Catalyst System. *Organometallics* **2021**, *40* (17), 2995–3002. https://doi.org/10.1021/acs.organomet.1c00347.
(152) Scott, N. W. J.; Ford, M. J.; Jeddi, N.; Eyles, A.; Simon, L.; Whitwood, A. C.; Tanner, T.; Willans, C. E.; Fairlamb, I. J. S. A Dichotomy in Cross-Coupling Site Selectivity in a Dihalogenated Heteroarene: Influence of Mononuclear Pd, Pd Clusters, and Pd Nanoparticles—the Case for Exploiting Pd Catalyst Speciation. *J. Am. Chem. Soc.* **2021**, *143* (25), 9682–9693. https://doi.org/10.1021/jacs.1c05294.
(153) Scott, N. W. J.; Ford, M. J.; Schotes, C.; Parker, R. R.; Whitwood, A. C.; Fairlamb, I. J. S. The Ubiquitous Cross-Coupling Catalyst System 'Pd(OAc)2'/2PPh3 Forms a Unique Dinuclear PdI Complex: An Important Entry Point into Catalytically Competent Cyclic Pd3 Clusters. *Chem. Sci.* **2019**, *10* (34), 7898–7906. https://doi.org/10.1039/C9SC01847F.
(154) Wei, C. S.; Davies, G. H. M.; Soltani, O.; Albrecht, J.; Gao, Q.; Pathirana, C.; Hsiao, Y.; Tummala, S.; Eastgate, M. D. The Impact of Palladium(II) Reduction Pathways on the Structure and Activity of Palladium(0) Catalysts. *Angew. Chem. Int. Ed.* **2013**, *52* (22), 5822–5826. https://doi.org/10.1002/anie.201210252.
(155) Vikse, K.; Naka, T.; McIndoe, J. S.; Besora, M.; Maseras, F. Oxidative Additions of Aryl Halides to Palladium Proceed through the Monoligated Complex. *ChemCatChem* **2013**, *5* (12), 3604–3609. https://doi.org/10.1002/cctc.201300723.
(156) Scharf, L. T.; Rodstein, I.; Schmidt, M.; Scherpf, T.; Gessner, V. H. Unraveling the High Activity of Ylide-Functionalized Phosphines in Palladium-Catalyzed Amination Reactions: A Comparative Study with CyJohnPhos and PtBu3. *ACS Catal.* **2020**, *10* (2), 999–1009. https://doi.org/10.1021/acscatal.9b04666.
(157) Niemeyer, Z. L.; Milo, A.; Hickey, D. P.; Sigman, M. S. Parameterization of Phosphine Ligands Reveals Mechanistic Pathways and Predicts Reaction Outcomes. *Nat. Chem.* **2016**, *8* (6), 610–617. https://doi.org/10.1038/nchem.2501.
(158) Besora, M.; Maseras, F. The Diverse Mechanisms for the Oxidative Addition of C–Br Bonds to Pd(PR3) and Pd(PR3)2 Complexes. *Dalton Trans.* **2019**, *48* (43), 16242–16248. https://doi.org/10.1039/C9DT03155C.
(159) Norman, J. P.; Larson, N. G.; Neufeldt, S. R. Different Oxidative Addition Mechanisms for 12- and 14-Electron Palladium(0) Explain Ligand-Controlled Divergent Site Selectivity. *ACS Catal.* **2022**, *12* (15), 8822–8828. https://doi.org/10.1021/acscatal.2c01698.
(160) Kania, M. J.; Reyes, A.; Neufeldt, S. R. Oxidative Addition of (Hetero)Aryl (Pseudo)Halides at Palladium(0): Origin and Significance of Divergent Mechanisms. *J. Am. Chem. Soc.* **2024**, *146* (28), 19249–19260. https://doi.org/10.1021/jacs.4c04496.

(161) Firsan, S. J.; Sivakumar, V.; Colacot, T. J. Emerging Trends in Cross-Coupling: Twelve-Electron-Based L1Pd(0) Catalysts, Their Mechanism of Action, and Selected Applications. *Chem. Rev.* **2022**, *122* (23), 16983–17027. https://doi.org/10.1021/acs.chemrev.2c00204.
(162) Biscoe, M. R.; Fors, B. P.; Buchwald, S. L. A New Class of Easily Activated Palladium Precatalysts for Facile C–N Cross-Coupling Reactions and the Low Temperature Oxidative Addition of Aryl Chlorides. *J. Am. Chem. Soc.* **2008**, *130* (21), 6686–6687. https://doi.org/10.1021/ja801137k.
(163) Bruno, N. C.; Tudge, M. T.; Buchwald, S. L. Design and Preparation of New Palladium Precatalysts for C–C and C–N Cross-Coupling Reactions. *Chem. Sci.* **2013**, *4* (3), 916–920. https://doi.org/10.1039/C2SC20903A.
(164) Bruneau, A.; Roche, M.; Alami, M.; Messaoudi, S. 2-Aminobiphenyl Palladacycles: The "Most Powerful" Precatalysts in C–C and C–Heteroatom Cross-Couplings. *ACS Catal.* **2015**, *5* (2), 1386–1396. https://doi.org/10.1021/cs502011x.
(165) Barnett, K. L.; Howard, J. R.; Treager, C. J.; Shipley, A. T.; Stullich, R. M.; Qu, F.; Gerlach, D. L.; Shaughnessy, K. H. Air-Stable [(R3P)PdCl2]2 Complexes of Neopentylphosphines as Cross-Coupling Precatalysts: Catalytic Application and Mechanism of Catalyst Activation and Deactivation. *Organometallics* **2018**, *37* (9), 1410–1424. https://doi.org/10.1021/acs.organomet.8b00082.
(166) Shaughnessy, K. H. Development of Palladium Precatalysts That Efficiently Generate LPd(0) Active Species. *Isr. J. Chem.* **2020**, *60* (3–4), 180–194. https://doi.org/10.1002/ijch.201900067.
(167) Hill, L. L.; Crowell, J. L.; Tutwiler, S. L.; Massie, N. L.; Hines, C. C.; Griffin, S. T.; Rogers, R. D.; Shaughnessy, K. H.; Grasa, G. A.; Johansson Seechurn, C. C. C.; Li, H.; Colacot, T. J.; Chou, J.; Woltermann, C. J. Synthesis and X-Ray Structure Determination of Highly Active Pd(II), Pd(I), and Pd(0) Complexes of Di(Tert-Butyl)Neopentylphosphine (DTBNpP) in the Arylation of Amines and Ketones. *J. Org. Chem.* **2010**, *75* (19), 6477–6488. https://doi.org/10.1021/jo101187q.
(168) Johansson Seechurn, C. C. C.; Parisel, S. L.; Colacot, T. J. Air-Stable Pd(R-Allyl)LCl (L= Q-Phos, P(t-Bu)3, Etc.) Systems for C–C/N Couplings: Insight into the Structure–Activity Relationship and Catalyst Activation Pathway. *J. Org. Chem.* **2011**, *76* (19), 7918–7932. https://doi.org/10.1021/jo2013324.
(169) Hruszkewycz, D. P.; Balcells, D.; Guard, L. M.; Hazari, N.; Tilset, M. Insight into the Efficiency of Cinnamyl-Supported Precatalysts for the Suzuki–Miyaura Reaction: Observation of Pd(I) Dimers with Bridging Allyl Ligands During Catalysis. *J. Am. Chem. Soc.* **2014**, *136* (20), 7300–7316. https://doi.org/10.1021/ja412565c.
(170) Melvin, P. R.; Nova, A.; Balcells, D.; Dai, W.; Hazari, N.; Hruszkewycz, D. P.; Shah, H. P.; Tudge, M. T. Design of a Versatile and Improved Precatalyst Scaffold for Palladium-Catalyzed Cross-Coupling: (H3-1-tBu-Indenyl)2(μ-Cl)2Pd2. *ACS Catal.* **2015**, *5* (6), 3680–3688. https://doi.org/10.1021/acscatal.5b00878.
(171) Nasielski, J.; Hadei, N.; Achonduh, G.; Kantchev, E. A. B.; O'Brien, C. J.; Lough, A.; Organ, M. G. Structure–Activity Relationship Analysis of Pd–PEPPSI Complexes in Cross-Couplings: A Close Inspection of the Catalytic Cycle and the Precatalyst Activation Model. *Chem. – Eur. J.* **2010**, *16* (35), 10844–10853. https://doi.org/10.1002/chem.201000138.
(172) Rio, J.; Liang, H.; Perrin, M.-E. L.; Perego, L. A.; Grimaud, L.; Payard, P.-A. We Already Know Everything about Oxidative Addition to Pd(0): Do We? *ACS Catal.* **2023**, *13* (17), 11399–11421. https://doi.org/10.1021/acscatal.3c01943.
(173) Labinger, J. A. Tutorial on Oxidative Addition. *Organometallics* **2015**, *34* (20), 4784–4795. https://doi.org/10.1021/acs.organomet.5b00565.
(174) Bickelhaupt, F. M.; Ziegler, T. Oxidative Insertion as Frontside SN2 Substitution: A Theoretical Study of the Model Reaction System Pd + CH3Cl. *Organometallics* **1995**, *14* (5), 2288–2296. https://doi.org/10.1021/om00005a030.

(175) de Jong, G. T.; Bickelhaupt, F. M. Catalytic Carbon–Halogen Bond Activation: Trends in Reactivity, Selectivity, and Solvation. *J. Chem. Theory Comput.* **2007**, *3* (2), 514–529. https://doi.org/10.1021/ct600342j.
(176) Vermeeren, P.; Sun, X.; Bickelhaupt, F. M. Arylic C–X Bond Activation by Palladium Catalysts: Activation Strain Analyses of Reactivity Trends. *Sci. Rep.* **2018**, *8* (1), 10729. https://doi.org/10.1038/s41598-018-28998-3.
(177) Köhler, K.; Wussow, K.; Wirth, A. S. Palladium-Catalyzed Cross-Coupling Reactions – A General Introduction. In *Palladium-Catalyzed Coupling Reactions*; John Wiley & Sons, Ltd, 2013; pp 1–30. https://doi.org/10.1002/9783527648283.ch1.
(178) Hansen, T.; Sun, X.; Dalla Tiezza, M.; van Zeist, W.-J.; van Stralen, J. N. P.; Geerke, D. P.; Wolters, L. P.; Poater, J.; Hamlin, T. A.; Bickelhaupt, F. M. C–X Bond Activation by Palladium: Steric Shielding versus Steric Attraction. *Chem. – Eur. J.* **2022**, *28* (44), e202201093. https://doi.org/10.1002/chem.202201093.
(179) Schoenebeck, F.; Houk, K. N. Ligand-Controlled Regioselectivity in Palladium-Catalyzed Cross Coupling Reactions. *J. Am. Chem. Soc.* **2010**, *132* (8), 2496–2497. https://doi.org/10.1021/ja9077528.
(180) Newman-Stonebraker, S. H.; Wang, J. Y.; Jeffrey, P. D.; Doyle, A. G. Structure–Reactivity Relationships of Buchwald-Type Phosphines in Nickel-Catalyzed Cross-Couplings. *J. Am. Chem. Soc.* **2022**, *144* (42), 19635–19648. https://doi.org/10.1021/jacs.2c09840.
(181) Newman-Stonebraker, S. H.; Smith, S. R.; Borowski, J. E.; Peters, E.; Gensch, T.; Johnson, H. C.; Sigman, M. S.; Doyle, A. G. Univariate Classification of Phosphine Ligation State and Reactivity in Cross-Coupling Catalysis. *Science* **2021**, *374* (6565), 301–308. https://doi.org/10.1126/science.abj4213.
(182) Johansson Seechurn, C. C. C.; Sperger, T.; Scrase, T. G.; Schoenebeck, F.; Colacot, T. J. Understanding the Unusual Reduction Mechanism of Pd(II) to Pd(I): Uncovering Hidden Species and Implications in Catalytic Cross-Coupling Reactions. *J. Am. Chem. Soc.* **2017**, *139* (14), 5194–5200. https://doi.org/10.1021/jacs.7b01110.
(183) Hills, I. D.; Netherton, M. R.; Fu, G. C. Toward an Improved Understanding of the Unusual Reactivity of Pd0/Trialkylphosphane Catalysts in Cross-Couplings of Alkyl Electrophiles: Quantifying the Factors That Determine the Rate of Oxidative Addition. *Angew. Chem. Int. Ed.* **2003**, *42* (46), 5749–5752. https://doi.org/10.1002/anie.200352858.
(184) Barrios-Landeros, F.; Carrow, B. P.; Hartwig, J. F. Effect of Ligand Steric Properties and Halide Identity on the Mechanism for Oxidative Addition of Haloarenes to Trialkylphosphine Pd(0) Complexes. *J. Am. Chem. Soc.* **2009**, *131* (23), 8141–8154. https://doi.org/10.1021/ja900798s.
(185) Widenhoefer, R. A.; Zhong, H. A.; Buchwald, S. L. Synthesis and Solution Structure of Palladium Tris(o-Tolyl)Phosphine Mono(Amine) Complexes. *Organometallics* **1996**, *15* (12), 2745–2754. https://doi.org/10.1021/om9509599.
(186) Lee, H. G.; Milner, P. J.; Buchwald, S. L. Pd-Catalyzed Nucleophilic Fluorination of Aryl Bromides. *J. Am. Chem. Soc.* **2014**, *136* (10), 3792–3795. https://doi.org/10.1021/ja5009739.
(187) McCann, S. D.; Reichert, E. C.; Arrechea, P. L.; Buchwald, S. L. Development of an Aryl Amination Catalyst with Broad Scope Guided by Consideration of Catalyst Stability. *J. Am. Chem. Soc.* **2020**, *142* (35), 15027–15037. https://doi.org/10.1021/jacs.0c06139.
(188) Dennis, J. M.; White, N. A.; Liu, R. Y.; Buchwald, S. L. Pd-Catalyzed C–N Coupling Reactions Facilitated by Organic Bases: Mechanistic Investigation Leads to Enhanced Reactivity in the Arylation of Weakly Binding Amines. *ACS Catal.* **2019**, *9* (5), 3822–3830. https://doi.org/10.1021/acscatal.9b00981.
(189) Hu, H.; Qu, F.; Gerlach, D. L.; Shaughnessy, K. H. Mechanistic Study of the Role of Substrate Steric Effects and Aniline Inhibition on the Bis(Trineopentylphosphine)Palladium(0)-Catalyzed

Arylation of Aniline Derivatives. *ACS Catal.* **2017**, *7* (4), 2516–2527. https://doi.org/10.1021/acscatal.7b00024.
(190) Ingoglia, B. T.; Buchwald, S. L. Oxidative Addition Complexes as Precatalysts for Cross-Coupling Reactions Requiring Extremely Bulky Biarylphosphine Ligands. *Org. Lett.* **2017**, *19* (11), 2853–2856. https://doi.org/10.1021/acs.orglett.7b01082.
(191) Timsina, Y. N.; Xu, G.; Colacot, T. J. It Is Not All about the Ligands: Exploring the Hidden Potentials of tBu3P through Its Oxidative Addition Complex as the Precatalyst. *ACS Catal.* **2023**, *13* (12), 8106–8118. https://doi.org/10.1021/acscatal.3c01582.
(192) Uehling, M. R.; King, R. P.; Krska, S. W.; Cernak, T.; Buchwald, S. L. Pharmaceutical Diversification via Palladium Oxidative Addition Complexes. *Science* **2019**, *363* (6425), 405–408. https://doi.org/10.1126/science.aac6153.
(193) Elango, V.; Murphy, M. A.; Smith, B. L.; Davenport, K. G.; Mott, G. N.; Zey, E. G.; Moss, G. L. Method for Producing Ibuprofen. US4981995A, January 1, 1991. https://patents.google.com/patent/US4981995A/en (accessed 2025-01-21).
(194) Larsen, R. D.; King, A. O.; Chen, C. Y.; Corley, E. G.; Foster, B. S.; Roberts, F. E.; Yang, C.; Lieberman, D. R.; Reamer, R. A.; Tschaen, D. M.; Verhoeven, T. R.; Reider, P. J.; Lo, Y. S.; Rossano, L. T.; Brookes, A. S.; Meloni, D.; Moore, J. R.; Arnett, J. F. Efficient Synthesis of Losartan, A Nonpeptide Angiotensin II Receptor Antagonist. *J. Org. Chem.* **1994**, *59* (21), 6391–6394. https://doi.org/10.1021/jo00100a048.
(195) Loiseleur, O.; Kaufmann, D.; Abel, S.; Buerger, H. M.; Meisenbach, M.; Schmitz, B.; Sedelmeier, G. N-Phenyl-2-Pyrimidine-Amine Derivatives. WO2003066613A1, August 14, 2003. https://patents.google.com/patent/WO2003066613A1/en (accessed 2025-01-21).
(196) WHO Expert Committee. The Selection and Use of Essential Medicines - 1049, 2024. https://www.who.int/publications/i/item/9789240089266 (accessed 2025-01-21).
(197) Camp, D.; Matthews, C. F.; Neville, S. T.; Rouns, M.; Scott, R. W.; Truong, Y. Development of a Synthetic Process towards a Hepatitis C Polymerase Inhibitor. *Org. Process Res. Dev.* **2006**, *10* (4), 814–821. https://doi.org/10.1021/op0600761.
(198) Davey, P. R. J.; Delouvrié, B.; Dorison-Duval, D.; Germain, H.; Harris, C. S.; Magnien, F.; Ouvry, G.; Tricotet, T. Facile Preparation and Suzuki–Miyaura Cross-Coupling of N-2-Alkylated 2H-1,2,3-Triazole 4-Boronates. *Tetrahedron Lett.* **2012**, *53* (50), 6849–6852. https://doi.org/10.1016/j.tetlet.2012.10.034.
(199) Chung, J. Y. L. Development of a Practical Synthesis of Naphthyridone P38 MAP Kinase Inhibitor MK-0913. In *Transition Metal-Catalyzed Couplings in Process Chemistry*; John Wiley & Sons, Ltd, 2003; pp 39–56. https://doi.org/10.1002/9783527658909.ch04.
(200) Krishna, A.; Lunchev, A. V.; Grimsdale, A. C. Suzuki Polycondensation. In *Synthetic Methods for Conjugated Polymers and Carbon Materials*; John Wiley & Sons, Ltd, 2017; pp 59–95. https://doi.org/10.1002/9783527695959.ch2.
(201) Jiang, K.; Zhang, L.; Zhao, Y.; Lin, J.; Chen, M. Palladium-Catalyzed Cross-Coupling Polymerization: A New Access to Cross-Conjugated Polymers with Modifiable Structure and Tunable Optical/Conductive Properties. *Macromolecules* **2018**, *51* (23), 9662–9668. https://doi.org/10.1021/acs.macromol.8b02163.
(202) Quagliotto, P.; Fin, A. Advances in Synthetic Methods for the Preparation of Poly(3-Hexylthiophene) (P3HT). *Lett. Org. Chem. 15* (12), 991–1006. https://doi.org/10.2174/1570178615666180322150512.
(203) Huang, X.; Wang, X.; Zou, Y.; An, M.; Wang, Y. The Renaissance of Poly(3-Hexylthiophene) as a Promising Hole-Transporting Material Toward Efficient and Stable Perovskite Solar Cells. *Small* **2024**, *20* (38), 2400874. https://doi.org/10.1002/smll.202400874.
(204) Lee, J.; Kim, H.; Park, H.; Kim, T.; Hwang, S.-H.; Seo, D.; Chung, T. D.; Choi, T.-L. Universal Suzuki–Miyaura Catalyst-Transfer Polymerization for Precision Synthesis of Strong

Donor/Acceptor-Based Conjugated Polymers and Their Sequence Engineering. *J. Am. Chem. Soc.* **2021**, *143* (29), 11180–11190. https://doi.org/10.1021/jacs.1c05080.
(205) Devendar, P.; Qu, R.-Y.; Kang, W.-M.; He, B.; Yang, G.-F. Palladium-Catalyzed Cross-Coupling Reactions: A Powerful Tool for the Synthesis of Agrochemicals. *J. Agric. Food Chem.* **2018**, *66* (34), 8914–8934. https://doi.org/10.1021/acs.jafc.8b03792.
(206) Committee for Medicinal Products for Human Use. ICH Guideline Q3D (R2) on Elemental Impurities, 2022. https://www.ema.europa.eu/en/documents/scientific-guideline/international-conference-harmonisation-technical-requirements-registration-pharmaceuticals-human-use-ich-q3d-elemental-impurities-step-5-revision-2_en.pdf (accessed 2025-01-18).
(207) Molnár, Á. Efficient, Selective, and Recyclable Palladium Catalysts in Carbon–Carbon Coupling Reactions. *Chem. Rev.* **2011**, *111* (3), 2251–2320. https://doi.org/10.1021/cr100355b.
(208) Remmel, A. Why Chemists Can't Quit Palladium. *Nature* **2022**, *606* (7914), 448–451. https://doi.org/10.1038/d41586-022-01612-3.
(209) McCarthy, S.; Braddock, D. C.; Wilton-Ely, J. D. E. T. Strategies for Sustainable Palladium Catalysis. *Coord. Chem. Rev.* **2021**, *442*, 213925. https://doi.org/10.1016/j.ccr.2021.213925.
(210) J. Lennox, A. J.; C. Lloyd-Jones, G. Selection of Boron Reagents for Suzuki–Miyaura Coupling. *Chem. Soc. Rev.* **2014**, *43* (1), 412–443. https://doi.org/10.1039/C3CS60197H.
(211) Molander, G. A.; Trice, S. L. J.; Dreher, S. D. Palladium-Catalyzed, Direct Boronic Acid Synthesis from Aryl Chlorides: A Simplified Route to Diverse Boronate Ester Derivatives. *J. Am. Chem. Soc.* **2010**, *132* (50), 17701–17703. https://doi.org/10.1021/ja1089759.
(212) Reeves, E. K.; Entz, E. D.; Neufeldt, S. R. Chemodivergence between Electrophiles in Cross-Coupling Reactions. *Chem. – Eur. J.* **2021**, *27* (20), 6161–6177. https://doi.org/10.1002/chem.202004437.
(213) Dumrath, A.; Lübbe, C.; Beller, M. Palladium-Catalyzed Cross-Coupling Reactions – Industrial Applications. In *Palladium-Catalyzed Coupling Reactions*; John Wiley & Sons, Ltd, 2013; pp 445–489. https://doi.org/10.1002/9783527648283.ch12.
(214) Dorval, C.; Dubois, E.; Bourne-Branchu, Y.; Gosmini, C.; Danoun, G. Sequential Organozinc Formation and Negishi Cross-Coupling of Amides Catalysed by Cobalt Salt. *Adv. Synth. Catal.* **2019**, *361* (8), 1777–1780. https://doi.org/10.1002/adsc.201801577.
(215) Liu, Y.; Li, P.; Wang, Y.; Qiu, Y. Electroreductive Cross-Electrophile Coupling (eXEC) Reactions. *Angew. Chem. Int. Ed.* **2023**, *62* (45), e202306679. https://doi.org/10.1002/anie.202306679.
(216) Hanna, L. E.; Jarvo, E. R. Selective Cross-Electrophile Coupling by Dual Catalysis. *Angew. Chem. Int. Ed.* **2015**, *54* (52), 15618–15620. https://doi.org/10.1002/anie.201509444.
(217) Prat, D.; Hayler, J.; Wells, A. A Survey of Solvent Selection Guides. *Green Chem.* **2014**, *16* (10), 4546–4551. https://doi.org/10.1039/C4GC01149J.
(218) Azzena, U.; Carraro, M.; Pisano, L.; Monticelli, S.; Bartolotta, R.; Pace, V. Cyclopentyl Methyl Ether: An Elective Ecofriendly Ethereal Solvent in Classical and Modern Organic Chemistry. *ChemSusChem* **2019**, *12* (1), 40–70. https://doi.org/10.1002/cssc.201801768.
(219) Watanabe, K.; Yamagiwa, N.; Torisawa, Y. Cyclopentyl Methyl Ether as a New and Alternative Process Solvent. *Org. Process Res. Dev.* **2007**, *11* (2), 251–258. https://doi.org/10.1021/op0680136.
(220) Granato, A. V.; Santos, A. G.; dos Santos, E. N. P-Cymene as Solvent for Olefin Metathesis: Matching Efficiency and Sustainability. *ChemSusChem* **2017**, *10* (8), 1832–1837. https://doi.org/10.1002/cssc.201700116.
(221) Lei, P.; Mu, Y.; Wang, Y.; Wang, Y.; Ma, Z.; Feng, J.; Liu, X.; Szostak, M. Green Solvent Selection for Suzuki–Miyaura Coupling of Amides. *ACS Sustain. Chem. Eng.* **2021**, *9* (1), 552–559. https://doi.org/10.1021/acssuschemeng.0c08044.

(222) Schäffner, B.; Holz, J.; Verevkin, S. P.; Börner, A. Organic Carbonates as Alternative Solvents for Palladium-Catalyzed Substitution Reactions. *ChemSusChem* **2008**, *1* (3), 249–253. https://doi.org/10.1002/cssc.200700142.
(223) Roger, J.; Verrier, C.; Le Goff, R.; Hoarau, C.; Doucet, H. Carbonates: Ecofriendly Solvents for Palladium-Catalyzed Direct 2-Arylation of Oxazole Derivatives. *ChemSusChem* **2009**, *2* (10), 951–956. https://doi.org/10.1002/cssc.200900148.
(224) Miao, X.; Fischmeister, C.; Bruneau, C.; Dixneuf, P. H. Dimethyl Carbonate: An Eco-Friendly Solvent in Ruthenium-Catalyzed Olefin Metathesis Transformations. *ChemSusChem* **2008**, *1* (10), 813–816. https://doi.org/10.1002/cssc.200800074.
(225) Kitanosono, T.; Masuda, K.; Xu, P.; Kobayashi, S. Catalytic Organic Reactions in Water toward Sustainable Society. *Chem. Rev.* **2018**, *118* (2), 679–746. https://doi.org/10.1021/acs.chemrev.7b00417.
(226) Jimenez-Gonzalez, C.; Ponder, C. S.; Broxterman, Q. B.; Manley, J. B. Using the Right Green Yardstick: Why Process Mass Intensity Is Used in the Pharmaceutical Industry To Drive More Sustainable Processes. *Org. Process Res. Dev.* **2011**, *15* (4), 912–917. https://doi.org/10.1021/op200097d.
(227) Sheldon, R. A. The E Factor 25 Years on: The Rise of Green Chemistry and Sustainability. *Green Chem.* **2017**, *19* (1), 18–43. https://doi.org/10.1039/C6GC02157C.
(228) Albéniz, A. C.; Carrera, N. Polymers for Green C–C Couplings. *Eur. J. Inorg. Chem.* **2011**, *2011* (15), 2347–2360. https://doi.org/10.1002/ejic.201100162.
(229) Karimi, B.; Abedi, S.; Zamani, A. Coupling Reactions Induced by Polymer-Supported Catalysts. In *Palladium-Catalyzed Coupling Reactions*; John Wiley & Sons, Ltd, 2013; pp 141–200. https://doi.org/10.1002/9783527648283.ch5.
(230) Markovič, M.; Lopatka, P.; Gracza, T.; Koóš, P. Recent Applications of Continuous Flow in Homogeneous Palladium Catalysis. *Synthesis* **2020**, *52* (23), 3511–3529. https://doi.org/10.1055/s-0040-1707212.
(231) Reynolds, W. R.; Frost, C. G. Coupling Reactions in Continuous-Flow Systems. In *Palladium-Catalyzed Coupling Reactions*; John Wiley & Sons, Ltd, 2013; pp 409–443. https://doi.org/10.1002/9783527648283.ch11.
(232) Sun, X.; Rocha, M. V. J.; Hamlin, T. A.; Poater, J.; Bickelhaupt, F. M. Understanding the Differences between Iron and Palladium in Cross-Coupling Reactions. *Phys. Chem. Chem. Phys.* **2019**, *21* (19), 9651–9664. https://doi.org/10.1039/C8CP07671E.
(233) Kaplaneris, N.; Ackermann, L. Earth-Abundant 3d Transition Metals on the Rise in Catalysis. *Beilstein J. Org. Chem.* **2022**, *18* (1), 86–88. https://doi.org/10.3762/bjoc.18.8.
(234) Hazari, N.; Melvin, P. R.; Beromi, M. M. Well-Defined Nickel and Palladium Precatalysts for Cross-Coupling. *Nat. Rev. Chem.* **2017**, *1* (3), 1–16. https://doi.org/10.1038/s41570-017-0025.

Chapter 2 – The Signal-to-Noise Issue in Mass Spectrometric Analysis of Polymers

This chapter has been reproduced with minor changes from "Ian C. Chagunda, Gregory T. Russel, and J. Scott McIndoe, *Polymer Chemistry*, **2021**, *12* (31), 4451–4461" and adapted with permission from Royal Society of Chemistry Publishing. This project was conceptualised by JSM. ICC's contributions included literature reviews, investigations of sample preparation challenges associated with each ionization method, and modeling of isotopic contributions. GTR assisted with mathematical modeling. All three authors collaborated in writing and refining this manuscript.

2.1 Abstract

Mass spectrometric approaches to polymer analysis become increasingly ineffective as the average molecular weight of the polymer increases. The reasons are several-fold and apply to both electrospray ionization (ESI) and matrix assisted laser desorption/ionization (MALDI) analysis commonly used for characterizing polymers. First, the distribution of signal over an increasing number of different species leads to diminishing signal-to-noise (S/N), even for distributions of narrowest possible dispersity. Second, each unique species' intensity is broadened over a wider range of *m/z* values as polyisotopic contributions become more significant. Third, the individual signal width becomes broader as *m/z* increases. Finally, solubility properties and solvent adducts can limit the analytical signal for polymer analysis. For MALDI analysis, an additional challenge arises. Effective sample preparation requires a specific weight percentage, which lowers the concentration of polymer in the matrix. Together, these factors create a S/N problem that fundamentally limits the ability of mass spectrometry to determine molecular weight distribution for high

mass polymers. This chapter will discuss these limitations in detail, exploring their implications for polymer characterization, and propose strategies to mitigate S/N issues.

2.2 Introduction

The stochastic nature of any polymerization process results in it producing molecules of differing mass and composition.[1,2] Unlike with most biomolecules, there is a general lack of homogeneity in a synthetic homopolymers that gives rise to both broad molar-mass distributions (MMDs) and distribution of endgroups.[3] This is further complicated in copolymer systems, which additionally show chemical composition distribution and functionality distribution.[4] Characterization of MMD and composition is therefore often the first step in the analysis of polymeric materials. Historically, methods of characterization were based on indirect properties such as light scattering and intrinsic viscosity, which provide limited chemical information about the polymer and only an average molar mass. End-group titration analysis provides some compositional information, allowing the estimation of molar mass in low mass polymers, and giving clues about the mechanism adopted in synthesis.[2,3] Nuclear magnetic resonance (NMR) spectroscopy is also frequently used to provide information on polymer structure including conformational analysis,[5–8] micellar structure[9] and crystalline morphology,[10,11] all of which can be correlated with mechanical behavior. Due to the nature of NMR, the information gained only yields an average of the polymer characteristics.[8]

Among the many techniques used for polymer analysis, MS is one of the most recently developed but has rapidly become one of the most prominent.[12] Using only minute amounts of sample, detailed information on polymer composition and structure can be gleaned from mass spectra of a wide variety of polymers.[3] The advent of soft ionization techniques, in particular electrospray ionization (ESI) and matrix assisted laser desorption/ionization (MALDI), has driven much research into optimizing mass spectrometric techniques for polymer analysis.[12,13] A comprehensive study by Ladavière and coworkers compared the ability of ESI and MALDI to ionize polystyrene carrying labile endgroups, showing that different doping salts result in significantly more intact endgroups

being detected when using ESI.[14] Significant fragmentation was observed in both ionization techniques, with the cationization salt found to play a key role in the degree of fragmentation. Koster and coworkers carried out endgroup and mass determination of poly(oxyalkyne)s between 400–8000 Da with ESI performed on a Fourier-transform ion-cyclotron resonance (FTICR) mass spectrometer, using the multi-charge states observed in ESI for increased accuracy.[15] However, mass discrimination remains a key disadvantage with ESI for high mass polymer samples owing to the charge-state distribution complexity of ESI spectra.[8,12–16] Solvent systems also have a significant effect on ESI polymer analysis, with solvent adducts shown to split the mass peaks and reduce the overall signal.[17]

On the other hand, MALDI-MS of polymeric systems enables significantly better detection of intact mass fragments up to a molecular weight of 30 kDa, generated primarily as singly charged ions.[14,16,18–21] However, regardless of whether MALDI or ESI is used, polymer chemists often encounter progressively poorer data quality as the average MW increases or the distribution broadens.[16,22–26] While MALDI-MS is well-established for analyzing biomacromolecules which typically exhibit narrow MMDs,[27–29] synthetic polymers pose greater challenges due to their much broader MMDs.[18] Precision in quantitative analysis is not fully understood, due to a number of factors that typically affect high *m/z* regions.[21,30,31]

This chapter provides an explanation for the phenomenon of poor MS data for high molecular weight polymers based on some simple physical limitations. Fundamentally, mass spectrometric techniques rapidly encounter a decreasing signal-to-noise (S/N) as the signal becomes distributed over more *m/z* values. The sources of this S/N problem are several-fold, and the various factors that conspire to prevent polymer chemists obtaining good results from mass spectrometric studies at high molecular weights are presented in the following sections.

First, consider a real example of the S/N problem. The MALDI-TOF-MS spectra in Figure 2.1, reproduced from the work of van Herk and coworkers,[32] illustrate styrene bulk polymerization with times of 0.02 s (top) to 1 s (bottom) between initiation-inducing laser pulses. This is a characteristic example of polymer analysis by MALDI, which serves as a reference for further discussion of the S/N problem. The same challenges are applicable

when using ESI. The resulting spectra in Figure 2.1 reach maxima at approximately 2400, 4000, 15 000, and 70 000 Da. Note the stark diminution of spectral quality as *m/z* increases.

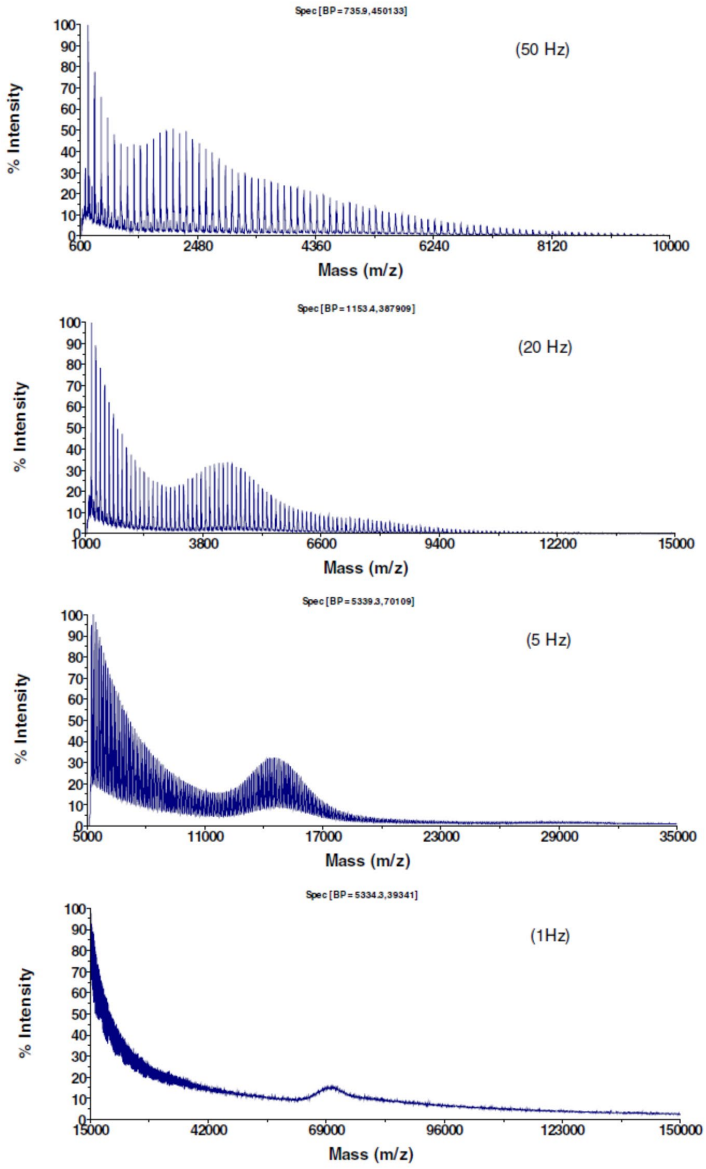

Figure 2.1: MALDI-ToF-MS spectra from bulk styrene pulsed-laser polymerization. Reprinted with permission from ref. 32. Copyright 2003 American Chemical Society.

2.3 Discussion

2.3.1 Isotope Pattern Contributions

Isotope patterns are analytical fingerprints that aid in the characterization polymers. This process typically involves computing theoretical isotope patterns and matching them to the measured mass spectra. For low molecular mass oligomers (<5000 Da), isotopic resolution can typically be achieved with a mass accuracy <100 ppm.[25] However, as the mass of a polymer increases, resolving the isotope peaks of an oligomer becomes difficult.[15,25,33,34] Consider the modeled isotope pattern of the styrene oligomer $H(C_2H_3Ph)_nH$ (with H assumed as the end groups for simplicity), where the *n* values were chosen to correspond closely to the positions of the peaks the experimental spectra shown in Figure 2.1.

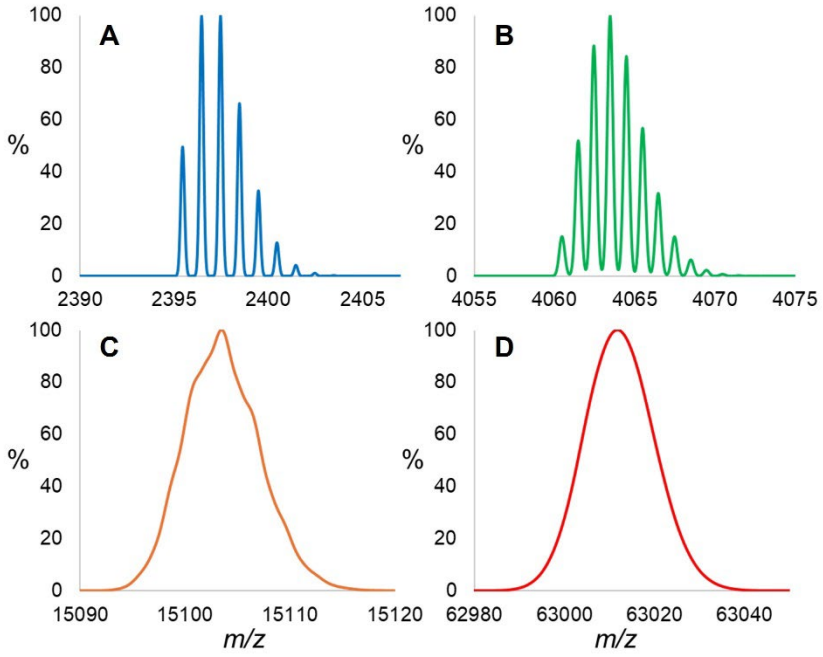

Figure 2.2: Isotope patterns for $H(C_2H_3Ph)_nH$, where *n* = 23 (blue, A), 39 (green, B), 145 (orange, C) and 605 (red, D), with isotopic envelope widths of *m/z* = 8 Da, 11 Da, 21 Da and 47 Da for *n* = 23, 39, 145 and 605 respectively.

For *n* =23 (*m/z* = 2397.4 Da for *z* = 1, Figure 2.2A) the pattern is considerably more complex than that observed for a low molecular weight ion, principally due to the contributions from ^{13}C (1% natural abundance) and, to a lesser extent, from ^{2}D (0.015%

natural abundance). The ion current from a single species is therefore distributed across approximately 7 peaks instead of mostly just one, greatly diminishing the S/N. For n =39 (m/z = 4063.8 Da for z = 1, Figure 2.2B), the pattern gets broader yet, distributed across approximately 10 peaks with even more contributions from ^{13}C and ^{2}D. For n = 145 (m/z = 15103.6 Da for z = 1, Figure 2.2C), the resolution is insufficient to provide an isotope pattern at all, although some shoulders resulting from the pattern may still be distinguished. For n = 605 (m/z = 63012.0 Da for z = 1, Figure 2.2D) there is no overt evidence of isotope pattern, as the curve is smooth and broad, with full-width of over 20 Da at half-maximum (for the full envelope). All isotope patterns were calculated using open-source tools from www.chemcalc.org.[35]

All modelled spectra here are presented at a resolution of 10000, defined by the full width at half maximum (FWHM).[36] This resolution was chosen to match that of the Voyager DE-STR MALDI-TOF-MS instrument used in the van Herk[32] study. Such a resolution is typical of a research-grade MALDI-TOF instrument, though high-end modern instruments are capable of achieving higher resolution.[12] For example, at an m/z value of 1000, an individual peak will have a width of m/z = 0.1 at half of its height. For higher molecular weights, the resolution results in isotopomers signals with increasingly broader widths and distinguished peaks, such the case in Figure 2.2C with peak width of 1.5 Da at half-height. These calculations, while illustrative, closely mirror the experimental data and demonstrate the challenges observed in Figure 2.1.

The data representation in Figure 2.2, plotted on increasing x-axis widths with plots normalized to a maximum of 100% for the most abundant peak in the spectrum, can be misleading. It suggests that resolution is the primary difference between the signals. To better highlight the impact of isotope patterns on the S/N, the same data is plotted with all four plots overlapping and scaled to have the same total peak area. This approach, shown in Figure 2.3, provides a more accurate depiction of how signal intensity is distributed across the isotopic envelope.

The combined plots of Figure 2.3 demonstrate that, as the molecular weight increases, signal from higher molecular mass polymers gradually blends into the baseline due to the cumulative effects of the isotopic contributions alone. This is evident in the

isotopic envelope widths, which increase progressively: *m/z* = 8 Da, 11 Da, 21 Da and 47 Da for *n* = 23, 39, 145 and 605 respectively. These widths were determined using the criterion of intensity being greater than 1% of the highest intensity peak of the envelope.[37] Notably, even the largest simulated polymer, where *n* = 605, is relatively small compared to commercial polystyrene. This highlights the inherent limitations of MS for high polymers compared to its performance for low molecular weight oligomers.

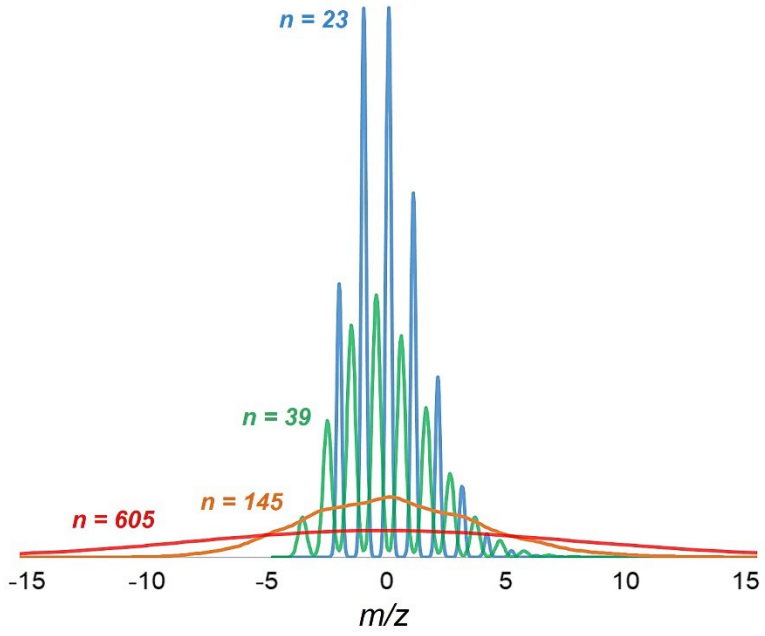

Figure 2.3: Isotope patterns for $H(C_2H_3Ph)_nH$, where *n* = 23 (blue, *m/z* ≈ 2400 Da), 39 (green, *m/z* ≈ 4000), 145 (orange, *m/z* ≈ 15000) and 605 (red, *m/z* ≈ 63000), recentered at the highest peak at an *m/z* value of 0.

It is important to emphasize that this is for two distinct reasons, both of which become more pronounced as mass increases: (1) Assuming constant instrument resolution the FWHM becomes larger with increasing mass, causing individual peaks to broaden and eventually become indistinguishable, as shown in Figure 2.2 and Figure 2.3; (2) Figure 2.3 also demonstrates that higher masses result in a greater number of peaks spread over a wider *m/z* range. This is due to the increasing number of possible isotopic contributions as the number of atoms in a molecule rises.

Point (2) is relevant for all polymers, and the magnitude of the effect depends on the atoms present. Most carbon-based polymers are dominated by ^{13}C contributions to isotopic

complexity, but other common elements also add to the broadness of these envelopes. For example, silicon has contributions from ^{29}Si (4.7%) and ^{30}Si (3.1%), nitrogen from ^{15}N (0.4%), oxygen from ^{17}O (0.04%) and ^{18}O (0.20%), and chlorine from ^{37}Cl (24%) along with the more abundant ^{35}Cl (76%). The latter makes poly(vinyl chloride) (PVC) particularly interesting. For example, Figure 2.4 shows that the pattern for an oligomer of PVC with just 23 repeat units is already significantly broader than the equivalent PS pattern (as in Figure 2.2A and Figure 2.3) thanks to the isotopic richness of Cl.

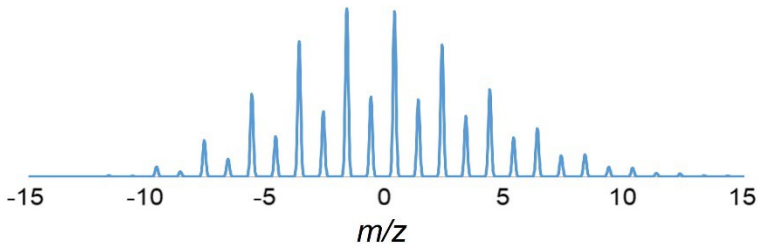

Figure 2.4: Isotope pattern for $H(C_2H_3Cl)_nH$ where n = 23, recentered at the highest peak at an m/z value of 0 (actual m/z = 1439.5 Da) for consistency with Figure 2.3.

Regarding the two effects giving rise to broad MS signals as mass increases, point (2) is part of the inherent nature of polymers and thus applies to all methods of analysis. For example, the spread of mass for a specific chain length is equally present in size exclusion chromatography (SEC).[38] However, this technique never operates with resolution in hydrodynamic volume that translates into a mass resolution of 1 Da, so this broadening effect never comes into consideration. Therefore, this should not be considered a weakness of MS methods. Instead, the individual molecular identification that is possible at low mass should be regarded as a strength. On the other hand, factor (1) – increasing FWHM as mass increases – is an MS instrumental factor, as other methods have instrumental broadening as well. Most notably, SEC has column broadening, which operates on a log mass rather than linear mass scale. This means SEC broadens over an exponentially increasing range of m as m increases, making it a far stronger effect than in MS.

2.3.2 Oligomeric and Polymeric Distributions

The identification of molecular properties is often the first step in the analysis of a polymer, with MS providing substantial information. This includes identification of monomer units and endgroups,[39,40] tracking of catalyst activity in the polymerization process,[41,42] and estimations of composition for complex copolymer systems.[43–46] Crotty and coworkers have extensively reviewed the application of MS and MS/MS techniques for probing synthetic polymer architecture of simple linear homopolymers through to complex copolymer systems.[47] The estimation of molar masses and MMDs is also of primary interest in polymer characterization.[23]

Contrary to proteins, which exhibit uniform chain lengths, synthetic polymers exhibit significant dispersity with mass ranges over many thousands of Daltons.[3] It is important to remember that dispersity reflects standard deviation relative to the mean. This means that broader distributions can have lower dispersity values because, although the standard deviation is larger, the mean is larger in proportion, resulting in a smaller ratio.[48] As MALDI-MS was originally developed for proteins, its extension to synthetic polymers has not been as straightforward, owing to the aforementioned dispersity of synthetic polymers.

Initial reports of molar mass and MMDs determined for low-mass synthetic polymers using MALDI-MS showed reasonable agreement with conventional methods such as viscometry, SEC and light scattering for samples with dispersity <1.2.[1,23] For samples possessing broader dispersity, however, reported molar mass values showed significant underestimation.[49] This issue, intrinsic to the polymerization process,[3,48] becomes more pronounced with higher molar mass polymers. This is because higher molar mass polymers generally produce a weaker signal response, resulting in a lower S/N as the signal intensity is distributed over a larger number of species with different degrees of polymerization. This problem can be mitigated to some extent by separation of polymer samples using chromatography methods prior to mass analysis.[16] However, such separations are rarely performed, as they can be challenging and costly.

This inherent limitation of mass spectrometric analysis of synthetic polymers is illustrated by again examining polystyrene. Bulk polystyrene is typically synthesized in batch reactors through chain polymerization, resulting in dispersity of roughly 2.[48] By assuming a dispersity far narrower than this, specifically the narrowest that can be achieved without further chromatographic separation, one can observe a Poisson distribution. A Poisson distribution describes the probability of a given number of events (such as chain growth steps) occurring within a fixed interval, assuming the events are independent and occur at a constant rate.[50] This distribution can be obtained by high purity anionic polymerization[3] and nearly achieved by various forms of reversible-deactivation radical polymerization.[51–53] The Poisson distributions for polystyrene are presented in Figure 2.5, with average degree of polymerization 23, 39, 145 and 605, matching the *n* values in Figure 2.2 and Figure 2.3. These previous calculations were for truly uniform polymers, whereas the current calculation in Figure 2.5 reflects a distribution of *n*.

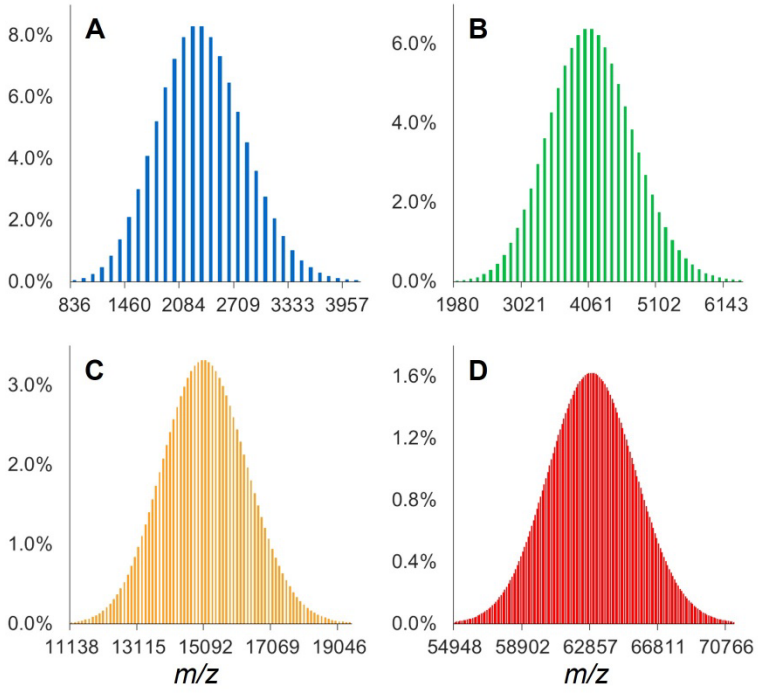

Figure 2.5: Poisson distributions for polystyrene with average degree of polymerization 23 (blue, A), 39 (green, B), 145 (orange, C) and 605 (red, D). These distributions have dispersity of 1.04, 1.03, 1.007 and 1.002 respectively, and peak widths of m/z = 2913.8, 3746.3, 7492.5, and 15401.3 Da, respectively.

When plotted with different x and y axes as in Figure 2.5, these distributions can appear deceptive. Resetting them such that they are all overlaid and have the same total area provides a more accurate depiction, as shown in Figure 2.6. This presentation reveals a more complex picture of the relationship between polymer mass distributions and their representation in mass spectra.

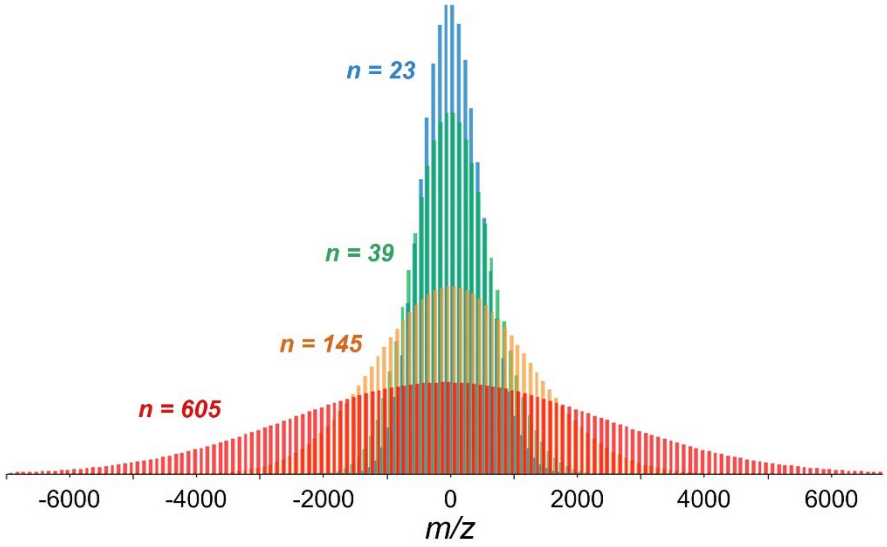

Figure 2.6: Poisson distributions from Figure 2.5, with disparities of 1.04, 1.03, 1.007 and 1.002 for *n* = 23, 39, 145, and 605 respectively, overlaid and with the same total intensity (summed heights), and recentered at the highest peak at an *m/z* value of 0.

Estimating how much the signal intensity at a given *m/z* value will be compromised involves considering a combination of isotopic broadening (Section 2.3.1) and oligomeric distributions (Section 2.3.2). The (average) *n* = 605 example in Figure 2.6 has a maximum intensity 1/4 that of the (average) *n* = 23 distribution due to a wider oligomeric distribution. Meanwhile, Figure 2.3 shows a 1/20 maximum intensity ratio for the same *n* due to isotopic broadening. This means that the maximum signal for a polystyrene ion at *m/z* = 60 000 Da is about 1/80 of that of a polystyrene on at 2500 Da. The falloff in intensity at any given *m/z* value due to these two effects alone can be quite dramatic and will be even more pronounced where polymerization gives rise to constant dispersity, as seen in Figure 2.5.

The preceding sections addressed general considerations for MS, while the next sections will focus on challenges and considerations specific to different ionization techniques.

2.3.3 Ionization Method-Specific Considerations: MALDI

MALDI mass spectrometers make use of intense pulses of laser light that induce vaporization of a co-crystallized mixture of a matrix, typically an organic acid with a UV chromophore, and analyte molecules.[54] Ionization occurs in the resulting energetic plume, with singly-charged ions being the survivors of a complex and rapid process. Several factors affect the spectral intensity of a polymer, many of which are related to its molecular weigh. These factors are responsible for the molecular weight distributions for high molecular weight polymer samples, especially those with high dispersity, in contrast to results from other quantitative methods.[55–59] Some of these factors are described below.

2.3.3.1 Molar Considerations

At a given power, the laser removes approximately the same amount of material in a single pulse due to the matrix being in great excess and responsible for the energy absorption.[12] If the matrix-to-analyte (M/A) weight ratio remains constant, the concentration of individual polymer molecules in the plume is inversely proportional to their molecular weight. As such, for the same amount of matrix and analyte material ablated, fewer high molecular weight polymer ions will be present in the ionized plume. This is simply a concentration effect, separate from any effect of molecular weight on ionization efficiency. Attempting to remedy this issue by boosting the polymer concentration when preparing the sample is not necessarily productive, as explained below.

2.3.3.2 Matrix-to-Analyte (M/A) Weight Ratio

M/A ratios are typically in the range 10^2:1 to 10^6:1.[54,60] This ratio tends to increase with polymer size, requiring more matrix to act as a dispersant, desorber, and ionization agent for each analyte molecule.[61] Increasing M/A ratios also act to minimize multimer formation.[30] Investigations into the effect of M/A ratio in MALDI analysis have shown diminishing returns for higher M/A for larger polymers.[30,62] As M/A increases beyond an

experimentally determined optimal zone for each polymer sample, less analyte signal is observed due to less analyte being available for ionization. Conversely, low M/A ratios, resulting in higher concentrations of analyte in the matrix, show decreasing ion intensity at lower masses, with significantly broader distributions shifted towards higher *m/z*.[63] This leads to an overestimation of number-average MW for a non-uniform polymer sample, where the higher mass components reach co-crystallization point before lower mass components.[30]

2.3.3.3 Sample Preparation

High mass oligomers in high concentration solutions have an increased tendency for polymer precipitation to occur prior to matrix co-crystallization.[25,64] Matrices usually tolerate only a certain percentage of analyte before co-crystallization fails, leading to altered polymer distribution in the ionized plume.[25] Most preparative protocols call for a particular weight of sample for optimal performance,[60] with the most common sample preparation method being the "dried droplet" (DD) method.[12,25,65] The DD method remains the most widely used MALDI sample preparation method due to its relatively simple preparation steps that are applicable to many different sample types. It involves depositing droplets of dissolved matrix and analyte onto a target plate, with co-crystallization occurring as the solvent evaporates.[23] However, uneven droplet distribution causes irregular crystallization and heterogeneous distribution, leading to mass distributions in the ionized plume that may not accurately represent the distribution in the analyte, complicating quantitative analysis.[65,66]

Other sample preparation methods have attempted to improve on this limitation, including the forced dried droplet method,[65] solvent-free methods,[67–69] freeze vacuum-drying method,[70] and electrowetting-assisted drying.[71] Although these methods show improved crystal homogeneity, they often require more preparation time and additional instruments in order to generate homogeneous microcrystal distribution.[12] Additionally, developments in automated chemistry have led to improvements in consistency and reductions in the time required for sample preparation.[38,72]

2.3.3.4 Laser Energy

Studies have shown that higher molecular masses of the same type of polymer require higher laser energies for efficient ionization.[73,74] However, increasing the laser energy beyond an optimal level does not increase ionization efficiency for high molecular mass components. Instead, excess laser energy leads to mass discrimination, where peak areas for higher molecular mases no longer increase.[74] The additional energy also causes fragmentation, resulting in a shift to lower *m/z* values and broader MMDs. Furthermore, the intensity of doubly charged peaks increases, adding complexity to the spectral analysis.[49,74]

2.3.3.5 Matrix Noise

MALDI noise primarily arises from matrix clusters, and their abundance decreases with increasing molecular weight.[75] For example, in Figure 2.1, the baseline becomes progressively lower as molecular weight increases. Other sources of chemical noise, such as impurities, fragments, and aggregates, will similarly diminish with greater molecular weight. As such, the S/N should see some mitigation from the reduction in noise at high molecular weight.

2.3.4 Ionization Method-Specific Considerations: ESI

2.3.4.1 Multiple Charge States

ESI-MS is sometimes used to characterize lower molecular weight oligomers,[40,76] but is usually more complicated than MALDI-MS because the signal is additionally distributed across multiple charge states or ionizing additives.[54] For example, as shown in Figure 2.7, an oligomeric phosphaalkene provides four series of ions in two different charge states. Each series arises from the oligomers associating with either $[Ag_2]^{2+}$, $[Ag_3]^{3+}$, $[Ag_3Cl]^{2+}$, or $[Ag_4Cl]^{3+}$.[77]

Higher molecular weight polymers further complicate ESI-MS analysis because their increased size provides more binding sites for cations, leading to higher charge states.[78,79] For example, Craido-Hidalgo and coworkers demonstrated that the high charge states observed in the ESI of polyethylene glycol (PEG) arise from the stretched gas-phase chain,

which more readily bind solution-phase cations.[80] To address this, they used strategies such as switching to a negative mode ESI-MS, which weakens cation binding, and carefully selecting combinations of solvent and solution ions that bind weakly to the polymer. These approached successfully modulated and reduced multiple ionizations. Their study also revealed a charge control mechanism, where the charge retained by a polymer globule is determined by ion evaporation from its dry surface.[80] Furthermore, they were able to distinguish between different polymer conformations, such as globular or linear, by incorporating ion mobility separation (IMS), resulting in narrower MMDs for each charge state. Similarly, Ozeki and coworkers used ESI-IMS-MS/MS to separate multiply charged, large intact polymers (>40 kDa) by using collision-induced charge stripping resulting in simplified spectra.[81]

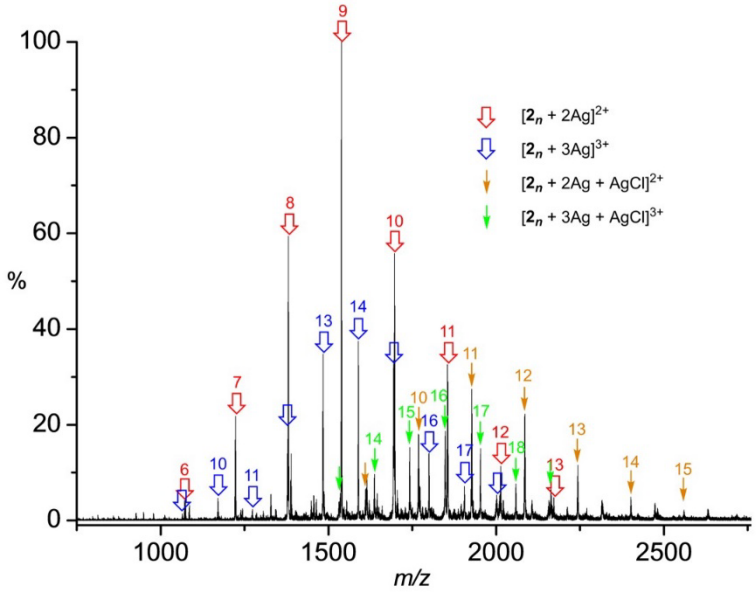

Figure 2.7: ESI(+)-MS spectrum of oligomerized phosphaalkene, recorded in acetonitrile with the addition of $AgNO_3$. Reprinted with permission from ref. 77. Copyright 2016 Canadian Science Publishing.

2.3.4.2 Polymer Chain Entanglement

The inherent entanglement of chains in high mass polymers presents a challenge to obtaining high-quality ESI mass spectra. Chain entanglement inhibits the droplet fission process as the solvent evaporates and oligomers acquire charge.[54] An investigation of

droplets in the ESI process revealed bimodal particle size distribution, with a significant large-particle component reflecting an inhibition of droplet fission.[82]

Entanglement also reduces sensitivity for samples at higher concentration, which may also be attributed to competition for available charge.[83] Interestingly, these decreased sensitivity issues are also observed at relatively low sample concentrations, as oligomer entanglement occurs early in the evaporation process. This limits the droplet fission process necessary to generate single-chain particles.[84] Detection of such entangled clusters is therefore limited by the *m/z* range of the spectrometer.

2.3.4.3 Solubility Issues in ESI-MS

A major challenge in ESI-MS analysis of polymers is the requirement for the polymer to dissolve well in a solvent that is compatible with the technique. ESI-MS relies on the formation of charged droplets in solution, making solubility a critical factor for successful ionization. However, polymers often have limited solubility in common ESI-MS solvents, such as methanol, acetonitrile, or water, particularly when the polymer is highly hydrophobic.[85] To address this, co-solvent mixtures, like THF, *N*,*N*-dimethylformamide (DMF) and dimethyl sulfoxide (DMSO), must be carefully chosen to both dissolve the polymer and maintain compatibility with the ESI process; this can significantly complicate sample preparation.[86] Nonpolar solvents that dissolve hydrophobic polymers may require the addition of volatile salts and weak acids or their conjugate bases, such as ammonium acetate (NH_4OAc), formic acid (FA), trifluoroacetic acid (TFA), or sodium trifluoroacetate (NaTFA), to promote ionization.[87–89] However, additive concentrations must be kept low (<10 mM) to prevent competitive ionization leading to signal suppression of multicomponent mixtures.[85] These added complexities can hinder the reproducibility and accessibility of ESI-MS for certain polymer systems.

2.3.4.4 Mass Discrimination at the Detector

Whether using ESI or MALDI, differences in detector response may be observed for oligomers of different mass, resulting in biasing of the MMDs. Microchannel plates (MCPs) can give lower responses for high-mass ions due to poor ion-to-electron conversion for heavy, low-velocity ions.[90] However, correcting for this effect is possible.[91] Ion-conversion

dynode detectors exhibit less mass bias, with lower mass ions exhibiting slightly lower responses.[92]

These additional complications contribute to the lower mass range of ESI-MS for polymers (currently <30 kDa) compared to MALDI-MS (<70 kDa). MALDI-MS has the added advantage of preferentially producing singly-charged ions,[13,16,18,25] which simplifies spectral analysis. Other ionization techniques are limited in their ability to transition high molecular weight materials into the gas phase, making ESI and MALDI the most commonly methods for polymer MS analysis.[12]

2.4 Conclusions

Every analytical method has strengths and weaknesses. In the case of mass spectrometric analysis of polymers, two strengths were immediately evident: (1) high-resolution separation of non-uniform samples so that individual species could be 'visualized' according to their precise molecular weights; and (2) the lack of need for calibration via narrow-dispersity polymer samples of known molecular weight. However, this chapter has explained why accurate determination of MMDs for high molecular weight polymer samples is not currently possible due to various weaknesses of MS methods, most notably S/N issues.

Understanding the source of the S/N problem helps propose solutions, some practical, some not. For example, synthesizing a ^{13}C-depleted polymer to reduce isotopic contributions and enhance data clarity would likely be prohibitively expensive in most cases. A more feasible approach is to conduct longer experiments, as extended acquisition times can improve S/N. Improved results can also be achieved by analyzing a polymer with low dispersity, where mass-selective separation such as SEC has been performed prior to analysis, as this reduces the distribution of ion current across multiple species. Optimizing matrix and solvent compositions, as well as tuning MALDI laser energy, can further enhance ionization and desorption efficiency, potentially improving data quality.

On a positive note, mass spectrometric innovation continues to be exceptionally vibrant. Instrumentation is in a process of continuous development, and better spectrometers (increased sensitivity, higher resolution, lower noise) and experimental methodologies (sample preparation, matrices, ionization methods, MS/MS methods) will continuously extend the limits of what is possible.

2.5 References

(1) Hanton, S. D. Mass Spectrometry of Polymers and Polymer Surfaces. *Chem. Rev.* **2001**, *101* (2), 527–570. https://doi.org/10.1021/cr9901081.

(2) O'Connor, P. B.; McLafferty, F. W. Oligomer Characterization of 4-23 kDa Polymers by Electrospray Fourier Transform Mass Spectrometry. *J. Am. Chem. Soc.* **1995**, *117* (51), 12826–12831. https://doi.org/10.1021/ja00156a021.

(3) Montaudo, G.; Montaudo, M. S. Polymer Characterization Methods. In *Mass Spectrometry of Polymers*; CRC Press, 2001; pp 41–112. https://doi.org/10.1201/9781420037753-2.

(4) Epping, R.; Panne, U.; Falkenhagen, J. Critical Conditions for Liquid Chromatography of Statistical Copolymers: Functionality Type and Composition Distribution Characterization by UP-LCCC/ESI-MS. *Anal. Chem.* **2017**, *89* (3), 1778–1786. https://doi.org/10.1021/acs.analchem.6b04064.

(5) Born, R.; Spiess, H. W. Ab Initio Calculations of Conformational Effects on 13C NMR Spectra of Amorphous Polymers. In *Ab Initio Calculations of Conformational Effects on 13C NMR Spectra of Amorphous Polymers*; Born, R., Spiess, H. W., Eds.; NMR Basic Principles and Progress; Springer: Berlin, Heidelberg, 1997; pp 1–121. https://doi.org/10.1007/978-3-642-60644-1_1.

(6) Tonelli, A. E. The Conformational Connection Between the Microstructures of Polymers and Their NMR Spectra. In *Annual Reports on NMR Spectroscopy*; Webb, G. A., Ando, I., Eds.; Academic Press, 1997; Vol. 34, pp 185–229. https://doi.org/10.1016/S0066-4103(08)60103-9.

(7) Danke, V.; Beiner, M.; Saalwächter, K.; Schäfer, M. Structure and Dynamics in a Polymorphic Nanophase-Separated Stiff Comblike Polymer. *Macromolecules* **2019**, *52* (18), 6943–6952. https://doi.org/10.1021/acs.macromol.9b00951.

(8) Smith, P. B.; Pasztor, A. J.; McKelvy, M. L.; Meunier, D. M.; Froelicher, S. W.; Wang, F. C.-Y. Analysis of Synthetic Polymers and Rubbers. *Anal. Chem.* **1999**, *71* (12), 61–80. https://doi.org/10.1021/a1990004f.

(9) Cerichelli, G.; Mancinit, G. NMR Techniques Applied to Micellar Systems. *Curr. Opin. Colloid Interface Sci.* **1997**, *2* (6), 641–648. https://doi.org/10.1016/S1359-0294(97)80058-1.

(10) De Rosa, C.; Capitani, D.; Cosco, S. Solid-State 13C Nuclear Magnetic Resonance Spectra of Four Crystalline Forms of Isotactic Poly(4-Methyl-1-Pentene). *Macromolecules* **1997**, *30* (26), 8322–8331. https://doi.org/10.1021/ma970706m.

(11) Ricci, G.; Alberti, E.; Zetta, L.; Motta, T.; Bertini, F.; Mendichi, R.; Arosio, P.; Famulari, A.; Meille, S. V. Synthesis, Characterization and Molecular Conformation of Syndiotactic 1,2 Polypentadiene: The Cis Polymer. *Macromolecules* **2005**, *38* (20), 8353–8361. https://doi.org/10.1021/ma047604y.

(12) Gruendling, T.; Weidner, S.; Falkenhagen, J.; Barner-Kowollik, C. Mass Spectrometry in Polymer Chemistry: A State-of-the-Art up-Date. *Polym. Chem.* **2010**, *1* (5), 599–617. https://doi.org/10.1039/B9PY00347A.

(13) Steinkoenig, J.; Cecchini, M. M.; Reale, S.; Goldmann, A. S.; Barner-Kowollik, C. Supercharging Synthetic Polymers: Mass Spectrometric Access to Nonpolar Synthetic Polymers. *Macromolecules* **2017**, *50* (20), 8033–8041. https://doi.org/10.1021/acs.macromol.7b02018.

(14) Ladavière, C.; Lacroix-Desmazes, P.; Delolme, F. First Systematic MALDI/ESI Mass Spectrometry Comparison to Characterize Polystyrene Synthesized by Different Controlled Radical Polymerizations. *Macromolecules* **2009**, *42* (1), 70–84. https://doi.org/10.1021/ma8013788.

(15) Koster, S.; Duursma, M. C.; Boon, J. J.; Heeren, R. M. A. Endgroup Determination of Synthetic Polymers by Electrospray Ionization Fourier Transform Ion Cyclotron Resonance Mass Spectrometry. *J. Am. Soc. Mass Spectrom.* **2000**, *11* (6), 536–543. https://doi.org/10.1016/S1044-0305(00)00115-X.

(16) *Mass Spectrometry in Polymer Chemistry*; Barner-Kowollik, C., Gruendling, T., Falkenhagen, J., Weidner, S., Eds.; Wiley-VCH: Weinheim, 2012.
(17) Gies, A. P. Ionization Techniques for Polymer Mass Spectrometry. In *Mass Spectrometry in Polymer Chemistry*; John Wiley & Sons, Ltd, 2012; pp 33–56. https://doi.org/10.1002/9783527641826.ch2.
(18) De Bruycker, K.; Welle, A.; Hirth, S.; Blanksby, S. J.; Barner-Kowollik, C. Mass Spectrometry as a Tool to Advance Polymer Science. *Nat. Rev. Chem.* **2020**, *4* (5), 257–268. https://doi.org/10.1038/s41570-020-0168-1.
(19) O'Connor, P. B.; Duursma, M. C.; van Rooij, G. J.; Heeren, R. M. A.; Boon, J. J. Correction of Time-of-Flight Shifted Polymeric Molecular Weight Distributions in Matrix-Assisted Laser Desorption/Ionization Fourier Transform Mass Spectrometry. *Anal. Chem.* **1997**, *69* (14), 2751–2755. https://doi.org/10.1021/ac961040h.
(20) Dey, Michael.; Castoro, J. A.; Wilkins, C. L. Determination of Molecular Weight Distributions of Polymers by MALDI-FTMS. *Anal. Chem.* **1995**, *67* (9), 1575–1579. https://doi.org/10.1021/ac00105a016.
(21) Karas, M.; Glückmann, M.; Schäfer, J. Ionization in Matrix-Assisted Laser Desorption/Ionization: Singly Charged Molecular Ions Are the Lucky Survivors. *J. Mass Spectrom.* **2000**, *35* (1), 1–12. https://doi.org/10.1002/(SICI)1096-9888(200001)35:1<1::AID-JMS904>3.0.CO;2-0.
(22) Tanaka, K.; Waki, H.; Ido, Y.; Akita, S.; Yoshida, Y.; Yoshida, T.; Matsuo, T. Protein and Polymer Analyses up to m/z 100 000 by Laser Ionization Time-of-Flight Mass Spectrometry. *Rapid Commun. Mass Spectrom.* **1988**, *2* (8), 151–153. https://doi.org/10.1002/rcm.1290020802.
(23) *Mass Spectrometry of Polymers*, 1st ed.; Montaudo, G., Lattimer, R., Eds.; CRC Press: Boca Raton, Fla, 2002.
(24) Shimada, K.; Nagahata, R.; Kawabata, S.; Matsuyama, S.; Saito, T.; Kinugasa, S. Evaluation of the Quantitativeness of Matrix-Assisted Laser Desorption/Ionization Time-of-Flight Mass Spectrometry Using an Equimolar Mixture of Uniform Poly(Ethylene Glycol) Oligomers. *J. Mass Spectrom.* **2003**, *38* (9), 948–954. https://doi.org/10.1002/jms.508.
(25) Li, L. MALDI-MS for Polymer Characterization. In *MALDI MS*; John Wiley & Sons, Ltd, 2013; pp 313–365. https://doi.org/10.1002/9783527335961.ch8.
(26) Waters. *Mass Spectrometry for Polymers*. www.waters.com. http://www.waters.com/waters/library.htm?lid=134827408 (accessed 2021-01-12).
(27) Mass Spectrometry of Biomolecules. In *Bioanalytical Chemistry*; John Wiley & Sons, Ltd, 2004; pp 295–321. https://doi.org/10.1002/0471623628.ch15.
(28) Leopold, J.; Popkova, Y.; Engel, K. M.; Schiller, J. Recent Developments of Useful MALDI Matrices for the Mass Spectrometric Characterization of Lipids. *Biomolecules* **2018**, *8* (4), 173. https://doi.org/10.3390/biom8040173.
(29) Keller, C.; Gemperline, E.; Li, L. MALDI Mass Spectrometry Imaging of Peptides in Medicago Truncatula Root Nodules. *Methods Mol. Biol. Clifton NJ* **2020**, *2139*, 341–351. https://doi.org/10.1007/978-1-0716-0528-8_25.
(30) Schriemer, D. C.; Li, L. Mass Discrimination in the Analysis of Polydisperse Polymers by MALDI Time-of-Flight Mass Spectrometry. 1. Sample Preparation and Desorption/Ionization Issues. *Anal. Chem.* **1997**, *69* (20), 4169–4175. https://doi.org/10.1021/ac9702610.
(31) Schriemer, D. C.; Li, L. Mass Discrimination in the Analysis of Polydisperse Polymers by MALDI Time-of-Flight Mass Spectrometry. 2. Instrumental Issues. *Anal. Chem.* **1997**, *69* (20), 4176–4183. https://doi.org/10.1021/ac9707794.
(32) Willemse, R. X. E.; Staal, B. B. P.; van Herk, A. M.; Pierik, S. C. J.; Klumperman, B. Application of Matrix-Assisted Laser Desorption Ionization Time-of-Flight Mass Spectrometry in Pulsed Laser Polymerization. Chain-Length-Dependent Propagation Rate Coefficients at High

Molecular Weight: An Artifact Caused by Band Broadening in Size Exclusion Chromatography? *Macromolecules* **2003**, *36* (26), 9797–9803. https://doi.org/10.1021/ma034789k.
(33) Whittal, R. M.; Schriemer, D. C.; Li, L. Time-Lag Focusing MALDI Time-of-Flight Mass Spectrometry for Polymer Characterization: Oligomer Resolution, Mass Accuracy, and Average Weight Information. *Anal. Chem.* **1997**, *69* (14), 2734–2741. https://doi.org/10.1021/ac970002a.
(34) Easterling, M. L.; Amster, I. J.; van Rooij, G. J.; Heeren, R. M. A. Isotope Beating Effects in the Analysis of Polymer Distributions by Fourier Transform Mass Spectrometry. *J. Am. Soc. Mass Spectrom.* **1999**, *10* (11), 1074–1082. https://doi.org/10.1021/jasms.8b01260.
(35) Patiny, L.; Borel, A. ChemCalc: A Building Block for Tomorrow's Chemical Infrastructure. *J. Chem. Inf. Model.* **2013**, *53* (5), 1223–1228. https://doi.org/10.1021/ci300563h.
(36) Gross, J. H. *Mass Spectrometry: A Textbook*; Springer, 2017.
(37) Yergey, James.; Heller, David.; Hansen, Gordon.; Cotter, R. J.; Fenselau, Catherine. Isotopic Distributions in Mass Spectra of Large Molecules. *Anal. Chem.* **1983**, *55* (2), 353–356. https://doi.org/10.1021/ac00253a037.
(38) Nielen, M. W. F. Polymer Analysis by Micro-Scale Size-Exclusion Chromatography/MALDI Time-of-Flight Mass Spectrometry with a Robotic Interface. *Anal. Chem.* **1998**, *70* (8), 1563–1568. https://doi.org/10.1021/ac9712409.
(39) van Rooij, G. J.; Duursma, M. C.; Heeren, R. M. A.; Boon, J. J.; de Koster, C. G. High Resolution End Group Determination of Low Molecular Weight Polymers by Matrix-Assisted Laser Desorption Ionization on an External Ion Source Fourier Transform Ion Cyclotron Resonance Mass Spectrometer. *J. Am. Soc. Mass Spectrom.* **1996**, *7* (5), 449–457. https://doi.org/10.1016/1044-0305(96)00003-7.
(40) Nyström, F.; Soeriyadi, A. H.; Boyer, C.; Zetterlund, P. B.; Whittaker, M. R. End-Group Fidelity of Copper(0)-Meditated Radical Polymerization at High Monomer Conversion: An ESI-MS Investigation. *J. Polym. Sci. Part Polym. Chem.* **2011**, *49* (24), 5313–5321. https://doi.org/10.1002/pola.25010.
(41) Binder, W. H.; Pulamagatta, B.; Kir, O.; Kurzhals, S.; Barqawi, H.; Tanner, S. Monitoring Block-Copolymer Crossover-Chemistry in ROMP: Catalyst Evaluation via Mass-Spectrometry (MALDI). *Macromolecules* **2009**, *42* (24), 9457–9466. https://doi.org/10.1021/ma902115j.
(42) Joshi, A.; Zijlstra, H. S.; Collins, S.; McIndoe, J. S. Catalyst Deactivation Processes during 1-Hexene Polymerization. *ACS Catal.* **2020**, *10* (13), 7195–7206. https://doi.org/10.1021/acscatal.0c01607.
(43) Wilczek-Vera, G.; Yu, Y.; Waddell, K.; Danis, P. O.; Eisenberg, A. Analysis of Diblock Copolymers of Poly(α-Methylstyrene)-Block-Polystyrene by Mass Spectrometry. *Macromolecules* **1999**, *32* (7), 2180–2187. https://doi.org/10.1021/ma981594h.
(44) Fouquet, T.; Nakamura, S.; Sato, H. MALDI SpiralTOF High-Resolution Mass Spectrometry and Kendrick Mass Defect Analysis Applied to the Characterization of Poly(Ethylene-Co-Vinyl Acetate) Copolymers. *Rapid Commun. Mass Spectrom.* **2016**, *30* (7), 973–981. https://doi.org/10.1002/rcm.7525.
(45) Town, J. S.; Jones, G. R.; Haddleton, D. M. MALDI-LID-ToF/ToF Analysis of Statistical and Diblock Polyacrylate Copolymers. *Polym. Chem.* **2018**, *9* (37), 4631–4641. https://doi.org/10.1039/C8PY00928G.
(46) Morgan, T. E.; Kerr, A.; Wootton, C. A.; Barrow, M. P.; Bristow, A. W. T.; Perrier, S.; O'Connor, P. B. Electron Capture Dissociation of Trithiocarbonate-Terminated Acrylamide Homo- and Copolymers: A Terminus-Directed Mechanism? *Anal. Chem.* **2020**, *92* (19), 12852–12859. https://doi.org/10.1021/acs.analchem.0c01224.
(47) Crotty, S.; Gerişlioğlu, S.; Endres, K. J.; Wesdemiotis, C.; Schubert, U. S. Polymer Architectures via Mass Spectrometry and Hyphenated Techniques: A Review. *Anal. Chim. Acta* **2016**, *932*, 1–21. https://doi.org/10.1016/j.aca.2016.05.024.

(48) *Polymerization Process Modeling*; Dotson, N. A., Ed.; Advances in interfacial engineering series; VCH: New York, 1996.
(49) Wetzel, S. J.; Guttman, C. M.; Girard, J. E. The Influence of Matrix and Laser Energy on the Molecular Mass Distribution of Synthetic Polymers Obtained by MALDI-TOF-MS. *Int. J. Mass Spectrom.* **2004**, *238* (3), 215–225. https://doi.org/10.1016/j.ijms.2004.04.019.
(50) Bryn D. Monnery. *How Narrow Can a Polymer Be? The Poisson Distribution*. The Quest for Monodispersity. https://brynmonnery.com/2017/08/20/how-narrow-can-a-polymer-be-the-poisson-distribution/ (accessed 2021-02-07).
(51) Chiefari, J.; Chong, Y. K. (Bill); Ercole, F.; Krstina, J.; Jeffery, J.; Le, T. P. T.; Mayadunne, R. T. A.; Meijs, G. F.; Moad, C. L.; Moad, G.; Rizzardo, E.; Thang, S. H. Living Free-Radical Polymerization by Reversible Addition−Fragmentation Chain Transfer: The RAFT Process. *Macromolecules* **1998**, *31* (16), 5559–5562. https://doi.org/10.1021/ma9804951.
(52) Cruz, A. R.; Hernandez, M. C. G.; Guzmán-Gutiérrez, M. T.; Zolotukhin, M. G.; Fomine, S.; Morales, S. L.; Kricheldorf, H.; Wilks, E. S.; Cárdenas, J.; Salmón, M. Precision Synthesis of Narrow Polydispersity, Ultrahigh Molecular Weight Linear Aromatic Polymers by A2 + B2 Nonstoichiometric Step-Selective Polymerization. *Macromolecules* **2012**, *45* (17), 6774–6780. https://doi.org/10.1021/ma301691f.
(53) Hong, J.; Wang, Q.; Fan, Z. Synthesis of Multiblock Polymer Containing Narrow Polydispersity Blocks. *Macromol. Rapid Commun.* **2006**, *27* (1), 57–62. https://doi.org/10.1002/marc.200500678.
(54) Montaudo, G.; Montaudo, M. S.; Samperi, F. Matrix-Assisted Laser Desorption Ionization/ Mass Spectrometry of Polymers (MALDI-MS). In *Mass Spectrometry of Polymers*; CRC Press, 2001; pp 419–522. https://doi.org/10.1201/9781420037753-10.
(55) Martin, K.; Spickermann, J.; Räder, H. J.; Müllen, K. Why Does Matrix-Assisted Laser Desorption/Ionization Time-of-Flight Mass Spectrometry Give Incorrect Results for Broad Polymer Distributions? *Rapid Commun. Mass Spectrom.* **1996**, *10* (12), 1471–1474. https://doi.org/10.1002/(SICI)1097-0231(199609)10:12<1471::AID-RCM693>3.0.CO;2-X.
(56) Axelsson, J.; Scrivener, E.; Haddleton, D. M.; Derrick, P. J. Mass Discrimination Effects in an Ion Detector and Other Causes for Shifts in Polymer Mass Distributions Measured by Matrix-Assisted Laser Desorption/Ionization Time-of-Flight Mass Spectrometry. *Macromolecules* **1996**, *29* (27), 8875–8882. https://doi.org/10.1021/ma960350z.
(57) McEwen, C. N.; Jackson, C.; Larsen, B. S. Instrumental Effects in the Analysis of Polymers of Wide Polydispersity by MALDI Mass Spectrometry. *Int. J. Mass Spectrom. Ion Process.* **1997**, *160* (1), 387–394. https://doi.org/10.1016/S0168-1176(96)04501-6.
(58) Schriemer, D. C.; Li, L. Detection of High Molecular Weight Narrow Polydisperse Polymers up to 1.5 Million Daltons by MALDI Mass Spectrometry. *Anal. Chem.* **1996**, *68* (17), 2721–2725. https://doi.org/10.1021/ac960442m.
(59) Hanton, S. D.; Liu, X. M. GPC Separation of Polymer Samples for MALDI Analysis. *Anal. Chem.* **2000**, *72* (19), 4550–4554. https://doi.org/10.1021/ac000095n.
(60) Owens, K. G.; Hanton, S. D. Conventional MALDI Sample Preparation. In *Maldi Mass Spectrometry for Synthetic Polymer Analysis*; John Wiley & Sons, Ltd, 2009; pp 129–158. https://doi.org/10.1002/9780470567234.ch6.
(61) Arakawa, R.; Watanabe, S.; Fukuo, T. Effects of Sample Preparation on Matrix-Assisted Laser Desorption/Ionization Time-of-Flight Mass Spectra for Sodium Polystyrene Sulfonate. *Rapid Commun. Mass Spectrom.* **1999**, *13* (11), 1059–1062. https://doi.org/10.1002/(SICI)1097-0231(19990615)13:11<1059::AID-RCM608>3.0.CO;2-1.
(62) Brandt, H.; Ehmann, T.; Otto, M. Investigating the Effect of Mixing Ratio on Molar Mass Distributions of Synthetic Polymers Determined by MALDI-TOF Mass Spectrometry Using Design of Experiments. *J. Am. Soc. Mass Spectrom.* **2010**, *21* (11), 1870–1875. https://doi.org/10.1021/jasms.8b03643.

(63) Schlosser, G.; Jakab, A.; Pocsfalvi, G.; Vékey, K.; Hudecz, F.; Mező, G. Matrix/Analyte Ratio Influencing Polymer Molecular Weight Distribution in Matrix-Assisted Laser Desorption/Ionization Time-of-Flight Mass Spectrometry. *Rapid Commun. Mass Spectrom.* **2009**, *23* (9), 1249–1254. https://doi.org/10.1002/rcm.3993.
(64) Yalcin, T.; Dai, Y.; Li, L. Matrix-Assisted Laser Desorption/Ionization Time-of-Flight Mass Spectrometry for Polymer Analysis: Solvent Effect in Sample Preparation. *J. Am. Soc. Mass Spectrom.* **1998**, *9* (12), 1303–1310. https://doi.org/10.1021/jasms.8b01128.
(65) Patil, A. A.; Chiang, C.-K.; Wen, C.-H.; Peng, W.-P. Forced Dried Droplet Method for MALDI Sample Preparation. *Anal. Chim. Acta* **2018**, *1031*, 128–133. https://doi.org/10.1016/j.aca.2018.05.056.
(66) Garden, R. W.; Sweedler, J. V. Heterogeneity within MALDI Samples As Revealed by Mass Spectrometric Imaging. *Anal. Chem.* **2000**, *72* (1), 30–36. https://doi.org/10.1021/ac9908997.
(67) Trimpin, S.; Keune, S.; Räder, H. J.; Müllen, K. Solvent-Free MALDI-MS: Developmental Improvements in the Reliability and the Potential of MALDI in the Analysis of Synthetic Polymers and Giant Organic Molecules. *J. Am. Soc. Mass Spectrom.* **2006**, *17* (5), 661–671. https://doi.org/10.1016/j.jasms.2006.01.007.
(68) Hortal, A. R.; Hurtado, P.; Martínez-Haya, B.; Arregui, A.; Bañares, L. Solvent-Free MALDI Investigation of the Cationization of Linear Polyethers with Alkali Metals. *J. Phys. Chem. B* **2008**, *112* (29), 8530–8535. https://doi.org/10.1021/jp802089r.
(69) Hortal, A. R.; Hurtado, P.; Martínez-Haya, B.; Arregui, A.; Bañares, L. Poly(Ethylene Glycol) Cationization with Alkali Metals in Matrix-Assisted Laser Desorption Ionization Investigated with the Solvent-Free Method. *Appl. Phys. A* **2008**, *92* (4), 859–863. https://doi.org/10.1007/s00339-008-4577-0.
(70) Shin, D.; Kim, I.; Paek, J.; Kim, J. A Novel "Freeze Vacuum Drying" Crystallization Method Toward Quantitative MALDI-MS. *Bull. Korean Chem. Soc.* **2017**, *38* (1), 133–135. https://doi.org/10.1002/bkcs.11046.
(71) Kudina, O.; Eral, B.; Mugele, F. E-MALDI: An Electrowetting-Enhanced Drop Drying Method for MALDI Mass Spectrometry. *Anal. Chem.* **2016**, *88* (9), 4669–4675. https://doi.org/10.1021/acs.analchem.5b04283.
(72) Meier, M. A. R.; Hoogenboom, R.; Fijten, M. W. M.; Schneider, M.; Schubert, U. S. Automated MALDI-TOF-MS Sample Preparation in Combinatorial Polymer Research. *J. Comb. Chem.* **2003**, *5* (4), 369–374. https://doi.org/10.1021/cc020101o.
(73) Guttman, C. M.; Wallace, W. E. MALDI Mass Spectrometry for the Quantitative Determination of Polymer Molecular Mass Distribution. In *Maldi Mass Spectrometry for Synthetic Polymer Analysis*; John Wiley & Sons, Ltd, 2009; pp 187–204. https://doi.org/10.1002/9780470567234.ch8.
(74) Zenobi, R. Ionization Processes and Detection in MALDI-MS of Polymers. In *Maldi Mass Spectrometry for Synthetic Polymer Analysis*; John Wiley & Sons, Ltd, 2009; pp 9–26. https://doi.org/10.1002/9780470567234.ch2.
(75) Dashtiev, M.; Wäfler, E.; Röhling, U.; Gorshkov, M.; Hillenkamp, F.; Zenobi, R. Positive and Negative Analyte Ion Yield in Matrix-Assisted Laser Desorption/Ionization. *Int. J. Mass Spectrom.* **2007**, *268* (2), 122–130. https://doi.org/10.1016/j.ijms.2007.07.001.
(76) J. Haven, J.; Vandenbergh, J.; Junkers, T. Watching Polymers Grow: Real Time Monitoring of Polymerizations via an on-Line ESI-MS/Microreactor Coupling. *Chem. Commun.* **2015**, *51* (22), 4611–4614. https://doi.org/10.1039/C4CC10426A.
(77) Gillon, B. H.; Gates, D. P.; Henderson, M. A.; Janusson, E.; McIndoe, J. S. Mass Spectrometric Characterization of Oligomeric Phosphaalkenes. *Can. J. Chem.* **2016**, *95* (3), 239–242. https://doi.org/10.1139/cjc-2016-0206.

(78) Ito, K.; Kitagawa, S.; Ohtani, H. Analysis of Multiply Charged Poly(Ethylene Oxide-Co-Propylene Oxide) Using Electrospray Ionization-Ion Mobility Spectrometry-Mass Spectrometry. *Anal. Sci.* **2019**, *35* (2), 169–174. https://doi.org/10.2116/analsci.18P332.
(79) Ishitsuka, K.; Kakiuchi, T.; Sato, H.; Fouquet, T. N. J. An Arsenal of Tools Based on Kendrick Mass Defects to Process Congested Electrospray Ionization High-Resolution Mass Spectra of Polymers with Multiple Charging. *Rapid Commun. Mass Spectrom.* **2020**, *34* (S2), e8584. https://doi.org/10.1002/rcm.8584.
(80) Criado-Hidalgo, E.; Fernández-García, J.; Fernández de la Mora, J. Mass and Charge Distribution Analysis in Negative Electrosprays of Large Polyethylene Glycol Chains by Ion Mobility Mass Spectrometry. *Anal. Chem.* **2013**, *85* (5), 2710–2716. https://doi.org/10.1021/ac303054x.
(81) Ozeki, Y.; Omae, M.; Kitagawa, S.; Ohtani, H. Electrospray Ionization-Ion Mobility Spectrometry–High Resolution Tandem Mass Spectrometry with Collision-Induced Charge Stripping for the Analysis of Highly Multiply Charged Intact Polymers. *Analyst* **2019**, *144* (10), 3428–3435. https://doi.org/10.1039/C8AN02500B.
(82) Festag, R.; Alexandratos, S. D.; Joy, D. C.; Wunderlich, B.; Annis, B.; Cook, K. D. Effects of Molecular Entanglements during Electrospray of High Molecular Weight Polymers. *J. Am. Soc. Mass Spectrom.* **1998**, *9* (4), 299–304. https://doi.org/10.1021/jasms.8b01156.
(83) Kebarle, P.; Tang, L. From Ions in Solution to Ions in the Gas Phase - the Mechanism of Electrospray Mass Spectrometry. *Anal. Chem.* **1993**, *65* (22), 972A-986A. https://doi.org/10.1021/ac00070a001.
(84) Konermann, L.; Metwally, H.; Duez, Q.; Peters, I. Charging and Supercharging of Proteins for Mass Spectrometry: Recent Insights into the Mechanisms of Electrospray Ionization. *Analyst* **2019**, *144* (21), 6157–6171. https://doi.org/10.1039/C9AN01201J.
(85) Wesdemiotis, C.; Williams-Pavlantos, K. N.; Keating, A. R.; McGee, A. S.; Bochenek, C. Mass Spectrometry of Polymers: A Tutorial Review. *Mass Spectrom. Rev.* **2024**, *43* (3), 427–476. https://doi.org/10.1002/mas.21844.
(86) Nitsche, T.; Sheil, M. M.; Blinco, J. P.; Barner-Kowollik, C.; Blanksby, S. J. Electrospray Ionization-Mass Spectrometry of Synthetic Polymers Functionalized with Carboxylic Acid End-Groups. *J. Am. Soc. Mass Spectrom.* **2021**, *32* (8), 2123–2134. https://doi.org/10.1021/jasms.1c00085.
(87) Kruve, A.; Kaupmees, K. Adduct Formation in ESI/MS by Mobile Phase Additives. *J. Am. Soc. Mass Spectrom.* **2017**, *28* (5), 887–894. https://doi.org/10.1007/s13361-017-1626-y.
(88) Henderson, M. A.; McIndoe, J. S. Ionic Liquids Enable Electrospray Ionisation Mass Spectrometry in Hexane. *Chem. Commun.* **2006**, No. 27, 2872–2874. https://doi.org/10.1039/B606938J.
(89) Ku, B. K.; Fernandez de la Mora, J.; Saucy, D. A.; Alexander. Mass Distribution Measurement of Water-Insoluble Polymers by Charge-Reduced Electrospray Mobility Analysis. *Anal. Chem.* **2004**, *76* (3), 814–822. https://doi.org/10.1021/ac034594a.
(90) Geno, P. W.; Macfarlane, R. D. Secondary Electron Emission Induced by Impact of Low-Velocity Molecular Ions on a Microchannel Plate. *Int. J. Mass Spectrom. Ion Process.* **1989**, *92*, 195–210. https://doi.org/10.1016/0168-1176(89)83028-9.
(91) Farmer, T. B.; Caprioli, R. M. Mass Discrimination in Matrix-Assisted Laser Desorption Ionization Time-of-Flight Mass Spectrometry: A Study Using Cross-Linked Oligomeric Complexes. *J. Mass Spectrom.* **1995**, *30* (9), 1245–1254. https://doi.org/10.1002/jms.1190300906.
(92) Weidmann, S.; Mikutis, G.; Barylyuk, K.; Zenobi, R. Mass Discrimination in High-Mass MALDI-MS. *J. Am. Soc. Mass Spectrom.* **2013**, *24* (9), 1396–1404. https://doi.org/10.1007/s13361-013-0686-x.

Chapter 3 – Comparative Assessment of ESI-MS Softness for Inorganic Complexes: How Soft is Your ESI-MS?

This chapter has been reproduced with minor changes from "Ian C. Chagunda, Peter J. H. Williams, Tiago Fisher, Naomi L. Stock, Daniel G. Beach, Gilian T. Thomas, Jane Zhu, and J. Scott McIndoe, *European Journal of Inorganic Chemistry*, **2024**, *27*, e202400077" and adapted with permission from Wiley-VCH GmbH. The project was conceptualized by ICC and JSM. The methodology was developed collaboratively by ICC, TF, and JSM. Investigations were carried out by ICC, PJHW, TF, NLS, DGB, GTT, and JZ, with ICC analyzing and interpreting the data. The original draft of this manuscript was written by ICC, with additional review and editing contributions from PJHW, NLS, DGB, and JSM.

3.1 Abstract

Electrospray ionization mass spectrometry (ESI-MS) is a powerful tool for identifying and characterizing organometallic and coordination compounds. However, detection of fragile structures bound by weaker intermolecular forces can be significantly limited in ESI-MS owing to the use of relatively harsh instrument conditions and configurations. In this study, a set of tests was developed to assess the softness of ESI-MS systems. Two variants are presented: positive ion mode, utilizing a mixture of sodium ions and triphenylphosphine oxide producing $[Na(OPPh_3)_n]^+$ ions (n = 1–4), and negative ion mode utilizing $Pd(PPh_3)_4$ and sulfonated triphenylphosphine producing $[Pd(\mathbf{L})(PPh_3)_n]^-$ ions (n = 0–2), where softer instrument conditions preserve a higher proportion of the high-coordinate ions and harsher conditions will result in increased detection of products of ion fragmentation. The results revealed notable variations in instrument softness, which were influenced by a combination of instrument design and experimental parameters. Meticulously optimizing experimental conditions and ESI-MS parameters is essential to achieving the softest

ionization possible, ensuring reliable analysis where applicable. This chapter offers valuable insight through straightforward tests that can be employed to assess the suitability of an instrument for specific research needs.

3.2 Introduction

In the field of organometallic chemistry, ESI-MS has emerged as a useful tool to identify and characterize new compounds, study reaction mechanisms and dynamics, and establish speciation in complex mixtures.[1–8] As a soft ionization technique, ESI is noted for producing ions with minimal fragmentation, making it highly suitable for thermally fragile species that are not amenable to other ionization techniques, such as electron ionization.[9] Despite the soft character of the ESI process, it is not immune to ion fragmentation and aggregation, which can complicate spectral interpretation and peak recognition, thus compromising analysis.[10]

The behavior and extent of fragmentation of ions is closely tied to the internal energy acquired during the ionization process, which encompasses the total energy above the ions' electronic, vibrational, and rotational ground states. The dissociation rate is influenced by both the internal energy as well as the timescale of the experiment, equal to the ion flight time between the source and the mass analyzer.[11,12] It is important to differentiate between the internal energy and the kinetic energy in ions, as conversion of kinetic energy to internal energy plays a significant role in influencing ion behavior and fragmentation outcomes. This conversion can be modelled by two energy transfer mechanisms: (1) the formation of long-lived complexes between the ion and background gas, leading to energy redistribution into internal energy and relative translation energy upon dissociation; and (2) the impulsive collision mechanisms where vibrational energy is transferred from the recoil energy of inelastic collision.[11]

Additionally, as ions or charged droplets are subjected to rapid decrease in pressure during their transition from the atmospheric pressure source into the high vacuum region of the mass analyzer (10^{-3} to 10^{-10} Torr, depending on the type of analyzer), they can

experience acceleration.[13] The axial velocity component is amplified as a result of supersonic expansion as ions and charged droplets pass through successive differential pumping stages separated by small orifices.[14] This acceleration and subsequent increased occurrence of collisions leads to an increase in the energy per particle, enhancing the likelihood of ion fragmentation.[11,15] Furthermore, acceleration by strong electric field gradients in the intermediate pressure regions intensifies the frequency of energetic collisions with residual background gases, thus promoting ion activation and fragmentation.[15–17]

Together, these aspects highlight the dynamic and multifaceted nature of in-source fragmentation and collision-induced dissociation (CID) in ESI-MS, where factors such as collision dynamics, energy transfer mechanisms, and the nature of interactions between ions and their surroundings all play a pivotal role in ion dissociation. Design of the ionization source, MS interface and ion optics, the composition of the solvent used, and the instrument settings can all contribute to an ESI instrument's ionization efficiency and softness.[18–21] As a result, spectra from different instruments might vary significantly, making it challenging to compare and to reproduce ESI-MS spectra.

Several studies on instrument parameter optimization have been published. One such study investigated the careful optimization of various parameters to enhance sampling efficiency, suggesting the use of fixed optimal values for key source parameters to simplify ESI-MS.[22] Another investigation focused on the internal energy distribution of benzylammonium ions produced through secondary electrospray ionization (SESI), revealing the relatively harsh instrument settings commonly used for SESI, and highlighting the need for precise instrument tuning necessary to take advantage of its softness.[23] The introduction of a new class of thermometer ions, benzhydrylpyridinium, has also offered a potential avenue for determining the internal energies of ions generated in ESI, with potential implications for optimization of instrument parameters for ESI-MS.[24]

Research in the McIndoe group focuses on investigating catalytic reactions with ESI-MS, particularly those characterized by weak interactions between organometallic metal complexes and substrates.[25–27] However, it is common to face challenges in obtaining consistent results due to substantial differences between ESI-MS instruments. Recognizing

the impact of these disparities is crucial and selecting the appropriate MS instrument and source is vital for accurate detection of the species of interest. Therefore, addressing these challenges becomes paramount in improving the reproducibility and comparability of our results.

To address this, a comparative assessment of ESI-MS instruments was conducted to evaluate their relative softness using a simple but sensitive experiment in both positive and negative ion mode. In this context, a source's "softness" is a qualitive measure of the minimum internal energy imparted to ions during ionization and subsequent transfer into the gas phase, while avoiding additional internal energy post-ionization that could promote fragmentation.[11] While the minimal energy required for ionization is largely determined by the ionization method and instrument design, additional energy transfer can be minimized by carefully adjusting experimental conditions and instrument parameters.

This chapter presents results from testing different ESI-MS instruments from various manufacturers, which revealed substantial differences in instrument softness. The aim of this work is to provide simple tests that allow researchers to qualitatively probe the energetic conditions of their instrument, with particular relevance for organometallic or inorganic chemists. These tests, unlike those developed using thermometer ions,[23,24,28] do not seek to provide a quantitative characterization of internal energies. Instead, they serve as a straightforward method for assessing instrument softness and offer practical tools for evaluating the suitability of instruments in detecting thermally fragile organometallic and coordination species.

3.3 Results and Discussion

3.3.1 Initial Assessment of Instrument Softness for Systems 1 and 2

The positive ion mode test used triphenylphosphine oxide ($OPPh_3$) and sodium chloride, both cheap and readily available starting materials. Phosphine oxide is notable due to the considerable basicity of the oxygen atom, and its propensity to aggregate with charged species in solution.[29,30] Charged species can be formed through Brönsted–Lowry acid–base

reactions, resulting in protonated molecules ($[M + H]^+$), or through the Lewis acid–base mechanism, which forms coordination complexes involving cations with neutral molecules (e.g., $[M + Na]^+$). Both the protonated and sodiated species are anticipated to be present in appreciable concentrations within the bulk solution,[31] despite binding constants in ESI-MS being reported to be on average two orders of magnitude larger than those detected in solution.[32] When $OPPh_3$ is sodiated, the resulting spectra appear uncomplicated, with $[Na(OPPh_3)_n]^+$ and a maximum of four coordinated ligands.[33] The $n = 4$ species emerges as the most diagnostic peak, appearing prominently in some instruments while being entirely absent in others.

Two mass spectrometers were used in the initial stages of method development: the Waters Tandem Quadrupole Detector (TQD) spectrometer (System 1) and the Waters Synapt G2-S*i* QuanTof ESI-ion mobility spectrometry (IMS) mass spectrometer (System 2). The instrument source parameters were not initially optimized, with settings based on values recommended by the manufacturer. Parameters were then optimized to minimize ion fragmentation using OptiMS,[34] (parameter details provided in Section 3.5). Both instruments are equipped with an atmospheric-pressure ionization (API) source, where differential pumping transfers ions from ambient pressure into the high vacuum of a mass analyzer.[13]

In System 1, samples are introduced into the ionization source, pass through the sample cone into the vacuum system, and proceed to the first quadrupole for mass filtering based on the *m/z* ratio. The ion beam proceeds to the T-Wave collision cell for CID or additional *m/z* filtering in the second quadrupole.[35] In contrast, System 2 directs samples through a sampling orifice in the ionization source, then via StepWave transfer optics with a narrow bore ion guide to eliminate neutral species. The ion beam is filtered by quadrupole, passes through the TriWave region with T-Wave ion guides for ion trapping, accumulation, release, and transfer to the time-of-flight (TOF) analyzer.[36]

Figure 3.1 shows mass spectra collected from the two initial ESI-MS test instruments in positive ion mode, using their non-optimized instrument parameters. The strongest relative signal intensity for the $n = 4$ ion peak was observed in System 1 (Figure 3.1A). The intensities of the observed peaks varied as anticipated, depending on the metal-ligand mole

ratio used in sample preparation. The best signal intensity for the tetrakis cation $[Na(OPPh_3)_4]^+$ is obtained with a 1:4 mole ratio of sodium ions to triphenylphosphine oxide.

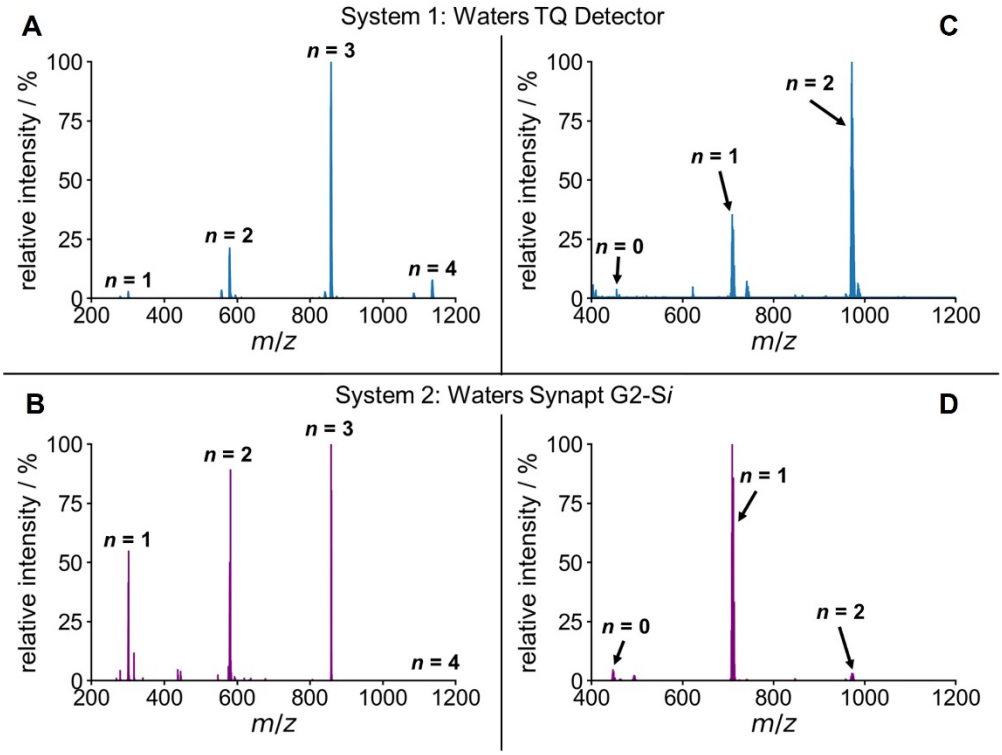

Figure 3.1: Left: ESI(+)-MS spectra for Systems 1 (A) and 2 (B) collected at 120 °C and 80 °C source temperatures, respectively. Samples consist of 0.05 mM and 0.2 mM NaCl and $OPPh_3$, respectively, producing $[Na(OPPh_3)_n]^+$ ions, where n = 1–4. Right: ESI(–)-MS spectra for Systems 1 (C) and 2 (D), collected at 100 °C source temperatures. Samples consist of 0.5 mM $Pd(PPh_3)_4$ and $[PPN]^+[P(Ph)_2(m\text{-}C_6H_4SO_3)]^-$ or [PPN][**1**], producing $[Pd(\mathbf{1})(PPh_3)_n]^-$ ions, where n = 0–2.

The tetrakis cation $[Na(OPPh_3)_4]^+$ was detected with minimal signal intensity in System 2 (Figure 3.1B). Its absolute intensity was 1.2×10^6 counts per second (cps.), which was three orders of magnitude less than the intensity of the n = 3 species, which was 2.2×10^9 cps. This low n = 4 signal intensity did not register significantly above the background noise level of 2.4×10^5 cps., even when excess $OPPh_3$ was added to the sample. This observation may not be attributed solely to in-source fragmentation, but rather to be a known effect of the instrument design. As a hybrid ESI-IMS-MS instrument, ions must pass through the IMS drift tube, regardless of whether IMS experiments are being undertaken, extending the experiment's timescale. This extended duration of transients may promote

an increase in the frequency of energetic ion collisions with background drift gas molecules, resulting in greater ion internal energy and promoting fragmentation.[37] Furthermore, recent investigations into structural rearrangements in trapped ion mobility spectrometry (TIMS) revealed that the effective vibrational temperature of ions inside the TIMS tunnel exceeds 500 K.[38] This suggests that a similar phenomenon is likely at play in System 2, where the upstream effective vibrational temperature of ions likely exceeds the source temperature.

In negative ion mode, a parallel test was developed using a charge-tagged triphenylphosphine derivative $[(Ph_3P)_2N]^+[PPh_2(m\text{-}C_6H_4SO_3)]^-$, hereafter referred to as [PPN][**1**], and tetrakis(triphenylphosphine)palladium(0), $Pd(PPh_3)_4$. This combination generated a series of $[Pd(\mathbf{1})(PPh_3)_n]^-$ ions, where n = 0-2. Since $Pd(PPh_3)_4$ primarily exists in solution as the tris-ligated $Pd(PPh_3)_3$ species formed following ligand dissociation,[39] the introduction of a charge-tagged analogue of PPh_3 facilitates the formation of anionic species through ligand exchange, making the complex detectable in negative mode ESI-MS. In this context, detection of the n = 2 tris-ligated ion implies preservation of weaker metal-ligand interactions in a "softer" source.

Similar trends to those observed in positive ion mode were also evident in the negative ion mode. System 1 produced the best results, prominently featuring the diagnostic n = 2 ion peak (Figure 3.1C). In contrast, System 2 produced distinct spectra characterized by a higher relative abundance of the n = 1 species with less than 5% relative abundance of the n = 2 ion peak (Figure 3.1D). The increased prevalence of the monophosphine ion, $[Pd(\mathbf{1})]^-$, for System 2 can be attributed to ion fragmentation, as high concentrations of this species are not accessible in solution.[40] These findings track closely with the observations from the positive mode test, where extensive fragmentation of the most fragile species occurred, likely due to additional energy imparted within the drift tube. The obtained data highlighted the spectral variability initially observed for both systems.

3.3.2 Enhancing Softness Through Automated Optimization of Instrument Parameters

To address the variability observed between the two test instruments, the potential for enhancing softness through instrument parameter optimization was explored. Achieving ideal spectral data often required substantial parameter optimization, as suboptimal settings during characterization can compromise the quality of results.[22] The difficulty of optimizing instrument parameters for unknown samples is recognized in real-world applications since the precise characteristics of a new sample are often unpredictable. However, the tests outlined in this chapter can facilitate the initial optimization of parameters for new sample analyses. By prioritizing softer ionization conditions that increase the relative abundance of highly coordinated ions, a favorable starting point for tuning instrument parameters can be established. This proactive approach encourages moving away from default instrument settings, which may be too harsh for fragile species, towards conditions that maximize the detection of thermally fragile compounds.

Identifying optimal parameters can be time consuming and complex, made more difficult by the fact that optimizing one parameter may deoptimize another.[41] To address this, a semi-systematic optimization of the instrument parameters was conducted using OptiMS.[34] This Bayesian optimization method used a multivariate approach to first randomly sample across the search space defined by the chosen parameters, followed by subsequent optimization for highest signal intensity. Here, parameters were optimized for "softness" as defined by converging on a set of parameters that maximized the signal intensity of the $[Na(OPPh_3)_4]^+$ (*m/z* 1135) or $[Pd(\mathbf{1})(PPh_3)_2]^-$ (*m/z* 971) corresponding peaks.

The open-source OptiMS software not only streamlined the process but also allowed for automated systematic exploration of various parameter settings. This enabled efficient identification of optimal conditions for System 1, which involved reducing capillary and cone voltages to 1.5 kV and 10 V, respectively in positive mode, from their default settings of 4 kV and 30 V. Optimizing instrument conditions led to notable improvements in softness, exemplified by the enhanced relative intensity achieved across all ions, including

the diagnostic n = 4 species, as well as an absolute signal intensity increase of the highest abundance n = 3 peak from 3.5 × 10^6 cps. (Figure 3.1) to 5.4 × 10^7 cps. (Figure 3.2). This highlights a crucial observation that default instrument parameters, tailored for ionization of large stable biomolecules, are often too harsh for preserving fragile assemblies such as coordination complexes.

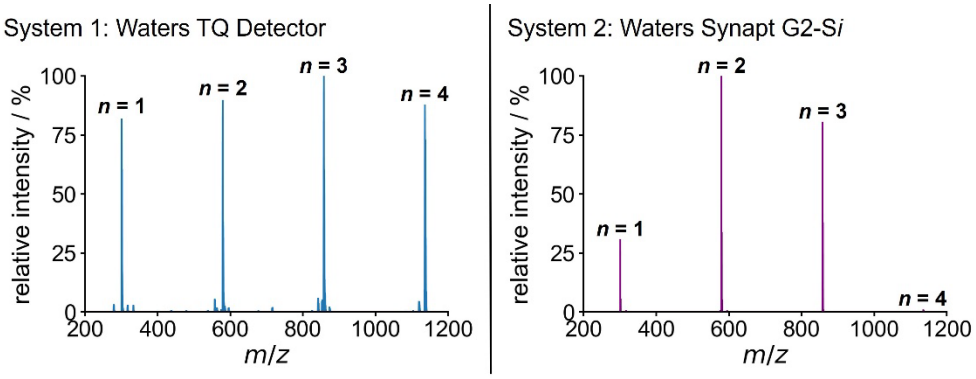

Figure 3.2: ESI(+)-MS spectra of $[Na(OPPh_3)_n]^+$ ions , where n = 1–4, for Systems 1 and 2, both collected at 80 °C source temperatures after automated optimization of instrument parameters using OptiMS.

As anticipated, higher cone voltages promote fragmentation, the degree of which depends on the voltage and the sample composition, whereas the use of lower cone voltages can result in the observation of intact molecular ions.[33] There is a trade-off between reducing the voltages to minimize fragmentation and maintaining a good signal intensity with higher applied potentials. Thus, optimal conditions are expected to be different for each instrument. When weighing the trade-off, lower capillary voltages were additionally beneficial to avoid phenomena such as corona discharge, which can result in an unstable or lost MS signal.

This automated optimization approach not only improved signal stability and signal-to-noise (S/N) ratio, but also offered the potential to fine-tune these settings for different instruments, ensuring optimal performance in each unique scenario. For System 2, the optimized parameters, determined using OptiMS, enhanced the signal intensity of the n = 4 corresponding peak to 3.2 × 10^7 cps. above a baseline noise level of 5.1 × 10^4 cps. as shown in Figure 3.2. This compared to the initial non-optimized settings shown in Figure

3.1 corresponds to an increase in the S/N ratio of two orders of magnitude. However, despite rigorous optimization attempts for System 2, no combination of parameter settings resulted in significantly large improvements in the absolute signal intensity of the tetrakis cation that matched the intensities of the n = 1–3 peaks, even with excess $OPPh_3$ present in solution.

3.3.3 Impact of Source Temperature on Ion Fragmentation Profiles

The positive-mode test was used to investigate how the source temperature affected fragmentation in Systems 1 and 2 (Figure 3.3). The instrument source temperature was ramped from 50-150 °C in 5 °C increments, covering a range that spanned the solvent boiling point (65 °C in this case). All other instrument settings used in these tests were kept at the optimized parameters determined from the OptiMS optimization experiments. For System 1, raising the source temperature above 85 °C led to a reduction in the relative intensity of the n = 4 ion peak, mirrored by a concurrent increase in relative intensity of the fragmentation product n = 3 ion. This temperature-induced effect for System 1 is consistent with a known phenomenon in mass spectrometry, where excessive source temperatures promote fragmentation and denaturation.[42,43]

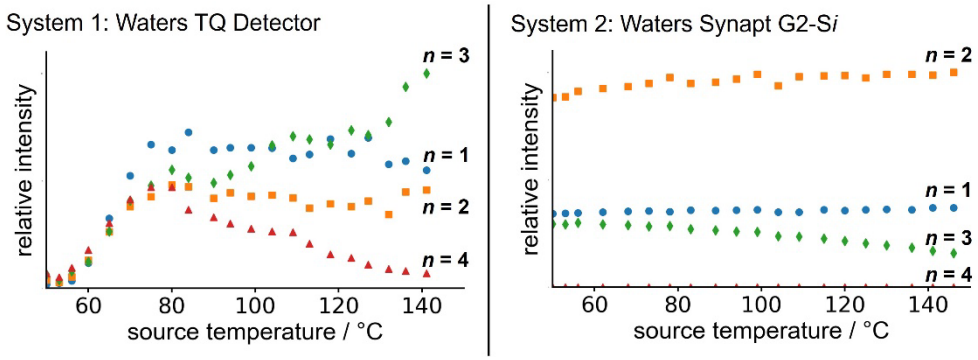

Figure 3.3: Normalized intensities of $[Na(OPPh_3)_n]^+$ ions, where n = 1–4, monitored during source temperature ramp (50-150 °C, 5 °C increments) obtained on Systems 1 and 2.

Applying the temperature ramp to System 2, it became evident that detection of the n = 4 ion was virtually non-existent, even at low source temperatures. The very low

abundance of high-coordinate ions further suggests that softness limitations in System 2 are due to other aspects of instrument design, rather than in-source thermal ion fragmentation. As noted previously, fragmentation is hypothesized to likely results from ions in the post-source region having a higher effective vibrational temperature.[38] Additional contributing factors may include the timescale of the experiment, trapping conditions, and auxiliary field parameters, all of which can lead to higher internal ion energy and increased ion fragmentation of high-coordinate ions.[29]

Furthermore, the discrepancy in relative ion intensities for System 2 observed at variable temperatures (Figure 3.3) compared to at 80 °C source temperature (Figure 3.1B) may stem from experimental or instrumental variations. Despite efforts to maintain consistency, changes in instrument performance over time and data collection at different times could contribute to these differences. Additionally, slight variations in sample preparation, including Na^+ and $OPPh_3$ concentrations may lead to differences in the relative ion intensities observed. Investigations of different molar ratios of Na^+ to $OPPh_3$ for these experiments revealed variations in the relative amounts of the produced ions in the mass spectra (Figure 3.4). As anticipated, a 1:4 NaCl:$OPPh_3$ molar ratio consistently yielded the highest relative intensity of the $n = 4$ peak, aligning with expectations.

These results highlight the pivotal role of instrument design, specifications, and source parameter configurations in defining instrument softness. This temperature-dependent distribution of various species also underscores the challenges associated with sensitively detecting species with different thermal stabilities simultaneously. The often-slow response time of instruments to temperature changes practically impedes the seamless oscillation between analyte-specific temperatures within a single experiment, often necessitating compromises. To overcome this limitation, exploring alternative instrument configurations or adopting experimental strategies that enable more dynamic temperature control in response to the specific thermal stabilities of targeted ions may be essential.

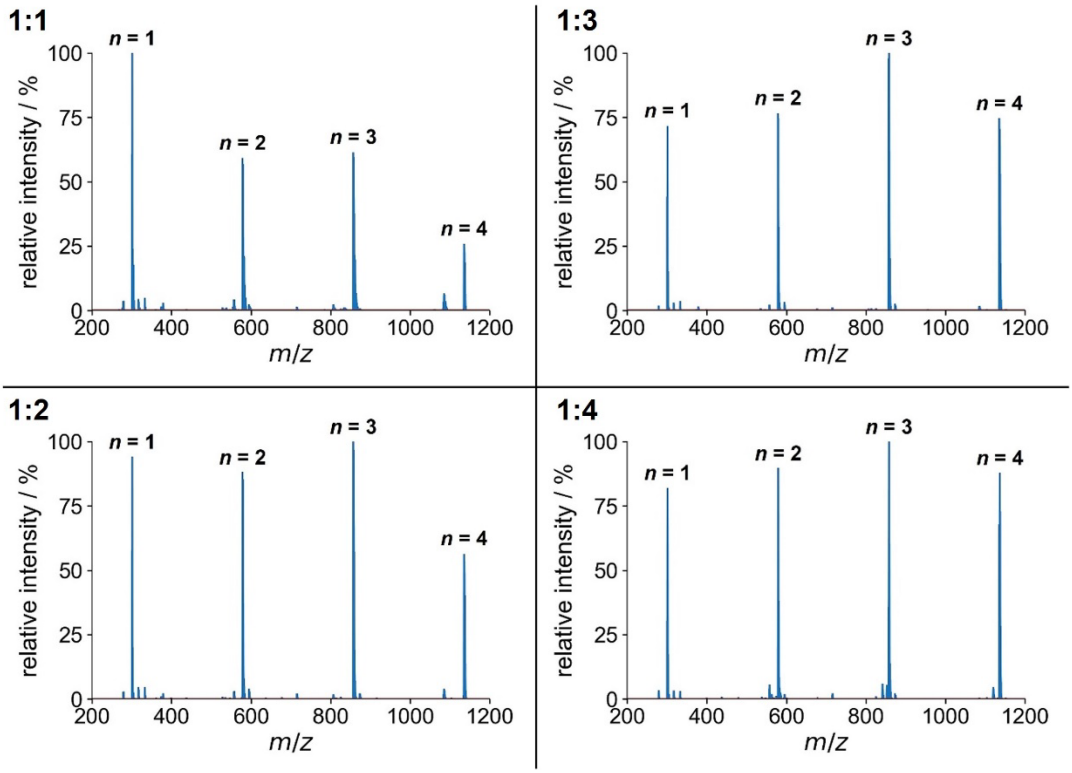

Figure 3.4: Effects of NaCl and $OPPh_3$ stoichiometry on positive-ion ESI mass spectra of $[Na(OPPh_3)_n]^+$ ions collected on System 1. Pane numbers represent the molar ratio of NaCl to $OPPh_3$.

3.3.4 Comparative Analysis of ESI-MS Softness Across Multiple Systems

Given the variability in results obtained from the two test instruments, the dataset was broadened through collaboration, incorporating ESI-MS instruments from different manufacturers. Six additional instruments (Systems 3–8) were used: two Sciex (Concorde, ON, Canada) QTRAP 5500 LC-MS/MS spectrometers equipped with a Sciex TurboSpray ion source (Systems 3 and 4); an Exactive Plus (ThermoFisher Scientific, MA) Orbitrap ESI-MS spectrometer (System 5) and a Q Exactive (ThermoFisher Scientific, MA) HF Hybrid Quadrupole-Orbitrap spectrometer (System 6), both equipped with an Ion Max API source with a HESI-II heated probe; a Bruker (Billerica, MA, USA) SolariX XR FT-ICR spectrometer with 7T magnet equipped with a dual ESI/MALDI source (System 7); and an Agilent (Mississauga, Canada) 6545 LC/Q-Tof spectrometer with a Dual-AJS ion source (System 8). The ESI source conditions for these systems were selected through user-driven parameter optimization, aiming to maximize the signal intensity of higher *n* species (details of

experimental parameter configurations are available in Appendix A, Tables A1–6). This broader dataset revealed significant variations in instrument softness across the different systems.

Figure 3.5 shows the mass spectra from the six additional ESI-MS instruments, operating in positive ion mode, offering additional insights. Notably, these investigations revealed variability in signal intensity, particularly for the diagnostic n = 4 ion peak. Consistent observation of the highest relative signal intensity for the n = 4 ion peak was found in both Systems 3 and 4. A comparative analysis of the two systems, both of which were Sciex QTRAP 5500 LC-MS/MS spectrometers, revealed congruent results, indicating reproducibility across different laboratories using identical instruments. Additionally, the effects of applying a declustering potential were observed. System 3, where a declustering potential was applied, did not show the protonated n = 1 and n = 2 peaks, which were observed as a doublet in System 4, where no declustering potential was applied.

System 5 and System 6 exhibited relatively modest signal intensities for the n = 4 cation. Previous studies on optimizing source parameter for the HESI-II heated electrospray ionization interface used in these two systems have pinpointed the tube lens voltage and skimmer voltage as having the most pronounced impact on in-source fragmentation of the analyzed lipids.[10] Excessive heating and voltages applied can induce thermal effects, influencing the desolvation and activation of ions, leading to variations in both the types and extent of fragmentation observed in the mass spectra.[44] These fragmentation discrepancies may also be related to orbitrap instruments applying strong fields to concentrate or trap ions in the C-trap prior to detection, potentially causing ion fragmentation within the mass analyzer.[45,46]

In contrast, System 7 detected only trace amounts of the $[Na(OPPh_3)_4]^+$ cation, with minimal signal above the baseline. This FT-ICR MS operates on the principles of ion cyclotron resonance in a magnetic field, offering exceptional mass resolution, resolving power, and mass accuracy by trapping and analyzing ions.[47] However, the confinement of ions in the trap can result in the accumulation of internal energy through mechanisms such as ion-neutral collisions, RF excitation inducing oscillatory motion in ions causing energy deposition, and resonant excitation of ions at their cyclotron frequencies.[48]

Similar ion-trapping effects were observed in System 3, involving linear ion traps, where the n = 3 signal intensity was significantly reduced (Figure 3.6). In this system, in addition to the pressure gradient that likely promotes energetic collisional activation, the coupling of radial and axial ion motion near the trap exit can result in ions receiving a proportionately higher kinetic energy boost, potentially leading to instability and fragmentation from collisions.[49] While the exact reason for the higher energy levels in the trapping modes of the QTRAP is not definitively established, this characteristic is specific to that particular instrument rather than a general feature of ion trap mass analyzers, which are not inherently less soft.

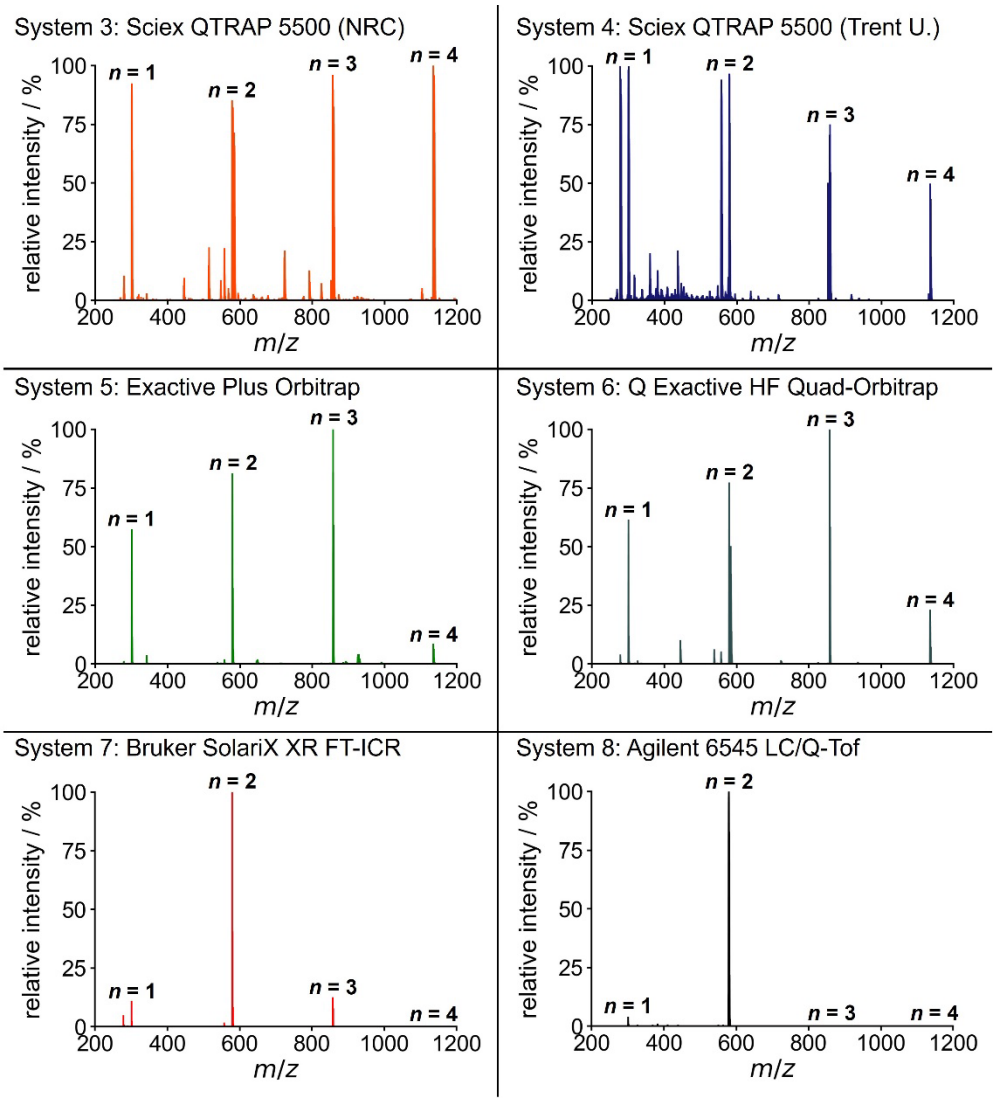

Figure 3.5: ESI(+)-MS spectra of $[Na(OPPh_3)_n]^+$ ions, where n = 1–4 collected on Systems 3–8, under varying manually optimized instrument parameters.

The impact of ion trapping on ion fragmentation is shown in Figure 3.6. In this experiment, ion trapping, which imparts an additional minimum trapping energy of 5 V, resulted in a reduction in the relative signal intensity of the n = 3 peak, accompanied by an increase in the relative intensity of the n = 2 peak (Figure 3.6A). The upper mass range limit (m/z 1000) hindered the detection of n = 4 ions. This observed shift in peak intensities is attributed to the additional ion fragmentation induced by the heightened internal energy caused by the ion trapping process, where additional energy is imparted to focus/trap ions in Q3. This shift is not attributed to in-source conditions, which were the same as in normal full scan mode (Figure 3.6B).

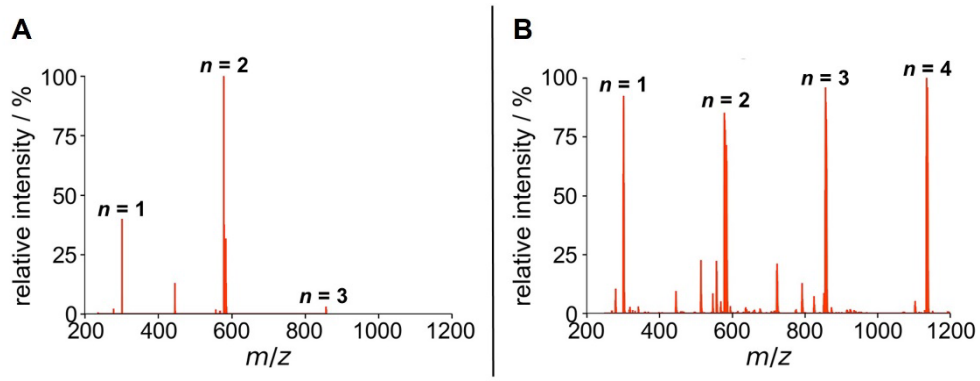

Figure 3.6: Full scan ESI(+)-MS spectra of $[Na(OPPh_3)_n]^+$ ions on System 3, obtained using A) Q3 as an ion trap and B) Q3 as a quadrupole filter.

For System 8, no substantial amounts of the four-coordinate cation were detected. In this system, excess energy is likely imparted on ions through the use of the Agilent Jet Stream (AJS) thermal gradient focusing technology, involving a superheated nitrogen sheath gas introduced collinear with the pneumatically assisted electrospray.[50]

In the negative ion mode, some analogous patterns were noted compared to the positive ion mode, albeit with a more limited set of instruments as shown in Figure 3.7. It is noteworthy that the relative abundance of the n = 2 species displayed variations among the instruments, further shedding light on the divergent softness of the tested systems. Additionally, sample preparation also played a significant role in these tests.

For System 5, where a Schlenk line was used in sample preparation, a high relative intensity of the n = 2 species was observed, however, significant chemical background was observed in this case. Systems 4 and 7, lacking access to a Schlenk line or glovebox, utilized degassed solvent and a quick "dump and mix" to minimize oxidation. Despite these efforts, some oxidation was observed as evidenced by the detection of dioxygenated palladium species $[Pd(O_2)(\mathbf{1})(PPh_3)]^-$ (*m/z* 741), along with minimal detection of the n = 2 species. In the case of System 6, the absence of an inert glovebox or Schlenk line likely led to increased oxidation. Moreover, other adducts and decomposition products were also identified in this system. These observations highlight the necessity of considering the availability of inert atmospheres during experimental design, and the impact of sample handling conditions on the detection outcomes and interpretation.

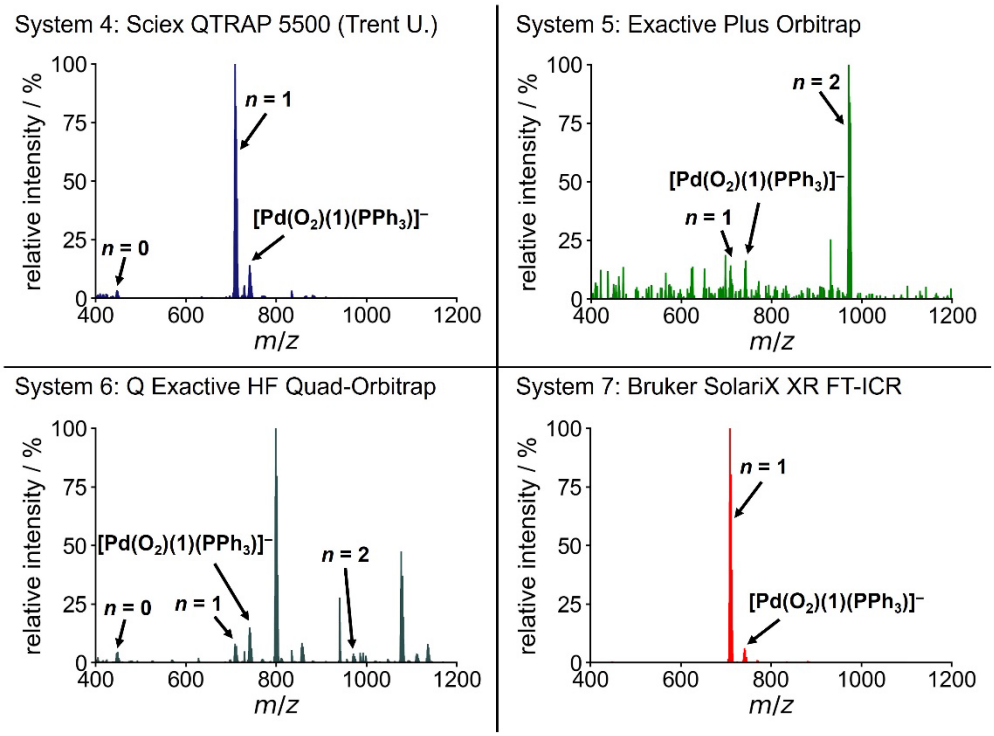

Figure 3.7: ESI(+)-MS spectra of $[Pd(\mathbf{1})(PPh_3)_n]^-$ ions, where n = 0–2, collected on Systems 4–7, under varying manually optimized instrument parameters.

3.3.5 Evaluating Sample Handling Techniques in Negative Ion Mode

When performing the negative ion mode test, a notable additional feature is the experiment's capability to detect O_2 exclusion. Maintaining moisture- and air-free conditions significantly impacts the reactivity and reproducibility of organometallic reactions.[51] In this context, this test provides additional utility by offering insight into the effectiveness of air-sensitive sample handling techniques. Previous studies have demonstrated the rapid catalytic oxidation of triphenylphosphine via $Pd(PPh_3)_4$ in the presence of O_2 in solution.[52] As such, this experiment can also function as a test for O_2 concentration, where detection of the phosphine oxide ion $[\mathbf{1}+O]^-$ (*m/z* 357) reveals the degree of O_2 contamination.

A comparison of poor and good sample handling techniques is shown in Figure 3.8. Figure 3.8A depicts the results of sample preparation in which solvent was collected directly from the solvent bottle without the use of any degassing procedures. This resulted in a phosphine-to-phosphine oxide signal intensity ratio of 1:0.26, as well as the detection of the dioxygenated palladium species $[Pd(O_2)(\mathbf{1})(PPh_3)_n]^-$ (*m/z* 741) in appreciable amounts. When oxygen is excluded by a freeze-pump-thaw cycle and suitable Schlenk line techniques, the intensity ratio of PPh_3 to $OPPh_3$ is reduced to 1:0.02, along with the minimal dioxygenated palladium species (Figure 3.8B). As such, the intensity of $OPPh_3$ indicates the presence of O_2 in an inert atmosphere, though such conditions are common in many catalytic reactions.

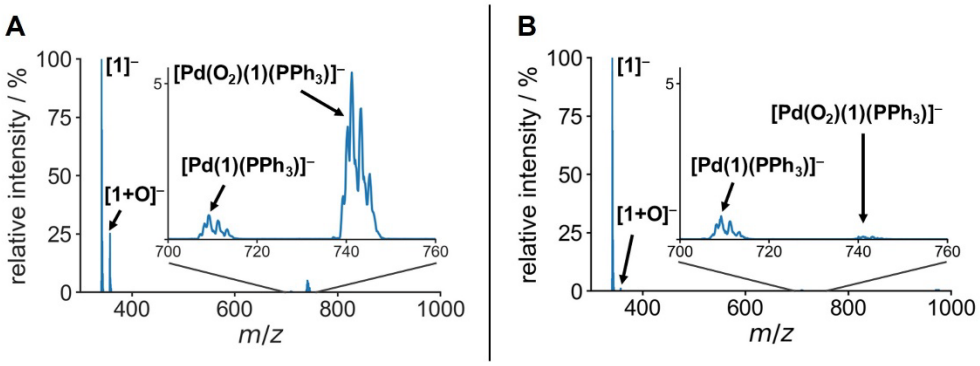

Figure 3.8: ESI(–)-MS spectra obtained for System 1 showing relative amounts of phosphine $[\mathbf{1}]^-$ (*m/z* 341.04) and phosphine oxide $[\mathbf{1}+O]^-$ (*m/z* 357.04) resulting from; A) poor O_2-free handling techniques, and B) O_2 exclusion by solvent degassing. Insets show low abundant species $[Pd(\mathbf{1})(PPh_3)]^-$ (*m/z* 709.04) and $[Pd(O_2)(\mathbf{1})(PPh_3)]^-$ (*m/z* 741.03) amplified ×20.

3.4 Conclusions

This chapter demonstrates the importance of assessing the softness of ESI-MS systems used for detecting easily fragmented species, such as coordination complexes and organometallic compounds. Using a set of tests designed for a quick, relative assessment of instrument softness revealed significant variations in instrument softness, even among instruments from the same manufacturer. These findings highlight the importance of selecting appropriate instrumentation and carefully controlling instrument energetics, such as trapping conditions and auxiliary field parameters where possible, to minimize excess ion energy and fragmentation.

Notably, the results also reveal that even after optimization, some systems exhibit varying levels of suitability for detecting fragile species, highlighting the importance of understanding instrument capabilities in the context of specific analytes and application. Additionally, the negative ion mode test proved effective as a probe for evaluating sample handling quality, such as the exclusion of O_2, further extending the utility of these assessments.

While this study provides a relative comparative assessment of ESI-MS softness, it does not cover all available instruments comprehensively. Nevertheless, these results can serve as a valuable guide for researchers to make informed decisions about instrument suitability for specific research needs. Conducting similar tests to optimize instrument conditions for a given sample composition is strongly recommended as a pathway to achieving reliable and reproducible results in ESI-MS analyses.

3.5 Materials and Methods

Triphenylphosphine oxide, 98%, tetrakis(triphenylphosphine)palladium(0), 99%, NaCl, 99%, and bis(triphenylphosphine)iminium chloride, 98%, were purchased from Sigma-Aldrich and used as received. Bis(triphenylphosphine)iminium triphenylphosphine monosulfonate $[PPN]^+[P(Ph)_2(m\text{-}C_6H_4SO_3)]^-$, or [PPN][**1**], was synthesized as reported previously and consistent characterization data obtained.[53,54] Methanol (HPLC grade) and

tetrahydrofuran (HPLC grade) were purchased from Fisher Scientific and degassed using the freeze-pump-thaw method and kept under inert atmosphere before use. N_2 (HP300 4.8) was purchased from Airgas (Calgary, Canada) and used without further purification. All chemicals were shared with collaborators at the University of British Columbia, Trent University – Water Quality Centre, Biotoxin Metrology – National Research Council Canada, and the University of Ottawa, and used without further processing. Experiments were done under ambient conditions for $[Na(OPPh_3)_n]^+$ tests, or under inert (N_2) atmosphere using standard glovebox and Schlenk line techniques for $[Pd(PPh_3)_n(\mathbf{1})]^-$ tests, where available.

Table 3.1 and Table 3.2 show the operating parameters for ESI-MS Systems 1 and 2. The non-optimized parameters refer to the "default" conditions used for spectra shown in Figure 3.1. Then, using OptiMS,[34] parameters were optimised for "softness" until a set of parameters that maximized the signal intensity of the $[Na(OPPh_3)_4]^+$ (*m/z* 1135.33) and $[Pd(\mathbf{1})(PPh_3)_2]^-$ (*m/z* 971.13) corresponding peaks was reached as in Figure 3.2. For Systems 3-8, ESI source parameters were chosen through manual user-driven optimization in each lab aimed at maximizing the signal intensity of higher *n* species, as summarized in Appendix A, Tables A1-6.

Table 3.1: Waters TQD parameters for instrument softness optimization.

Parameter	Non-optimized		OptiMS optimized	
	Positive Mode	Negative Mode	Positive Mode	Negative Mode
Flow rate	20 µL min^{-1}	20 µL min^{-1}	20 µL min^{-1}	20 µL min^{-1}
Capillary voltage	4.0 kV	3.0 kV	2.0 kV	3.0 kV
Cone voltage	30 V	15 V	12 V	12 V
Extractor voltage	3.0 V	3.0 V	2.0 V	3.0 V
RF Lens voltage	0.5 V	0.3 V	0.3 V	0.3 V
Source temperature	120 °C	100 °C	80 °C	80 °C
Desolvation temperature	250 °C	180 °C	180 °C	180 °C
Cone gas flow	50 L hr^{-1}	100 L hr^{-1}	100 L hr^{-1}	100 L hr^{-1}
Desolvation gas flow	300 L hr^{-1}	200 L hr^{-1}	200 L hr^{-1}	200 L hr^{-1}
FWHM			485	550

Table 3.2: Waters Synapt G2-S*i* instrument parameters for softness optimization.

Parameter	Non-optimized		OptiMS optimized	
	Positive Mode	Negative Mode	Positive Mode	Negative Mode
Flow rate	20 μL min^{-1}	20 μL min^{-1}	20 μL min^{-1}	20 μL min^{-1}
Capillary voltage	3.0 kV	2.5 kV	1.5 kV	2.0 kV
Cone voltage	40 V	40 V	0 V	0 V
Extractor voltage	80 V	80 V	5 V	5 V
RF Lens voltage	80 °C	100 °C	80 °C	80 °C
Source temperature	200 °C	200 °C	200 °C	180 °C
Desolvation temperature	50 L hr^{-1}	50 L hr^{-1}	50 L hr^{-1}	100 L hr^{-1}
Cone gas flow	600 L hr^{-1}	600 L hr^{-1}	200 L hr^{-1}	200 L hr^{-1}
Desolvation gas flow	1.0 V	1.0 V	1.0 V	1.0 V
FWHM			17160	15750

3.5.1 Procedures for ESI-MS Tests

Specifics for ESI(+)-MS mode: In a typical experiment, aliquots of a NaCl solution (1.0 mM in H_2O, 0.1 mL, 0.1 μmol) and a triphenylphosphine oxide ($OPPh_3$) solution (1.0 mM in MeOH, 0.4 mL, 0.1 μmol) were mixed, and the sample made up to 2 mL with methanol (MeOH) to form a 1:4 equivalent sample (0.05 mM NaCl and 0.20 mM $OPPh_3$). Infusion of the sample into a mass spectrometer yielded a spectrum of $[Na(OPPh_3)_n]^+$, where n = 1–4, with expected peaks at *m/z* 301.0753, 579.1613, 875.2474, and 1135.3334 for n = 1–4, respectively.

Specifics for ESI(–)-MS mode: An equimolar solution of 0.5 mM $Pd(PPh_3)_4$ and 0.5 mM bis(triphenylphosphine)iminium triphenylphosphine monosulfonate $[PPN]^+[P(Ph)_2(m\text{-}C_6H_4SO_3)]^-$,or [PPN][**1**], was prepared in 9:1 MeOH/tetrahydrofuran (THF). The solution was prepared using standard Schlenk line techniques,[55] and kept under inert atmosphere where available. A 1 mL sample of the solution was collected, with infusion into a mass spectrometer yielding a spectrum of $[Pd(\mathbf{1})(PPh_3)_n]^-$, where n = 0–2, with expected peaks at *m/z* 446.9442, 709.0353, and 971.1264 for n = 0–2, respectively.

3.6 References

(1) Cheng, G.-J.; Zhong, X.-M.; Wu, Y.-D.; Zhang, X. Mechanistic Understanding of Catalysis by Combining Mass Spectrometry and Computation. *Chem. Commun.* **2019**, *55* (85), 12749–12764. https://doi.org/10.1039/C9CC05458H.

(2) Traeger, J. C. Electrospray Mass Spectrometry of Organometallic Compounds. *Int. J. Mass Spectrom.* **2000**, *200* (1), 387–401. https://doi.org/10.1016/s1387-3806(00)00346-8.

(3) Oliveira, C. C.; Marques, M. V.; Godoi, M. N.; Regiani, T.; Santos, V. G.; Santos, E. A. F. dos; Eberlin, M. N.; Sá, M. M.; Correia, C. R. D. Chemo-, Regio- and Stereoselective Heck Arylation of Allylated Malonates: Mechanistic Insights by ESI-MS and Synthetic Application toward 5-Arylmethyl-γ-Lactones. *Org. Lett.* **2014**, *16* (19), 5180–5183. https://doi.org/10.1021/ol502529v.

(4) Sabino, A. A.; Machado, A. H. L.; Correia, C. R. D.; Eberlin, M. N. Probing the Mechanism of the Heck Reaction with Arene Diazonium Salts by Electrospray Mass and Tandem Mass Spectrometry. *Angew. Chem.* **2004**, *116* (19), 2568–2572. https://doi.org/10.1002/ange.200353076.

(5) Deuker, M.; Yang, Y.; O'Hair, R. A. J.; Koszinowski, K. Tetraorganylargentate(III) Complexes: Key Intermediates in Silver-Mediated Cross-Coupling Reactions. *Organometallics* **2021**, *40* (14), 2354–2363. https://doi.org/10.1021/acs.organomet.1c00118.

(6) Chung, R.; Yu, D.; Thai, V. T.; Jones, A. F.; Veits, G. K.; Read de Alaniz, J.; Hein, J. E. Tandem Reaction Progress Analysis as a Means for Dissecting Catalytic Reactions: Application to the Aza-Piancatelli Rearrangement. *ACS Catal.* **2015**, *5* (8), 4579–4585. https://doi.org/10.1021/acscatal.5b01087.

(7) Schröder, D. Applications of Electrospray Ionization Mass Spectrometry in Mechanistic Studies and Catalysis Research. *Acc. Chem. Res.* **2012**, *45* (9), 1521–1532. https://doi.org/10.1021/ar3000426.

(8) Konermann, L.; Metwally, H.; Duez, Q.; Peters, I. Charging and Supercharging of Proteins for Mass Spectrometry: Recent Insights into the Mechanisms of Electrospray Ionization. *Analyst* **2019**, *144* (21), 6157–6171. https://doi.org/10.1039/C9AN01201J.

(9) Kebarle, P. A Brief Overview of the Present Status of the Mechanisms Involved in Electrospray Mass Spectrometry. *J. Mass Spectrom.* **2000**, *35* (7), 804–817. https://doi.org/10.1002/1096-9888(200007)35:7<804::aid-jms22>3.0.co;2-q.

(10) Gathungu, R. M.; Larrea, P.; Sniatynski, M. J.; Marur, V. R.; Bowden, J. A.; Koelmel, J. P.; Starke-Reed, P.; Hubbard, V. S.; Kristal, B. S. Optimization of Electrospray Ionization Source Parameters for Lipidomics To Reduce Misannotation of In-Source Fragments as Precursor Ions. *Anal. Chem.* **2018**, *90* (22), 13523–13532. https://doi.org/10.1021/acs.analchem.8b03436.

(11) Gabelica, V.; Pauw, E. D. Internal Energy and Fragmentation of Ions Produced in Electrospray Sources. *Mass Spectrom. Rev.* **2005**, *24* (4), 566–587. https://doi.org/10.1002/mas.20027.

(12) Nishimura, T. Unimolecular Dissociations in Mass Spectrometry. In *Fundamentals of Mass Spectrometry*; Hiraoka, K., Ed.; Springer: New York, NY, 2013; pp 29–54. https://doi.org/10.1007/978-1-4614-7233-9_2.

(13) Gross, J. H. Electrospray Ionization. In *Mass Spectrometry: A Textbook*; Gross, J. H., Ed.; Springer International Publishing: Cham, 2017; pp 721–778. https://doi.org/10.1007/978-3-319-54398-7_12.

(14) Hayes, J. M.; Small, G. J. Supersonic Jets, Rotational Cooling, and Analytical Chemistry. *Anal. Chem.* **1983**, *55* (4), 565A-574A. https://doi.org/10.1021/ac00255a784.

(15) Davidson, J. T.; Sasiene, Z. J.; Jackson, G. P. Comparison of In-Source Collision-Induced Dissociation and Beam-Type Collision-Induced Dissociation of Emerging Synthetic Drugs Using a High-Resolution Quadrupole Time-of-Flight Mass Spectrometer. *J. Mass Spectrom.* **2021**, *56* (2), e4679. https://doi.org/10.1002/jms.4679.

(16) Markert, C.; Thinius, M.; Lehmann, L.; Heintz, C.; Stappert, F.; Wissdorf, W.; Kersten, H.; Benter, T.; Schneider, B. B.; Covey, T. R. Observation of Charged Droplets from Electrospray Ionization (ESI) Plumes in API Mass Spectrometers. *Anal. Bioanal. Chem.* **2021**, *413* (22), 5587–5600. https://doi.org/10.1007/s00216-021-03452-y.
(17) Rovelli, G.; I. Jacobs, M.; D. Willis, M.; J. Rapf, R.; M. Prophet, A.; R. Wilson, K. A Critical Analysis of Electrospray Techniques for the Determination of Accelerated Rates and Mechanisms of Chemical Reactions in Droplets. *Chem. Sci.* **2020**, *11* (48), 13026–13043. https://doi.org/10.1039/D0SC04611F.
(18) Raji, M. A.; Schug, K. A. Chemometric Study of the Influence of Instrumental Parameters on ESI-MS Analyte Response Using Full Factorial Design. *Int. J. Mass Spectrom.* **2009**, *279* (2), 100–106. https://doi.org/10.1016/j.ijms.2008.10.013.
(19) Page, J. S.; Kelly, R. T.; Tang, K.; Smith, R. D. Ionization and Transmission Efficiency in an Electrospray Ionization—Mass Spectrometry Interface. *J. Am. Soc. Mass Spectrom.* **2007**, *18* (9), 1582–1590. https://doi.org/10.1016/j.jasms.2007.05.018.
(20) Liigand, J.; Kruve, A.; Liigand, P.; Laaniste, A.; Girod, M.; Antoine, R.; Leito, I. Transferability of the Electrospray Ionization Efficiency Scale between Different Instruments. *J. Am. Soc. Mass Spectrom.* **2015**, *26* (11), 1923–1930. https://doi.org/10.1007/s13361-015-1219-6.
(21) Cox, J. T.; Marginean, I.; Smith, R. D.; Tang, K. On the Ionization and Ion Transmission Efficiencies of Different ESI-MS Interfaces. *J. Am. Soc. Mass Spectrom.* **2015**, *26* (1), 55–62. https://doi.org/10.1007/s13361-014-0998-5.
(22) Kang, Y.; Schneider, B. B.; Bedford, L.; Covey, T. R. Design Characteristics to Eliminate the Need for Parameter Optimization in Nanoflow ESI-MS. *J. Am. Soc. Mass Spectrom.* **2019**, *30* (11), 2347–2357. https://doi.org/10.1007/s13361-019-02301-8.
(23) Kaeslin, J.; Wüthrich, C.; Giannoukos, S.; Zenobi, R. How Soft Is Secondary Electrospray Ionization? *J. Am. Soc. Mass Spectrom.* **2022**, *33* (10), 1967–1974. https://doi.org/10.1021/jasms.2c00201.
(24) Rahrt, R.; Auth, T.; Demireva, M.; Armentrout, P. B.; Koszinowski, K. Benzhydrylpyridinium Ions: A New Class of Thermometer Ions for the Characterization of Electrospray-Ionization Mass Spectrometers. *Anal. Chem.* **2019**, *91* (18), 11703–11711. https://doi.org/10.1021/acs.analchem.9b02257.
(25) Belli, R. G.; Wu, Y.; Ji, H.; Joshi, A.; Yunker, L. P. E.; McIndoe, J. S.; Rosenberg, L. Competitive Ligand Exchange and Dissociation in Ru Indenyl Complexes. *Inorg. Chem.* **2019**, *58* (1), 747–755. https://doi.org/10.1021/acs.inorgchem.8b02915.
(26) Thomas, G. T.; Janusson, E.; Zijlstra, H. S.; McIndoe, J. S. Step-by-Step Real Time Monitoring of a Catalytic Amination Reaction. *Chem. Commun.* **2019**, *55* (78), 11727–11730. https://doi.org/10.1039/C9CC05076K.
(27) Joshi, A.; Zijlstra, H. S.; Collins, S.; McIndoe, J. S. Catalyst Deactivation Processes during 1-Hexene Polymerization. *ACS Catal.* **2020**, *10* (13), 7195–7206. https://doi.org/10.1021/acscatal.0c01607.
(28) Asakawa, D.; Yamamoto, R.; Hanari, N.; Saikusa, K. Differences in the Internal Energies of Ions in Electrospray Ionization Mass Spectrometers Equipped with Capillary–Skimmer and Capillary–RF Lens Interfaces. *Anal. Methods* **2023**, *15* (45), 6150–6158. https://doi.org/10.1039/D3AY01450A.
(29) Henderson, W.; McIndoe, J. S. *Mass Spectrometry of Inorganic and Organometallic Compounds*; John Wiley & Sons, Ltd.: New York, 2005.
(30) Kruve, A.; Kaupmees, K.; Liigand, J.; Oss, M.; Leito, I. Sodium Adduct Formation Efficiency in ESI Source. *J. Mass Spectrom.* **2013**, *48* (6), 695–702. https://doi.org/10.1002/jms.3218.
(31) Kruve, A.; Kaupmees, K. Adduct Formation in ESI/MS by Mobile Phase Additives. *J. Am. Soc. Mass Spectrom.* **2017**, *28* (5), 887–894. https://doi.org/10.1007/s13361-017-1626-y.

(32) Breitbach, Z. S.; Wanigasekara, E.; Dodbiba, E.; Schug, K. A.; Armstrong, D. W. Mechanisms of ESI-MS Selectivity and Sensitivity Enhancements When Detecting Anions in the Positive Mode Using Cationic Pairing Agents. *Anal. Chem.* **2010**, *82* (21), 9066–9073. https://doi.org/10.1021/ac102115w.
(33) Bonnington, L. S.; Coll, R. K.; Gray, E. J.; Flett, J. I.; Henderson, W. Electrospray Mass Spectrometric Investigation of the Relative Ligand Properties of EPh_3 Ligands (E=P, As, Sb or Bi) towards Ag^+ and Cu^+. *Inorganica Chim. Acta* **1999**, *290* (2), 213–221. https://doi.org/10.1016/S0020-1693(99)00151-6.
(34) Williams, P. J. H.; Chagunda, I. C.; McIndoe, J. S. OptiMS: An Accessible Program for Automating Mass Spectrometry Parameter Optimization and Configuration. *J. Am. Soc. Mass Spectrom.* **2024**, *35* (3), 449–455. https://doi.org/10.1021/jasms.3c00354.
(35) Corporation, W. *Waters TQ Detector Operator's Guide*; Operator's Guide 71500126802/Revision G; Waters Corporation: Milford, USA, 2015; pp 1–174. https://www.waters.com/webassets/cms/support/docs/71500126802rg.pdf (accessed 2024-03-13).
(36) Corporation, W. *SYNAPT G2-Si HDMS Mass Spectrometer Overview and Maintenance Guide*; Overview and Maintenance Guide 715004159/Revision C; Waters Corporation: Milford, USA, 2016; pp 1–358. https://www.waters.com/webassets/cms/support/docs/715004159rc.pdf (accessed 2024-03-13).
(37) Gross, J. H. Tandem Mass Spectrometry. In *Mass Spectrometry: A Textbook*; Gross, J. H., Ed.; Springer International Publishing: Cham, 2017; pp 539–612. https://doi.org/10.1007/978-3-319-54398-7_9.
(38) Morsa, D.; Hanozin, E.; Eppe, G.; Quinton, L.; Gabelica, V.; Pauw, E. D. Effective Temperature and Structural Rearrangement in Trapped Ion Mobility Spectrometry. *Anal. Chem.* **2020**, *92* (6), 4573–4582. https://doi.org/10.1021/acs.analchem.9b05850.
(39) Sherwood, J.; Clark, J. H.; Fairlamb, I. J. S.; Slattery, J. M. Solvent Effects in Palladium Catalysed Cross-Coupling Reactions. *Green Chem.* **2019**, *21* (9), 2164–2213. https://doi.org/10.1039/C9GC00617F.
(40) Vidossich, P.; Ujaque, G.; Lledós, A. Palladium Monophosphine $Pd(PPh_3)$: Is It Really Accessible in Solution? *Chem. Commun.* **2013**, *50* (6), 661–663. https://doi.org/10.1039/C3CC47404F.
(41) Elpa, D. P.; Prabhu, G. R. D.; Wu, S.-P.; Tay, K. S.; Urban, P. L. Automation of Mass Spectrometric Detection of Analytes and Related Workflows: A Review. *Talanta* **2020**, *208*, 120304. https://doi.org/10.1016/j.talanta.2019.120304.
(42) Rockwood, A. L.; Busman, M.; Udseth, H. R.; Smith, R. D. Thermally Induced Dissociation of Ions from Electrospray Mass Spectrometry. *Rapid Commun. Mass Spectrom.* **1991**, *5* (12), 582–585. https://doi.org/10.1002/rcm.1290051203.
(43) Alexander Harrison, J.; Pruška, A.; Oganesyan, I.; Bittner, P.; Zenobi, R. Temperature-Controlled Electrospray Ionization: Recent Progress and Applications. *Chem. – Eur. J.* **2021**, *27* (72), 18015–18028. https://doi.org/10.1002/chem.202102474.
(44) Bernier, L.; Pinfold, H.; Pauly, M.; Rauschenbach, S.; Reiss, J. Gas Flow and Ion Transfer in Heated ESI Capillary Interfaces. *J. Am. Soc. Mass Spectrom.* **2018**, *29* (4), 761–773. https://doi.org/10.1007/s13361-018-1895-0.
(45) Zubarev, R. A.; Makarov, A. Orbitrap Mass Spectrometry. *Anal. Chem.* **2013**, *85* (11), 5288–5296. https://doi.org/10.1021/ac4001223.
(46) Hecht, E. S.; Scigelova, M.; Eliuk, S.; Makarov, A. Fundamentals and Advances of Orbitrap Mass Spectrometry. In *Encyclopedia of Analytical Chemistry*; John Wiley & Sons, Ltd, 2019; pp 1–40. https://doi.org/10.1002/9780470027318.a9309.pub2.
(47) Tiquet, M.; La Rocca, R.; Kirnbauer, S.; Zoratto, S.; Van Kruining, D.; Quinton, L.; Eppe, G.; Martinez-Martinez, P.; Marchetti-Deschmann, M.; De Pauw, E.; Far, J. FT-ICR Mass Spectrometry

Imaging at Extreme Mass Resolving Power Using a Dynamically Harmonized ICR Cell with 1ω or 2ω Detection. *Anal. Chem.* **2022**, *94* (26), 9316–9326. https://doi.org/10.1021/acs.analchem.2c00754.

(48) Marshall, A. G. Milestones in Fourier Transform Ion Cyclotron Resonance Mass Spectrometry Technique Development. *Int. J. Mass Spectrom.* **2000**, *200* (1), 331–356. https://doi.org/10.1016/S1387-3806(00)00324-9.

(49) Hager, J. W. A New Linear Ion Trap Mass Spectrometer. *Rapid Commun. Mass Spectrom.* **2002**, *16* (6), 512–526. https://doi.org/10.1002/rcm.607.

(50) Wasito, H.; Causon, T.; Hann, S. Alternating In-Source Fragmentation with Single-Stage High-Resolution Mass Spectrometry with High Annotation Confidence in Non-Targeted Metabolomics. *Talanta* **2022**, *236*, 122828. https://doi.org/10.1016/j.talanta.2021.122828.

(51) Joshi, A.; Killeen, C.; Thiessen, T.; Zijlstra, H. S.; McIndoe, J. S. Handling Considerations for the Mass Spectrometry of Reactive Organometallic Compounds. *J. Mass Spectrom.* **2022**, *57* (3). https://doi.org/10.1002/jms.4807.

(52) Hesketh, A. V.; Nowicki, S.; Baxter, K.; Stoddard, R. L.; McIndoe, J. S. Simplified Real-Time Mass Spectrometric Analysis of Reactions. *Organometallics* **2015**, *34* (15), 3816–3819. https://doi.org/10.1021/acs.organomet.5b00460.

(53) Vikse, K. L.; Henderson, M. A.; Oliver, A. G.; McIndoe, J. S. Direct Observation of Key Intermediates by Negative-Ion Electrospray Ionisation Mass Spectrometry in Palladium-Catalysed Cross-Coupling. *Chem. Commun.* **2010**, *46* (39), 7412–7414. https://doi.org/10.1039/C0CC02773A.

(54) Barton, M. R.; Zhang, Y.; Atwood, J. D. Mono-Sulfonated Derivatives of Triphenylphosphine, $[NH_4]$TPPMS and M(TPPMS)$_2$ (TPPMS = P(Ph)$_2$(*m*-$C_6H_4SO^-_3$); M = Mn^{2+}, Fe^{2+}, Co^{2+} and Ni^{2+}). Crystal Structure Determinations for $[NH_4]$[TPPMS]·½H_2O, $[Fe(H_2O)_5$(TPPMS)]TPPMS, $[Co(H_2O)_5$TPPMS]TPPMS and $[Ni(H_2O)_6](TPPMS)_4 \cdot H_2O$. *J. Coord. Chem.* **2002**, *55* (8), 969–983. https://doi.org/10.1080/0095897022000002295.

(55) Borys, A. M. An Illustrated Guide to Schlenk Line Techniques. *Organometallics* **2023**, *42* (3), 182–196. https://doi.org/10.1021/acs.organomet.2c00535.

Chapter 4 – Poisonous Truth about the Mercury Drop Test: The Effect of Elemental Mercury on Pd(0) and Pd(II)ArX Intermediates

This chapter has been reproduced with minor changes from "Ian C. Chagunda, Tiago Fisher, Makenna Schierling, and J. Scott McIndoe, *Organometallics*, **2023**, *42* (19), 2938–2945" and adapted with permission from American Chemical Society Publications. The project was conceptualized by ICC and JSM. The methodology was developed by ICC and TF, and all investigations carried out by ICC, TF, and MS. Data interpretation and authorship of the original manuscript was by ICC, with additional review and editing from TF and JSM.

4.1 Abstract

The mercury drop test is a widely used method often regarded as decisive for discriminating between homogeneous and heterogeneous catalysis in organometallic systems. However, recent research has highlighted the limitations of this test due to the intrinsic reactivity of some organometallic compounds towards elemental mercury. In this chapter, real-time mass spectrometry was used to investigate the effect of elemental mercury on L_nPd(0) and L_nPd(II)ArX intermediates common in palladium-catalyzed cross-coupling reactions. The findings demonstrate that mercury can interact with both species through redox-transmetallation and amalgamation processes, leading to inhibition of catalytic activity which would often be misinterpreted as evidence for heterogeneous catalysis. These results further call into question the widely held assumption that mercury reacts selectively with heterogeneous catalytic species. Consequently, this chapter will emphasize the need for careful evaluation of results from the test and advocate for the incorporation of alternative kinetic analysis to better understand catalyst behaviour.

4.2 Introduction

Palladium-catalyzed cross-coupling (PdCC) reactions have had a huge impact on the way in which chemists think about building fine chemicals, with innovative applications of palladium cross-coupling garnering new synthetic approaches to natural products,[1,2,3] pharmaceuticals,[4,5] and organic materials.[6,7] These reactions can be classified as either homogeneous or heterogeneous, depending on the nature of the palladium catalyst.

Recent research has challenged the traditional classification of catalysts into homogeneous and heterogeneous domains, as a more complex picture of complementary catalysis from multiple types of catalytic sites has emerged.[8–11] Homogeneous catalysts are defined as having a single type of active site, existing in the same phase as the reactants. These catalysts' reactivity and selectivity are highly dependent on their auxiliary ligands.[12–14] In contrast, a heterogeneous catalyst can have multiple types of active sites on metallic surfaces. The nature of the active site can be ambiguous as illustrated by literature supporting both soluble molecular and nanoparticle catalysts, as well as truly heterogeneous insoluble palladium catalysts.[15–17]

Since most significant catalytic properties including activity, selectivity, stability, and lifetime are affected differently for these two classes of catalysts, it is crucial to differentiate between true homogeneous catalysis and heterogeneous catalysis. Notably, a variety of industrial processes, such as efficient catalyst recovery, rely on the knowledge of the catalyst's identity.[18,19] However, accurately identifying whether a system involves metal-complex homogeneous catalysis or metal-particle heterogeneous catalysis is a difficult issue that has generated a lot of debate in the literature.[20–22]

The mercury drop test is the most widely used poisoning test for heterogeneous catalysis.[19,23] Because of historical precedence and literature descriptions, this test is often regarded as a decisive test for distinguishing between homogeneous and heterogeneous catalysis in organometallic systems. It is based on the simple assumption that elemental mercury, Hg(0), will amalgamate with metal nanoparticles, M(0), considerably reducing or eliminating their catalytic activity (Scheme 4.1A).[22,24] The absence of inhibition is often used as evidence for catalysis by homogenous species, due to the common misconception

that homogeneous metal species bearing protective ligands, $L_nM(X)$, will be left unaffected by Hg(0).[19,22] However, this absence of inhibition is only interpretable as strong evidence against M(0) nanoparticle catalysis known to be inhibited by mercury amalgamation (true for the platinum group metals).[22] Catalyst inhibition can be caused by multiple factors, and is therefore not easily interpretable. This inhibition could result from interactions with molecular M(0) species, or from the amalgamation of soluble M(0) nanoparticles that are often present in equilibrium with the active molecular species.[25] Despite this, there is a prevalent misconception in the literature about the mercury drop test that both outcomes summarized in Scheme 4.1A are equally interpretable.

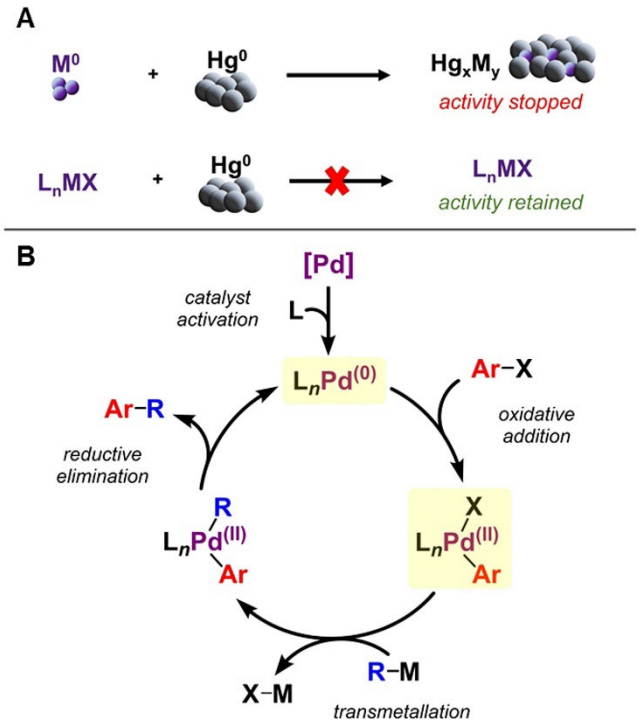

Scheme 4.1: A) General misconception about the interpretable outcomes of the mercury drop test for organometallic catalysis. B) Generic palladium-catalyzed cross-coupling catalytic cycle, highlighting Pd(0) and Pd(II) species formed following catalyst activation and oxidative addition, respectively.

The accuracy of this test has been called into question due to limitations in reaction conditions and the reactivity of some organometallic compounds towards mercury. Warnings about the these drawbacks date back to the 1980s, pointing to the possibility of interactions between mercury and some organometallic compounds.[26] More recent

research has provided evidence of interactions between mercury and palladium (pre)catalysts in catalyzed reactions. For example, the reactivity of mercury with palladium in *N*-heterocyclic carbene (NHC), and in *C,N*- and *C,P*-palladacycle ligand systems, has raised concerns about the accuracy of the test.[27–29]

While many have used the inhibition of catalysis upon the addition of mercury prior to catalyst activation as evidence for the involvement of heterogeneous species,[30,31] Gorunova and coworkers suggested that this could rather indicate reactivity with the homogeneous precatalyst.[28] Work by Chernychev and coworkers recently provided evidence for such interactions by demonstrating the reaction of Hg(0) with the precatalyst tris(dibenzylideneacetone)dipalladium(0), $Pd_2(dba)_3$, to form free dba and other organomercuric species, leading to the near-complete disappearance of dissolved palladium within 30 minutes.[32] Well-defined Pd(II) complexes involving other monophosphines and NHCs were also demonstrated to be poisoned by Hg(0). In addition, reaction conditions such as stoichiometry, stir rate, and temperature were shown to significantly impact the test's sensitivity, further casting doubt on the validity of some results. Given these limitations, the effectiveness of the mercury drop test, and the interpretation of the results attained remains contentious.

This chapter describes the use of PSI-ESI-MS to monitor the effects of the mercury drop test on a model palladium-catalyzed cross-coupling reaction, providing important insights into reaction intermediates. Specifically, the work focusses on interrogating how mercury interacts with the first two intermediates in the reaction cycle: the Pd(0) species formed following catalyst activation of the precatalyst with a ligand, and the Pd(II) species formed after oxidative addition of ArX (Scheme 4.1B). Intermediates further along in the cycle are more challenging to examine unambiguously, as the addition of the nucleophilic cross-coupling partner allows the cycle to turn over, resulting in a system complicated by the simultaneous presence of multiple intermediates. Nevertheless, real-time monitoring of these reactions enabled the identification of significant catalytic and mercuric species, shedding light on their reactivity.

4.3 Results and Discussion

4.3.1 Effects of Mercury on Catalyst Activation: Pd(0) Species

The investigations began with monitoring the *in situ* activation of Pd precatalyst, and the effects of mercury thereupon. Addition of $Pd_2(dba)_3$ to the solution of a charge-tagged triphenylphosphine derivative $[(Ph_3P)_2N]^+[PPh_2(m\text{-}C_6H_4SO_3)]^-$, hereafter [PPN][**1**], at 5 minutes resulted in catalyst activation, with rapid formation of ligated Pd(0) species $[Pd(\mathbf{1})_n(dba)_m]^{n-}$, where n = 1–2 and m = 0–1 (Figure 4.1), as previously reported.[34] Reaction species were identified by their m/z ratios, MS/MS fragmentation products, and matching measured to calculated isotopic distribution patterns (see Appendix B, Table AB.1 for detailed MS/MS characterization). These activated catalyst resting states remained stable in solution for >25 minutes. $[Pd(\mathbf{1})_n(dba)_m]^{n-}$ formation occurred faster than the solution transferred from the reaction flask to the spectrometer (approximately 25 s delay),[33] implying $t_{1/2}$ <10 s.

Upon adding mercury into the reaction (Figure 4.1, 10 min), the relative abundance of the catalyst resting state $[Pd(\mathbf{1})_n(dba)_m]^{n-}$ decreased. No species with characteristic mercury isotope patterns were detected, suggesting that Pd(0) nanoparticles and/or Hg_xPd_y amalgamation as the likely destination of the Pd. The favourable thermodynamics of amalgamation with Pd(0) species further supports this observation ($PdHg_4$ ΔG_{298} = –84.0 kJ mol^{-1}).[35] However, addition of Hg(0) to $[Pd(\mathbf{1})_n(dba)_m]^{n-}$ resulted in a decrease in the relative abundance of both $[Pd(\mathbf{1})_n(dba)_m]^{n-}$ and $[\mathbf{1}]^-$. This was accompanied by an increase in the relative abundance of the oxide of $[\mathbf{1}]^-$, presumably due to phosphine oxidation, which can lead to catalyst deactivation and termination of the reaction.[36] Previous work in the McIndoe group has demonstrated the effects of dioxygen in solution resulting in palladium-catalyzed triphenylphosphine oxidation.[37] It is likely that introduction of uncontrolled amounts of air from the syringe at the addition of Hg(0) accelerated phosphine oxidation in $[Pd(\mathbf{1})_n(dba)_m]^{n-}$, leading to observed decrease in $[\mathbf{1}]^-$ intensity. The summed intensities of the two species remained unchanged after Hg(0) addition (Figure 4.2), indicating an increase and decrease in the relative abundances of $[\mathbf{1}+O]^-$ and $[\mathbf{1}]^-$ respectively.

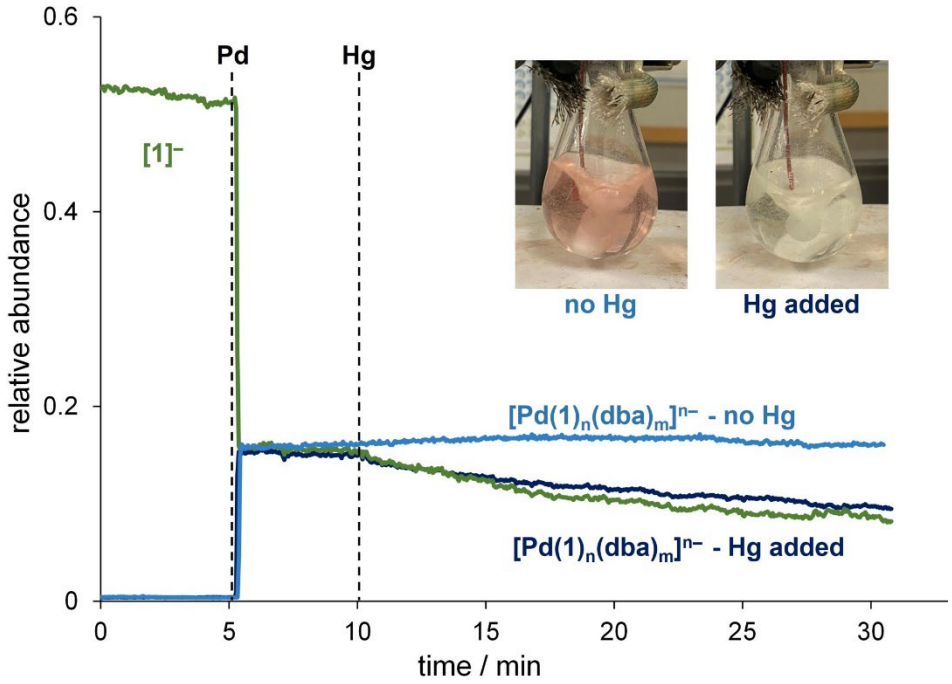

Figure 4.1: PSI-ESI(–)-MS reaction monitoring showing the effects of mercury addition on catalyst activation. A decrease in relative abundance of catalyst resting state [Pd(**1**)$_n$(dba)$_m$]$^{n-}$ (dark blue) and [**1**]$^-$ (green) is observed upon mercury addition (10 min). Control experiment with no mercury added shown in light blue. Inset: Solution colour change observed upon mercury addition.

Repeating the previous control experiment (Figure 4.1), but with air injected into the reaction flask headspace at 20 minutes instead of mercury yielded only a minimal increase in phosphine oxide formation (and no colour change). This suggested that the extensive catalyst decomposition was predominantly due to the interaction of Hg(0) with Pd(0) intermediates. Despite their reputation and widespread use, these results show that triphenylphosphine and similar monodentate phosphine ligands are ineffective at protecting homogeneous Pd(0) intermediates in mercury drop testing under these conditions.[24] The minimal protective properties of monodentate phosphines are likely due to their easy dissociation from the metal complex.

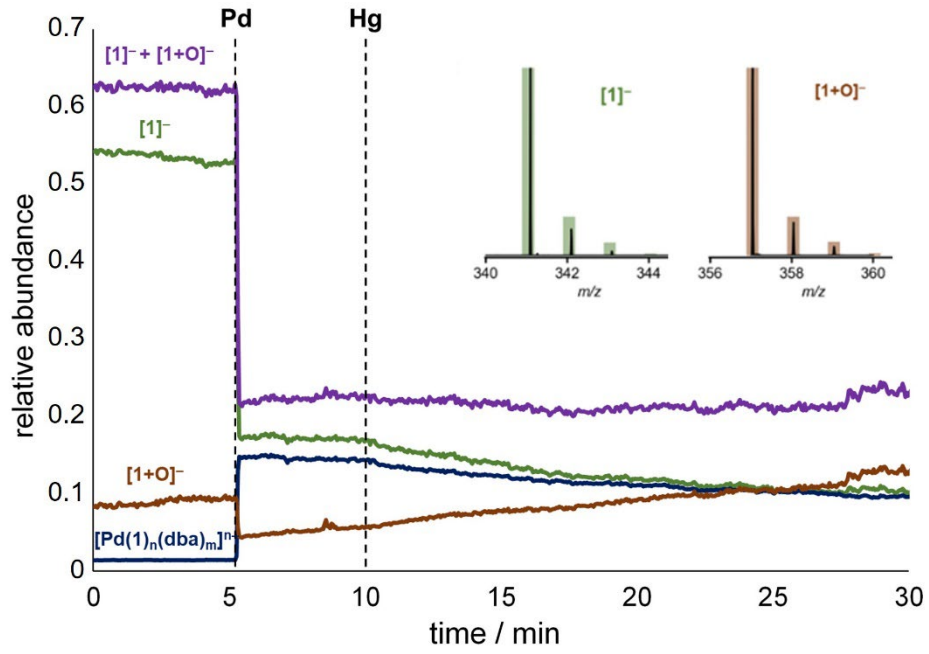

Figure 4.2: PSI-ESI(–)-MS reaction monitoring as in Figure 4.1, showing phosphine ligand **1** and phosphine oxide [**1**+O]⁻ upon Hg addition at 10 minutes, with the summed phosphine intensities remaining unchanged. Insets show the predicted isotope patterns (bars) overlaid on the experimental mass spectra (lines).

4.3.2 Effects of Mercury on Oxidative Addition: Pd(II) Species

After observing decomposition of Pd(0) catalyst activation intermediates, the reactivity of Hg(0) with the monodentate phosphine ligated Pd(II) species formed following the oxidative addition step was investigated. After catalyst activation had reached a steady state, an excess of PhI was added, causing [Pd(**1**)$_n$(dba)$_m$]$^{n-}$ to be consumed and primarily replaced by the Pd(II) species [Pd(**1**)(Ph)(I)]⁻ (Figure 4.3, 10-30 min). Oxidative addition occurred at a significantly slower rate than catalyst activation, likely due to the requirement of dba decoordination prior to the reaction occurring.[38] For the first 10 minutes until equilibrium was reached, the disappearance of [Pd(**1**)$_n$(dba)$_m$]$^{n-}$ exhibited first order kinetics, with $t_{1/2}$ = 3.3 min (Figure 4.3, inset). Additionally, I⁻ was detected, likely resulting from a dissociative equilibrium between [Pd(**1**)(Ph)(I)]⁻ and unobserved Pd(**1**)(Ph). In polar solvents, L$_n$Pd(Ar)(X) complexes feature cationic [L$_n$Pd(Ar)]⁺ species,[39] making the halide dissociation product Pd(**1**)(Ph) zwitterionic. The anionic bisligated [Pd(**1**)$_2$(Ph)]⁻ was also detected in much lower abundance, following a similar temporal profile, indicating its involvement in halide dissociation equilibria.

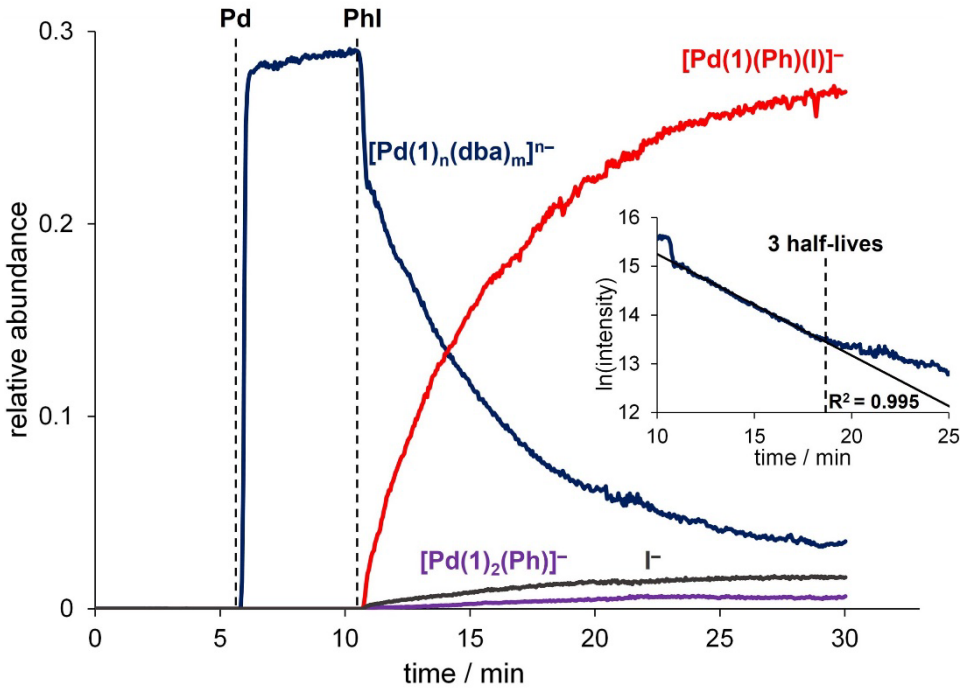

Figure 4.3: PSI-ESI(–)-MS reaction monitoring of the oxidative addition of PhI to $[Pd(\mathbf{1})_n(dba)_m]^{n-}$, where n = 1–2, m = 0–1 over 30 min. Inset: natural log of intensity of $[Pd(\mathbf{1})_n(dba)_m]^{n-}$ over time showing pseudo-first-order kinetics up to 3 half-lives.

Mercury was added to the reaction after the intensity of the oxidative addition product stabilized (Figure 4.4, 20 min), resulting in significant changes in the reaction profiles of multiple species. Firstly, consumption of the catalyst resting state $[Pd(\mathbf{1})_n(dba)_m]^{n-}$ was accelerated (as in Figure 4.1). There was no recovery in the abundance of $[Pd(\mathbf{1})_n(dba)_m]^{n-}$, suggesting that the principal destination of the palladium is to Pd(0) nanoparticles and amalgamation. Additionally, we observed that an increase in $[\mathbf{1}]^-$ intensity mirrored the disappearance of $[Pd(\mathbf{1})Ph(I)]^-$, suggesting that phosphine is decoordinated from the Pd(II) intermediate during reaction with Hg(0). We also observed an increase in $[Pd(\mathbf{1})_2Ph]^-$ intensity, which accounts for approx. 60% of the intensity of Ph-containing ions present after Hg(0) addition. Furthermore, trace quantities of the organomercuric species $[Hg(I)_2Ph]^-$ (Figure 4.4, inset), as well as $[Pd(\mathbf{1})Ph_2(dba)]^-$ were detected, accounting for some of the "missing" Ph-containing ions. However, the mass balance obtained by ESI-MS is not reliable due to differences in surface activities of the

various ions in solution,[40] and these activities are not measurable due to the impracticalities of isolating the individual components.

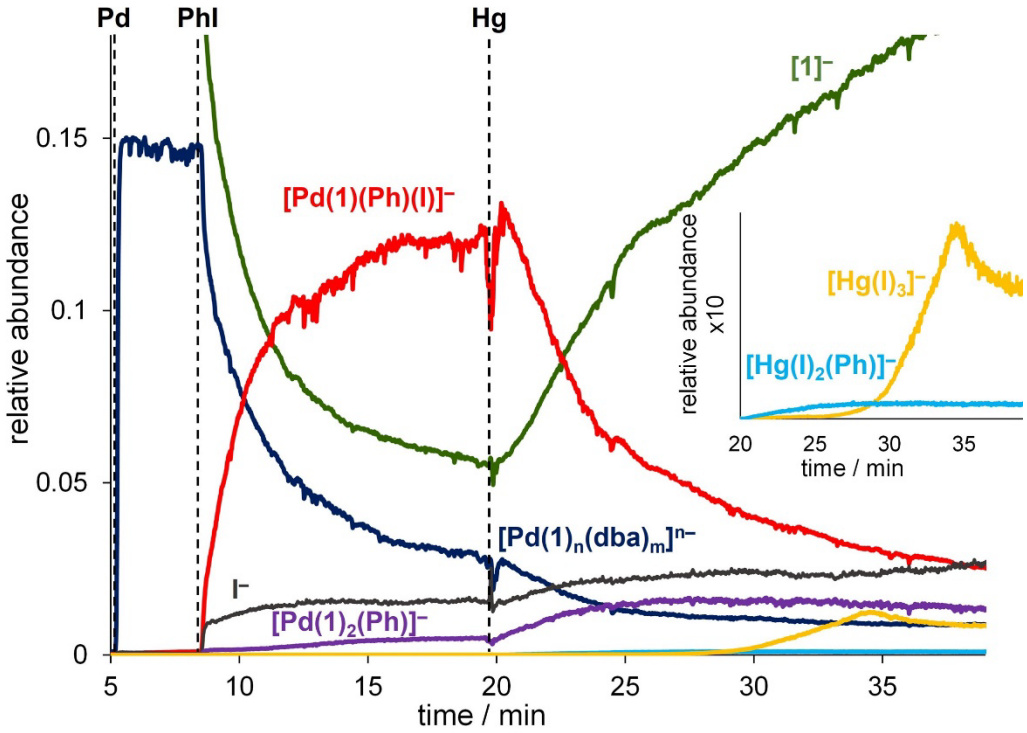

Figure 4.4: PSI-ESI(–)-MS reaction monitoring of the effects of Hg on the oxidative addition of PhI to $[Pd(1)_n(dba)_m]^{n-}$, where n = 1–2, m = 0–1. Inset amplifies low abundance species.

Studies have shown that both dissolved Hg(0) species and liquid mercury readily oxidize in aqueous media in the presence of halides.[41–43] We observed evidence of this oxidation occurring in methanol with the detection of $[HgI_3]^-$ 10 minutes after adding mercury. A proposed mechanism (Scheme 4.2) involves the Pd(II) intermediate adsorbing onto Hg(0), followed by reduction of Pd(II) via electron transfer from Hg(0), and I^- transfer to form $[HgI]^+$ and $[Pd(\mathbf{1})(Ph)]^{2-}$. The resulting Pd(0) species likely form Hg_xPd_y amalgams. The increase in abundance of $[Pd(\mathbf{1})_2(Ph)]^-$ is likely due to I^- abstraction from $[Pd(\mathbf{1})(Ph)(I)]^-$ by $[HgI]^+$, and subsequent free phosphine **1** coordination. These findings suggest that Hg(0) oxidation in the presence of halides is a complex process with multiple steps.

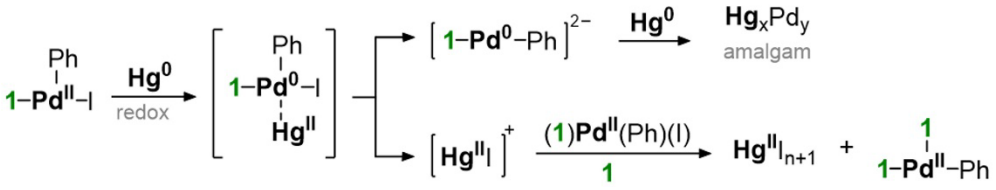

Scheme 4.2: Proposed pathways for the mercury redox decomposition of Pd(II) oxidative addition intermediate forming mercuric iodide, $[Pd(\mathbf{1})_2Ph]^-$ and Hg_xPd_y amalgam.

A gradual increase in abundance of I^- occurred before reaching a steady state after approx. 10 minutes (Figure 4.4). Tandem MS experiments on $[HgI_3]^-$ revealed that I^- dissociation occurred at collision energy (CE) <2 V; ligand dissociation more typically occurs at >10 V under these conditions. This dissociation may occur in the spectrometer under standard source conditions. According to the literature, $[HgI_3]^-$ and $[HgI_4]^{2-}$ have similar stability constants.[44] However, $[HgI_4]^{2-}$ was not observed, likely due to the limited stability of polyanionic gas phase species, which, when not stabilized by solvation, are prone to X^- loss or evaporation of an electron.[45] Plateauing I^- dissociation indicates equilibria being reached between $[HgI]^+$, HgI_2, $[HgI_3]^-$, and $[HgI_4]^{2-}$. In addition, we observed formation of $[Hg(I)_2Ph]^-$ and trace amounts of $[Pd(\mathbf{1})(Ph)_2(dba)]^-$, suggesting transmetallation occurred between Hg(0) and Pd(II). Given these findings, the next step was to investigate transmetallation with Hg(II) species generated via *in situ* oxidation of Hg(0).

4.3.3 Investigations of Pd/Hg Redox-Transmetallation

When $Pd(PPh_3)_4$ is added to a solution of the aryl iodide $[PPN]^+[p\text{-}IC_6H_4CH_2SO_3]^-$, hereafter $[PPN][\mathbf{2}]$,[46] the expected Pd(II) oxidative addition products $[(PPh_3)_mPd(I)(C_6H_4CH_2SO_3)]^-$ (m = 1–2) quickly formed. After the signal stabilized, mercury was added, which resulted in the formation of the organomercuric species $[Hg(I)(C_6H_4CH_2SO_3)]^-$ via transmetallation (Figure 4.5). $[Hg(I)_2X]^-$ (X = I or Cl) was also detected approx. 5 minutes after mercury addition, an induction period presumably due to the requirement for preceding formation of $[HgI]^+$ and HgI_2.

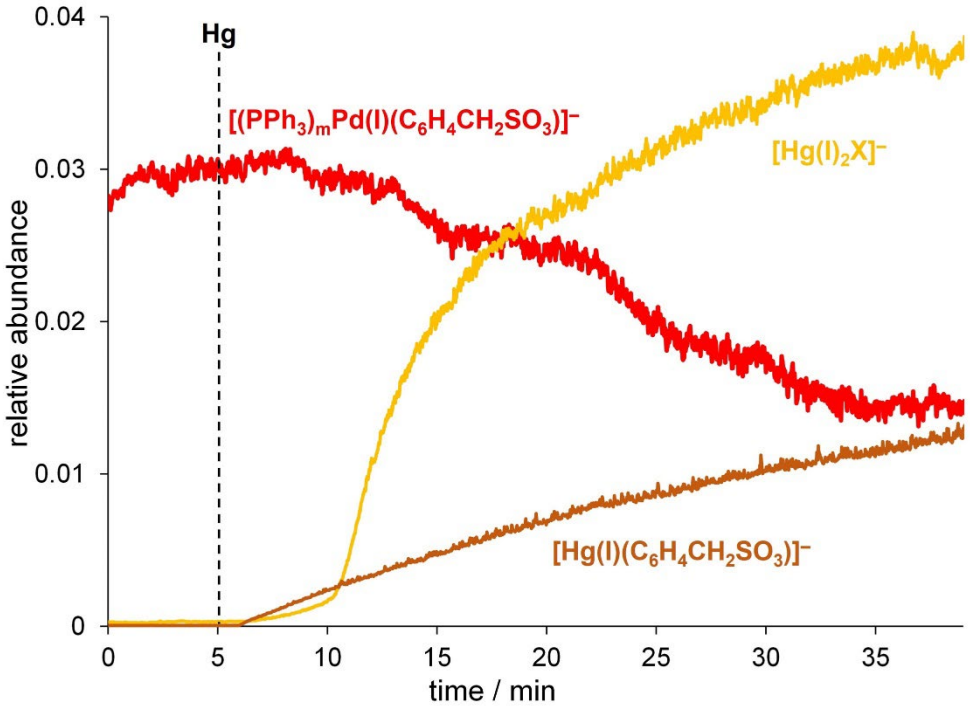

Figure 4.5: PSI-ESI(–)-MS reaction monitoring of the effects of Hg on the Pd(0) oxidative addition intermediate $[(PPh_3)_mPd(I)(C_6H_4CH_2SO_3)]^-$, where m = 1–2. Pd/Hg transmetallation of substrate occurs with the immediate formation of $[Hg(I)(C_6H_4CH_2SO_3)]^-$, as well as $[Hg(I)_2X]^-$ (X = I or Cl).

The transmetallation between organopalladium intermediates and Hg(0) likely occurs via an inner-sphere mechanism mediated by activated iodide or aryl ligands forming bridged intermediates (Scheme 4.3A).[47] Following this, a ligand transfer to mercury occurs, with ligand coordination being thermodynamically favourable for less electronegative mercury. This may occur as a concerted process involving both bridged ligands (Scheme 4.3A) or via a more complex stepwise mechanism. Alternatively, Pd-Hg-X intermediates may form via an initial insertion of Hg(0) into a weakened Pd–X bond,[48–50] followed by an aryl ligand *cis*-migration to mercury (Scheme 4.3B).

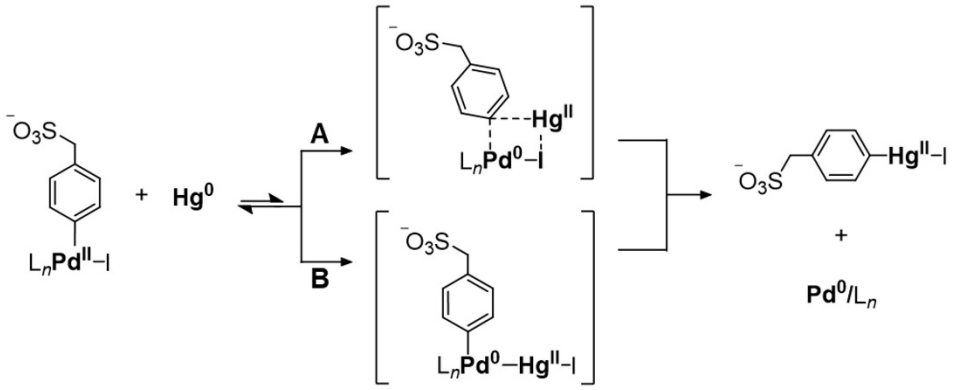

Scheme 4.3: Proposed pathway for Pd/Hg redox transmetallation forming $[Hg(I)(C_6H_4CH_2SO_3)]^-$, via A) iodide- and aryl-bridged intermediate, and B) insertion of Hg into a weakened Pd–I bond.

Control experiments showed that in the absence of palladium, $[Hg(I)(C_6H_4CH_2SO_3)]^-$ was not formed, indicating it as a redox-transmetallation product, rather than resulting from a C–I bond insertion. Subsequent addition of equimolar amounts of PhI and the charge-tagged analogue **2** yielded no peaks corresponding to neither the transmetallation intermediate $[(PPh_3)Pd(Ph)(C_6H_4CH_2SO_3)]^-$ nor the expected reductive elimination product $[Ph(C_6H_4CH_2SO_3)]^-$. This could be due to the presence of the anionic sulfonate group disfavoring coordination to palladium, due to electrostatic repulsion. Additionally, the bulky counterion $[PPN]^+$, may hinder entry of organomercurials into the coordination sphere of palladium.

Collision-induced dissociation (CID) was used to fragment the transmetallation species $[(PPh_3)Pd(I)(C_6H_4CH_2SO_3)]^-$ and $[Hg(I)(C_6H_4CH_2SO_3)]^-$, with CEs optimized to reduce the precursor ions' abundance to 10% of their initial intensity (Figure 4.6). At a CE of 8 V for the Pd(II) ion, we detected an initial neutral loss of *m/z* 262.1 (PPh_3). PPh_3 readily dissociates from palladium as an L-type ligand through simple ligand dissociation, hence the lower voltage. This low energy PPh_3 dissociation was also observed for the bisligated $[(PPh_3)_2Pd(I)(C_6H_4CH_2SO_3)]^-$ ion at CE 1 V. In contrast, X-type ligands require more energy for homolytic dissociation due to the necessity of radical formation.[51] We also observed a product ion at *m/z* 296.9 assigned to the reductive elimination of the charge-tagged aryl halide $[IC_6H_4CH_2SO_3]^-$ (Figure 4.6A).

The Hg(II) transmetallation intermediate showed different unimolecular decomposition pathways, with the charge-tagged aryl fragment $[C_6H_4CH_2SO_3]^-$ having the greatest relative abundance (Figure 4.6B). This product ion, as well as I^-, results from homolytic cleavage of the X-type ligands. This CID reaction pathway was not observed for the Pd(II) precursor ion, which has a square planar geometry, making reductive elimination a more favorable pathway. In contrast, the linear geometry of the Hg(II) species, disfavors reductive elimination, and hence the homolytic cleavage product ions are more abundant.

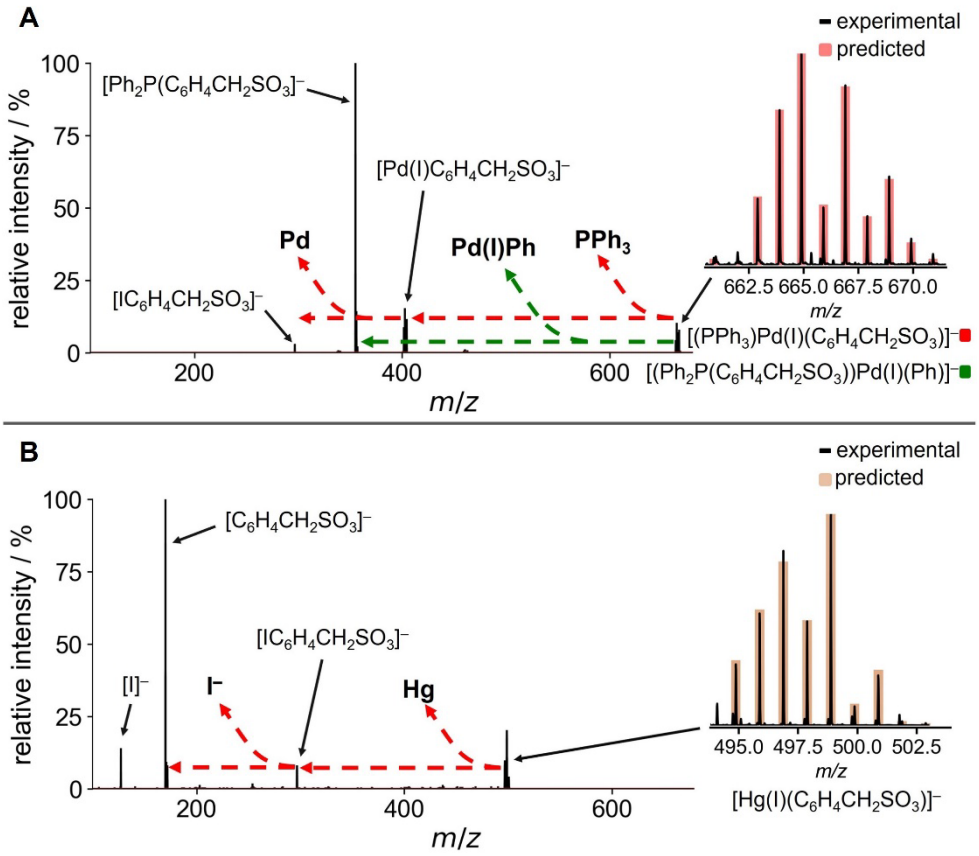

Figure 4.6: A) ESI(–)-MS/MS (CE = 16 V) of $[(PPh_3)Pd(I)(C_6H_4CH_2SO_3)]^-$, showing product ions $[Pd(I)(C_6H_4CH_2SO_3)]^-$, $[IC_6H_4CH_2SO_3]^-$, and phosphine scrambling product ion $[Ph_2P(C_6H_4CH_2SO_3)]^-$. B) ESI(–)-MS/MS (CE = 15 V) of $[Hg(I)(C_6H_4CH_2SO_3)]^-$, showing product ions $[IC_6H_4CH_2SO_3]^-$, $[C_6H_4CH_2SO_3]^-$, and I^-. Insets: the predicted isotope pattern (bars) overlaid on the experimental mass spectrum (lines) of $[Hg(I)(C_6H_4CH_2SO_3)]^-$ and $[(PPh_3)Pd(I)(C_6H_4CH_2SO_3)]^-$.

4.3.4 Aryl-Phosphine Scrambling

Detection of the Pd(II) product ion $[Ph_2P(C_6H_4CH_2SO_3)]^-$, indicates the occurrence of intramolecular aryl-phosphine scrambling (Figure 4.6A, green), a known side reaction in palladium-catalyzed cross-coupling reactions, often leading to undesired scrambled side products and catalyst deactivation.[52–54] These results suggest that the scrambling process is facile,[55,56] and can be easily initiated under energetic CID conditions. Evidence for aryl-phosphine scrambling was also observed in full scan ESI(–)-MS experiments, indicating that it occurs in the absence of high energy CID conditions (Figure 4.7).

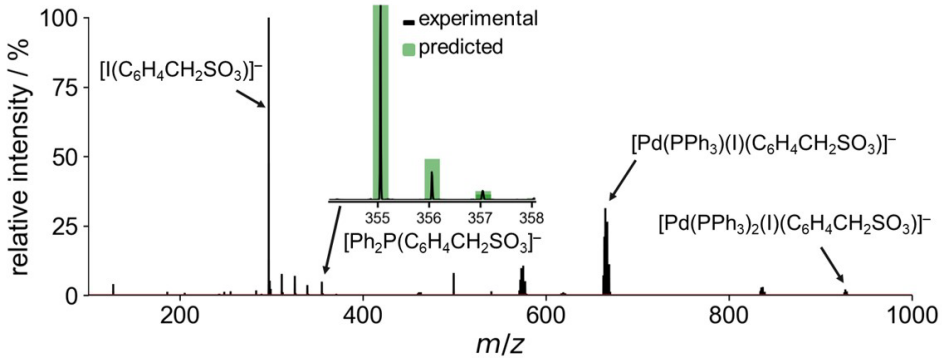

Figure 4.7: PSI-ESI(–)-MS full scan of $Pd(PPh_3)_4$ (10μM) added to [PPN][**2**] (80 μM) in MeOH, showing intramolecular aryl-phosphine scrambling product $[Ph_2P(C_6H_4CH_2SO_3)]^-$ (*m/z* 355.1) occurring even in the absence of high energy CID conditions. Inset: the predicted isotope pattern (bars) overlaid on the experimental mass spectrum (lines) of $[Ph_2P(C_6H_4CH_2SO_3)]^-$.

A proposed mechanism for the solution-phase aryl-phosphine scrambling pathway is shown in Scheme 4.4. This involves the reductive elimination of a phosphonium salt intermediate, a known by-product in cross-coupling reactions.[70,71] This intermediate undergoes an oxidative addition to produce the aryl-phosphine scrambling Pd species with a new P–C bond,[62,72] which further fragments by CID to produce the detected product ion $[Ph_2P(C_6H_4CH_2SO_3)]^-$. These findings provide insight into the characteristics of Pd(II) and Hg(II) transmetallation intermediates and can be used to diagnose substrate binding strength and composition.[73]

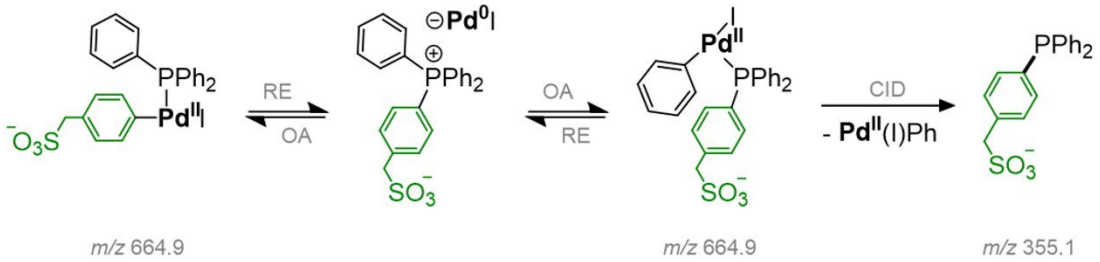

Scheme 4.4: Proposed mechanism of aryl-phosphine scrambling showing reductive elimination (RE) and oxidative addition (OA) resulting in new P–C bond formation and product ion $[Ph_2P(C_6H_4CH_2SO_3)]^-$ following collision-induced dissociation (CID).

4.4 Conclusions

Real-time mass spectrometric analysis of the effects of mercury on a model palladium catalyzed cross-coupling reaction has revealed the limitations of the mercury drop test. These findings indicate that mercury can interact with both L_nPd(0) and L_nPd(II)ArX intermediates. Mercury accelerated the consumption of Pd(0/II) homogeneous catalyst resting states, resulting in the formation of organomercuric ions, mercuric halides, and catalyst deactivation likely through Pd(0) nanoparticles and amalgamation. Additionally, transmetallation has been observed between organopalladium intermediates and Hg(0). It is postulated that the ligand transfer occurs through a thermodynamically favorable inner-sphere redox-transmetallation process, although the exact nature of ligand and electron transfer remains unresolved.

These findings add to the recent efforts that highlight the misconceptions surrounding the mercury drop test and encourage the development of alternate methods for the analysis of organometallic catalytic systems. These results refute the widely held assumption that protective ligands, such as triphenylphosphine, prevent Hg(0) from interacting with palladium complexes of elevated oxidation states. The observed inhibition of catalytic activity resulting from such interactions, would often be misinterpreted as evidence for heterogeneous catalysis. As such, the mercury drop test should be just one step in a comprehensive kinetic analysis of the catalyst to distinguish heterogeneous from homogeneous catalysis, bearing in mind that not all outcomes are equally interpretable.

4.5 Materials and Methods

All experiments were set-up and performed under an inert (Ar or N_2) atmosphere using standard glovebox and Schlenk line techniques.[64] Ar (UHP200 5.0) and N_2 (HP300 4.8) were purchased from Airgas (Calgary, Canada) and used without further purification. All solvents were purchased from Fisher Scientific and kept under inert atmosphere before use; methanol (MeOH, HPLC-grade) was degassed using the freeze-pump-thaw method, and tretrahydrofuran (THF) was distilled under a standard benzophenone-sodium still.

Tetrakis(triphenylphosphine)-palladium(0), $Pd(PPh_3)_4$ 99% and tris(dibenzylideneacetone)dipalladium(0), $Pd_2(dba)_3$ 99%, were purchased from Sigma-Aldrich and used as received. PhI, 98%, was purchased from Sigma-Aldrich and purified by washing 3 times with 10% HCl, followed by freeze-pump-thaw degassing. Bis(triphenylphosphine)iminium triphenylphosphine mono-sulfonate $[PPN]^+[P(Ph)_2(m\text{-}C_6H_4SO_3)]^-$ or [PPN][**1**], was synthesized as reported previously.[65,66] The charge-tagged aryl iodide $[PPN]^+[p\text{-}IC_6H_4CH_2SO_3]^-$ or [PPN][**2**], was synthesized according to a literature procedure and consistent characterization data obtained.[67] Elemental mercury was generously donated by the University of Victoria, Department of Chemistry Undergraduate Teaching Laboratory. All reagent stock solutions were prepared under an inert N_2 atmosphere in a glovebox or on a Schlenk line.

4.5.1 ESI-MS Instrument Parameters

Mass spectra were collected on a Waters (Milford, USA) Synapt G2-S*i* mass spectrometer and analyzed using Waters MassLynx V4.2 software, PythoMS, and the IsoSpecPy package.[68,69] The Synapt G2-S*i* was operated in negative ion resolution full scan mode, with all MS chromatograms normalized to the total ion current (TIC). Instrument parameters used are summarized in Table 4.1.

Table 4.1: Waters Synapt G2-S*i* Instrument Parameters for Hg Test.

Parameter	Negative Mode
Flow rate (PSI)	20 μL min^{-1}
Scan time	1 s
Capillary voltage	2.5 kV
Sampling cone voltage	40 V
Source offset	80 V
Source temperature	80 °C
Desolvation temperature	250 °C
Cone gas flow	50 L hr^{-1}
Desolvation gas flow	200 L hr^{-1}
Nebuliser	2.8 bar
m/z range	100-1200
FWHM	11500

4.5.2 General Procedures for PSI-ESI-MS Reaction Monitoring

General methodology applicable to both **1** and **2** are as follows: Degassed HPLC-grade MeOH (20 mL) was transferred to a Schlenk flask equipped with a stirrer bar and sparged with N_2 (15 min) before being connected to the spectrometer inlet via PEEK tubing (TubPEEK Red, 1/16 in. OD, 0.005 in. ID, 18 in. L). The reaction mixture was monitored by PSI-ESI-MS techniques[42] until a steady signal intensity was achieved. Sequential additions of each subsequent reagent followed, with the reaction allowed to proceed for up to 40 minutes. All reactions were stirred at 450 rpm at room temperature (22 °C).

Specifics for **1**: [PPN][**1**] (1.0 mM in MeOH, 0.05 mL, 0.05 μmol, 0.25 eq.) was injected into the flask at time zero, followed by injection of $Pd_2(dba)_3$ (1.0 mM in THF, 0.2 mL, 0.20 μmol, 1.0 equiv. Pd) at 5 minutes, and PhI (4.0 mM in MeOH, 0.4 mL, 1.60 μmol, 8.0 equiv.) at 10 minutes. A bead of mercury (0.5±0.05 g, 2500 μmol, >12500 equiv. Hg) was injected either after the catalyst activation stage (10 min), or after the oxidative addition stage (20 min).

Specifics for **2**: $Pd(PPh_3)_4$ (1.0 mM in THF, 0.2 mL, 0.20 μmol, 1.0 equiv. Pd) was injected at time zero, followed by injection of [PPN][**2**] (4.0 mM in MeOH, 0.4 mL, 1.60 μmol, 8.0 equiv.) at 1 minute. After steady state of the oxidative intermediate Pd^{II} species was reached, a bead of mercury (0.5±0.05 g, 2500 μmol, >12500 equiv. Hg) was injected into the reaction flask (5 min).

4.6 References

(1) Johansson Seechurn, C. C. C.; Kitching, M. O.; Colacot, T. J.; Snieckus, V. Palladium-Catalyzed Cross-Coupling: A Historical Contextual Perspective to the 2010 Nobel Prize. *Angew. Chem. Int. Ed.* **2012**, *51* (21), 5062–5085. https://doi.org/10.1002/anie.201107017.

(2) Touré, B. B.; Hall, D. G. Natural Product Synthesis Using Multicomponent Reaction Strategies. *Chem. Rev.* **2009**, *109* (9), 4439–4486. https://doi.org/10.1021/cr800296p.

(3) Wang, D.; Gao, S. Sonogashira Coupling in Natural Product Synthesis. *Org. Chem. Front.* **2014**, *1* (5), 556–566. https://doi.org/10.1039/C3QO00086A.

(4) Torborg, C.; Beller, M. Recent Applications of Palladium-Catalyzed Coupling Reactions in the Pharmaceutical, Agrochemical, and Fine Chemical Industries. *Adv. Synth. Catal.* **2009**, *351* (18), 3027–3043. https://doi.org/10.1002/adsc.200900587.

(5) Rayadurgam, J.; Sana, S.; Sasikumar, M.; Gu, Q. Palladium Catalyzed C–C and C–N Bond Forming Reactions: An Update on the Synthesis of Pharmaceuticals from 2015–2020. *Org. Chem. Front.* **2021**, *8* (2), 384–414. https://doi.org/10.1039/D0QO01146K.

(6) Messina, C.; Douglas, L. Z.; Liu, J. T.; Forgione, P. Successive Pd-Catalyzed Decarboxylative Cross-Couplings for the Modular Synthesis of Non-Symmetric Di-Aryl-Substituted Thiophenes. *Eur. J. Org. Chem.* **2020**, *2020* (32), 5182–5191. https://doi.org/10.1002/ejoc.202000780.

(7) Rohand, T.; Qin, W.; Boens, N.; Dehaen, W. Palladium-Catalyzed Coupling Reactions for the Functionalization of BODIPY Dyes with Fluorescence Spanning the Visible Spectrum. *Eur. J. Org. Chem.* **2006**, *2006* (20), 4658–4663. https://doi.org/10.1002/ejoc.200600531.

(8) Appleby, K. M.; Dzotsi, E.; Scott, N. W. J.; Dexin, G.; Jeddi, N.; Whitwood, A. C.; Pridmore, N. E.; Hart, S.; Duckett, S. B.; Fairlamb, I. J. S. Bridging the Gap from Mononuclear Pd^{II} Precatalysts to Pd Nanoparticles: Identification of Intermediate Linear $[Pd_3(XPh_3)_4]^{2+}$ Clusters as Catalytic Species for Suzuki–Miyaura Couplings (X = P, As). *Organometallics* **2021**, *40* (21), 3560–3570. https://doi.org/10.1021/acs.organomet.1c00452.

(9) Scott, N. W. J.; Ford, M. J.; Jeddi, N.; Eyles, A.; Simon, L.; Whitwood, A. C.; Tanner, T.; Willans, C. E.; Fairlamb, I. J. S. A Dichotomy in Cross-Coupling Site Selectivity in a Dihalogenated Heteroarene: Influence of Mononuclear Pd, Pd Clusters, and Pd Nanoparticles—the Case for Exploiting Pd Catalyst Speciation. *J. Am. Chem. Soc.* **2021**, *143* (25), 9682–9693. https://doi.org/10.1021/jacs.1c05294.

(10) Ananikov, V. P.; Beletskaya, I. P. Toward the Ideal Catalyst: From Atomic Centers to a "Cocktail" of Catalysts. *Organometallics* **2012**, *31* (5), 1595–1604. https://doi.org/10.1021/om201120n.

(11) Prima, D. O.; Madiyeva, M.; Burykina, J. V.; Minyaev, M. E.; Boiko, D. A.; Ananikov, V. P. Evidence for "Cocktail"-Type Catalysis in Buchwald–Hartwig Reaction. A Mechanistic Study. *Catal. Sci. Technol.* **2021**, *11* (21), 7171–7188. https://doi.org/10.1039/D1CY01601F.

(12) Vanden Broeck, S. M. P.; Nahra, F.; Cazin, C. S. J. Bulky-Yet-Flexible Carbene Ligands and Their Use in Palladium Cross-Coupling. *Inorganics* **2019**, *7* (6), 78. https://doi.org/10.3390/inorganics7060078.

(13) Onoabedje, E. A.; Okoro, U. C. Ligand-Supported Palladium-Catalyzed Cross-Coupling Reactions of (Hetero) Aryl Chlorides. *Synth. Commun.* **2019**, *49* (17), 2117–2146. https://doi.org/10.1080/00397911.2019.1587778.

(14) Perry, G. L.; Schley, N. D. Tris(Bicyclo[1.1.1]Pentyl)Phosphine: An Exceptionally Small Tri-Tert-Alkylphosphine and Its Bis-Ligated Pd(0) Complex. *J. Am. Chem. Soc.* **2023**, *145* (12), 7005–7010. https://doi.org/10.1021/jacs.3c00885.

(15) Veerakumar, P.; Thanasekaran, P.; Lu, K.-L.; Lin, K.-C.; Rajagopal, S. Computational Studies of Versatile Heterogeneous Palladium-Catalyzed Suzuki, Heck, and Sonogashira Coupling Reactions. *ACS Sustain. Chem. Eng.* **2017**, *5* (10), 8475–8490. https://doi.org/10.1021/acssuschemeng.7b00922.

(16) Yin; Liebscher, J. Carbon–Carbon Coupling Reactions Catalyzed by Heterogeneous Palladium Catalysts. *Chem. Rev.* **2007**, *107* (1), 133–173. https://doi.org/10.1021/cr0505674.
(17) Mpungose, P. P.; Vundla, Z. P.; Maguire, G. E. M.; Friedrich, H. B. The Current Status of Heterogeneous Palladium Catalysed Heck and Suzuki Cross-Coupling Reactions. *Molecules* **2018**, *23* (7), 1676. https://doi.org/10.3390/molecules23071676.
(18) Astruc, D.; Lu, F.; Aranzaes, J. R. Nanoparticles as Recyclable Catalysts: The Frontier between Homogeneous and Heterogeneous Catalysis. *Angew. Chem. Int. Ed.* **2005**, *44* (48), 7852–7872. https://doi.org/10.1002/anie.200500766.
(19) Widegren, J. A.; Finke, R. G. A Review of the Problem of Distinguishing True Homogeneous Catalysis from Soluble or Other Metal-Particle Heterogeneous Catalysis under Reducing Conditions. *J. Mol. Catal. -Chem.* **2003**, *198* (1), 317–341. https://doi.org/10.1016/s1381-1169(02)00728-8.
(20) Crabtree, R. H. *The Organometallic Chemistry of the Transition Metals*, Seventh edition.; Wiley: Hoboken, NJ, 2019.
(21) Schmidt, A. F.; Kurokhtina, A. A. Distinguishing between the Homogeneous and Heterogeneous Mechanisms of Catalysis in the Mizoroki-Heck and Suzuki-Miyaura Reactions: Problems and Prospects. *Kinet. Catal.* **2012**, *53* (6), 714–730. https://doi.org/10.1134/s0023158412060109.
(22) Crabtree, R. H. Resolving Heterogeneity Problems and Impurity Artifacts in Operationally Homogeneous Transition Metal Catalysts. *Chem. Rev.* **2012**, *112* (3), 1536–1554. https://doi.org/10.1021/cr2002905.
(23) Molnár, Á. Efficient, Selective, and Recyclable Palladium Catalysts in Carbon–Carbon Coupling Reactions. *Chem. Rev.* **2011**, *111* (3), 2251–2320. https://doi.org/10.1021/cr100355b.
(24) Phan, N. T. S.; Van Der Sluys, M.; Jones, C. W. On the Nature of the Active Species in Palladium Catalyzed Mizoroki–Heck and Suzuki–Miyaura Couplings – Homogeneous or Heterogeneous Catalysis, A Critical Review. *Adv. Synth. Catal.* **2006**, *348* (6), 609–679. https://doi.org/10.1002/adsc.200505473.
(25) Richardson, J. M.; Jones, C. W. Poly(4-Vinylpyridine) and Quadrapure TU as Selective Poisons for Soluble Catalytic Species in Palladium-Catalyzed Coupling Reactions – Application to Leaching from Polymer-Entrapped Palladium. *Adv. Synth. Catal.* **2006**, *348* (10–11), 1207–1216. https://doi.org/10.1002/adsc.200606021.
(26) Whitesides, G. M.; Hackett, Marifaith.; Brainard, R. L.; Lavalleye, J. P. P. M.; Sowinski, A. F.; Izumi, A. N.; Moore, S. S.; Brown, D. W.; Staudt, E. M. Suppression of Unwanted Heterogeneous Platinum(0)-Catalyzed Reactions by Poisoning with Mercury(0) in Systems Involving Competing Homogeneous Reactions of Soluble Organoplatinum Compounds: Thermal Decomposition of Bis(Triethylphosphine)-3,3,4,4-Tetramethylplatinacyclopentane. *Organometallics* **1985**, *4* (10), 1819–1830. https://doi.org/10.1021/om00129a023.
(27) Gorunova, O. N.; Livantsov, M. V.; Grishin, Y. K.; Ilyin, M. M.; Kochetkov, K. A.; Churakov, A. V.; Kuz'mina, L. G.; Khrustalev, V. N.; Dunina, V. V. Evidence on Palladacycle-Retaining Pathway for Suzuki Coupling. Inapplicability of Hg-Drop Test for Palladacycle Catalysed Reactions. *J. Organomet. Chem.* **2013**, *737*, 59–63. https://doi.org/10.1016/j.jorganchem.2013.03.050.
(28) Gorunova, O. N.; Novitskiy, I. M.; Grishin, Y. K.; Gloriozov, I. P.; Roznyatovsky, V. A.; Khrustalev, V. N.; Kochetkov, K. A.; Dunina, V. V. When Applying the Mercury Poisoning Test to Palladacycle-Catalyzed Reactions, One Should Not Consider the Common Misconception of Mercury(0) Selectivity. *Organometallics* **2018**, *37* (17), 2842–2858. https://doi.org/10.1021/acs.organomet.8b00363.
(29) Gorunova, O. N.; Novitskiy, I. M.; Grishin, Y. K.; Gloriozov, I. P.; Roznyatovsky, V. A.; Khrustalev, V. N.; Kochetkov, K. A.; Dunina, V. V. The Use of Control Experiments as the Sole Route to Correct the Mechanistic Interpretation of Mercury Poisoning Test Results: The Case of

P,C-Palladacycle-Catalysed Reactions. *J. Organomet. Chem.* **2020**, *916*, 121245. https://doi.org/10.1016/j.jorganchem.2020.121245.
(30) Baier, H.; Kelling, A.; Holdt, H.-J. PEPPSI-Effect on Suzuki–Miyaura Reactions Using 4,5-Dicyano-1,3-Dimesitylimidazol-2-Ylidene-Palladium Complexes: A Comparison between Trans-Ligands. *Eur. J. Inorg. Chem.* **2015**, *2015* (11), 1950–1957. https://doi.org/10.1002/ejic.201500010.
(31) Baier, H.; Kelling, A.; Schilde, U.; Holdt, H.-J. Investigation of the Catalytic Activity of a 2-Phenylidenepyridine Palladium(II) Complex Bearing 4,5-Dicyano-1,3-Bis(Mesityl)Imidazol-2-Ylidene in the Mizoroki-Heck Reaction. *Z. Für Anorg. Allg. Chem.* **2016**, *642* (2), 140–147. https://doi.org/10.1002/zaac.201500625.
(32) Chernyshev, V. M.; Astakhov, A. V.; Chikunov, I. E.; Tyurin, R. V.; Eremin, D. B.; Ranny, G. S.; Khrustalev, V. N.; Ananikov, V. P. Pd and Pt Catalyst Poisoning in the Study of Reaction Mechanisms: What Does the Mercury Test Mean for Catalysis? *ACS Catal.* **2019**, *9* (4), 2984–2995. https://doi.org/10.1021/acscatal.8b03683.
(33) Thomas, G. T.; Donnecke, S.; Chagunda, I. C.; McIndoe, J. S. Pressurized Sample Infusion. *Chemistry–Methods* **2022**, *2* (1). https://doi.org/10.1002/cmtd.202100068.
(34) Janusson, E.; Zijlstra, H. S.; Nguyen, P. P. T.; MacGillivray, L.; Martelino, J.; McIndoe, J. S. Real-Time Analysis of Pd2(Dba)3 Activation by Phosphine Ligands. *Chem. Commun.* **2017**, *53* (5), 854–856. https://doi.org/10.1039/C6CC08824D.
(35) Barański, A.; Kryska, A.; Galus, Z. On the Electrochemical Properties of the Pd + Hg System. *J. Electroanal. Chem.* **1993**, *349* (1), 341–354. https://doi.org/10.1016/0022-0728(93)80183-I.
(36) Tereniak, S. J.; Landis, C. R.; Stahl, S. S. Are Phosphines Viable Ligands for Pd-Catalyzed Aerobic Oxidation Reactions? Contrasting Insights from a Survey of Six Reactions. *ACS Catal.* **2018**, *8* (4), 3708–3714. https://doi.org/10.1021/acscatal.8b01009.
(37) Hesketh, A. V.; Nowicki, S.; Baxter, K.; Stoddard, R. L.; McIndoe, J. S. Simplified Real-Time Mass Spectrometric Analysis of Reactions. *Organometallics* **2015**, *34* (15), 3816–3819. https://doi.org/10.1021/acs.organomet.5b00460.
(38) Weber, P.; Biafora, A.; Doppiu, A.; Bongard, H.-J.; Kelm, H.; Gooßen, L. J. A Comparative Study of Dibenzylideneacetone Palladium Complexes in Catalysis. *Org. Process Res. Dev.* **2019**, *23* (7), 1462–1470. https://doi.org/10.1021/acs.oprd.9b00214.
(39) Yunker, L. P. E.; Ahmadi, Z.; Logan, J. R.; Wu, W.; Li, T.; Martindale, A.; Oliver, A. G.; McIndoe, J. S. Real-Time Mass Spectrometric Investigations into the Mechanism of the Suzuki–Miyaura Reaction. *Organometallics* **2018**, *37* (22), 4297–4308. https://doi.org/10.1021/acs.organomet.8b00705.
(40) Omari, I.; Randhawa, P.; Randhawa, J.; Yu, J.; McIndoe, J. S. Structure, Anion, and Solvent Effects on Cation Response in ESI-MS. *J. Am. Soc. Mass Spectrom.* **2019**, *30* (9), 1750–1757. https://doi.org/10.1007/s13361-019-02252-0.
(41) de Magalhães, M. E. A.; Tubino, M. A Possible Path for Mercury in Biological Systems: The Oxidation of Metallic Mercury by Molecular Oxygen in Aqueous Solutions. *Sci. Total Environ.* **1995**, *170* (3), 229–239. https://doi.org/10.1016/0048-9697(95)04711-5.
(42) Amyot, M.; Morel, F. M. M.; Ariya, P. A. Dark Oxidation of Dissolved and Liquid Elemental Mercury in Aquatic Environments. *Environ. Sci. Technol.* **2005**, *39* (1), 110–114. https://doi.org/10.1021/es035444k.
(43) Hocsman, A.; Di Nezio, S.; Charlet, L.; Avena, M. On the Mechanisms of Dissolution of Montroydite [HgO(s)]: Dependence of the Dissolution Rate on pH, Temperature, and Stirring Rate. *J. Colloid Interface Sci.* **2006**, *297* (2), 696–704. https://doi.org/10.1016/j.jcis.2005.11.020.

(44) Amini, M. K.; Ghaedi, M.; Rafi, A.; Habibi, M. H.; Zohory, M. M. Iodide Selective Electrodes Based on Bis(2-Mercaptobenzothiazolato) Mercury(II) and Bis(4-Chlorothiophenolato) Mercury(II) Carriers. *Sensors* **2003**, *3* (11), 509–523. https://doi.org/10.3390/s31100509.
(45) Butcher, C. P. G.; Johnson, B. F. G.; McIndoe, J. S.; Yang, X.; Wang, X.-B.; Wang, L.-S. Collision-Induced Dissociation and Photodetachment of Singly and Doubly Charged Anionic Polynuclear Transition Metal Carbonyl Clusters: Ru3Co(CO)13−, Ru6C(CO)162−, and Ru6(CO)182−. *J. Chem. Phys.* **2002**, *116* (15), 6560–6566. https://doi.org/10.1063/1.1462579.
(46) Liu, S.; Dockendorff, C.; Taylor, S. D. Synthesis of Protected L-4-[Sulfono(Difluoromethyl)]Phenylalanine and Its Incorporation into a Peptide. *Org. Lett.* **2001**, *3* (10), 1571–1574. https://doi.org/10.1021/ol0158664.
(47) Rasmussen, S. C. Transmetalation: A Fundamental Organometallic Reaction Critical to Synthesis and Catalysis. *ChemTexts* **2020**, *7* (1), 1. https://doi.org/10.1007/s40828-020-00124-9.
(48) Gubin, S. P.; Rubezhov, A. Z.; Denisovich, L. I.; Nesmeyanov, A. N. Reaction of Metallic Mercury with π-Allyl Compounds of Palladium. *Bull. Acad. Sci. USSR Div. Chem. Sci.* **1966**, *15* (9), 1630–1630. https://doi.org/10.1007/BF00848943.
(49) Nesmeyanov, A. N.; Rubezhov, A. Z.; Leites, L. A.; Gubin, S. P. The Reactions of Metallic Mercury with π-Allyl Compounds of Ni, Pd and Pt. *J. Organomet. Chem.* **1968**, *12* (1), 187–198. https://doi.org/10.1016/S0022-328X(00)90912-4.
(50) Harvey, P. D.; Aye, K. T.; Hierso, K.; Isabel, E.; Lognot, I.; Mugnier, Y.; Rochon, F. D. Electron-Ligand Interchange Reactions between Palladium(II) Complexes and Mercury and Single-Crystal X-Ray Characterization of the D10-D10 Binuclear [Hg2(Dppm)2Cl3]Cl Complex. *Inorg. Chem.* **1994**, *33* (26), 5981–5982. https://doi.org/10.1021/ic00104a002.
(51) Henderson, W.; McIndoe, J. S. *Mass Spectrometry of Inorganic and Organometallic Compounds*; John Wiley & Sons, Ltd.: New York, 2005.
(52) Alcazar-Roman, L. M.; Hartwig, J. F.; Rheingold, A. L.; Liable-Sands, L. M.; Guzei, I. A. Mechanistic Studies of the Palladium-Catalyzed Amination of Aryl Halides and the Oxidative Addition of Aryl Bromides to Pd(BINAP)2 and Pd(DPPF)2: An Unusual Case of Zero-Order Kinetic Behavior and Product Inhibition. *J. Am. Chem. Soc.* **2000**, *122* (19), 4618–4630. https://doi.org/10.1021/ja9944599.
(53) Fiebig, L.; Schlörer, N.; Schmalz, H.-G.; Schäfer, M. Aryl–Phenyl Scrambling in Intermediate Organopalladium Complexes: A Gas-Phase Study of the Mizoroki–Heck Reaction. *Chem. – Eur. J.* **2014**, *20* (17), 4906–4910. https://doi.org/10.1002/chem.201400115.
(54) Lee, Y. H.; Morandi, B. Transition Metal-Mediated Metathesis between P–C and M–C Bonds: Beyond a Side Reaction. *Coord. Chem. Rev.* **2019**, *386*, 96–118. https://doi.org/10.1016/j.ccr.2018.12.001.
(55) Ting, M. Y. C.; Yunker, L. P. E.; Chagunda, I. C.; Hatlelid, K.; Vieweg, M.; McIndoe, J. S. A Mechanistic Investigation of the Suzuki Polycondensation Reaction Using MS/MS Methods. *Catal. Sci. Technol.* **2021**, *11* (13), 4406–4416. https://doi.org/10.1039/D1CY00743B.
(56) Agrawal, D.; Zins, E.-L.; Schröder, D. Intramolecular Scrambling of Aryl Groups in Organopalladium Complexes [ArPd(PPh3)2]+: From Solution to the Gas Phase, Back Again, and In-Between. *Chem. – Asian J.* **2010**, *5* (7), 1667–1676. https://doi.org/10.1002/asia.201000086.

Chapter 5 – Ligand Substitution, Catalyst Activation, and Oxidative Addition Studies of a Stable Dialkyl Palladium Precatalyst

This chapter has been reproduced with minor changes from "Ian C. Chagunda, Antonia Kropp, David C. Leitch, and J. Scott McIndoe, *Organometallics*, **2025**, *44* (5), 628–636" and adapted with permission from American Chemical Society Publications. The project was conceptualized by ICC, DCL, and JSM. The research methodology was developed by ICC, and investigations carried out by ICC and AK. The original manuscript was written by ICC, with additional review and editing from DCL and JSM. This article was a Front Cover Feature, with the cover artwork conceptualized by ICC and jointly produced by ICC and JSM.

5.1 Abstract

Palladium-catalyzed cross-coupling reactions are indispensable in chemical synthesis, but efficient *in situ* catalyst activation remains a persistent challenge. Current Pd(II) precatalysts often lead to inefficient catalyst activation, necessitating higher catalyst loadings and limiting selectivity. The ligand substitution and activation mechanism of the stable Pd(II) dialkyl complex (^{DMP}DAB)Pd(CH_2SiMe_3)$_2$ was investigated in real-time using mass spectrometric monitoring. The introduction of charge-tagged phosphine ligands enabled the detection of key catalytic intermediates and identification of off-cycle species. The results demonstrate a low activation energy for the ligand dissociation of the ^{DMP}DAB ligand and the reductive elimination of (Me_3SiCH_2)$_2$ resulting in rapid formation of monoligated LPd(0) species, which are the active catalytic species for oxidative addition. These mechanistic insights offer a path towards developing more efficient and selective Pd-catalyzed processes, offering valuable guidance for the future design of precatalysts with improved performance.

5.2 Introduction

The nature of the active species in the catalytic cycle is one of the main issues in cross-coupling reactions. Precursors like $Pd_2(dba)_3$•*solvent*,[1,2] $[Pd(allyl)Cl]_2$, and $Pd(OAc)_2$[3] have typically been used with appropriate ligands to produce the active Pd(0) complexes *in situ* (Figure 5.1A); however, the formation of a specific active catalytic species can be challenging to achieve when using *in situ* catalysis.[4] This method may lead to catalytic processes that are not as efficient in terms of catalyst loading, conversion, and selectivity, owing to unwanted off-cycle reaction pathways.[5,6]

While $L_nPd(0)$ complexes are widely recognized as the active catalytic species, the exact ligation state – monoligated (n = 1), bisligated (n = 2), or both – remains unclear in many cases.[6] Monoligated LPd(0) complexes are sufficiently reactive that they have not been isolated,[7,8] whereas many examples of bisligated $L_2Pd(0)$ complexes are commercially available.[9,10] Notably the catalytic activity of monoligated and bisligated complexes can significantly differ, even with the same ligand used.[11] Factors such as ligand size and ligand-to-precatalyst molar ratio play a crucial role in determining the preference for mono- or bisligation.[12–14] Crucially, the ligation state also influences the mechanistic pathways for oxidative addition, where LPd(0) tends towards a 3-centered concerted mechanism, while $L_2Pd(0)$ complexes can favor a nucleophilic displacement mechanism.[15–17] This mechanistic divergence can lead to differential site-selectivity preferences in certain cases.[15–18]

The activation of appropriate precatalysts has made it possible to generate highly reactive LPd(0) species under controlled reaction conditions thanks to advancements in ligand and catalyst design.[19–31] Many of these new-generation precatalysts exist as preligated Pd(II) complexes that are air- and moisture-stable, and rapidly activate under the reaction conditions. This leads to high reactivity with lower catalyst loadings, enabling expanded applicability and selectivity.[32] In parallel, preligated Pd(0) precatalysts bearing throw-away ligands such as cyclopentadiene (COD), divinyl-disiloxanes (dvds), or maleic anhydride have also been developed.[33–38] These ligands serve as sacrificial components, stabilizing the Pd(0) species during handling while dissociating readily under reaction conditions, offering another route to accessing reactive LPd(0) species. However, these

precatalysts all require preinstallation of the ancillary ligand L, and options for *in situ* ligation/activation are still limited.

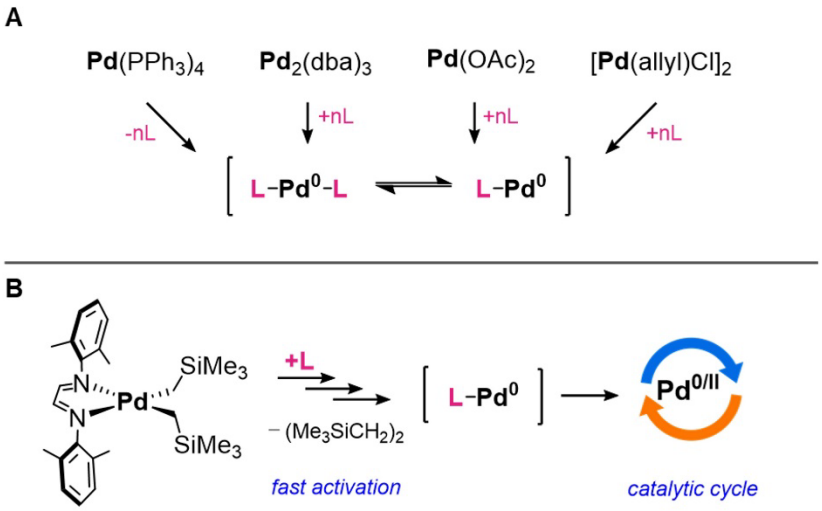

Figure 5.1: A) Common Pd(II) and Pd(0) sources for *in situ* LnPd(0) catalyst formation, where controlling the ligation state can be challenging. B) New dialkyl Pd(II) precatalyst (^{DMP}DAB)Pd(CH_2SiMe_3)$_2$ for controlled *in situ* LPd(0) generation without the need for preinstallation of ligand L.

A recent solution to these issues is the Pd(II) dialkyl complex (^{DMP}DAB)Pd(CH_2SiMe_3)$_2$ (^{DMP}DAB = *N,N′*-bis(2,6-dimethylphenyl)diazabutadiene, Figure 5.1B).[39] This precatalyst does not require the preinstallation of ancillary ligands, potentially enabling greater versatility in a broader range of reaction conditions. It has shown high activity for *in situ* catalyst formation in challenging Suzuki and Heck reactions. It is also an ideal precursor to generate isolable oxidative addition complexes (OACs), a class of complexes relevant to both mechanistic studies and late-stage functionalization of pharmaceutical scaffolds.[23,39,40] Additionally, its thermal and air stability and high solubility in many organic solvents make (^{DMP}DAB)Pd(CH_2SiMe_3)$_2$ a versatile Pd source for high-throughput experimentation.

This chapter covers work examining the mechanism of catalyst activation for (^{DMP}DAB)Pd(CH_2SiMe_3)$_2$ using charge-tagged phosphine ligands, as well as the subsequent oxidative addition reaction with aryl halides. Through the use of pressurized sample infusion-electrospray ionization-mass spectrometry (PSI-ESI-MS),[41] the catalytic

intermediates and off-cycle reaction pathways are studied in real-time. PSI-ESI-MS has proved to be a valuable tool for these investigations, with charge-tagged ligands facilitating the detection of transient catalytic intermediates which can be challenging to identify using other techniques. Specifically, experiments with sSPhos revealed extremely rapid formation of LPd(0) by ligand substitution and C–C reductive elimination, even at low concentration. Additionally, key intermediates and potential off-cycle species, where the ^{DMP}DAB ligand remains coordinated to Pd, were identified. This work provides a more complete mechanistic picture of how (^{DMP}DAB)Pd(CH_2SiMe_3)$_2$ operates as a precursor for ArX oxidative addition or catalysis.

5.3 Results and Discussion

5.3.1 Investigation of Catalyst Activation Processes

Monoligated LPd(0) species have been described as difficult, if not impossible, to define clearly in solution.[42] While theoretical investigations have provided some insight into the energetics of such species,[43–45] definitive solution phase detection remains elusive due to their coordinatively unsaturated and consequently highly reactive nature. Advancements in this area has been made with identification by MS.[11,46] However, using MS techniques to determine the solution phase structures does have limitations, particularly if the ionization process imparts enough internal energy to ions resulting in fragmentation of weakly coordinating ligands.[47–49] A semi-systemic optimization of instrument parameters was therefore conducted using OptiMS[50] to minimize ion fragmentation and mitigate the stated limitation in characterization by MS.

Initial investigations of the catalyst activation process were conducted using a charge-tagged phosphine [(Ph_3P)$_2$N]$^+$[sSPhos]$^-$ (hereafter [PPN][**3**]), obtained following a counterion exchange from the commercially available sulfonated dialkylbiaryl phosphine ligand [Na]$^+$[sSPhos]$^-$. Using charge-tagged ligands enabled operating the instruments at low source voltages, while maintaining strong signal intensities as previously demonstrated.[5,51,52] Catalyst activation was initiated by introduction of a solution of

precatalyst (^{DMP}DAB)Pd(CH_2SiMe_3)$_2$ (tetrahydrofuran solvent) into a solution of [PPN][**3**] (methanol solvent) and monitoring the disappearance of [**3**]$^-$ (*m/z* 498) and the appearance of catalyst activation species (Figure 5.2A).

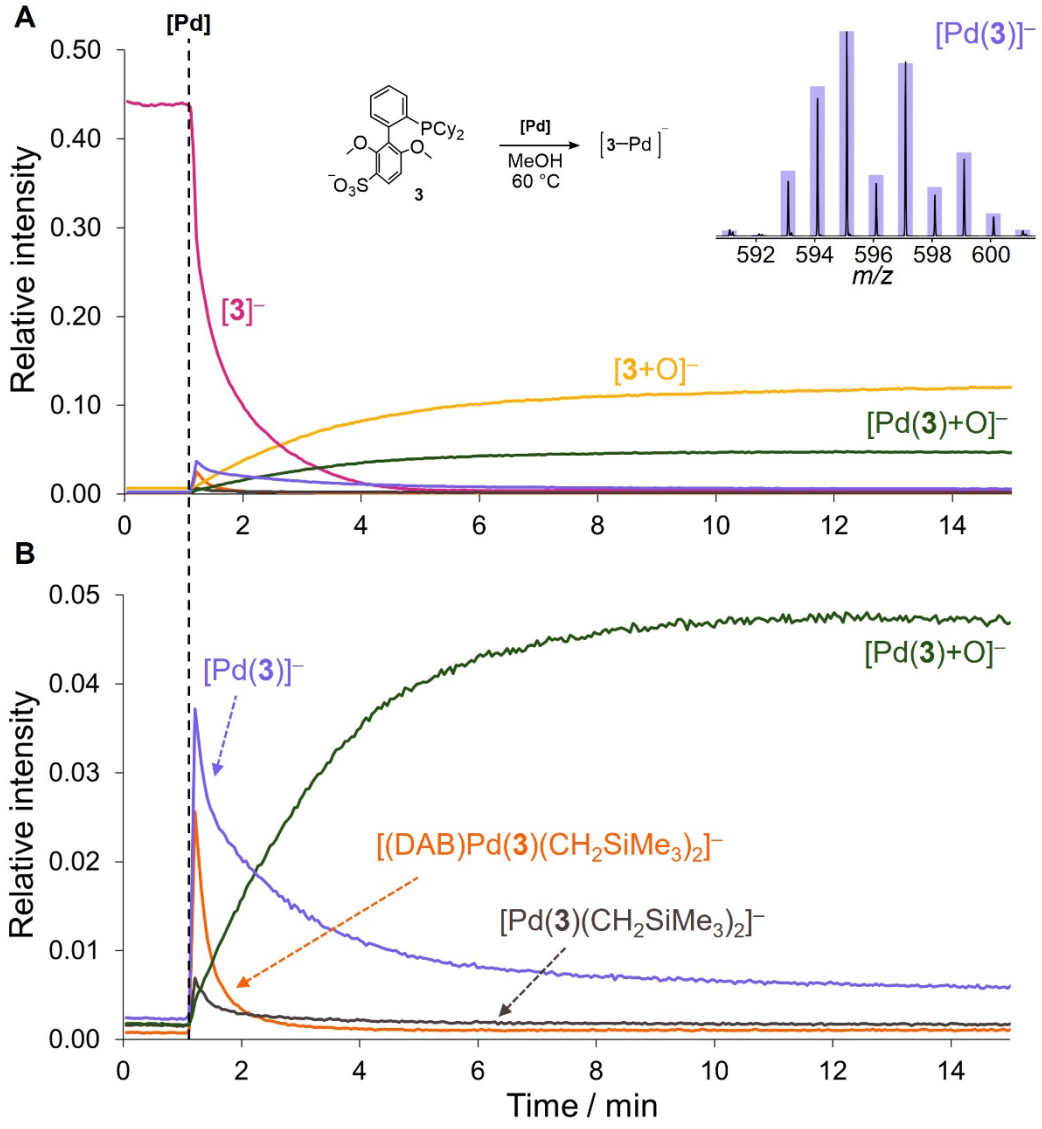

Figure 5.2: A) PSI-ESI(–)-MS reaction monitoring of catalyst activation upon addition of (^{DMP}DAB)Pd(CH_2SiMe_3)$_2$ (10 μM, 1.0 equiv, at 1.0 min) to a solution of [PPN][**3**] (10 μM, 1.0 equiv) in MeOH, resulting in formation of [Pd(**3**)]$^-$, associative ligand exchange intermediates [(^{DMP}DAB)Pd(**3**)(CH_2SiMe_3)$_2$]$^-$ and [Pd(**3**)(CH_2SiMe_3)$_2$]$^-$, and ligand oxidation product [**3**+O]$^-$. B) Relative intensities axis amplified ×10, highlighting key reaction intermediates. Inset: calculated isotopic distribution pattern (bars) overlaid on the experimental isotopic distribution (lines) for monoligated [Pd(**3**)]$^-$.

Several Pd-containing species were observed and identified by their *m/z* ratios; measured isotopic distribution patterns also matched calculated patterns (see Appendix C, Table C.1, Figure C.2). The primary species, generated immediately upon addition of (^{DMP}DAB)Pd(CH_2SiMe_3)$_2$, is assigned as monoligated [Pd(**3**)]$^-$ (*m/z* 595) (Figure 5.2). The formation of [Pd(**3**)]$^-$ was evident within the time required to transfer the solution from the reaction flask to the spectrometer inlet (approx. 25 seconds),[41] suggesting a rapid initiation process. This species is formed by ligand exchange and C–C reductive elimination, both of which happen extremely rapidly even at low concentration (10 μM). The observed consumption of free ligand (Figure 5.2A) occurs over a longer timescale (approx. 5 minutes), indicating that ligand coordination and subsequent reduction likely proceed with a half-life closer to 60 seconds under the experimental conditions. No bisligated [Pd(**3**)$_2$]$^{2-}$ species were observed under these conditions, even when 2 equivalents of **3** were added; however, bisligation is evident with a larger excess of **3** (see below). Over time, evidence of phosphine oxidation was observed, a common deactivation pathway in palladium-catalyzed reactions.[53] The major Pd species observed is assigned as [Pd(**3**)+O]$^-$ (*m/z* 611), which is generated alongside the phosphine oxide [**3**+O]$^-$ (*m/z* 517). This deactivation of monoligated [Pd(**3**)]$^-$ is consistent with the highly reactive nature of this coordinatively unsaturated species.

Despite following best practices to maintain an anaerobic environment, minor air contamination can occur during the injection of solutions into reaction flasks. This air contamination, along with trace dissolved gases in the solvent, can lead to excessive observable oxidation side products, further accentuated by the extremely low operating concentrations used for ESI-MS experiments.[41] Consequently, the oxidation side products observed may be more prominent in these experiments than they would be under typical preparative-scale conditions.

In addition to [Pd(**3**)]$^-$, two Pd(II) ligand exchange intermediates were detected: [(^{DMP}DAB)Pd(**3**)(CH_2SiMe_3)$_2$]$^-$ (*m/z* 1033) and [Pd(**3**)(CH_2SiMe_3)$_2$]$^-$ (*m/z* 769). Further investigation focused on the intermediate [(^{DMP}DAB)Pd(**3**)(CH_2SiMe_3)$_2$]$^-$ using ESI-MS/MS techniques, where inducing the unimolecular decomposition provided a detailed picture of the fragmentation pathway. Under collision-induced dissociation (CID) conditions, the

precursor ion fragmented into three product ions: (1) [Pd(**3**)(CH_2SiMe_3)$_2$]$^-$ through loss of ^{DMP}DAB via ligand dissociation; (2) [Pd(**3**)]$^-$ through loss of (Me_3SiCH_2)$_2$ by reductive elimination; and (3) free [**3**]$^-$ from ligand dissociation of the phosphine (Figure 5.3A). Notably, even at collision energy (CE) of 0 V, precursor ion fragmentation occurred, indicating a low activation energy for dissociation of this intermediate. While we cannot definitively assign this as 4- or 5-coordinate, a monodentate binding mode for ^{DMP}DAB is consistent with both the bonding preferences of d^8 Pd(II), and the facile ligand dissociation at 0 V. This 4-coordinate species likely arises from **3** displacing one of the imine arms. The relatively low intensity of product ion [Pd(**3**)]$^-$ at CE 0 V contrasts with its higher abundance observed in the MS scans (Figure 5.2). This indicates that the monoligated [Pd(**3**)]$^-$ catalyst activation species in Figure 5.2 is not solely a result of in-source fragmentation.

A transfer collision energy ramp from 0 to 30 V (in 1 V increments) was applied to [(^{DMP}DAB)Pd(**3**)(CH_2SiMe_3)$_2$]$^-$, revealing the energy-dependent changes in precursor and product ion intensities (Figure 5.3B). The results indicate that [(^{DMP}DAB)Pd(**3**)(CH_2SiMe_3)$_2$]$^-$ forms via a ligand association reaction, which undergoes further reactivity to generate the active catalyst. Initially, the precursor ion was at maximum intensity at CE 0 V and decreased rapidly as CE was increased. Notably, dissociation of ^{DMP}DAB is facile, as evidenced by the low activation energy required for fragmentation leading to [Pd(**3**)(CH_2SiMe_3)$_2$]$^-$. Subsequent reductive elimination of (Me_3SiCH_2)$_2$ generates the monoligated active catalyst [Pd(**3**)]$^-$, with the phosphine assisting the reductive elimination process through steric compression and transition state stabilization by coordination to the pendant arene.[54–56] Crucially, the absence of a [(^{DMP}DAB)Pd(**3**)]$^-$ fragment ion indicates that the mechanistic steps follow a sequential pathway, as in Figure 5.3A, with ^{DMP}DAB ligand dissociation preceding the reductive elimination of (Me_3SiCH_2)$_2$. This observation aligns with literature studies demonstrating how reductive elimination in 4-coordinate d^8 complexes is often preceded by ligand dissociation, which generates a 3-coordinate intermediate.[57,58] This reductive elimination is facilitated by the relative ease of polytopal rearrangement in this intermediate, enabling geometry distortion for advantageous orbital overlap.[59–61]

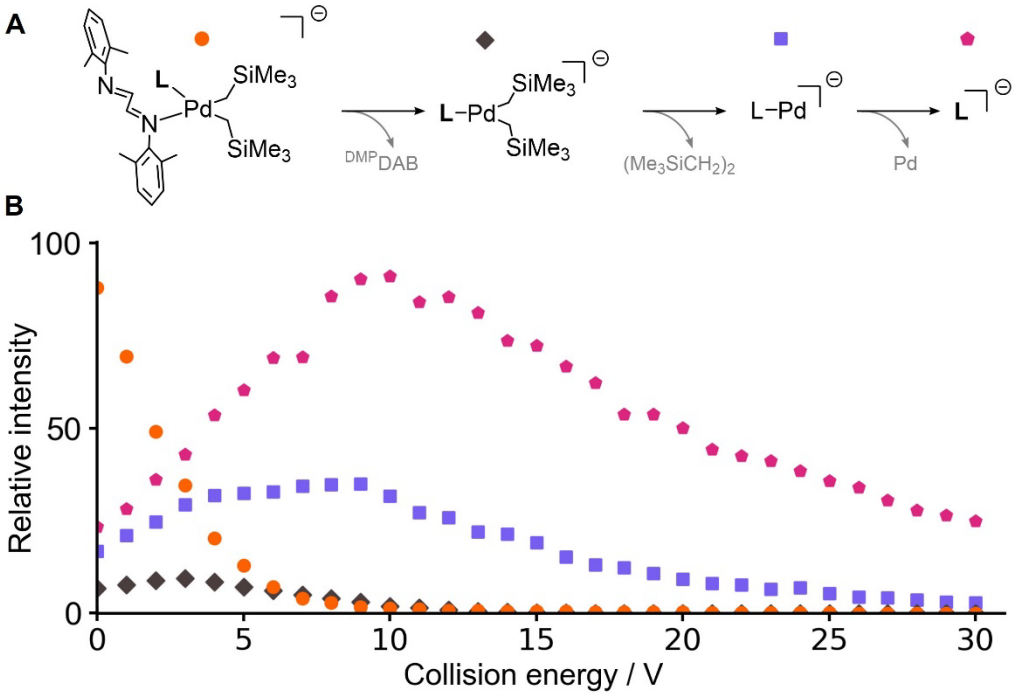

Figure 5.3: A) Reaction pathway of [(^{DMP}DAB)Pd(**3**)(CH_2SiMe_3)$_2$]$^-$ ion fragmentation upon CID with argon gas, showing collision energies that maximized each product ion. Undetected neutral fragments shown in grey. B) Relative intensities of precursor and product ions over a collision energy ramp (0–30 V, 1 V increments), highlighted with colors as in A.

5.3.2 *In Situ* Trapping of Monoligated [Pd(**3**)]$^-$

Once coordinatively unsaturated LPd(0) forms *in situ*, it should be susceptible to rapid trapping, either by ArX via oxidative addition, or alternatively through coordination with a stabilizing ligand such as an electron-deficient olefin.[62] To investigate this, [Pd(**3**)]$^-$ in solution was trapped by adding an excess of the π-acidic ligand maleic anhydride (MAH). This approach was designed to evaluate whether [Pd(**3**)]$^-$ was a true solution phase species, rather than an in-source MS ion fragment of [(^{DMP}DAB)Pd(**3**)(CH_2SiMe_3)$_2$]$^-$ or of the bisligated [Pd(**3**)$_2$]$^{2-}$ species. Accordingly, after catalyst activation, 2 equivalents of MAH were introduced to the reaction mixture (Figure 5.4). A sudden decrease in the signal intensity of [Pd(**3**)]$^-$ was observed, accompanied by a matching increase in the olefin-trapped Pd(0) species [Pd(**3**)(MAH)]$^-$ (*m/z* 693). A much slower conversion between the two followed, which likely reflects the rate of reductive elimination of (Me_3SiCH_2)$_2$ from [(^{DMP}DAB)Pd(**3**)(CH_2SiMe_3)$_2$]$^-$ and/or the rate of bimolecular ligand association at these

low concentrations. Upon CID of [Pd(**3**)(MAH)]⁻ at CE 13 V, the primary fragment ion observed was [Pd(**3**)]⁻.

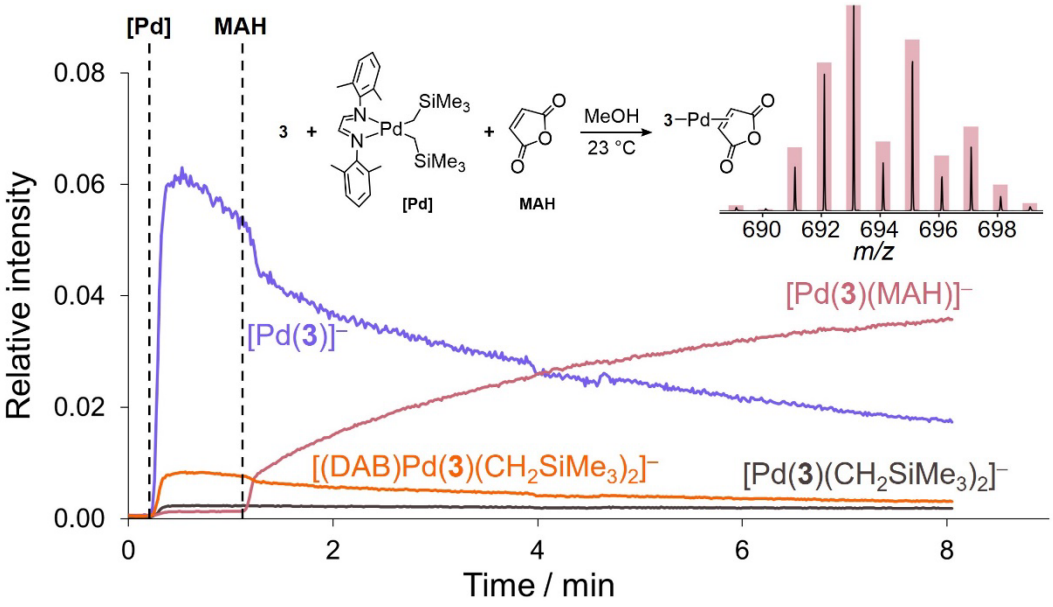

Figure 5.4: Relative species intensities for the introduction of maleic anhydride (MAH, 20 μM, 2 equiv, at 1.1 min) into a MeOH solution of [PPN][**3**] (10 μM, 1 equiv) and (^{DMP}DAB)Pd(CH_2SiMe_3)$_2$ (10 μM, 1 equiv, at 0.1 min), monitored by PSI-ESI(–)-MS. MAH trapping yielded [Pd(**3**)(MAH)]⁻. Inset: calculated isotopic distribution patterns (bars) overlaid on the experimental isotopic distribution (lines) for [Pd(**3**)(MAH)]⁻.

This trapping experiment further supports the assertion that [Pd(**3**)]⁻ is indeed a solution-phase species, where the only other ligands are weakly-bound and rapidly-exchanging solvent molecules. This distinguishes it from a mere product of in-source ion fragmentation, where under these conditions (stoichiometric **3**) the solution equilibrium strongly favors LPd(0) over L_2Pd(0).

5.3.3 Ligand Competition Experiments

Previous studies have highlighted how ligand size influences the coordination number in L_nPd(0) species.[13,18,56,63] The impact different ligands have on catalyst activation was explored through competitive experiments involving three phosphine ligands with varying sizes and denticity. To initiate catalyst activation, a precatalyst solution was introduced to

a reaction flask containing equimolar amounts of charge-tagged phosphines TPPMS (**1**), sSPhos (**3**), and ssXantphos (**4**). By maintaining a low precatalyst to ligand ratio (1:3 Pd/L), we aimed to observe preferential activation among these ligands.

Figure 5.5 shows the results of this experiment, with all three ligands exhibiting monoligated species upon activation. As a bidentate phosphine, **4** appears to form the more stable intermediate, although ion effects from the dianion likely result in suppression of the monoanionic intermediates. Additionally, all three ligands exhibited the associative ligand substitution intermediates $[(^{DMP}DAB)Pd(L)(CH_2SiMe_3)_2]^-$ and $[Pd(L)(CH_2SiMe_3)_2]^-$, consistent with similar activation mechanisms. Notably, detection of $[Pd(\mathbf{4})(CH_2SiMe_3)_2]^-$ aligns favorably with previous work, where the analogous $Pd(xantphos)(CH_2SiMe_3)_2$ complex was successfully isolated from $(^{DMP}DAB)Pd(CH_2SiMe_3)_2$ in 68% yield.[39]

No homoleptic or heteroleptic bisligated species were observed for any of the ligands used in these experiments (Figure 5.6). The observed preference for monoligation under stoichiometric conditions implies an appreciable barrier to the formation of $L_2Pd(0)$ species. This is attributed to steric hindrance posed by bulky ligands, electrostatic repulsion of the anionic ligands, and the low concentration of these reaction mixtures. Additionally, dialkylbiaryl phosphine ligands exhibit conformational flexibility and diverse binding modes. Among these, strong pendant arene-metal interactions effectively stabilize the metal in a bidentate manner. These interactions occur through coordination where the non-phosphine-containing ring of the biaryl framework can serve as a ligand for the Pd center via the *ipso* or *ortho* carbon, or alternatively through the 2-methoxy substituent for **3**.[23,55,64–66]

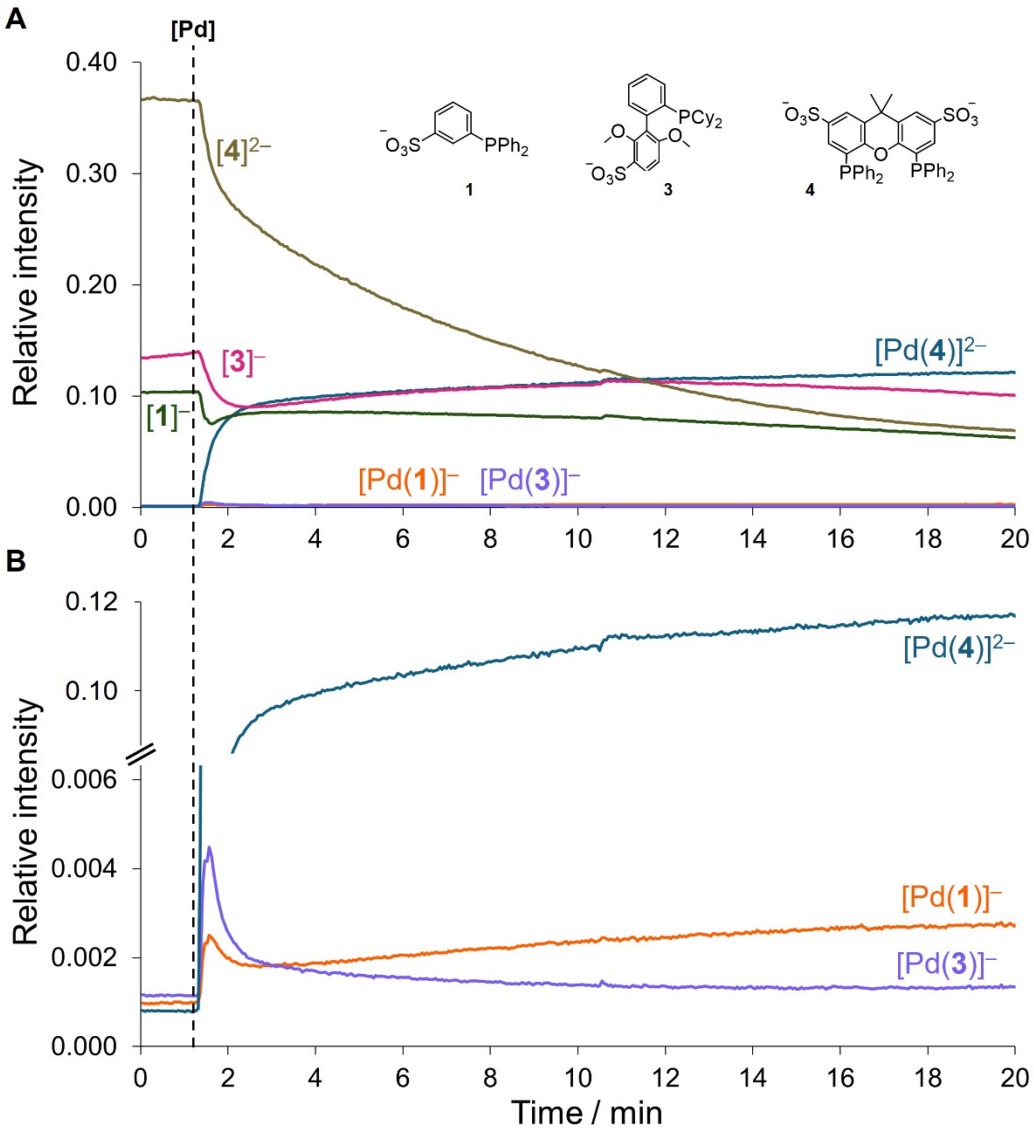

Figure 5.5: A) PSI-ESI(–)-MS reaction monitoring of the addition of (^{DMP}DAB)Pd(CH_2SiMe_3)$_2$ (2.5 μM, 1 equiv, at 1.5 min) into an equimolar MeOH solution at 40 °C containing [PPN][**3**] (2.5 μM, 1 equiv), [PPN][**1**] (2.5 μM, 1 equiv), and [PPN]$_2$[**4**] (2.5 μM, 1 equiv),showing relative rates of phosphine activation and formation of LPd(0) intermediates. B) Relative intensities axis amplified ×5 to highlight key reaction intermediates.

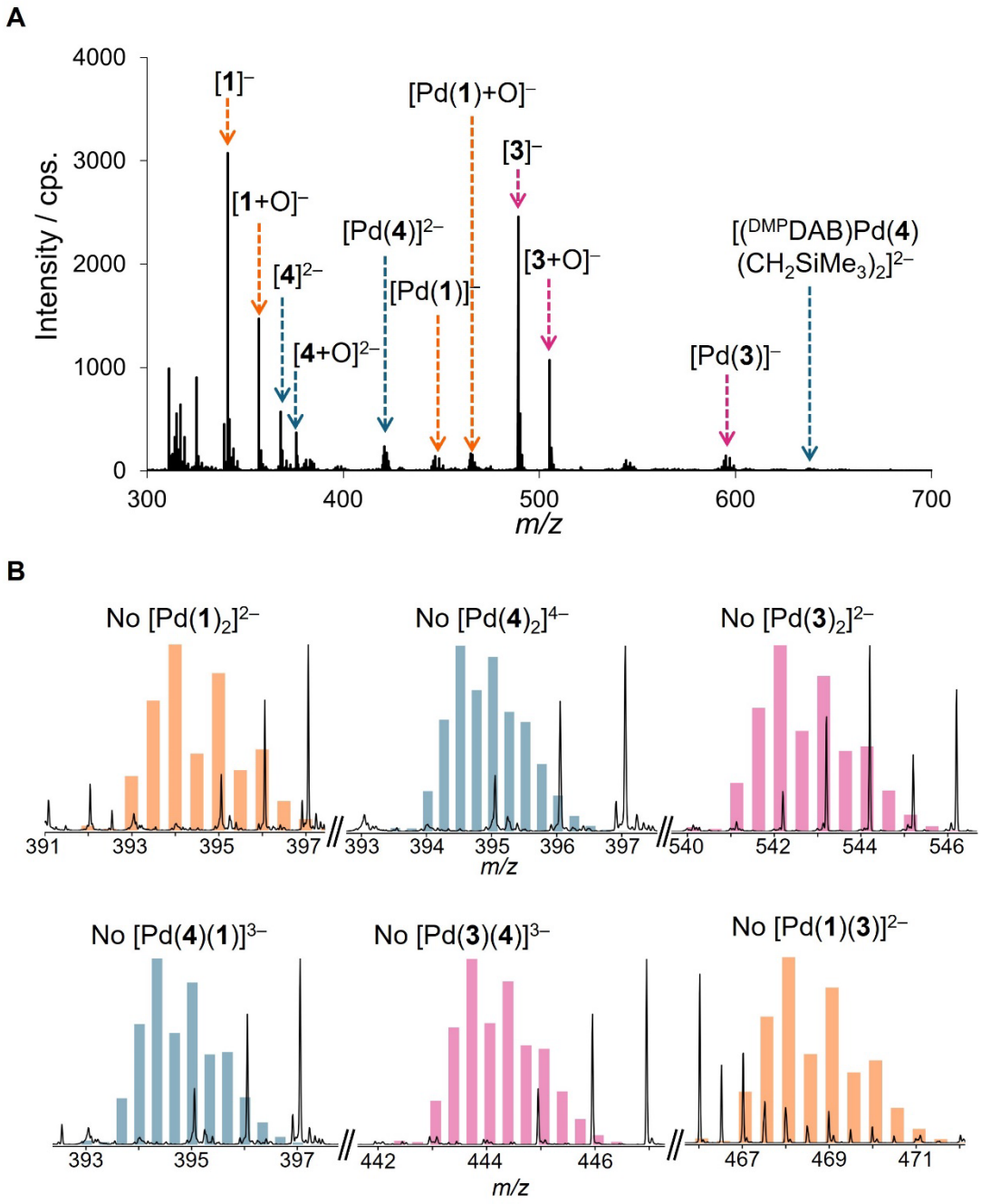

Figure 5.6: A) Representative mass spectrum collected at 1 min after addition of (^{DMP}DAB)Pd(CH_2SiMe_3)$_2$ (2.5 μM) to an equimolar solution of [PPN][**1**], [PPN][**3**], and [PPN]$_2$[**4**] (2.5 μM) in MeOH, showing free phosphine, phosphine oxides, and catalyst activation [Pd(L)]$^{n-}$ species. B) Zoomed-in mass spectra of *m/z* regions where homoleptic or heteroleptic bisligated [Pd(L)$_2$]$^{n-}$ species are expected to be observed, with calculated isotopic distribution patterns (bars) overlaid on the experimental isotopic distribution (lines), showing no characteristic isotopic distribution patterns for species of interest above the background threshold.

Despite the smaller size of TPPMS (**1**), the formation of bisligated palladium species was unexpectedly elusive in initial stoichiometric trials. This outcome contradicts previous studies under similar conditions, where $Pd_2(dba)_3$ was used as the palladium source, and bisligation of **1** was readily observed, as in Chapter 4.[67,68] To promote bisligation, control experiments were conducted by adding an excess of **1** (3:1 L/Pd molar ratio) to the reaction flask prior to introducing the precatalyst. Upon adding the precatalyst, bisligated $[Pd(\mathbf{1})_2]^{2-}$ (and the protonated $[Pd(\mathbf{1})_2{+}H]^-$) was observed, with a relative abundance 1/5th that of $[Pd(\mathbf{1})]^-$ under these conditions (Figure 5.7).

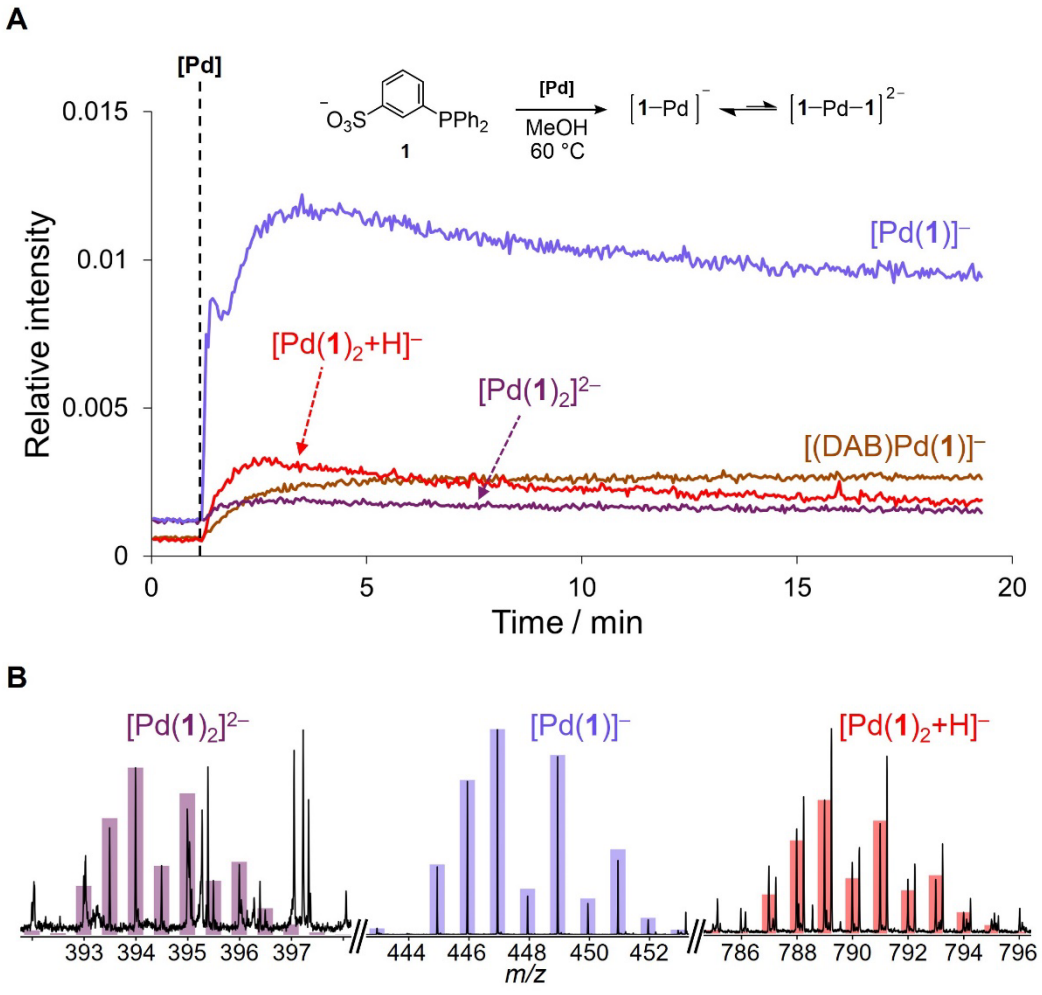

Figure 5.7: PSI-ESI(–)-MS reaction monitoring of catalyst activation upon addition of (^{DMP}DAB)Pd(CH_2SiMe_3)$_2$ (10 μM, 1.0 equiv, at 1.0 min) to a solution of 3× excess [PPN][**1**] (30 μM, 3.0 equiv) in MeOH, showing formation of $[Pd(\mathbf{1})_n]^{n-}$ species. B) Zoomed-in mass spectra of *m/z* regions for $[Pd(\mathbf{1})_n]^{n-}$ species collected 2 minutes after precatalyst addition with calculated isotopic distribution patterns (bars) overlaid on the experimental isotopic distribution (lines).

In further control experiments, the formation of bisligated palladium species was investigated by adding an excess of [PPN][**3**] prior to introduction of precatalyst. Bisligation was also observed for **3** when using a 3:1 L/Pd molar ratio (Figure 5.8). As expected, the consumption of ligand proceeded at a slower rate, with a half-life of approx. 5 min, compared to a half-life less than 1 minute in stoichiometric experiments. The relatively low ion fragmentation energy of $[Pd(\mathbf{3})_2]^{2-}$ at 7 V compared to $[Pd(\mathbf{3})]^-$ at 20 V further indicates unfavourable coordination of the second phosphine.

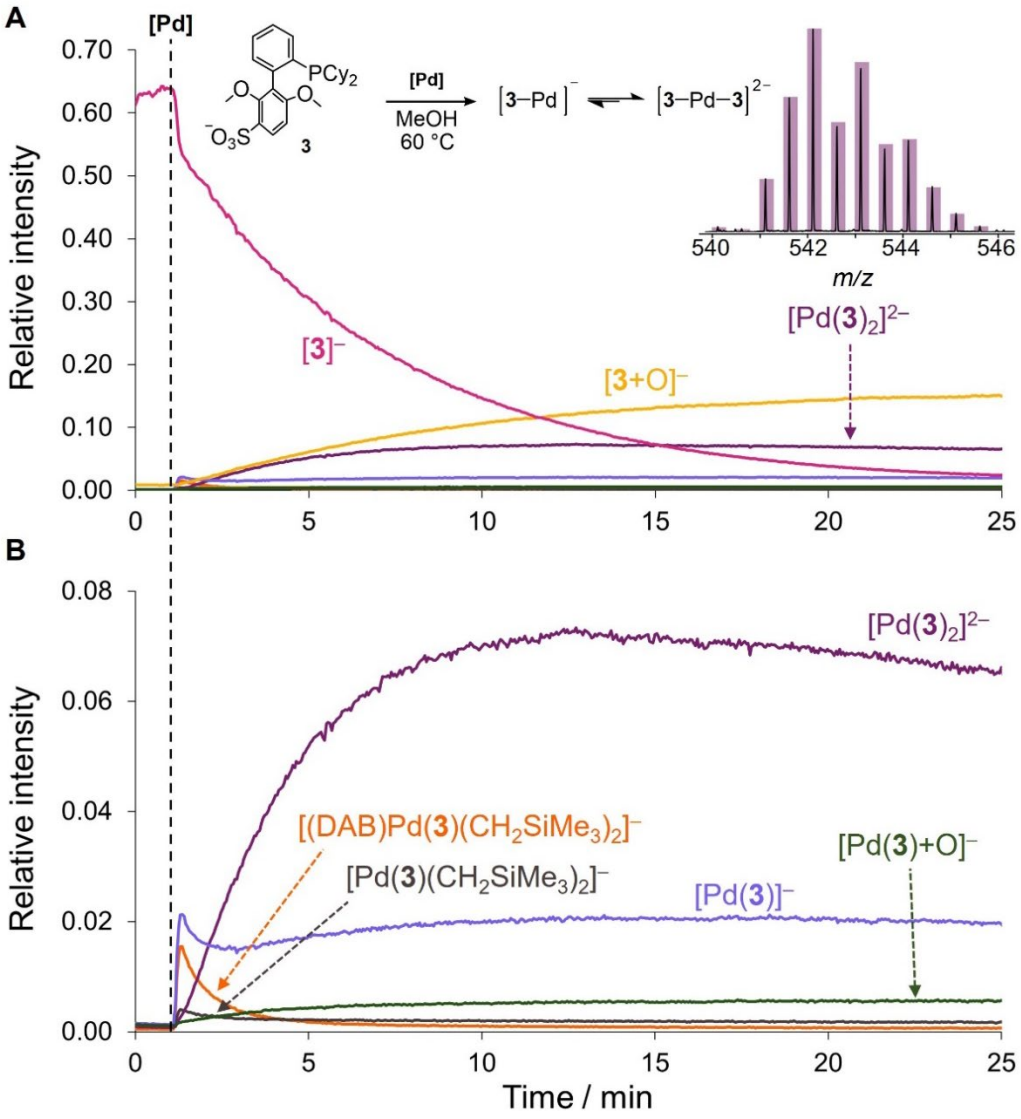

Figure 5.8: A) PSI-ESI(–)-MS reaction monitoring of catalyst activation upon addition of $(^{DMP}DAB)Pd(CH_2SiMe_3)_2$ (10 μM, 1.0 equiv, at 1.0 min) to a solution of 3× excess [PPN][**3**] (30 μM, 3.0 equiv) in MeOH, showing formation of $[Pd(\mathbf{3})_2]^{2-}$. B) Relative intensities axis amplified ×10, highlighting key reaction intermediates. Inset: calculated isotopic distribution pattern (bars) overlaid on the experimental isotopic distribution (lines) for bisligated $[Pd(\mathbf{3})_2]^{2-}$ (*m/z* 542).

While these studies provide valuable insights into the activation mechanisms of (^{DMP}DAB)Pd(CH_2SiMe_3)$_2$ using phosphines **1**, **3**, and **4**, these ligands primarily feature phenyl and secondary alkyl groups. The activation mechanism may differ when using bulkier phosphines such as PAd_3, (*t*-Bu)XPhos, or (*t*-Bu)BrettPhos which introduce greater steric hindrance.

5.3.4 Oxidative Addition Reactivity

With the mechanisms of *in situ* catalyst activation to LPd(0) established, the next step was to investigate the oxidative addition of this species with ArX. Initial investigations using the charge-tagged phosphine sSPhos (**3**) yielded no detectable oxidative addition products by MS. Since oxidative addition complexes $L_nPd(Ar)(X)$ tend to produce cationic $[L_nPd(Ar)]^+$ species following halide dissociation in polar solvents under ESI-MS conditions,[52,68–70] the charge-tagged analogue Pd(**3**)(Ar) would be zwitterionic and undetectable by MS. To address this, the investigation shifted to using the neutral dialkylbiaryl phosphine SPhos (**5**) while operating the instruments in positive ion mode, where **5** was observed as the protonated species [**5**+H]$^+$ (*m/z* 411).

Investigation of the formation of OACs was achieved by introducing precatalyst into a solution containing **5** and an excess of 4'-bromoacetophenone (ArBr). Upon adding (^{DMP}DAB)Pd(CH_2SiMe_3)$_2$, the primary Pd(II) intermediate [Pd(**5**)(Ar)]$^+$ (*m/z* 635) formed rapidly through oxidative addition to ArBr (Figure 5.9A). After approx. 10 minutes, this species reached a steady state. Analysis of the reaction intermediates (Figure 5.9B) identified the ligand exchange intermediate [Pd(**5**)(CH_2SiMe_3)]$^+$ (*m/z* 603), which ionized via [CH_2SiMe_3]$^-$ loss, as the most abundant Pd-containing species immediately following precatalyst addition. As its abundance decreased, [Pd(**5**+H)]$^+$ (*m/z* 517) was also detected, maintaining a steady abundance. These sequential temporal profiles lend support to the proposed ligand exchange and reductive elimination mechanism, consistent with the relative activation energies determined by CID (Figure 5.3).

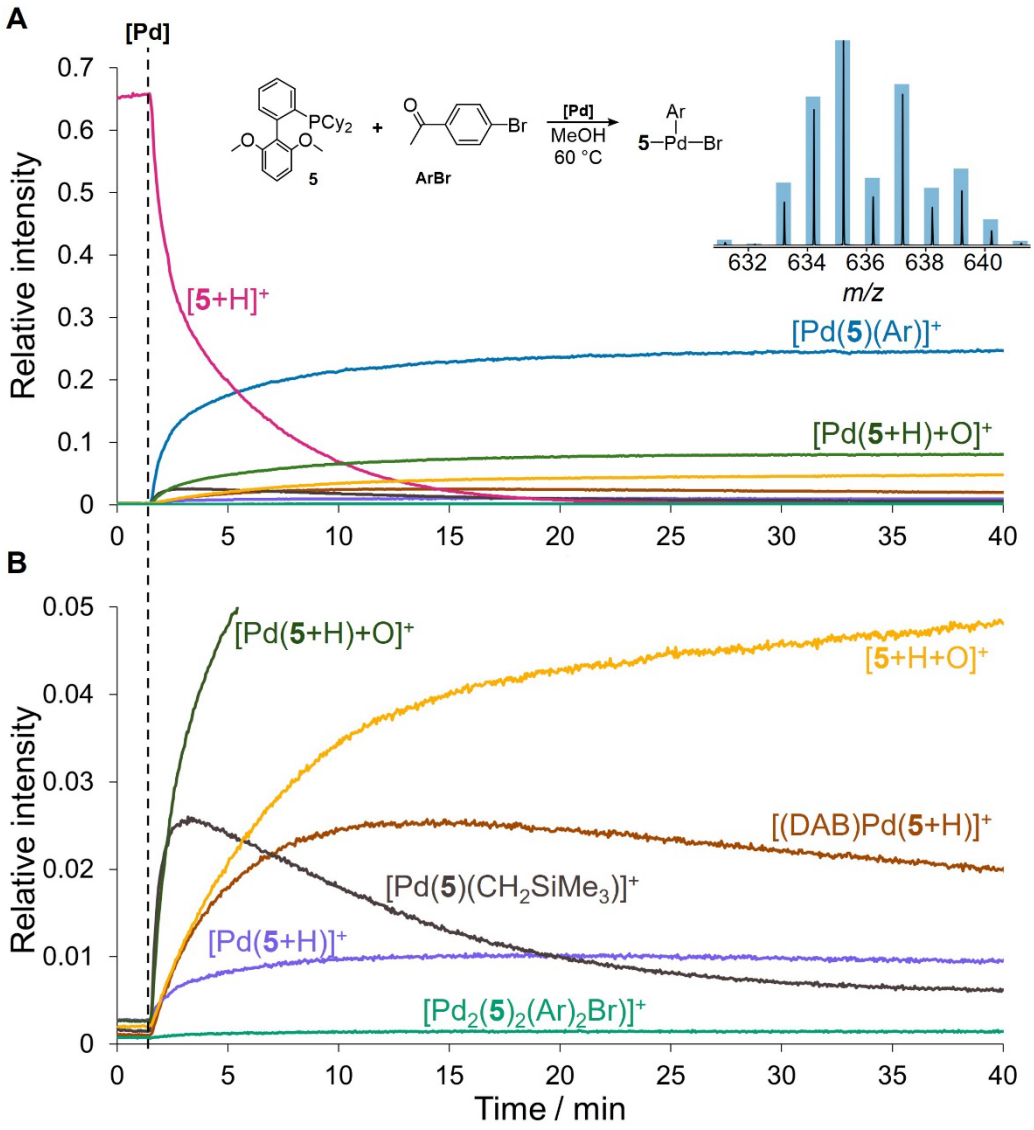

Figure 5.9: A) PSI-ESI(+)-MS reaction monitoring of oxidative addition upon introduction of (^{DMP}DAB)Pd(CH_2SiMe_3)$_2$ (2.5 μM, 1 equiv, at 1.0 min) into a MeOH solution containing **5** (2.5 μM, 1 equiv) and ArBr (50 μM, 20 equiv), forming [Pd(**5**)(Ar)]$^+$. B) Key reaction intermediates and off-cycle products observed, with relative intensities axis amplified ×10. Inset: calculated isotopic distribution patterns (bars) overlaid on the experimental isotopic distribution (lines) for [Pd(**5**)(Ar)]$^+$.

Studies on Pd(L)(Ph)X OACs have highlighted their solvent-dependent behavior. Specifically, the halide-bridged dimeric form [Pd(L)(Ph)(μ-X)]$_2$ tends to persist in non-coordinating solvents.[71] In this investigation, evidence of dimer formation was detected as the fragment ion [Pd$_2$(**5**)$_2$(Ar)$_2$Br]$^+$ (*m/z* 1351), which exhibited a kinetic profile similar to that of [Pd(**5**)(Ar)]$^+$. This equilibrium between dimers and monomers plays a crucial role,

with dimer dissociation necessary for coordinating the nucleophilic coupling partner. Notably, no [(^{DMP}DAB)Pd(Ar)]$^+$ species was observed, which would result either from direct oxidative addition to a (^{DMP}DAB)Pd(0) intermediate, or from ligand substitution between ^{DMP}DAB and [Pd(**5**)(Ar)(Br).

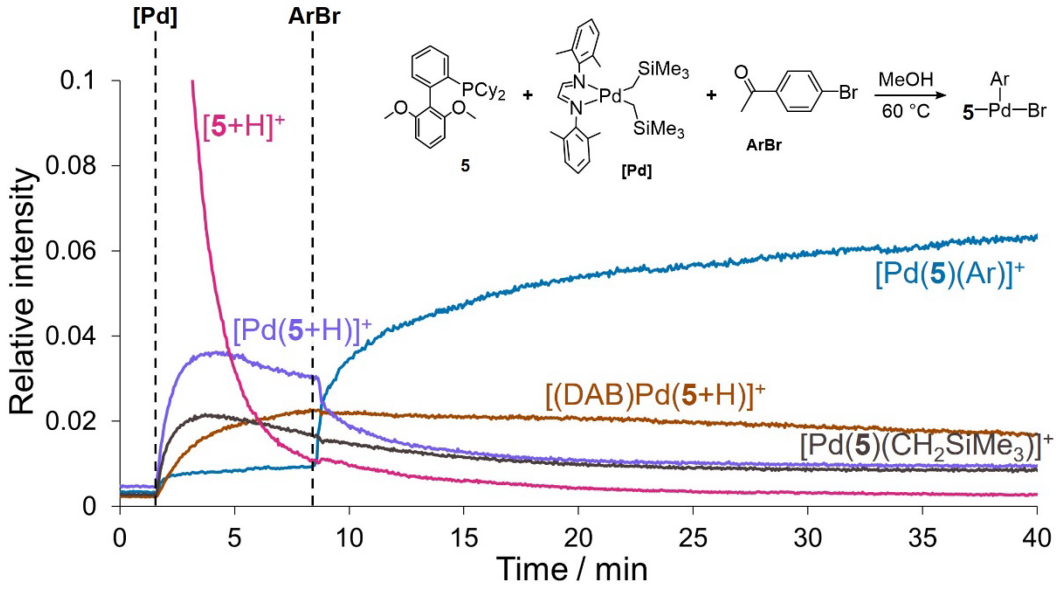

Figure 5.10: Relative species intensities for OAC formation by the sequential additions of (^{DMP}DAB)Pd(CH_2SiMe_3)$_2$ (2.5 μM, 1 equiv, at 1.0 min) and ArBr (50 μM, 20 equiv, at 8.0 min) into a MeOH solution containing **5** (2.5 μM, 1.0 equiv). Experiment conducted under the same conditions as Figure 5.6, monitored by PSI-ESI(+)-MS.

Beyond OAC formation, additional potential off-cycle reaction pathways and product formation was observed. Notably, palladium-catalyzed phosphine oxidation resulted in the formation of [Pd(**5**+H)+O]$^-$ (*m/z* 533) and [(**5**+H+O)]$^+$ (*m/z* 427), consistent with prior observations in the absence of ArX. Importantly, the mixed ligand Pd(0) species [(^{DMP}DAB)Pd(**5**+H)]$^+$ (*m/z* 781) was detected, which also appeared in negative mode experiments as [(^{DMP}DAB)Pd(**3**)]$^-$ (*m/z* 861). This species likely arises from the coordination of free ^{DMP}DAB ligand to LPd(0). This means that ^{DMP}DAB could act as a catalyst inhibitor, maintaining a reservoir of less-reactive Pd(0). This behavior becomes evident when ArBr is sequentially added following catalyst activation (Figure 5.10). Moreover, this sequential addition of precatalyst and ArBr further solidifies the role of monoligated

[Pd(**5**+H)]$^+$ (*m/z* 517) as the active catalytic species, with its relative abundance decreasing in tandem with the formation of [Pd(**5**)(Ar)]$^+$.

Upon CID of [Pd(**5**)(Ar)]$^+$ at 32 V, multiple fragment ions emerged (Figure 5.11). Notably, one fragment ion, [Pd(Ar')]$^+$, emerged as a product of aryl exchange reactions between an aryl group originating from the Pd centre (Ar) and another from the phosphine (Ar'). The aryl exchange reaction competes with the catalytic cycle, potentially contaminating the desired reaction product with products derived from the aryl group originally bound to the phosphorus. Generally, electron-rich aryl groups make exchange more facile, especially in polar solvents and under dilute conditions.[72–74] Additionally, trace amounts of the phosphonium salt [**5**Ar]$^+$ (*m/z* 529), a proposed intermediate for aryl exchange, were generated through CID-induced reductive elimination of [Pd(**5**)(Ar)]$^+$.

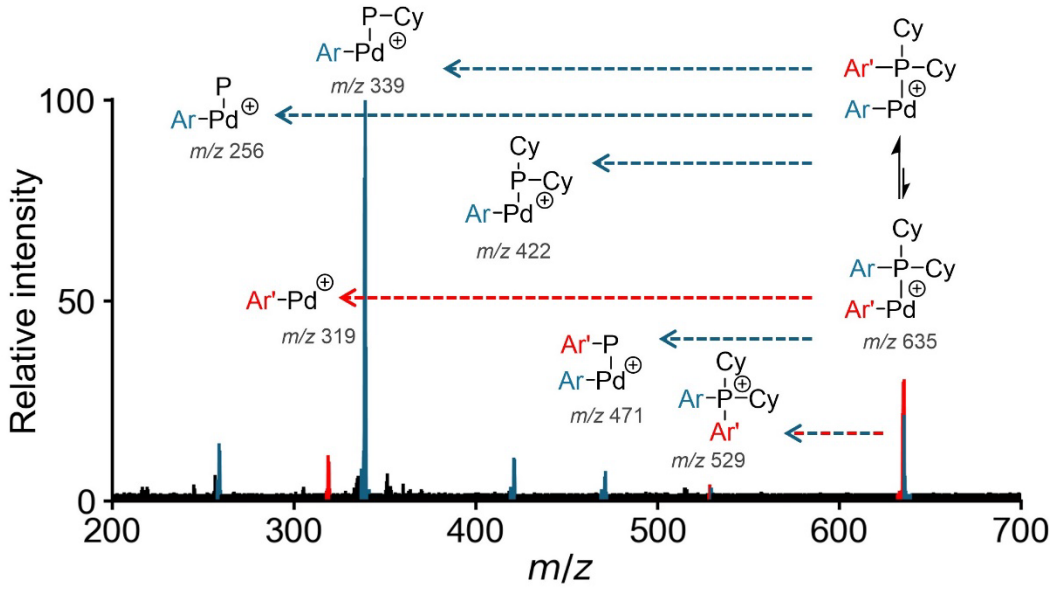

Figure 5.11: ESI(+)-MS/MS (CE = 32 V) of [Pd(**5**)Ar]+ (*m/z* 635.4) showing product ions highlighted in blue, with product ion resulting from Pd-aryl/P-aryl exchange reaction [Pd(Ar')]$^+$ (*m/z* 319.1) highlighted in red. Key: Ar = [$C_6H_4COCH_3$] originating from ArBr; Ar' = [$C_6H_4(C_6H_3(OMe)_2)$] originating from **5**.

5.3.5 Model Suzuki-Miyaura Reaction

A test Suzuki cross-coupling reaction involving 4'-bromoacetophenone (ArBr) and 4-methoxyphenylboronic acid ($RB(OH)_2$) was investigated, to observe any contaminants

resulting from aryl exchange reactions. Species were primarily ionized through sodiation, resulting from an excess of Na_2CO_3, and the detection of Pd-containing intermediates was suppressed by the high sodium concentration (Figure 5.12).

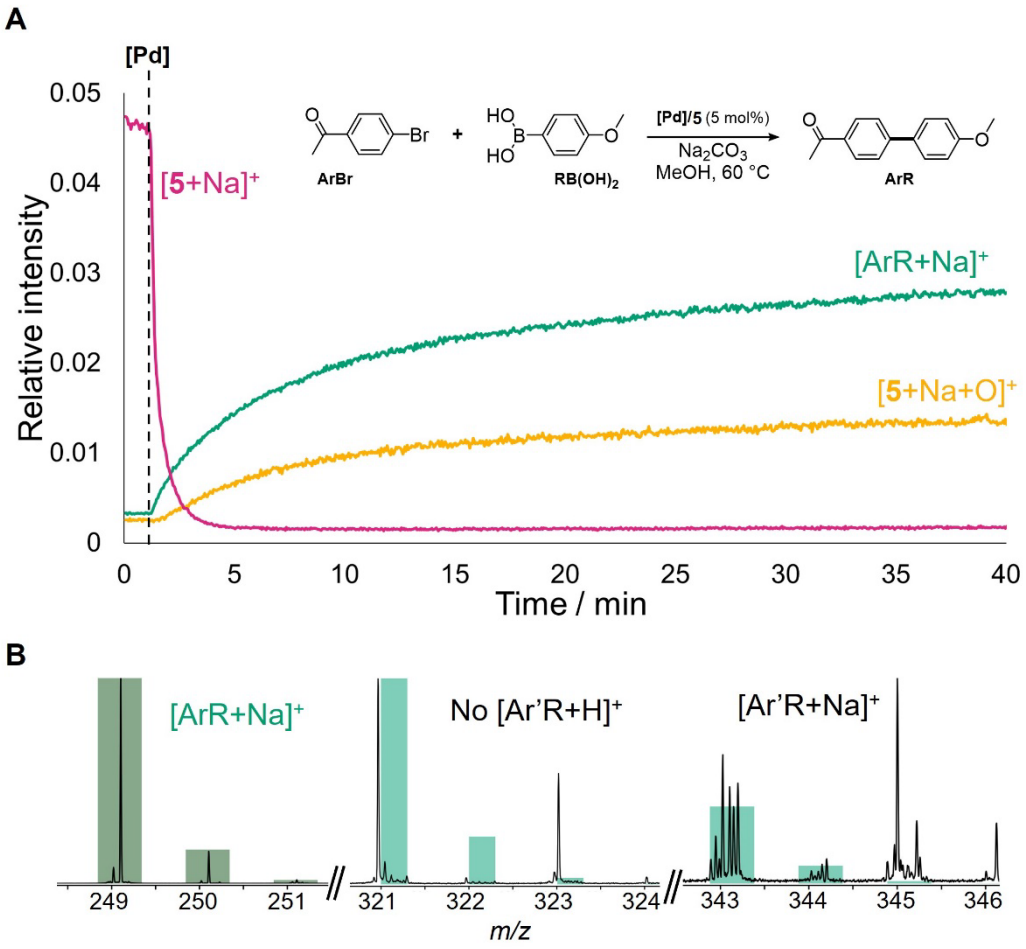

Figure 5.12: A) Relative species intensities for Suzuki coupling of 4'-bromoacetophenone (ArBr) and 4-methoxyphenylboronic acid ($RB(OH)_2$), yielding $[ArR+Na]^+$ (*m/z* 249). B) Zoomed-in mass spectrum collected at 20 min, showing trace amounts of aryl exchange product $[Ar'R+Na]^+$ (*m/z* 343). Key: Ar = $[C_6H_4COCH_3]$ originating from ArBr; Ar' = $[C_6H_4(C_6H_3(OMe)_2)]$ originating from **5**.

Only trace contamination (< 1%) from the aryl exchange product was detected. This observation is consistent with the aryl exchange rate being significantly lower than the rates of transmetallation and reductive elimination. The steric bulk and added stabilization from the pendant arene of the ligand likely disfavors formation of the phosphonium salt intermediate in the solution phase,[75] a process that occurred more readily with a less bulky

phosphine as seen in Chapter 4. Nonetheless, this aryl transfer pathway is a potential source of both catalyst decomposition and product contamination and should therefore be considered as a possible failure mode.

5.3.6 Proposed Catalytic Cycle

Drawing from the discussed observations, the following general reaction pathways are proposed for the *in situ* catalyst activation of (^{DMP}DAB)Pd(CH_2SiMe_3)$_2$ to L_nPd(0) and the subsequent formation of OACs (Figure 5.13). The active Pd(0) species emerges through an associative ligand substitution, initially forming the 4-coordinate mixed ligand (^{DMP}DAB)Pd(L)(CH_2SiMe_3)$_2$, followed by dissociation of ^{DMP}DAB. Subsequent reductive elimination of the two alkyl groups yields the monoligated LPd(0), which remains stable due to interactions with ligand pendant arenes and/or coordinating solvent molecules. This highly active species then initiates the catalytic cycle for cross-coupling reactions, with the product of oxidative addition of ArX partially existing as monomeric $[Pd(L)Ar]^+$ following halide loss in polar solvents under these ESI-MS conditions. Identified off-cycle pathways include phosphine oxidation if O_2 is present, as well as competitive inhibition by ^{DMP}DAB. This latter aspect is an important consideration for achieving maximum catalytic rates, where a non-innocent ^{DMP}DAB 'throw-away' ligand would impede catalytic turnover.

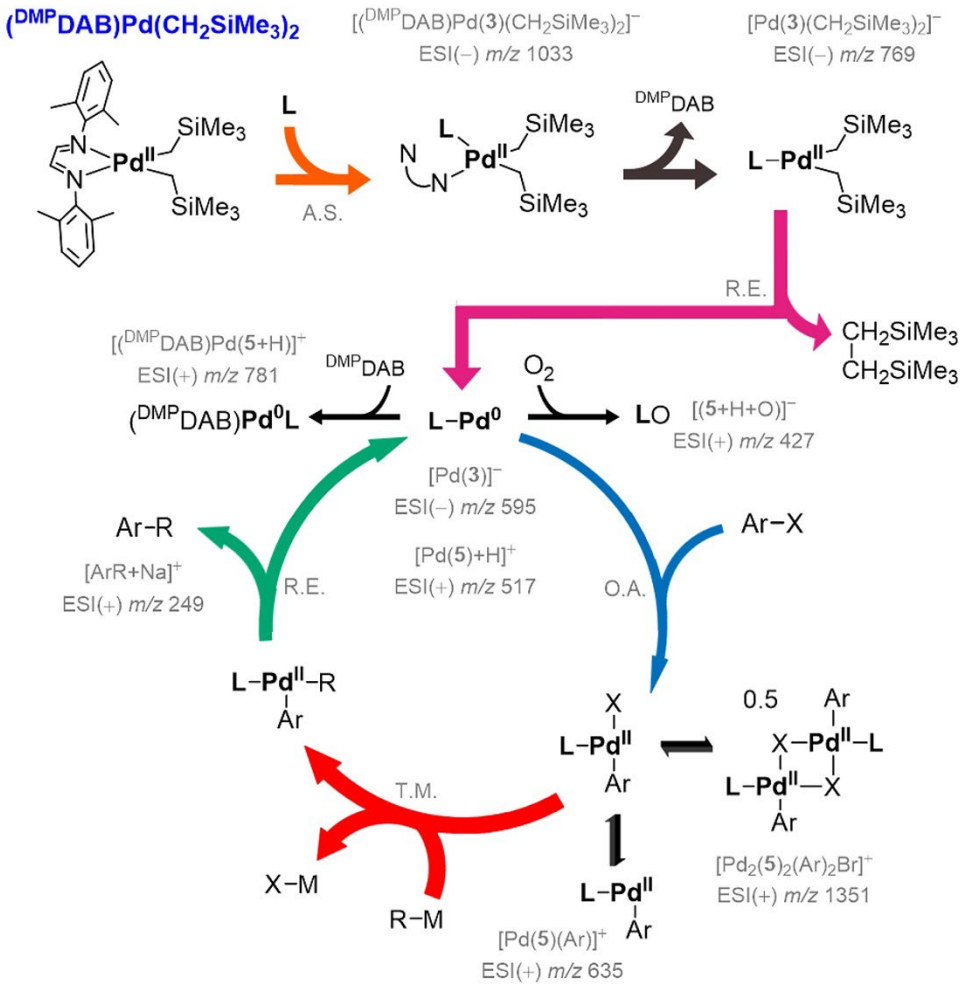

Figure 5.13: Proposed pathways for formation of LPd(0) and LPd(II)(Ar) species from (^{DMP}DAB)Pd(CH_2SiMe_3)$_2$ precatalyst activation with diarylbialkyl phosphine **3** and **5** at 1:1 Pd/L molar ratios, and oxidative addition to ArBr. Key: A.S. = associative substitution, O.A. = oxidative addition, T.M. = transmetallation, R.E. = reductive elimination; *m/z* ratios of key detected intermediates shown in grey; arrow thicknesses qualitatively represent rate constants; catalytic cycle made using www.catacycle.com.[76]

5.4 Conclusions

This chapter has examined the activation mechanisms of the dialkyl-palladium precatalyst (^{DMP}DAB)Pd(CH_2SiMe_3)$_2$, with a focus on the role played by the activating phosphine ligand and the formation of active species in solution. Using PSI-ESI-MS has allowed for the real-time monitoring of these processes. The results demonstrate that after phosphine coordination to (^{DMP}DAB)Pd(CH_2SiMe_3)$_2$, the ^{DMP}DAB ligand dissociates before the

reductive elimination of $(Me_3SiCH_2)_2$. This sequence leads to the generation of the monoligated active catalyst LPd(0), which is identified as the active species responsible for oxidative addition. Notably, a considerable mechanistic barrier to bisligation favours the formation of the highly active monoligated catalyst. Additionally, potential off-cycle pathways have been identified, including the possibility of competitive inhibition by ^{DMP}DAB. These findings contribute to a broader understanding of how this precatalyst functions, providing a foundation for the development of more active and robust catalyst systems for cross-coupling reactions.

5.5 Materials and Methods

All experiments were set-up and performed under an inert (Ar or N_2) atmosphere using standard glovebox and Schlenk line techniques.[77] Ar (UHP200 5.0) and N_2 (HP300 4.8) were purchased from Airgas (Calgary, Canada) and used without further purification. Solvents were purchased from Fisher Scientific and kept under inert atmosphere before use; methanol (MeOH, HPLC-grade) and tetrahydrofuran (THF) were degassed using the freeze-pump-thaw method.

SPhos (**5**) (Sigma-Aldrich, 98 %), sSPhos-sodium salt (Sigma-Aldrich, >99.5%), xantphos (Sigma-Aldrich, 97%), triphenylphosphine (Sigma-Aldrich, ReagentPlus, 99%), bis(triphenylphosphine)iminium chloride (Sigma-Aldrich, 97%), maleic anhydride (Sigma-Aldrich, 99%), 4'-bromoacetophenone (Sigma-Aldrich, 98%), 4-methoxyphenylboronic acid (Oakwood Chemicals, ≥95.0%), and sodium carbonate anhydrous (Bio Basic Canada, ACS, ≥99.5%) were obtained from the commercial suppliers and used without further purification.

(^{DMP}DAB)Pd(CH_2SiMe_3)$_2$ was synthesized according to a literature procedure and consistent characterization data obtained.[2] Bis(triphenylphosphine)iminium triphenylphosphine mono-sulfonate, or [PPN][**1**], was synthesized from triphenylphosphine as reported previously.[60] [PPN][**3**] was obtained by salt metathesis of $[Na]^+[sSPhos]^-$ dissolved in minimal hot methanol mixed with 1.0 equivalent of

bis(triphenylphosphine)iminium chloride [PPN][Cl] dissolved in water, with the precipitate washed using a cold methanol/water mixture (1:1) and collected under vacuum. Synthesis of 2,7-bis(SO_3Na)-xantphos, or $[Na]_2$[**4**], was from xantphos as previously reported,[5] followed by its salt metathesis in 1:1 water:methanol with 2.0 equivalents of bis(triphenylphosphine)iminium chloride [PPN][Cl] to afford $[PPN]_2$[**4**] that was collected using vacuum filtration.

5.5.1 MS Instrument Parameters

Experiments were conducted on a Waters (Milford, USA) Synapt G2-S*i* mass spectrometer and analyzed using Waters MassLynx V4.2 software. The mass spectrometer was operated in full scan resolution mode in a range of *m/z* 50–1500 for both negative and positive ion modes, with parameters optimized by OptiMS[50] as summarized in Table 5.1. Calculation of theoretical *m/z* ratios and isotope patterns were done using PythoMS[78] and the IsoSpecPy[79] package, with identified *m/z* ratios summarized in Appendix C. Signal intensities for all chromatograms were normalized to the total ion current (TIC).

Table 5.1: Waters Synapt G2-S*i* instrument parameters for dialkyl-Pd experiments.

Parameter	Positive Mode	Negative Mode
Flow rate (PSI)	20 µL min^{-1}	20 µL min^{-1}
Scan time	1 s	1 s
Capillary voltage	2.9 kV	2.6 kV
Sampling cone voltage	63 V	50 V
Source offset	72 V	80 V
Source temperature	90 °C	90 °C
Desolvation temperature	200 °C	200 °C
Cone gas flow	70 L hr^{-1}	100 L hr^{-1}
Desolvation gas flow	350 L hr^{-1}	400 L hr^{-1}
Nebuliser	2.8 bar	2.8 bar
FWHM	18510	24150

5.5.2 General Procedures for PSI-ESI-MS Reaction Monitoring

Stock solutions of (^{DMP}DAB)Pd(CH_2SiMe_3)$_2$ were prepared in degassed tetrahydrofuran (THF), with all other chemical stock solutions prepared in degassed HPLC-grade methanol (MeOH). In a typical reaction, degassed HPLC-grade MeOH (10 mL or 20 mL) was transferred to a Schlenk flask equipped with a stirrer bar, with an aliquot of ligand and/or substrate added, and the solution sparged with nitrogen for 15 minutes. The inlet system and the ESI source of the mass spectrometer were flushed with MeOH for 10 minutes before each experiment. The sealed flask was then connected to the inlet via PEEK tubing (TubPEEK Red, 1/16 in. OD, 0.005 in. ID, 18 in. L). The reaction mixture was monitored by PSI-ESI-MS techniques, where an overpressure of argon gas was applied to transfer the sample solution from the Schlenk flask into the spectrometer inlet at an infusion rate of 20 μL min^{-1}. Reactions were initiated by additions of (^{DMP}DAB)Pd(CH_2SiMe_3)$_2$ or substrate at specified time intervals, with the reaction allowed to proceed for up to 40 minutes. All reactions were stirred at 400 rpm and monitored at 60°C (unless otherwise specified). Detailed experimental conditions are summarized in the Table 5.2.

Table 5.2: Summary of reagent and injection details for figures.

Figure	Reagents in Flask (Concentration / μM, Equivalents)	Reaction Volume / mL	Reagents Added (Concentration / μM, Equivalents, at Injection Time)
5.2	[PPN][**3**] (10, 1.0)	20	(^{DMP}DAB)Pd(CH_2SiMe_3)$_2$ (10, 1.0, at 1.0 min)
5.4	[PPN][**3**] (10, 1.0)	10 (23 °C)	(^{DMP}DAB)Pd(CH_2SiMe_3)$_2$ (10, 1.0, at 0.1 min), MAH (20, 2.0, at 1.1 min)
5.5, 5.6	[PPN][**1**] (10, 1.0), [PPN][**3**] (10, 1.0), [PPN]$_2$[**4**] (10, 1.0)	20 (40 °C)	(^{DMP}DAB)Pd(CH_2SiMe_3)$_2$ (10, 1.0, at 1.0 min)
5.7	[PPN][**1**] (30, 3.0)	20	(^{DMP}DAB)Pd(CH_2SiMe_3)$_2$ (10, 1.0, at 1.0 min)
5.8	[PPN][**3**] (30, 3.0)	20	(^{DMP}DAB)Pd(CH_2SiMe_3)$_2$ (10, 1.0, at 1.0 min)
5.9	**5** (2.5, 1.0)	20	(^{DMP}DAB)Pd(CH_2SiMe_3)$_2$ (2.5, 1.0, at 1.0 min)
5.10	**5** (2.5, 1.0)	20	(^{DMP}DAB)Pd(CH_2SiMe_3)$_2$ (10, 1.0, at 1.0 min), ArBr (50, 20.0 at 8.0 min)
5.12	**5** (2.5, 1.0), ArBr (50, 20.0), RB(OH)$_2$ (50, 20.0), Na_2CO_3 (2.0 mg, 19 μmol)	20	(^{DMP}DAB)Pd(CH_2SiMe_3)$_2$ (2.5, 1.0, at 1.0 min)

5.6 References

(1) Zalesskiy, S. S.; Ananikov, V. P. Pd2(Dba)3 as a Precursor of Soluble Metal Complexes and Nanoparticles: Determination of Palladium Active Species for Catalysis and Synthesis. *Organometallics* **2012**, *31* (6), 2302–2309. https://doi.org/10.1021/om201217r.

(2) Weber, P.; Biafora, A.; Doppiu, A.; Bongard, H.-J.; Kelm, H.; Gooßen, L. J. A Comparative Study of Dibenzylideneacetone Palladium Complexes in Catalysis. *Org. Process Res. Dev.* **2019**, *23* (7), 1462–1470. https://doi.org/10.1021/acs.oprd.9b00214.

(3) Carole, W. A.; Colacot, T. J. Understanding Palladium Acetate from a User Perspective. *Chem. – Eur. J.* **2016**, *22* (23), 7686–7695. https://doi.org/10.1002/chem.201601450.

(4) Slack, E. D.; Tancini, P. D.; Colacot, T. J. Process Economics and Atom Economy for Industrial Cross Coupling Applications via LnPd(0)-Based Catalysts. In *Organometallics in Process Chemistry*; Colacot, T. J., Sivakumar, V., Eds.; Springer International Publishing: Cham, 2019; pp 161–198. https://doi.org/10.1007/3418_2019_28.

(5) Ting, M. Y. C.; Yunker, L. P. E.; Chagunda, I. C.; Hatlelid, K.; Vieweg, M.; McIndoe, J. S. A Mechanistic Investigation of the Suzuki Polycondensation Reaction Using MS/MS Methods. *Catal. Sci. Technol.* **2021**, *11* (13), 4406–4416. https://doi.org/10.1039/D1CY00743B.

(6) Firsan, S. J.; Sivakumar, V.; Colacot, T. J. Emerging Trends in Cross-Coupling: Twelve-Electron-Based L1Pd(0) Catalysts, Their Mechanism of Action, and Selected Applications. *Chem. Rev.* **2022**, *122* (23), 16983–17027. https://doi.org/10.1021/acs.chemrev.2c00204.

(7) Lau, S. H.; Chen, L.; Kevlishvili, I.; Davis, K.; Liu, P.; Carrow, B. Capturing the Most Active State of a Palladium(0) Cross-Coupling Catalyst. ChemRxiv October 13, 2021. https://doi.org/10.26434/chemrxiv-2021-477kn.

(8) Semeniuchenko, V.; Sharif, S.; Rana, N.; Chandrasoma, N.; Braje, W. M.; Baker, R. T.; Manthorpe, J. M.; Pietro, W. J.; Organ, M. G. Experimental Evidence for Zerovalent Pd(NHC) as a Competent Catalyst in C–N Cross-Coupling (NHC = DiMeIHeptCl). *J. Am. Chem. Soc.* **2024**, *146* (42), 29224–29236. https://doi.org/10.1021/jacs.4c12203.

(9) MacQueen, P. M.; Holley, R.; Ghorai, S.; Colacot, T. J. Convenient One-Pot Synthesis of L2Pd(0) Complexes for Cross-Coupling Catalysis. *Organometallics* **2023**, *42* (18), 2644–2650. https://doi.org/10.1021/acs.organomet.3c00059.

(10) Li, H.; Johansson Seechurn, C. C. C.; Colacot, T. J. Development of Preformed Pd Catalysts for Cross-Coupling Reactions, Beyond the 2010 Nobel Prize. *ACS Catal.* **2012**, *2* (6), 1147–1164. https://doi.org/10.1021/cs300082f.

(11) Vikse, K.; Naka, T.; McIndoe, J. S.; Besora, M.; Maseras, F. Oxidative Additions of Aryl Halides to Palladium Proceed through the Monoligated Complex. *ChemCatChem* **2013**, *5* (12), 3604–3609. https://doi.org/10.1002/cctc.201300723.

(12) Scharf, L. T.; Rodstein, I.; Schmidt, M.; Scherpf, T.; Gessner, V. H. Unraveling the High Activity of Ylide-Functionalized Phosphines in Palladium-Catalyzed Amination Reactions: A Comparative Study with CyJohnPhos and PtBu3. *ACS Catal.* **2020**, *10* (2), 999–1009. https://doi.org/10.1021/acscatal.9b04666.

(13) Newman-Stonebraker, S. H.; Smith, S. R.; Borowski, J. E.; Peters, E.; Gensch, T.; Johnson, H. C.; Sigman, M. S.; Doyle, A. G. Univariate Classification of Phosphine Ligation State and Reactivity in Cross-Coupling Catalysis. *Science* **2021**, *374* (6565), 301–308. https://doi.org/10.1126/science.abj4213.

(14) Scott, N. W. J.; Ford, M. J.; Jeddi, N.; Eyles, A.; Simon, L.; Whitwood, A. C.; Tanner, T.; Willans, C. E.; Fairlamb, I. J. S. A Dichotomy in Cross-Coupling Site Selectivity in a Dihalogenated Heteroarene: Influence of Mononuclear Pd, Pd Clusters, and Pd Nanoparticles—the Case for Exploiting Pd Catalyst Speciation. *J. Am. Chem. Soc.* **2021**, *143* (25), 9682–9693. https://doi.org/10.1021/jacs.1c05294.

(15) Besora, M.; Maseras, F. The Diverse Mechanisms for the Oxidative Addition of C–Br Bonds to Pd(PR3) and Pd(PR3)2 Complexes. *Dalton Trans.* **2019**, *48* (43), 16242–16248. https://doi.org/10.1039/C9DT03155C.
(16) Norman, J. P.; Larson, N. G.; Neufeldt, S. R. Different Oxidative Addition Mechanisms for 12- and 14-Electron Palladium(0) Explain Ligand-Controlled Divergent Site Selectivity. *ACS Catal.* **2022**, *12* (15), 8822–8828. https://doi.org/10.1021/acscatal.2c01698.
(17) Kania, M. J.; Reyes, A.; Neufeldt, S. R. Oxidative Addition of (Hetero)Aryl (Pseudo)Halides at Palladium(0): Origin and Significance of Divergent Mechanisms. *J. Am. Chem. Soc.* **2024**, *146* (28), 19249–19260. https://doi.org/10.1021/jacs.4c04496.
(18) Niemeyer, Z. L.; Milo, A.; Hickey, D. P.; Sigman, M. S. Parameterization of Phosphine Ligands Reveals Mechanistic Pathways and Predicts Reaction Outcomes. *Nat. Chem.* **2016**, *8* (6), 610–617. https://doi.org/10.1038/nchem.2501.
(19) Marion, N.; Navarro, O.; Mei, J.; Stevens, E. D.; Scott, N. M.; Nolan, S. P. Modified (NHC)Pd(Allyl)Cl (NHC = N-Heterocyclic Carbene) Complexes for Room-Temperature Suzuki−Miyaura and Buchwald−Hartwig Reactions. *J. Am. Chem. Soc.* **2006**, *128* (12), 4101–4111. https://doi.org/10.1021/ja057704z.
(20) Johansson Seechurn, C. C. C.; Parisel, S. L.; Colacot, T. J. Air-Stable Pd(R-Allyl)LCl (L= Q-Phos, P(t-Bu)3, Etc.) Systems for C–C/N Couplings: Insight into the Structure–Activity Relationship and Catalyst Activation Pathway. *J. Org. Chem.* **2011**, *76* (19), 7918–7932. https://doi.org/10.1021/jo2013324.
(21) Hill, L. L.; Crowell, J. L.; Tutwiler, S. L.; Massie, N. L.; Hines, C. C.; Griffin, S. T.; Rogers, R. D.; Shaughnessy, K. H.; Grasa, G. A.; Johansson Seechurn, C. C. C.; Li, H.; Colacot, T. J.; Chou, J.; Woltermann, C. J. Synthesis and X-Ray Structure Determination of Highly Active Pd(II), Pd(I), and Pd(0) Complexes of Di(Tert-Butyl)Neopentylphosphine (DTBNpP) in the Arylation of Amines and Ketones. *J. Org. Chem.* **2010**, *75* (19), 6477–6488. https://doi.org/10.1021/jo101187q.
(22) Melvin, P. R.; Nova, A.; Balcells, D.; Dai, W.; Hazari, N.; Hruszkewycz, D. P.; Shah, H. P.; Tudge, M. T. Design of a Versatile and Improved Precatalyst Scaffold for Palladium-Catalyzed Cross-Coupling: (H3-1-tBu-Indenyl)2(μ-Cl)2Pd2. *ACS Catal.* **2015**, *5* (6), 3680–3688. https://doi.org/10.1021/acscatal.5b00878.
(23) Ingoglia, B. T.; Buchwald, S. L. Oxidative Addition Complexes as Precatalysts for Cross-Coupling Reactions Requiring Extremely Bulky Biarylphosphine Ligands. *Org. Lett.* **2017**, *19* (11), 2853–2856. https://doi.org/10.1021/acs.orglett.7b01082.
(24) Biscoe, M. R.; Fors, B. P.; Buchwald, S. L. A New Class of Easily Activated Palladium Precatalysts for Facile C–N Cross-Coupling Reactions and the Low Temperature Oxidative Addition of Aryl Chlorides. *J. Am. Chem. Soc.* **2008**, *130* (21), 6686–6687. https://doi.org/10.1021/ja801137k.
(25) Bruno, N. C.; Tudge, M. T.; Buchwald, S. L. Design and Preparation of New Palladium Precatalysts for C–C and C–N Cross-Coupling Reactions. *Chem. Sci.* **2013**, *4* (3), 916–920. https://doi.org/10.1039/C2SC20903A.
(26) Barnett, K. L.; Howard, J. R.; Treager, C. J.; Shipley, A. T.; Stullich, R. M.; Qu, F.; Gerlach, D. L.; Shaughnessy, K. H. Air-Stable [(R3P)PdCl2]2 Complexes of Neopentylphosphines as Cross-Coupling Precatalysts: Catalytic Application and Mechanism of Catalyst Activation and Deactivation. *Organometallics* **2018**, *37* (9), 1410–1424. https://doi.org/10.1021/acs.organomet.8b00082.
(27) Nasielski, J.; Hadei, N.; Achonduh, G.; Kantchev, E. A. B.; O'Brien, C. J.; Lough, A.; Organ, M. G. Structure–Activity Relationship Analysis of Pd–PEPPSI Complexes in Cross-Couplings: A Close Inspection of the Catalytic Cycle and the Precatalyst Activation Model. *Chem. – Eur. J.* **2010**, *16* (35), 10844–10853. https://doi.org/10.1002/chem.201000138.

(28) Durà-Vilà, V.; P. Mingos, D. M.; Vilar, R.; White, A. J. P.; Williams, D. J. Reactivity Studies of [Pd2(μ-X)2(PBut3)2] (X = Br, I) with CNR (R = 2,6-Dimethylphenyl), H2 and Alkynes. *J. Organomet. Chem.* **2000**, *600* (1), 198–205. https://doi.org/10.1016/S0022-328X(00)00187-X.
(29) Carole, W.; Colacot, T.; Seechurn, C.; Scrase, T. WO2018073559, April 26, 2018. https://patentscope.wipo.int/search/en/detail.jsf?docId=WO2018073559 (accessed 2024-08-27).
(30) Aufiero, M.; Scattolin, T.; Proutière, F.; Schoenebeck, F. Air-Stable Dinuclear Iodine-Bridged Pd(I) Complex - Catalyst, Precursor, or Parasite? The Additive Decides. Systematic Nucleophile-Activity Study and Application as Precatalyst in Cross-Coupling. *Organometallics* **2015**, *34* (20), 5191–5195. https://doi.org/10.1021/acs.organomet.5b00766.
(31) Schmid, T. E.; Jones, D. C.; Songis, O.; Diebolt, O.; Furst, M. R. L.; Slawin, A. M. Z.; Cazin, C. S. J. Mixed Phosphine/N-Heterocyclic Carbene Palladium Complexes: Synthesis, Characterization and Catalytic Use in Aqueous Suzuki–Miyaura Reactions. *Dalton Trans.* **2013**, *42* (20), 7345–7353. https://doi.org/10.1039/C2DT32858E.
(32) Shaughnessy, K. H. Development of Palladium Precatalysts That Efficiently Generate LPd(0) Active Species. *Isr. J. Chem.* **2020**, *60* (3–4), 180–194. https://doi.org/10.1002/ijch.201900067.
(33) Andreu, M. G.; Zapf, A.; Beller, M. Molecularly Defined Palladium(0) Monophosphine Complexes as Catalysts for Efficient Cross-Coupling of Aryl Chlorides and Phenylboronic Acid1. *Chem. Commun.* **2000**, No. 24, 2475–2476. https://doi.org/10.1039/B006791L.
(34) Tschan, M. J.-L.; García-Suárez, E. J.; Freixa, Z.; Launay, H.; Hagen, H.; Benet-Buchholz, J.; van Leeuwen, P. W. N. M. Efficient Bulky Phosphines for the Selective Telomerization of 1,3-Butadiene with Methanol. *J. Am. Chem. Soc.* **2010**, *132* (18), 6463–6473. https://doi.org/10.1021/ja100521m.
(35) Lee, H. G.; Milner, P. J.; Buchwald, S. L. An Improved Catalyst System for the Pd-Catalyzed Fluorination of (Hetero)Aryl Triflates. *Org. Lett.* **2013**, *15* (21), 5602–5605. https://doi.org/10.1021/ol402859k.
(36) Lee, H. G.; Milner, P. J.; Colvin, M. T.; Andreas, L.; Buchwald, S. L. Structure and Reactivity of [(L·Pd)*n*·(1,5-Cyclooctadiene)] (*n* = 1–2) Complexes Bearing Biaryl Phosphine Ligands. *Inorganica Chim. Acta* **2014**, *422*, 188–192. https://doi.org/10.1016/j.ica.2014.06.008.
(37) Huang, J.; Isaac, M.; Watt, R.; Becica, J.; Dennis, E.; Saidaminov, M. I.; Sabbers, W. A.; Leitch, D. C. DMPDAB–Pd–MAH: A Versatile Pd(0) Source for Precatalyst Formation, Reaction Screening, and Preparative-Scale Synthesis. *ACS Catal.* **2021**, *11* (9), 5636–5646. https://doi.org/10.1021/acscatal.1c00288.
(38) Bigler, R.; Spiess, D.; Wellauer, J.; Binder, M.; Carré, V.; Fantasia, S. Synthesis of Biaryl Phosphine Palladium(0) Precatalysts. *Organometallics* **2021**, *40* (15), 2384–2388. https://doi.org/10.1021/acs.organomet.1c00288.
(39) Huang, J.; Ho, D. B.; Gaube, G.; Celuszak, H.; Becica, J.; Thomas, G. T.; Schley, N. D.; Leitch, D. C. A Thermally Stable, Alkene-Free Palladium Source for Oxidative Addition Complex Formation and High-Turnover Catalysis. *Organometallics* **2024**, *43* (20), 2403–2412. https://doi.org/10.1021/acs.organomet.4c00125.
(40) Uehling, M. R.; King, R. P.; Krska, S. W.; Cernak, T.; Buchwald, S. L. Pharmaceutical Diversification via Palladium Oxidative Addition Complexes. *Science* **2019**, *363* (6425), 405–408. https://doi.org/10.1126/science.aac6153.
(41) Thomas, G. T.; Donnecke, S.; Chagunda, I. C.; McIndoe, J. S. Pressurized Sample Infusion. *Chemistry–Methods* **2022**, *2* (1), e202100068. https://doi.org/10.1002/cmtd.202100068.
(42) McMullin, C. L.; Fey, N.; Harvey, J. N. Computed Ligand Effects on the Oxidative Addition of Phenyl Halides to Phosphine Supported Palladium(0) Catalysts. *Dalton Trans.* **2014**, *43* (36), 13545–13556. https://doi.org/10.1039/C4DT01758G.

(43) Vidossich, P.; Ujaque, G.; Lledós, A. Palladium Monophosphine Pd(PPh_3): Is It Really Accessible in Solution? *Chem. Commun.* **2013**, *50* (6), 661–663. https://doi.org/10.1039/C3CC47404F.
(44) Ahlquist, M.; Fristrup, P.; Tanner, D.; Norrby, P.-O. Theoretical Evidence for Low-Ligated Palladium(0): [Pd–L] as the Active Species in Oxidative Addition Reactions. *Organometallics* **2006**, *25* (8), 2066–2073. https://doi.org/10.1021/om060126q.
(45) Li, Z.; Fu, Y.; Guo, Q.-X.; Liu, L. Theoretical Study on Monoligated Pd-Catalyzed Cross-Coupling Reactions of Aryl Chlorides and Bromides. *Organometallics* **2008**, *27* (16), 4043–4049. https://doi.org/10.1021/om701065f.
(46) Zheng, Q.; Liu, Y.; Chen, Q.; Hu, M.; Helmy, R.; Sherer, E. C.; Welch, C. J.; Chen, H. Capture of Reactive Monophosphine-Ligated Palladium(0) Intermediates by Mass Spectrometry. *J. Am. Chem. Soc.* **2015**, *137* (44), 14035–14038. https://doi.org/10.1021/jacs.5b08905.
(47) Chagunda, I. C.; Williams, P. J. H.; Fisher, T.; Stock, N. L.; Beach, D. G.; Thomas, G. T.; Zhu, J.; McIndoe, J. S. Comparative Assessment of ESI-MS Softness for Inorganic Complexes: How Soft Is Your ESI-MS? *Eur. J. Inorg. Chem.* **2024**, No. 27, e202400077. https://doi.org/10.1002/ejic.202400077.
(48) Schröder, D. Applications of Electrospray Ionization Mass Spectrometry in Mechanistic Studies and Catalysis Research. *Acc. Chem. Res.* **2012**, *45* (9), 1521–1532. https://doi.org/10.1021/ar3000426.
(49) McDonald, L. W. I.; Campbell, J. A.; Clark, S. B. Failure of ESI Spectra to Represent Metal-Complex Solution Composition: A Study of Lanthanide–Carboxylate Complexes. *Anal. Chem.* **2014**, *86* (2), 1023–1029. https://doi.org/10.1021/ac401751r.
(50) Williams, P. J. H.; Chagunda, I. C.; McIndoe, J. S. OptiMS: An Accessible Program for Automating Mass Spectrometry Parameter Optimization and Configuration. *J. Am. Soc. Mass Spectrom.* **2024**, *35* (3), 449–455. https://doi.org/10.1021/jasms.3c00354.
(51) Thomas, G. T.; Janusson, E.; Zijlstra, H. S.; McIndoe, J. S. Step-by-Step Real Time Monitoring of a Catalytic Amination Reaction. *Chem. Commun.* **2019**, *55* (78), 11727–11730. https://doi.org/10.1039/C9CC05076K.
(52) Yunker, L. P. E.; Ahmadi, Z.; Logan, J. R.; Wu, W.; Li, T.; Martindale, A.; Oliver, A. G.; McIndoe, J. S. Real-Time Mass Spectrometric Investigations into the Mechanism of the Suzuki–Miyaura Reaction. *Organometallics* **2018**, *37* (22), 4297–4308. https://doi.org/10.1021/acs.organomet.8b00705.
(53) Tereniak, S. J.; Landis, C. R.; Stahl, S. S. Are Phosphines Viable Ligands for Pd-Catalyzed Aerobic Oxidation Reactions? Contrasting Insights from a Survey of Six Reactions. *ACS Catal.* **2018**, *8* (4), 3708–3714. https://doi.org/10.1021/acscatal.8b01009.
(54) Barder, T. E.; Buchwald, S. L. Insights into Amine Binding to Biaryl Phosphine Palladium Oxidative Addition Complexes and Reductive Elimination from Biaryl Phosphine Arylpalladium Amido Complexes via Density Functional Theory. *J. Am. Chem. Soc.* **2007**, *129* (39), 12003–12010. https://doi.org/10.1021/ja073747z.
(55) Arrechea, P. L.; Buchwald, S. L. Biaryl Phosphine Based Pd(II) Amido Complexes: The Effect of Ligand Structure on Reductive Elimination. *J. Am. Chem. Soc.* **2016**, *138* (38), 12486–12493. https://doi.org/10.1021/jacs.6b05990.
(56) Newman-Stonebraker, S. H.; Wang, J. Y.; Jeffrey, P. D.; Doyle, A. G. Structure–Reactivity Relationships of Buchwald-Type Phosphines in Nickel-Catalyzed Cross-Couplings. *J. Am. Chem. Soc.* **2022**, *144* (42), 19635–19648. https://doi.org/10.1021/jacs.2c09840.
(57) Milstein, D.; Stille, J. K. Mechanism of Reductive Elimination. Reaction of Alkylpalladium(II) Complexes with Tetraorganotin, Organolithium, and Grignard Reagents. Evidence for Palladium(IV) Intermediacy. *J. Am. Chem. Soc.* **1979**, *101* (17), 4981–4991. https://doi.org/10.1021/ja00511a031.

(58) Gillie, A.; Stille, J. K. Mechanisms of 1,1-Reductive Elimination from Palladium. *J. Am. Chem. Soc.* **1980**, *102* (15), 4933–4941. https://doi.org/10.1021/ja00535a018.
(59) Tatsumi, K.; Hoffmann, R.; Yamamoto, A.; Stille, J. K. Reductive Elimination of D8-Organotransition Metal Complexes. *Bull. Chem. Soc. Jpn.* **1981**, *54* (6), 1857–1867. https://doi.org/10.1246/bcsj.54.1857.
(60) Komiya, S.; Albright, T. A.; Hoffmann, R.; Kochi, J. K. Reductive Elimination and Isomerization of Organogold Complexes. Theoretical Studies of Trialkylgold Species as Reactive Intermediates. *J. Am. Chem. Soc.* **1976**, *98* (23), 7255–7265. https://doi.org/10.1021/ja00439a024.
(61) Pérez-Rodríguez, M.; Braga, A. A. C.; de Lera, A. R.; Maseras, F.; Álvarez, R.; Espinet, P. A DFT Study of the Effect of the Ligands in the Reductive Elimination from Palladium Bis(Allyl) Complexes. *Organometallics* **2010**, *29* (21), 4983–4991. https://doi.org/10.1021/om1001974.
(62) Christmann, U.; Vilar, R. Monoligated Palladium Species as Catalysts in Cross-Coupling Reactions. *Angew. Chem. Int. Ed.* **2005**, *44* (3), 366–374. https://doi.org/10.1002/anie.200461189.
(63) Schoenebeck, F.; Houk, K. N. Ligand-Controlled Regioselectivity in Palladium-Catalyzed Cross Coupling Reactions. *J. Am. Chem. Soc.* **2010**, *132* (8), 2496–2497. https://doi.org/10.1021/ja9077528.
(64) Barder, T. E.; Biscoe, M. R.; Buchwald, S. L. Structural Insights into Active Catalyst Structures and Oxidative Addition to (Biaryl)phosphine−Palladium Complexes via Density Functional Theory and Experimental Studies. *Organometallics* **2007**, *26* (9), 2183–2192. https://doi.org/10.1021/om0701017.
(65) Martin, R.; Buchwald, S. L. Palladium-Catalyzed Suzuki−Miyaura Cross-Coupling Reactions Employing Dialkylbiaryl Phosphine Ligands. *Acc. Chem. Res.* **2008**, *41* (11), 1461–1473. https://doi.org/10.1021/ar800036s.
(66) Yadav, M. R.; Nagaoka, M.; Kashihara, M.; Zhong, R.-L.; Miyazaki, T.; Sakaki, S.; Nakao, Y. The Suzuki–Miyaura Coupling of Nitroarenes. *J. Am. Chem. Soc.* **2017**, *139* (28), 9423–9426. https://doi.org/10.1021/jacs.7b03159.
(67) Janusson, E.; Zijlstra, H. S.; Nguyen, P. P. T.; MacGillivray, L.; Martelino, J.; McIndoe, J. S. Real-Time Analysis of Pd2(Dba)3 Activation by Phosphine Ligands. *Chem. Commun.* **2017**, *53* (5), 854–856. https://doi.org/10.1039/C6CC08824D.
(68) Chagunda, I. C.; Fisher, T.; Schierling, M.; McIndoe, J. S. Poisonous Truth about the Mercury Drop Test: The Effect of Elemental Mercury on Pd(0) and Pd(II)ArX Intermediates. *Organometallics* **2023**, *42* (19), 2938–2945. https://doi.org/10.1021/acs.organomet.3c00340.
(69) Henderson, W.; Evans, C. Electrospray Mass Spectrometric Analysis of Transition-Metal Halide Complexes. *Inorganica Chim. Acta* **1999**, *294* (2), 183–192. https://doi.org/10.1016/S0020-1693(99)00212-1.
(70) Santos, L. S.; Rosso, G. B.; Pilli, R. A.; Eberlin, M. N. The Mechanism of the Stille Reaction Investigated by Electrospray Ionization Mass Spectrometry. *J. Org. Chem.* **2007**, *72* (15), 5809–5812. https://doi.org/10.1021/jo062512n.
(71) Brazier, J. B.; Newton, M. A.; Barreiro, E. M.; Adrio, L. A.; Naya, L.; Hii, K. K. (Mimi). Solvent-Dependent Nuclearity, Geometry and Catalytic Activity of [(SPhos)Pd(Ph)Cl]2. *Dalton Trans.* **2017**, *46* (22), 7223–7231. https://doi.org/10.1039/C7DT01019B.
(72) Agrawal, D.; Zins, E.-L.; Schröder, D. Intramolecular Scrambling of Aryl Groups in Organopalladium Complexes [ArPd(PPh3)2]+: From Solution to the Gas Phase, Back Again, and In-Between. *Chem. - Asian J.* **2010**, *5* (7), 1667–1676. https://doi.org/10.1002/asia.201000086.
(73) Morita, D. K.; Stille, J. K.; Norton, J. R. Methyl/Phenyl Exchange between Palladium and a Phosphine Ligand. Consequences for Catalytic Coupling Reactions. *J. Am. Chem. Soc.* **1995**, *117* (33), 8576–8581. https://doi.org/10.1021/ja00138a012.

(74) Fiebig, L.; Schlörer, N.; Schmalz, H.-G.; Schäfer, M. Aryl–Phenyl Scrambling in Intermediate Organopalladium Complexes: A Gas-Phase Study of the Mizoroki–Heck Reaction. *Chem. – Eur. J.* **2014**, *20* (17), 4906–4910. https://doi.org/10.1002/chem.201400115.
(75) Lee, Y. H.; Morandi, B. Transition Metal-Mediated Metathesis between P–C and M–C Bonds: Beyond a Side Reaction. *Coord. Chem. Rev.* **2019**, *386*, 96–118. https://doi.org/10.1016/j.ccr.2018.12.001.
(76) McFarlane, J.; Henderson, B.; Donnecke, S.; McIndoe, J. S. An Information-Rich Graphical Representation of Catalytic Cycles. *Organometallics* **2019**, *38* (21), 4051–4053. https://doi.org/10.1021/acs.organomet.9b00563.
(77) Borys, A. M. An Illustrated Guide to Schlenk Line Techniques. *Organometallics* **2023**, *42* (3), 182–196. https://doi.org/10.1021/acs.organomet.2c00535.
(78) Yunker, L. P. E.; Donnecke, S.; Ting, M.; Yeung, D.; McIndoe, J. S. PythoMS: A Python Framework To Simplify and Assist in the Processing and Interpretation of Mass Spectrometric Data. *J. Chem. Inf. Model.* **2019**, *59* (4), 1295–1300. https://doi.org/10.1021/acs.jcim.9b00055.
(79) Łącki, M. K.; Startek, M.; Valkenborg, D.; Gambin, A. IsoSpec: Hyperfast Fine Structure Calculator. *Anal. Chem.* **2017**, *89* (6), 3272–3277. https://doi.org/10.1021/acs.analchem.6b01459.

Chapter 6 – Conclusions and Outlook

6.1 Summary of Key Findings

This dissertation set out to investigate two fundamental questions: the limitations of ESI-MS in studying complex chemical systems, and how PSI-ESI-MS can be used to uncover key reaction intermediates and pathways involved in the *in situ* mechanisms of Pd precatalysts. An investigation of the limitations of ESI-MS was first necessary to establish its role in this research, particularly in probing palladium-catalyzed cross-coupling reactions. This enabled investigations into the interaction of palladium precatalysts with reaction conditions and substrates, advancing both the analytical methodologies and mechanistic understanding.

Chapter 2 highlighted the challenges of using MS to characterize complex systems such as high molecular weight polymers, particularly due to isotopic contributions and signal broadening, which accumulate into pronounced signal-to-noise issues. Effective sample preparation was discussed as a factor in improving analytical outcomes, as well as the need for methodological refinement and optimizing instrument conditions to enhance data quality.

Chapter 3 investigated the performance of ESI-MS across multiple instruments, focusing on their capability to preserve and detect weak interactions in inorganic and organometallic complexes. This study revealed significant variability in instrument performance, even among systems from the same manufacturer. To address these inconsistence, simple tests were developed and proposed to help researchers assess instrument softness and optimize conditions for specific analytes. These findings reinforce the necessity of methodical instrument assessment and optimization.

Chapter 4 explored the mechanisms of catalyst activation, focussing on $Pd_2(dba)_3$ as a classic Pd(0) source. A critical evaluation of the mercury drop test demonstrated its limitations, challenging the assumption that elemental mercury is unreactive towards ligated molecular palladium species. This work crucially highlights that Pd(0) and Pd(II)

intermediates interact with mercury in ways that may lead to misinterpretations about catalytic activity. This chapter contributes to a more nuanced understanding of how to evaluate catalytic activity and the necessity of using multiple analytical approaches to gain a more comprehensive understanding of reaction mechanisms and catalyst reactivity.

Building on these methodologies, Chapter 5 examined the activation and oxidative addition processes of a next-generation palladium precatalyst, (^{DMP}DAB)Pd(CH_2SiMe_3)$_2$. Through PSI-ESI-MS investigations with charge-tagged and neutral phosphine ligands, this chapter revealed *in situ* activation pathways and the formation of key intermediates. Additionally, the study identified off-cycle species, particularly the role of ^{DMP}DAB as a competitive inhibitor of the active LPd(0) species. This approach can prove insightful in investigating potential catalyst inhibition mechanisms caused by "throw-away" ligands, which are typically assumed to be innocent spectators.

6.2 Opportunities for Further Research

Building on the findings presented in Chapters 2–5, several avenues for future research emerge that could yield insights into palladium-catalyzed cross-coupling reactions, and reaction monitoring by ESI-SMS. These are presented in the following sections.

6.2.1 Instrument Optimization and Methodology Development

Further research can enhance our understanding of ESI-MS and its implications for detecting fragile inorganic complexes. One promising avenue involves establishing a comprehensive benchmarking study of various ESI-MS instruments using the assessment tests presented in Chapter 3. An evaluation of a broader range of instruments under controlled conditions could generate a robust dataset detailing instrument performance. This analysis would help identify specific design features or configurations that contribute most significantly to optimal performance, facilitating better instrument selection tailored to organometallic research applications.

Additionally, further exploration of auxiliary fields and their impact on ion behavior during fragmentation could yield significant insights. The work in Chapter 3 demonstrated one such example of how varying the source temperature can influence signal stability and the effective transition of ions into the gas phase. Expanding this research to investigate the effects of other instrument parameters on ion preservation would refine strategies aimed at minimizing undesired fragmentation. This effort could help develop standardized methodologies for optimizing ESI-MS conditions across diverse applications within organometallic and inorganic chemistry, ultimately expanding the limits of mass spectrometric analysis for fragile complexes.

Recent work in the McIndoe group developed an open-source program for semi-automated optimization of instrument parameters[1] in tandem with the instrument assessment studies of Chapter 3. Expanding this OptiMS system to incorporate set benchmarks or targets for optimal instrument conditions based on the proposed softness tests, could further improve its utility. Such developments would provide researchers with accessible tools for fine-tuning their instruments, ensuring more consistent and reliable results in complex synthetic environments.

6.2.2 Reaction Monitoring and Mechanistic Studies

6.2.2.1 Formation and Stability of Polynuclear Palladium Species

One key area for continued research could therefore focus on monitoring the formation of polynuclear palladium species. These species are commonly observed as precursors to the generation of Pd black, a major deactivation pathway in catalysis.[2] Fairlamb and coworkers explored the formation of various polynuclear palladium complexes by varying the palladium to ligand ($Pd(OAc)_2$: PPh_3) ratio in their studies. Their findings indicated that a Pd/PPh_3 ratio of 1:2 resulted in the formation of the dinuclear complex $[Pd_2(\mu\text{-}PPh_2)(\mu_2\text{-}OAc)(PPh_3)_2]$, while higher ratios of 1:3 led to the generation of more complex Pd_3 clusters.[3] They further proposed that ligated Pd_n clusters act as intermediates, bridging monoligated Pd species and Pd nanoparticles (PdNPs), rather than merely serving as precursors to catalyst deactivation.[4] Understanding and harnessing the reactivity of these clusters could

therefore present an opportunity for innovative catalyst design. The unique framework of these clusters could provide alternatives to conventional $L_nPd(0)$ complexes or small PdNPs, with potential benefits in efficiency, atom economy, selectivity, and catalytic reactivity.

The effects of solvents on the stability of active Pd species and clusters remain an active area for exploration with significant implications for catalysis. Solvent choice influences the stability of ionic species and can, in some cases, accelerate palladium decomposition.[5] The careful selection of solvents in ESI-MS is additionally important for optimizing ion detection and achieving accurate representations of analyte concentrations.[6] By varying solvent polarity and coordinating ability, it may be possible to identify conditions that stabilize Pd_n clusters and enhance catalytic efficiency. Real-time MS could provide deeper insights into how solvent properties influence catalytic activity, species stability, and the formation of polynuclear structures. Gaining control over the dynamics of Pd_n cluster formation and propagation may further unlock new catalytic activity and expand accessible chemical space.

6.2.2.2 Investigating Structure-Activity Relationships of ^{R}DAB Ligands

Building on the findings of Chapter 5, further research could explore the inhibitory effects of *N,N*'-diaryl diazabutadiene (^{R}DAB) ligands on the activation process. Understanding the competitive inhibition by ^{R}DAB ligands could prove important for achieving maximum catalytic rates, as non-innocent ligands can impede catalytic turnover rather than act as benign 'throw-away' ligands. Recent work by Leitch and coworkers examined isopropyl- and methyl-substituted ^{R}DAB ligands used for stabilizing Ni(0) catalyst precursor for *in situ* catalyst formation.[7] Notably, the more sterically hindered diisopropyl-substituted ^{DIPP}DAB precatalyst outperformed dimethyl-substituted ^{DMP}DAB precatalyst in Suzuki-Miyaura and C–N coupling reactions. The improved reactivity likely stems from steric shielding by the isopropyl groups, which stabilizes reactive intermediates while promoting substrate binding. This steric stabilization effect has been well studied and rationalized for various ligand classes.[8–12] Additionally, the increased bulk of ^{DIPP}DAB may disfavours ^{R}DAB re-coordinating to the LPd(0) species, thereby reducing inhibitory effects.

An evaluation of ^{R}DAB ligands with varying steric properties could help clarify their influence on catalyst inhibition, providing insight into structure-activity relationships that govern their reactivity. This proposal draws inspiration from work by Doyle and coworkers, who used a data-driven approach to analyze the structure-activity relationships of dialkylbiaryl phosphine ligands in nickel and palladium complexes.[13] Their study revealed that the minimum percent buried volume (%V_{burr} (*min*))—a conformationally representative descriptor of ligand size—enabled the discovery of a reactivity threshold for the formation of active monoligated vs inactive bisligated catalytic species. A similar strategy, as illustrated in Figure 6.1, could be applied to uncover ^{R}DAB ligand structure properties that influence catalyst inhibition. MS/MS trapping and fragmentation experiments would be particularly effective in assessing relative ligand binding strengths and correlating them with observed reactivity. These experiments could further be supported by density functional theory (DFT) calculations, which would provide theoretical low-energy structures and transition states for comparison with experimental data.

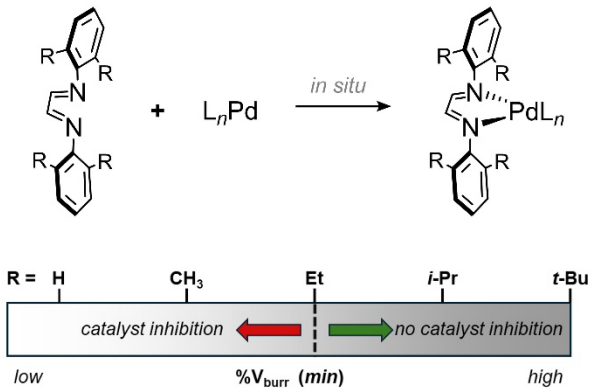

Figure 6.1: Conceptual representation of study of the structure-activity relationships of ^{R}DAB ligands on LPd(0) catalyst inhibition. A survey of ^{R}DAB ligands with R substituents across a spectrum of steric bulk (%V_{burr} (*min*)) may reveal a structural threshold for mitigating catalyst inhibition.

Expanding these studies would require the developing of synthetic routes for isolating and purifying an expanded class of dialkyl-Pd precatalysts, presenting an opportunity for further collaborative research with synthetic expertise from the Leitch group. Furthermore, these synthetic endeavours could include isolating oxidative addition

complexes for mechanistic investigations. Such efforts would build on the findings of this work and open new avenues for optimizing catalyst design and performance.

6.2.2.3 Ligand Effects on Catalyst Activation

Further exploration on the (DAB)Pd(CH_2SiMe_3)$_3$ precatalyst could additionally focus on investigating bulkier phosphine ligands beyond those studied in Chapter 5. Examining the steric effects of these ligands on activation pathways can clarify the generality of the mechanisms observed with smaller ligands. This research could also be expanded to include *N*-heterocyclic carbene (NHC) ligands, giving indication of their interactions compared to traditional phosphines. NHCs offer a variety of steric profiles and different bonding character compared to phosphines, which could significantly influence the activation and reactivity properties of the precatalyst. For instance, the stronger σ-donating ability of NHCs may stabilize Pd intermediates differently, potentially altering the rate and pathway of activation.[14] Additionally, the tunable steric bulk of NHCs could provide insights into how ligand size and shape impact the formation and stability of key intermediates. The charge-tagged NHC ligand ESIMes,[15] recently developed in the McIndoe group, could enable detailed real-time MS reaction monitoring.

Moreover, exploring charge-tagged ligands, such as sulfonated dialkylbiaryl phosphines, could be particularly advantageous for assessing catalytic activity under aqueous conditions, aligning with green chemistry principles aimed at minimizing the use of harmful organic solvents.[16] The Buchwald group has demonstrated scalable methods for synthesizing sulfonated ligands,[17] some of which are commercially available. These ligands could facilitate probing catalytic activity under aqueous or biphasic conditions.

6.2.2.4 Simultaneous Orthogonal Reaction Monitoring in Biphasic Systems

The use of biphasic conditions in cross-coupling reactions presents the possibility of recyclability, where the aqueous phase containing the catalyst can be by reused after product extraction from the organic phase.[18,19] Monitoring biphasic reactions, however, presents unique challenges, particularly in ESI-MS where different solvents require distinct instrument parameters for optimal desolvation.[20] Despite these challenges, the high sensitivity of MS makes it well suited for detecting ligated catalyst intermediates at low

concentration in the aqueous phase, while bulk reactants and product in the organic phase can be monitored using orthogonal techniques such as flow Fourier-transform infrared (FTIR) or UV-Vis spectroscopy (Figure 6.2). Work in the McIndoe group has demonstrated the utility of simultaneous orthogonal monitoring, enabling a more comprehensive analysis of reaction components.[21,22] Extending PSI-ESI-MS to accommodate biphasic systems would broaden its applicability in reaction monitoring, and could prove advantageous to understanding catalytic dynamics and phase behaviors.

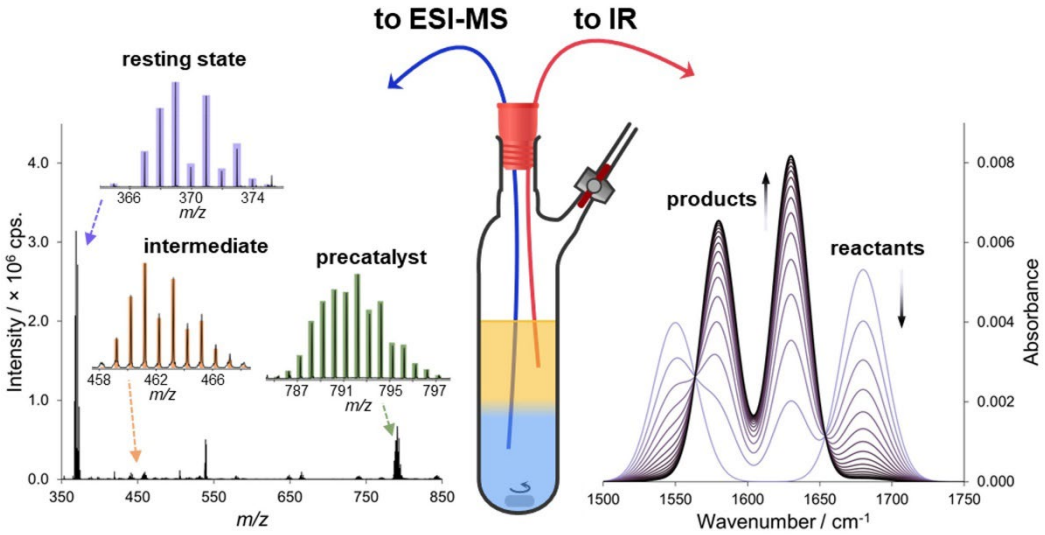

Figure 6.2: Conceptual representation of simultaneous reaction monitoring, where sampling of the aqueous phase directs to the ESI-MS, while tubing circulates the organic phase through a flow FTIR spectrometer.

Investigating the reactivity and efficiency of palladium catalysts in alternative solvent systems could contribute to the development of more sustainable catalytic processes and broaden the application scope of palladium catalysis in organic synthesis. Importantly, these proposed methodologies and approaches would be equally applicable to other precatalyst systems. As discussed in Chapter 1, the rapidly expanding field of tailored precatalysts would greatly benefit from such investigations, further advancing the understanding and optimization of cross-coupling reactions.

6.3 Outlook

The work presented in this dissertation reinforces the role of mass spectrometry in advancing modern synthetic chemistry and encourages researchers to harness its full potential. By enabling the direct observation of catalytic intermediates and speciation under reaction conditions, PSI-ESI-MS provides valuable mechanistic insights that can drive the optimization of cross-coupling reactions. Real-world catalytic system, involving diverse metal sources, supporting ligands, additives, and structurally diverse reaction substrates, are undoubtably very complex. However, with the aid of modern on-line analysis techniques, researchers can elucidate these dynamic systems and develop models that will bridge the gaps in our understanding.

However, as demonstrated throughout the chapters, limitations remain, particularly in preserving fragile organometallic species and accurate monitoring of increasingly complex systems. Addressing these challenges requires continued advancements in sample handling techniques, instrument design and optimization, and ionization strategies to improve the robustness and reliability of mass spectrometric analysis for dynamic catalytic systems.

Looking ahead, PSI-ESI-MS could play a transformative role in mechanistic studies and reaction optimization when integrated with emerging technologies in automation and robotics. The potential for automated reactors equipped with on-line MS for real-time analysis and feedback control could streamline reaction development, accelerating the discovery of more efficient and sustainable catalytic systems. As the field of cross-coupling chemistry continues to evolve, incorporating green chemistry principles—such as earth-abundant metal catalysts, solvent-free or aqueous-phase reactions, and using less toxic atom-economic processes—will also be key to maintaining its relevance and impact in both academic and industrial settings.

6.4 References

(1) Williams, P. J. H.; Chagunda, I. C.; McIndoe, J. S. OptiMS: An Accessible Program for Automating Mass Spectrometry Parameter Optimization and Configuration. *J. Am. Soc. Mass Spectrom.* **2024**, *35* (3), 449–455. https://doi.org/10.1021/jasms.3c00354.

(2) Böck, K.; Feil, J. E.; Karaghiosoff, K.; Koszinowski, K. Catalyst Activation, Deactivation, and Degradation in Palladium-Mediated Negishi Cross-Coupling Reactions. *Chem. – Eur. J.* **2015**, *21* (14), 5548–5560. https://doi.org/10.1002/chem.201406408.

(3) Scott, N. W. J.; Ford, M. J.; Schotes, C.; Parker, R. R.; Whitwood, A. C.; Fairlamb, I. J. S. The Ubiquitous Cross-Coupling Catalyst System 'Pd(OAc)2'/2PPh3 Forms a Unique Dinuclear PdI Complex: An Important Entry Point into Catalytically Competent Cyclic Pd3 Clusters. *Chem. Sci.* **2019**, *10* (34), 7898–7906. https://doi.org/10.1039/C9SC01847F.

(4) Jeddi, N.; Scott, N. W. J.; Fairlamb, I. J. S. Well-Defined Pdn Clusters for Cross-Coupling and Hydrogenation Catalysis: New Opportunities for Catalyst Design. *ACS Catal.* **2022**, 11615–11638. https://doi.org/10.1021/acscatal.2c03345.

(5) Sherwood, J.; Clark, J. H.; Fairlamb, I. J. S.; Slattery, J. M. Solvent Effects in Palladium Catalysed Cross-Coupling Reactions. *Green Chem.* **2019**, *21* (9), 2164–2213. https://doi.org/10.1039/C9GC00617F.

(6) Omari, I.; Randhawa, P.; Randhawa, J.; Yu, J.; McIndoe, J. S. Structure, Anion, and Solvent Effects on Cation Response in ESI-MS. *J. Am. Soc. Mass Spectrom.* **2019**, *30* (9), 1750–1757. https://doi.org/10.1007/s13361-019-02252-0.

(7) Thomas, G. T.; Cruise, O. D.; Peel-Smith, D.; Fernández, N. P.; Killeen, C.; Leitch, D. C. Easily Accessible and Solution-Stable Ni(0) Precatalysts for High-Throughput Experimentation. *Chem. – Eur. J. n/a* (n/a), e202403960. https://doi.org/10.1002/chem.202403960.

(8) Clavier, H.; Nolan, S. P. Percent Buried Volume for Phosphine and N-Heterocyclic Carbene Ligands: Steric Properties in Organometallic Chemistry. *Chem. Commun.* **2010**, *46* (6), 841–861. https://doi.org/10.1039/B922984A.

(9) Fleckenstein, C. A.; Plenio, H. Sterically Demanding Trialkylphosphines for Palladium-Catalyzed Cross Coupling Reactions—Alternatives to PtBu3. *Chem. Soc. Rev.* **2010**, *39* (2), 694–711. https://doi.org/10.1039/B903646F.

(10) Hamann, B. C.; Hartwig, J. F. Sterically Hindered Chelating Alkyl Phosphines Provide Large Rate Accelerations in Palladium-Catalyzed Amination of Aryl Iodides, Bromides, and Chlorides, and the First Amination of Aryl Tosylates. *J. Am. Chem. Soc.* **1998**, *120* (29), 7369–7370. https://doi.org/10.1021/ja981318i.

(11) Kendall, A. J.; Zakharov, L. N.; Tyler, D. R. Steric and Electronic Influences of Buchwald-Type Alkyl-JohnPhos Ligands. *Inorg. Chem.* **2016**, *55* (6), 3079–3090. https://doi.org/10.1021/acs.inorgchem.5b02996.

(12) Hansen, T.; Sun, X.; Dalla Tiezza, M.; van Zeist, W.-J.; van Stralen, J. N. P.; Geerke, D. P.; Wolters, L. P.; Poater, J.; Hamlin, T. A.; Bickelhaupt, F. M. C–X Bond Activation by Palladium: Steric Shielding versus Steric Attraction. *Chem. – Eur. J.* **2022**, *28* (44), e202201093. https://doi.org/10.1002/chem.202201093.

(13) Newman-Stonebraker, S. H.; Smith, S. R.; Borowski, J. E.; Peters, E.; Gensch, T.; Johnson, H. C.; Sigman, M. S.; Doyle, A. G. Univariate Classification of Phosphine Ligation State and Reactivity in Cross-Coupling Catalysis. *Science* **2021**, *374* (6565), 301–308. https://doi.org/10.1126/science.abj4213.

(14) Hopkinson, M. N.; Richter, C.; Schedler, M.; Glorius, F. An Overview of N-Heterocyclic Carbenes. *Nature* **2014**, *510* (7506), 485–496. https://doi.org/10.1038/nature13384.

(15) Killeen, C.; Oliver, A. G.; McIndoe, J. S. An Electrospray-Active N-Heterocyclic Carbene Ligand for Real-Time Analysis of Organometallic Reactions. *Dalton Trans.* **2025**, *54* (4), 1365–1369. https://doi.org/10.1039/D4DT03243H.

(16) Sheldon, R. A. The E Factor 25 Years on: The Rise of Green Chemistry and Sustainability. *Green Chem.* **2017**, *19* (1), 18–43. https://doi.org/10.1039/C6GC02157C.
(17) Rodriguez, J.; Dhanjee, H. H.; Buchwald, S. L. Amphiphilic Biaryl Monophosphine Ligands by Regioselective Sulfonation. *Org. Lett.* **2021**, *23* (3), 777–780. https://doi.org/10.1021/acs.orglett.0c04001.
(18) Hanhan, M. E.; Cetinkaya, C.; Shaver, M. P. Effective Binuclear Pd(II) Complexes for Suzuki Reactions in Water. *Appl. Organomet. Chem.* **2013**, *27* (10), 570–577. https://doi.org/10.1002/aoc.3034.
(19) Hanhan, M. E.; Senemoglu, Y. Microwave-Assisted Aqueous Suzuki Coupling Reactions Catalyzed by Ionic Palladium(II) Complexes. *Transit. Met. Chem.* **2012**, *37* (1), 109–116. https://doi.org/10.1007/s11243-011-9564-1.
(20) Killeen, C.; Kropp, A.; Chagunda, I. C.; Jackson, E. C.; Scott McIndoe, J. The Amenability of Different Solvents to Electrospray Ionization Mass Spectrometry. *Int. J. Mass Spectrom.* **2024**, *506*, 117349. https://doi.org/10.1016/j.ijms.2024.117349.
(21) Theron, R.; Wu, Y.; Yunker, L. P. E.; Hesketh, A. V; Pernik, I.; Weller, A. S.; Mcindoe, J. S. Simultaneous Orthogonal Methods for the Real-Time Analysis of Catalytic Reactions. *ACS Catal.* **2016**, *6*, 6911–6917. https://doi.org/10.1021/acscatal.6b01489.
(22) Janusson, E.; Zijlstra, H. S.; Nguyen, P. P. T.; MacGillivray, L.; Martelino, J.; McIndoe, J. S. Real-Time Analysis of Pd2(Dba)3 Activation by Phosphine Ligands. *Chem. Commun.* **2017**, *53* (5), 854–856. https://doi.org/10.1039/C6CC08824D.

Appendices

A – Supporting Information for Chapter 3

Table A.1–6 show the operating parameters for ESI-MS Systems 3-8. The ESI source parameters were chosen through manual user-driven optimization in each lab aimed at maximizing the signal intensity of higher *n* species. The absolute intensities for the 100% relative intensity peaks shown in Figures 3.1-8 are shown in Table A.7.

Table A.1: Sciex QTRAP 5500 parameters. (NRC)

Parameter	Positive Mode	Negative Mode
Flow rate	5 µL min^{-1}	
IonSpray voltage	4.5 kV	
Declustering potential	120 V	
Spray temperature	200 °C	
Curtain gas	10 L min^{-1}	
Ion Source gas 1	5 L min^{-1}	
Ion Source gas 2	2 L min^{-1}	

Table A.2: Thermo Exactive+ Orbitrap parameters.

Parameter	Positive Mode	Negative Mode
Flow rate	0.1 mL min^{-1}	0.10 mL min^{-1}
Spray voltage	3.5 kV	2.5 kV
Capillary temperature	250 °C	250 °C
Probe heater temperature	200 °C	200 °C
S-Lens RF level	50	50
Sheath gas	35	35
Aux gas	20	20

Table A.3: Sciex QTRAP 5500 parameters. (Trent U.)

Parameter	Positive Mode	Negative Mode
Flow rate	7 µL min^{-1}	7 µL min^{-1}
IonSpray voltage	5.5 kV	4.5 kV
Entrance potential	10 V	10 V
Declustering potential	0 V	200 V
Spray temperature	43 °C	43 °C
Curtain gas	20 L min^{-1}	20 L min^{-1}
Ion Source gas 1	20 L min^{-1}	20 L min^{-1}

Table A.4: Thermo QE HF Quad-Orbi parameters.

Parameter	Positive Mode	Negative Mode
Flow rate	3 µL min^{-1}	5 µL min^{-1}
Spray voltage	3.75 kV	3.75 kV
Capillary temperature	200 °C	250 °C
S-lens	70	70
Sheath gas	2	0
Aux gas	2	2
Sweep gas	0	0

Table A.5: Bruker SolariX XR FT-ICR parameters.

Parameter	Positive Mode	Negative Mode
Flow rate	180 µL hr^{-1}	180 µL hr^{-1}
Capillary voltage	5.5 kV	5.5 kV
Desolvation temp.	180 °C	180 °C
Desolvation gas flow	4 L min^{-1}	4 L min^{-1}
Nebulizer gas	1 bar	1 bar
Free ion decay (FID)	0.2621 s	0.2621 s
ICR cell accumulation	0.004 s	0.8 s

Table A.6: Agilent 6545 LC/Q-Tof MS parameters.

Parameter	Positive Mode	Negative Mode
Capillary voltage	4.0 kV	
Nozzle voltage	0 V	
Gas temperature	325 °C	
Drying gas flow	10 L min^{-1}	
Sheath gas temp.	400 °C	
Sheath gas flow	12 L min^{-1}	
Nebulizer gas	20 psi	

Table A.7: Absolute ion intensities for the 100% relative intensity peaks.

ESI-MS Instrument	Ion mode	100% relative intensity peak	Absolute ion intensity / cps.
Waters TQD (non optimized)	+	n = 3	3.2×10^6
	–	n = 2	2.6×10^5
Waters Synapt G2-S*i* (non optimized)	+	n = 3	2.2×10^9
	–	n = 1	1.8×10^9
Waters TQD (optimized)	+	n = 3	5.4×10^7
Waters Synapt G2-S*i* (optimized)	+	n = 2	3.0×10^9
Sciex QTRAP 5500 (NRC)	+	n = 4	1.7×10^7
Sciex QTRAP 5500 (Trent U.)	+	n = 1	3.8×10^8
	–	n = 1	1.5×10^8
Thermo Exactive Plus Orbitrap	+	n = 3	1.6×10^8
	–	n = 2	3.3×10^5
Thermo QE HF Quad-Orbitrap	+	n = 3	1.2×10^9
	–	*m/z* 799	3.4×10^7
Bruker SolariX	+	n = 2	4.6×10^{10}
	–	n = 1	1.1×10^{11}
Agilent 6545	+	n = 2	1.0×10^6

B – Supporting Information for Chapter 4

Caution! Mercury and its compounds are highly toxic and can cause serious health problems if inhaled, absorbed, or ingested. Precautions must be taken when handling mercury, including wearing appropriate personal protective equipment (PPE), and working in a well-ventilated fume hood. Proper disposal of mercury must be followed according to local regulations, to ensure the safety of individuals and the environment.

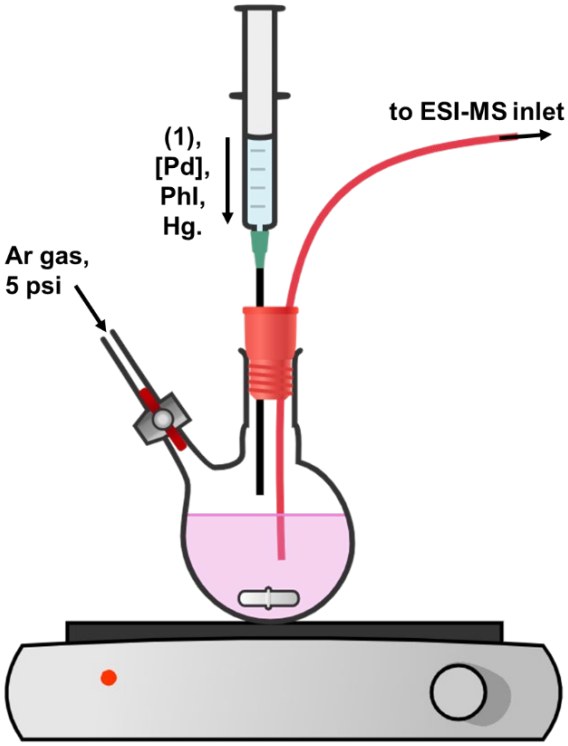

Figure B.1: Experimental set-up for PSI-ESI-MS reaction monitoring.

NMR spectra of charge-tagged reagents

The ^{1}H and ^{31}P NMR spectra are recorded on a Bruker AV III 300 MHz instrument. ^{1}H NMR spectra are reported in δ units, parts per million (ppm), and were measured relative to the signals for residual solvent; CD_3OD(4.87, 3.31 ppm). All $^{31}P\{^{1}H\}$ NMR spectra are reported in ppm referenced to an external 85% aqueous phosphoric acid standard (0.00 ppm).

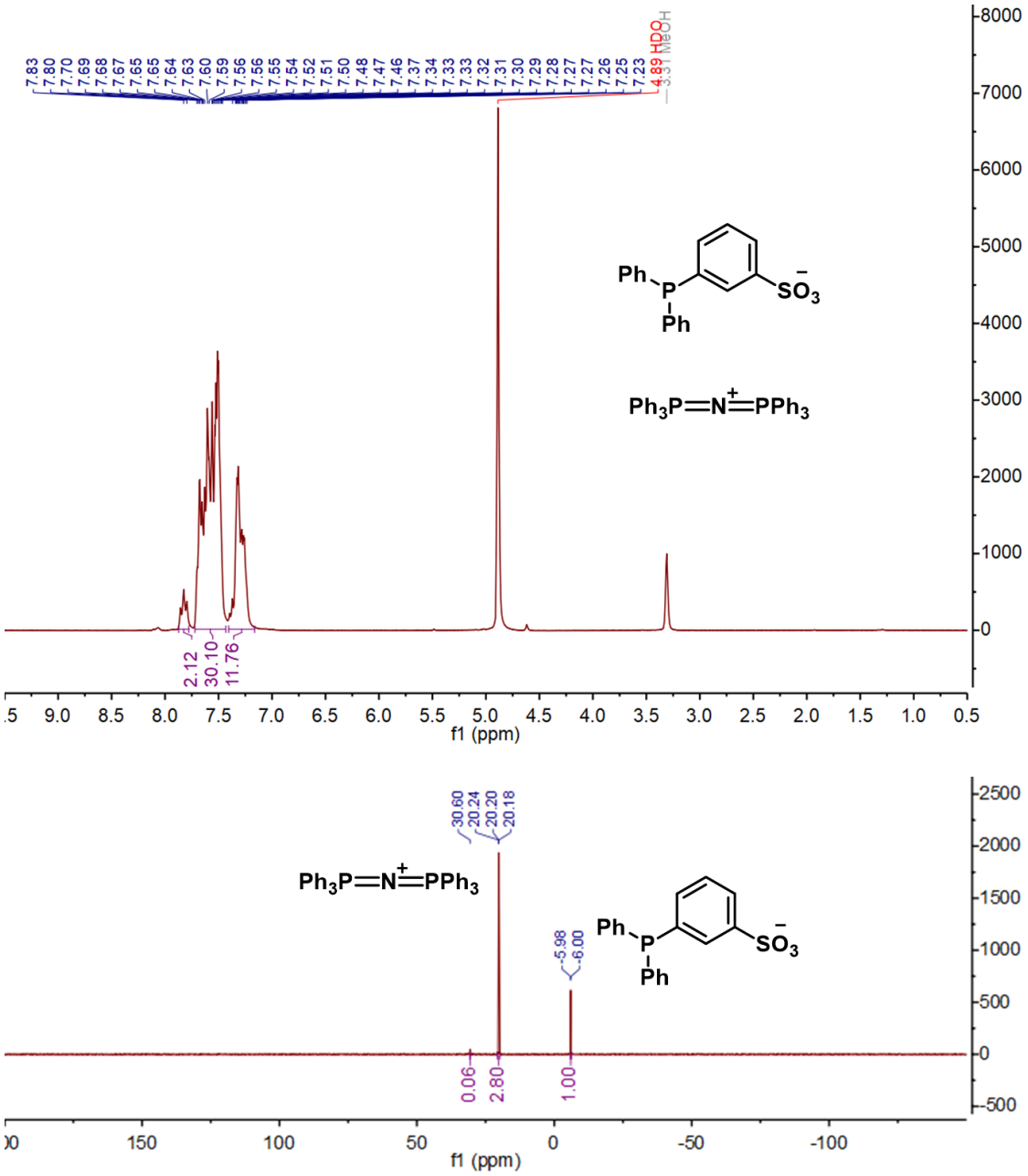

Figure B.2: Top: ^{1}H NMR of $[PPN]^{+}[P(Ph)_2(C_6H_4SO_3)]^{-}$, (300 MHz, MeOD-$d_4$) δ 7.83 (t, J = 9.0 Hz, 2H), 7.72 – 7.43 (m, 30H), 7.41 – 7.16 (m, 12H). **Bottom:** ^{31}P NMR of $[PPN]^{+}[P(Ph)_2(C_6H_4SO_3)]^{-}$, (122 MHz, MeOD-$d_4$) δ 20.20, -5.99 (d, J = 2.1 Hz).

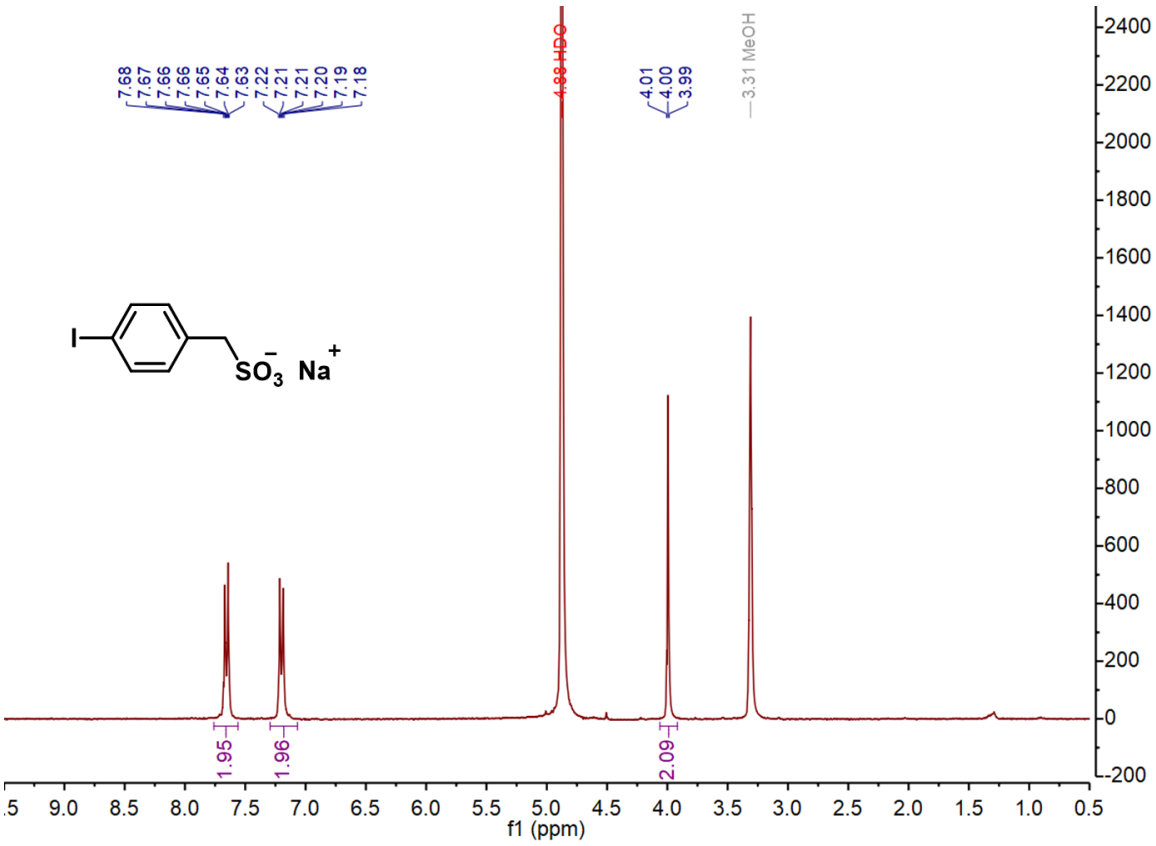

Figure B.3: ^{1}H NMR of $[Na]^{+}[IC_6H_4CH_2SO_3]^{-}$, (300 MHz, MeOD-$d_4$) δ 7.76 – 7.56 (m, 2H), 7.29 – 7.07 (m, 2H), 3.99 (d, J = 2.8 Hz, 2H).

MS/MS Reaction Species Characterization

All MS/MS spectra were collected using PSI-ESI-MS technique with the same tuning parameters as in full scan conditions. In addition, the optimised CID collision energies for each identified species are listed in Table B.1. The product ions detected in each CID experiment along with isotope pattern matching were diagnostic for identifying the catalytically relevant species in each experiment.

Table B.1: CID scan specifications for relevant Hg and Pd reaction intermediates.

Precursor Ion / *m/z*		Product Ion(s) / *m/z*		Collision Energy / V
[**1**]$^-$	341.0	[P(Ph)($C_6H_4SO_3$)]$^-$ [P($C_6H_4SO_3$)(MeOH]$^-$	264.0 218.9	20 25
[Pd(**1**)]$^-$	446.9	[Pd(**1**)+(MeOH)]$^-$ [Pd(P(Ph)($C_6H_4SO_3$))]$^-$ [**1**]$^-$	478.9 369.9 341.1	0 1 1
[Pd(**1**)(dba)]$^-$	681.0	[Pd(**1**)]$^-$ [Pd(**1**)+(MeOH]$^-$ [Pd(P(Ph)($C_6H_4SO_3$))]$^-$	446.9 478.9 369.9	1 5 10
[Pd(**1**)$_2$(dba)]$^{2-}$	511.0	[Pd(**1**)(dba)]- [**1**]$^-$ [Pd(**1**)$_2$]$^{2-}$	681.0 341.1 393.9	2 2 1
[Pd(**1**)$_2$]$^{2-}$	393.9	[**1**]$^-$ [Pd(**1**)]$^-$	341.1 446.9	1 1
[Pd(**1**)(Ph)(I)]$^-$	650.9	[**1**]$^-$ [Pd(**1**)]$^-$	341.1 446.9	0 12
[Pd(**1**)$_2$Ph]$^-$	865.0	[Pd($C_6H_4SO_3$)(P(Ph)$_2$($C_6H_4SO_3$))]$^-$ [**1**]$^-$ [Pd(**1**)]$^-$ [P(Ph)$_2$($C_6H_4SO_3$)$_2$]$^-$	602.9 341.1 446.9 497.0	5 8 15 22
[Pd(PPh_3)($C_6H_4CH_2SO_3$)(I)]$^-$	664.9	[P(Ph)$_2$($C_6H_4CH_2SO_3$)]$^-$ [Pd(I)($C_6H_4CH_2SO_3$)]$^-$ [I$C_6H_4CH_2SO_3$]$^-$	355.1 402.8 296.9	8 8 16
[Pd(PPh_3)$_2$($C_6H_4CH_2SO_3$)(I)]$^-$	923.0	[Pd(PPh_3)($C_6H_4CH_2SO_3$)(I)]$^-$ [P(Ph)$_2$($C_6H_4CH_2SO_3$]$^-$	664.9 355.1	1 12
[Hg(I)($C_6H_4CH_2SO_3$)]$^-$	498.9	[I$C_6H_4CH_2SO_3$]$^-$ [I]$^-$ [$C_6H_4CH_2SO_3$]$^-$	296.9 126.9 170.0	13 15 15
[Hg(I)$_2$(Ph)]$^-$	532.8	[I]$^-$	126.9	1
[Hg(I)$_3$]$^-$	582.7	[I]$^-$	126.9	2
[Hg(I)$_2$Cl]$^-$	490.7	[I]$^-$	126.9	2

Key: **1** = $C_{18}H_{14}O_3PS$; dba = $C_{17}H_{14}O$

Additional MS Reaction Monitoring Data

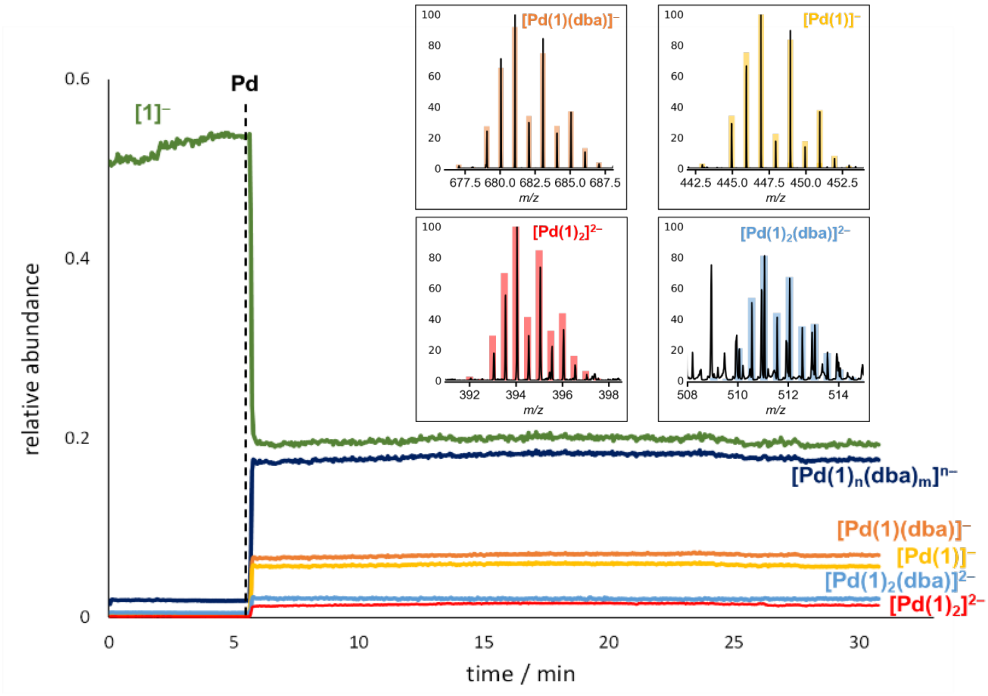

Figure B.4: Relative abundances of monoligated and bisligated catalyst activation resting states $[Pd(\mathbf{1})_n(dba)_m]^{n-}$ showing good stability in MeOH for at least 25 min. Insets show the predicted isotope patterns (bars) overlaid on the experimental mass spectra (lines).

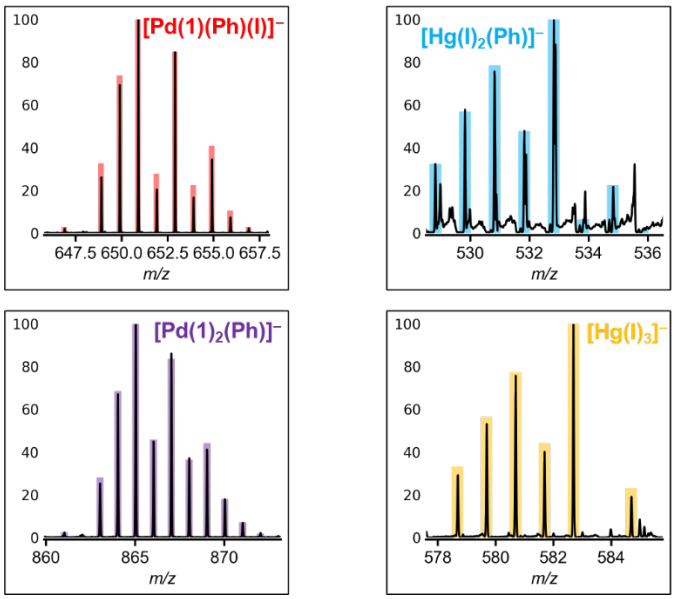

Figure B.5: The predicted isotope patterns (bars) overlaid on the experimental mass spectra (lines) of key palladium and mercuric ion observed upon addition of mercury.

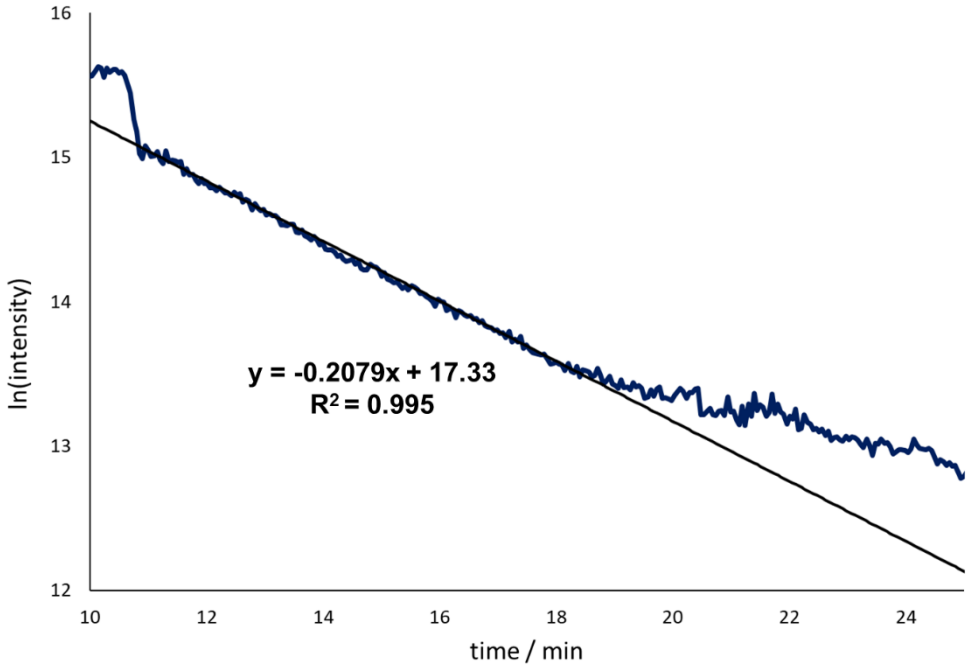

Figure B.6: Kinetic plot of ln(intensity) vs time for $[Pd(1)_n(dba)_m]^{n-}$ species.

Rate constant for $[Pd(1)_n(dba)]^{n-}$

slope = –0.2079. First order, therefore k = 0.2079 min^{-1}

$$t_{1/2} = \frac{0.693}{k} = \frac{0.693}{0.2079\ min^{-1}} = \mathbf{3.3\ min}$$

Redox-transmetallation

In addition to $[Hg(I)_3]^-$, $[Hg(I)_2Cl]^-$ was also observed to form in redox-transmetallation experiments, following similar kinetic profiles (Figure B.7). Formation of $[Hg(I)_2Cl]^-$ is attributed to residual chloride counterions presumably from the synthesis of [PPN][**2**], competing for mercury coordination with iodide ions. These species intensities are summed as shown in Figure 4.5. All species were characterized thoroughly using isotope pattern matching and MS/MS experiments.

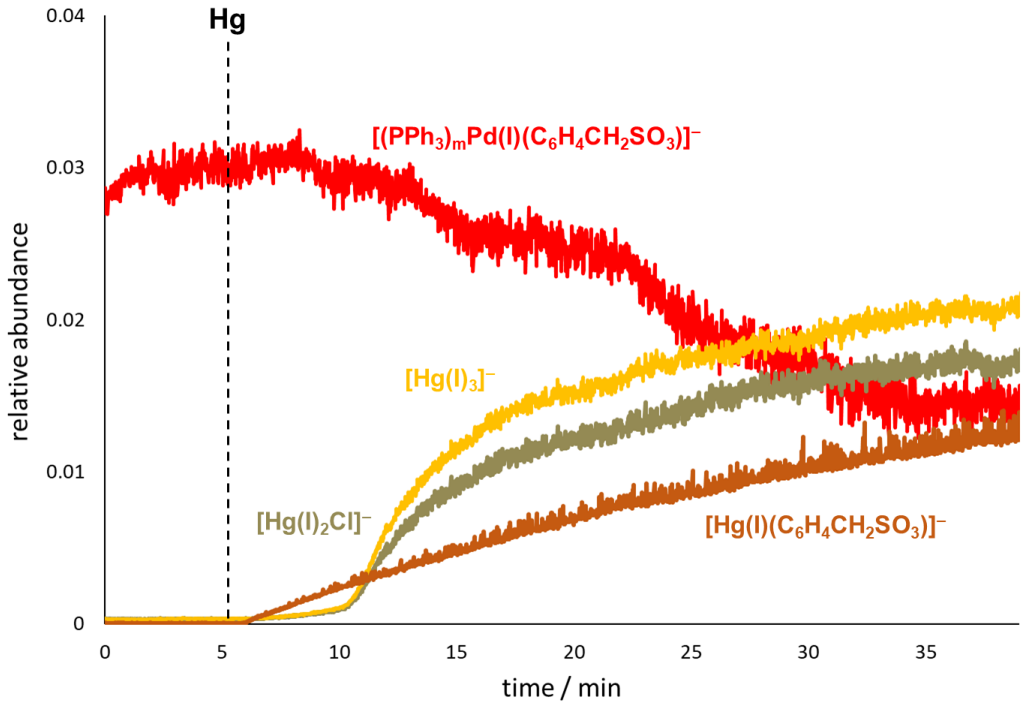

Figure B.7: PSI-ESI(–)-MS reaction monitoring of the effects of Hg on the Pd^{II} oxidative addition intermediate $[(PPh_3)_mPd(I)(C_6H_4CH_2SO_3)]^-$, where m = 1–2. Pd/Hg transmetallation of substrate occurs with the immediate formation of $[Hg(I)(C_6H_4CH_2SO_3)]^-$, as well as $[Hg(I)_2X]^-$ (X = I or Cl).

C – Supporting Information for Chapter 5

The manuscript for Chapter 5 was featured as a Front Cover in *Organometallics* (Figure C.1). ICC conceptualised this cover, with initial sketches aimed at depicting the catalyst activation in action. Discussions with JSM evolved this concept into making a 3D render. Molecule geometries were then constructed and optimized in Avogadro, and further refined in Mercury, before exporting as .stl files into Fusion 360. Initial renderings were done by JSM, with ICC refining the design with colours and lighting.

Figure C.1: Front Cover feature artwork for *Organometallics* by Ian C. Chagunda and J. Scott McIndoe.

MS/MS Reaction Species Characterization

All MS/MS spectra were collected using the same instrument parameters as in full scan experiments. The optimised collision-induced dissociation (CID) transfer collision energies for each identified species are listed in Table C.1. The collision energy (CE) for each precursor ion was chosen such that the ion fragmented to <10% of its initial intensity at CE = 0 V. The product ions detected in each CID experiment along with isotope pattern matching were diagnostic for identifying the catalytically relevant species in each experiment. Experimental and overlaid calculated isotope patterns for relevant catalytic intermediates are shown in Figure C.2.

Table C.1: CID scan specifications for relevant (^{DMP}DAB)Pd(CH_2SiMe_3)$_2$ reaction intermediates.

Precursor Ion / *m/z*		Product Ion(s) / *m/z*		Collision Energy / V
[**3**]$^-$	489.20	[**3**−((PCy)(OMe))]$^-$ [**3**−(PCy_2)]$^-$	375.09 292.01	40
[**3**+O]$^-$	505.19	[**3**]$^-$ [**3**−((Cy)(OMe))]$^-$	489.15 391.09	45
[Pd(**3**)]$^-$	595.09	[**3**]$^-$	489.19	20
[Pd(**3**)$_2$]$^{2-}$	542.10	[Pd(**3**)]$^-$ [**3**]$^-$	595.04 489.16	7
[Pd(**3**)+O]$^-$	611.09	[**3**+O]$^-$ [Pd(**3**)+O−(C_6H_{10})]$^-$	505.19 529.02	22
[(^{DMP}DAB)Pd(**3**)(CH_2SiMe_3)$_2$]$^-$	1033.54	[Pd(**3**)(CH_2SiMe_3)$_2$]$^-$ [Pd(**3**)]$^-$ [**3**]$^-$	769.36 595.09 489.20	3
[Pd(**3**)(CH_2SiMe_3)$_2$]$^-$	769.36	[Pd(**3**)]$^-$ [**3**]$^-$	595.09 489.17	5
[(^{DMP}DAB)Pd(**3**)]$^-$	859.25	[Pd(**3**)]$^-$ [**3**]$^-$	595.03 489.08	25
[Pd(**3**)(MAH)]$^-$	693.09	[Pd(**3**)]$^-$	595.20	13
[**1**]$^-$	341.04	[**1**−(C_6H_5)]$^-$ [**1**−(PPh)]$^-$	264.01 156.00	40
[**1**+O]$^-$	357.04	[**1**+O−(C_6H_5)]$^-$	280.00	47
[Pd(**1**)]$^-$	446.96	[**1**]$^-$	341.05	15

		[Pd(**1**)−(C_6H_5)]$^-$	369.91	
[Pd(**1**)$_2$]$^{2-}$	437.98	[Pd(**1**)]$^-$ [**1**]$^-$	446.92 341.04	10
[Pd(**1**)(CH_2SiMe_3)$_2$]$^-$	621.07	Abundance too low for CID trapping		
[(^{DMP}DAB)Pd(**1**)(CH_2SiMe_3)$_2$]$^-$	885.24	Abundance too low for CID trapping		
[**4**]$^{2-}$	368.06	[**4**−(O)]$^{2-}$ [**4**−(C_6H_5)]$^{2-}$ [**4**−PPh_2]$^{2-}$	360.54 329.53 275.02	23
[**4**+O]$^{2-}$	376.04	[**4**]$^{2-}$	368.06	24
[Pd(**4**)]$^{2-}$	421.24	[**4**]$^{2-}$	368.05	10
[Pd(**4**)+O]$^{2-}$	437.01	[Pd(**4**)]$^{2-}$ [Pd(**4**)−(O(C_6H_5))]$^{2-}$	421.01 381.98	12
[Pd(**4**)(CH_2SiMe_3)$_2$]$^{2-}$	509.06	Abundance too low for CID trapping		
[(^{DMP}DAB)Pd(**4**)(CH_2SiMe_3)$_2$]$^{2-}$	641.14	Abundance too low for CID trapping		
[**5**+H]$^+$	411.24	[(**5**)-($HPCy_2$)]$^+$	213.00	22
[**5**+H+O]$^+$	427.26	[(**5**+H+O)−(Cy_2)]$^+$ [(**5**+H+O)−(HCy)]$^+$	261.11 343.19	35
[Pd(**5**+H)]$^+$	517.14	[Pd(**5**−Cy)]$^+$ [Pd(**5**−Cy_2)]$^+$ [Pd(PCy)]$^+$	434.05 351.00 219.97	30
[Pd(**5**+H+O)]$^+$	533.48	[Pd(**5**+H+O)−Cy_2]$^+$ [Pd(PCyO)]$^+$	367.32 235.22	33
[Pd(**5**)(CH_2SiMe_3)]$^+$	603.19	[Pd(PCy)(CH_2SiMe_3)]$^+$ [Pd(PCy_2)(CH_2SiMe_3)]$^+$ [Pd(**5**−Cy)]$^+$ [Pd(**5**)]$^+$	307.03 389.11 433.05 516.15	19
[(^{DMP}DAB)Pd(**5**+H)]+	781.30	[Pd(**5**+H)]$^+$	517.16	15
[Pd(**5**)(Ar)]$^+$	635.15	[**5**]$^+$ [Pd(**5**)]$^+$	410.23 516.15	32
[Pd_2(**5**)$_2$($Ar)_2$Br]$^+$	1349.30	Abundance too low for CID trapping		
[ArR+Na]$^+$	249.10	[($C_6H_4COCH_3$)+Na]$^+$ [(C_6H_4CO)($C_6H_4OCH_3$)+Na]$^+$	142.98 235.01	10

Key: **1** = $C_{18}H_{14}O_3PS$; **3** = $C_{26}H_{34}O_5PS$; **4** = $C_{39}H_{30}O_7P_2S_2$; **5** = $C_{26}H_{35}O_2P$; ^{DMP}DAB = $C_{18}H_{20}N_2$; Ar = C_8H_7O; R = C_7H_7O; MAH = $C_4H_2O_3$

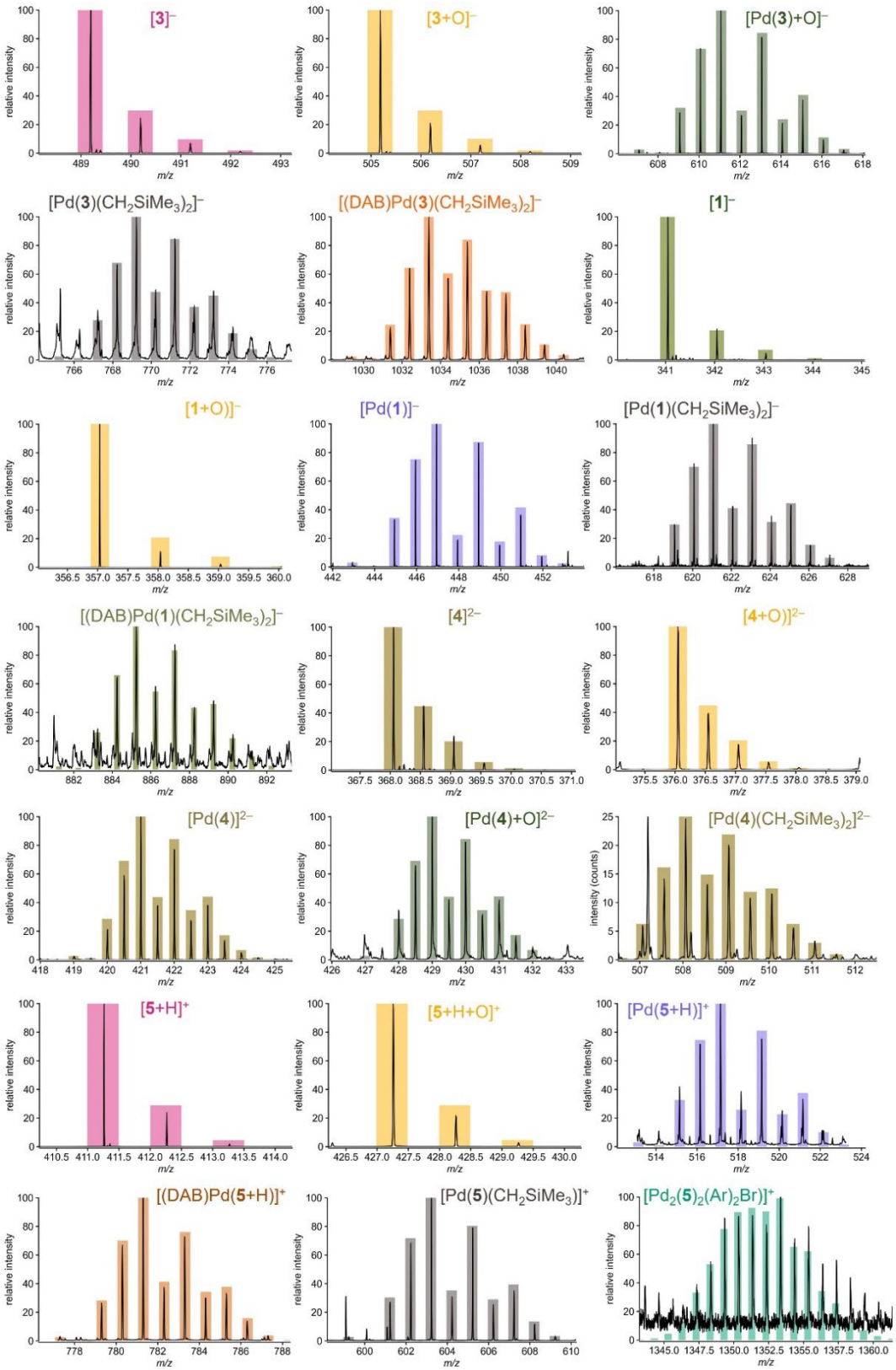

Figure C.2: Additional calculated isotopic distribution patterns (bars) overlaid on the experimental isotopic distribution (lines) for relevant catalytic species.

Supporting Investigations of LPd(0) Formation

Control experiments for the activation of (^{DMP}DAB)Pd(CH_2SiMe_3)$_2$ to promote the formation of the bisligated [Pd(**3**)$_2$]$^{2-}$ complex by adding an excess (2 equiv.) of sSPhos (**3**). The excess phosphine was introduced either in a single aliquot prior to adding the precatalyst, or as a second equivalent aliquot following precatalyst addition. Figure C.3 shows a representative example of these experiments. Despite monitoring the reaction species after adding excess [PPN][**3**], no detectable [Pd(**3**)$_2$]$^{2-}$ species were observed (Figure C.3B).

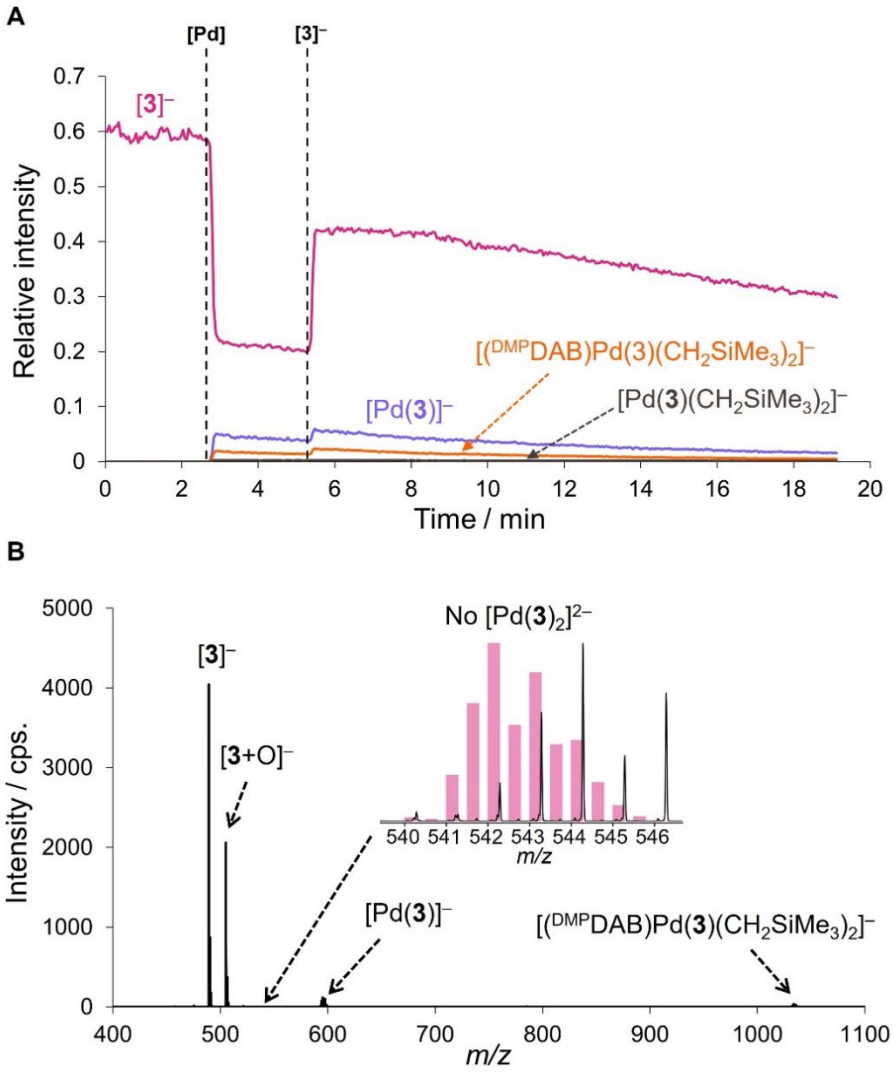

Figure C.3: A) PSI-ESI(–)-MS reaction monitoring of catalyst activation upon addition of (^{DMP}DAB)Pd(CH_2SiMe_3)$_2$ (10 μM, 1.0 equiv, at 2.6 min) to a solution of [PPN][**3**] (10 μM, 1.0 equiv) in MeOH. Subsequent addition of [PPN][**3**] (10 μM, 1.0 equiv) was done at 5 min. B) Cumulative mass spectra collected at 7 min, showing no detectable bisligated [Pd(**3**)$_2$]$^{2-}$ (*m/z* 542). Inset: zoomed-in experimental isotopic distribution (lines) with calculated isotopic distribution patterns (bars) for spectra region *m/z* 540-546, showing no diagnostic Pd-pattern.

CID of [(^{DMP}DAB)Pd(**3**)(CH_2SiMe_3)$_2$]$^-$ at various collision voltages of an applied transfer collision energy ramp (0 to 30 V, in 1 V increments) resulted no [(^{DMP}DAB)Pd(**3**)]$^-$ fragment ion detected (Figure C.4). This absence of a [(^{DMP}DAB)Pd(**3**)]$^-$ fragment ion suggests a sequential pathway involving the ligand dissociation and reductive elimination of ^{DMP}DAB and (CH_2SiMe_3)$_2$, leading to the formation of LPd(0).

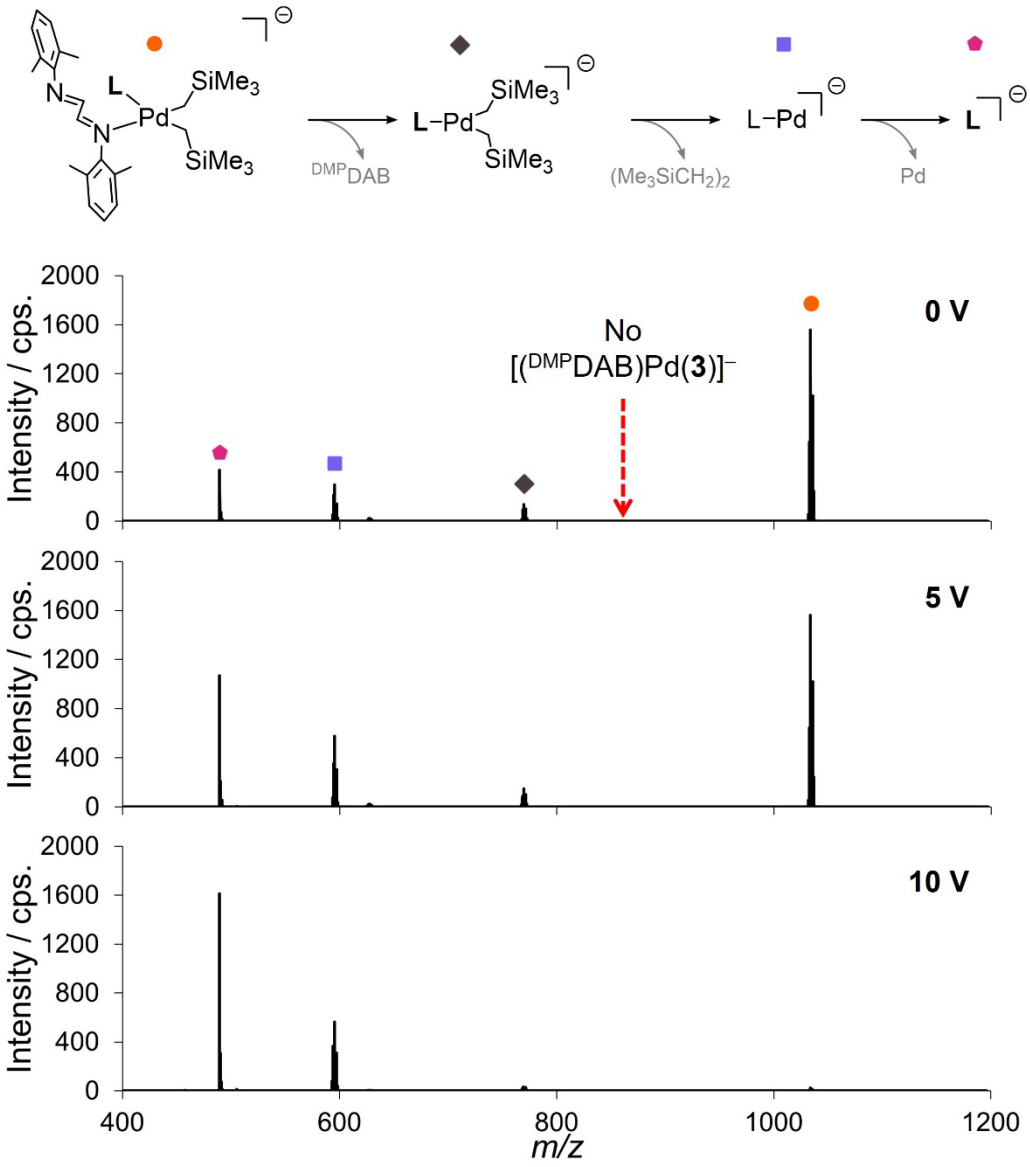

Figure C.4: ESI(–)-MS/MS CID of [(^{DMP}DAB)Pd(**3**)(CH_2SiMe_3)$_2$]$^-$ at collision energies 0, 5, and 10 V.